Assessment of Surface Water Pollution Caused by Tannery Effluents and Its Mitigation Strategies in Bangladesh

By

Fatema-Tuj-Zohra

A Dissertation

Submitted to the Dept. of Applied Chemistry and Chemical Engineering

University of Dhaka

in Partial Fulfilment of the Requirements for

the Degree of Doctor of Philosophy

December 2022

Declaration

It is hereby declared that this thesis or any part of it has not been submitted elsewhere for awarding any degree or diploma.

Signature of the Candidate
Fatema-Tuj-Zohra
Registration Number: 26/2019-2020
Session: 2019-2020
Department of Applied Chemistry and Chemical Engineering
University of Dhaka

CERTIFICATE

This is to certify that the thesis entitled "Assessment of Surface Water Pollution Caused by Tannery Effluents and Its Mitigation Strategies in Bangladesh" being submitted by Fatema-Tuj-Zohra, Registration No. 26/2019-2020, Session: 2019-2020, Department of Applied Chemistry and Chemical Engineering, University of Dhaka, in partial fulfillment of the requirement for the degree of the Doctor of Philosophy, is an original study of the author carried out under the joint supervisions. The thesis or any part this thesis has not been submitted before to any other University or Institute for the award of any Degree or Diploma.

Dr. Md. Zahangir Alam
Professor and Supervisor
Department of Applied Chemistry and
Chemical Engineering
University of Dhaka

Dr. Md. Nurnabi
Professor and Supervisor
Department of Applied Chemistry and
Chemical Engineering
University of Dhaka

Dr. Nazia Rahman
Principal Scientific Officer and Supervisor
Institute of Nuclear Science and Technology
Atomic Energy Research Establishment
Bangladesh Atomic Energy Commission

Dedicated

To

All of My Teachers

Acknowledgment

At first, I Wish to express my gratitude to the most gracious, merciful Almighty Allah, since without his blessings I would not be able to complete my PhD work.

My heartiest gratitude goes to my honorable supervisors, **Professor Dr. Md. Zahangir Alam,** Department of Applied Chemistry and Chemical Engineering, University of Dhaka and Vice-Chancellor, Atish Dipankar University of Science and Technology, Dhaka, **Professor Dr. Md. Nurnabi**, Chairman, Department of Applied Chemistry and Chemical Engineering, University of Dhaka, and **Dr. Nazia Rahman,** Principal Scientific Officer, Institute of Nuclear Science and Technology, Atomic Energy Research Establishment, Bangladesh Atomic Energy Commission for giving me the opportunity, courage and trusts that boosting me to explore. It is my great pleasure to express my sincere and deep gratefulness to them for their immense guidance, information, and practical suggestion in order to finish this thesis work and to write the dissertation.

My sincere thanks to **Professor Dr. Mohammed Mizanur Rahman**, Director, Institute of Leather Engineering and Technology, University of Dhaka, for providing tremendous support during the completion of the dissertation.

I am very grateful to all the faculty members, Department of Applied Chemistry and Chemical Engineering, University of Dhaka, for their incredible support and cooperation throughout my research.

Special thanks to my daughter for her support, passionate inspiration and prolonged patience that helped me to complete this research work.

December. 2022 Author

Abstract

Wastewater from leather processing industries generally contain high amount of toxic metal ions, organic and inorganic pollutants, which poses high risk to the ecosystem and human civilization. This thesis focuses on the assessment of pollution level of surface water collected from the river adjacent to the leather processing industries. The research also focuses on the use of peanut shell, Bagasse, and potato peel for the treatment of prepared wastewater and tannery effluents.

First of all, various physico-chemical properties including pH, temperature, TDS, EC, NaCl %, BOD, and COD along with heavy metals (Cr, Ni, Cu, Cd, and Pb) of the surface water samples were analyzed. These sample were collected from three layers at three different locations of Dhaleshwari, Buriganga, Bhairab and Karnaphuli rivers nearby the tannery where the effluents were discharged. In the next step, chemically activated pyrolyzed peanut shell (PNS), chemically activated peanut shell (NS), and chemically activated pyrolyzed bagasse (PB) were prepared to remove Cr(III) from $Cr_2(SO_4)_3.6H_2O$ aqueous solution and from chrome tanning effluents. Adsorbent PNS, NS and PB was characterized through EDX, FTIR, SEM, XRD and BET analysis. The adsorption capacity of PNS, NS, and PB were 104.82 mg/g, 58.28 mg/g and 74.63 mg/g respectively for removal of Cr(III) from aqueous solution at pH 5.0, while, it was 72.79 mg/g, 58.11 mg/g, and 72.45 mg/g respectively for removal of chromium from chrome tanning effluents. In this research, another adsorbent was prepared from potato peel powder (PP) and characterized through EDX, FTIR, SEM, XRD and BET analysis. The PP was applied for removal of leather dye C.I. Acid Red 73 (AR73) from aqueous solution and dyeing effluent. The adsorption capacity of PP was 258.39 mg/g for removal of AR73 from aqueous solution at pH 2.0, and 137.39 mg/g for removal of AR73 dye from dyeing effluent.

The Langmuir and Freundlich isotherm model were applied to explain the distribution of adsorbate (Cr^{3+} and dye) on adsorbents (PNS, NS, PB and PP) surface. The values signify that the adsorption of Cr^{3+} on adsorbents comply both Langmuir and Freundlich isotherm model, preferably the Langmuir model. Pseudo-first-order and pseudo-second-order kinetic models were employed to justify the adsorption process. It was observed that pseudo-second-order kinetic models provide better correlation for all adsorbents. The thermodynamic analyses were also carried out for all adsorbents and it was revealed that the adsorption process was spontaneous at low temperature. The regeneration was studied for the spent PNS, NS, PB and PP, and it was found that the used adsorbents could be regenerated and reused.

Table of Contents

List of abbreviations

AC	Activated Carbon
AR73	C.I. Acid Red 73
BCS	basic chromium sulfate
BET	Brunauer-Emmett-Teller
BOD	Biochemical Oxygen Demand
CETP	Central Effluent Treatment Plant
COD	Chemical Oxygen Demand
DoE	Department of Environment
DSP_{50}	Downstream point at 50 cm deep
DSP_{100}	Downstream point at 100 cm deep
DSP_S	Downstream point at surface
EC	Electrical Conductivity
ECR	Environmental Conservation Rule
ED	Electrodialysis
EDX	Energy Dispersive X-ray
EPB	Export Promotion Bureau
FTIR	Fourier Transform Infrared Spectroscopy
GO	Graphene Oxide
HCA	Hierarchical Cluster Analysis
ICP-MS	Inductively Coupled Plasma-Mass-Spectrometry
LCAs	Low-cost adsorbents
MCL	Maximum contaminant level
MF	Microfiltration
MP_{50}	Main discharge point at 50 cm deep
MP_{100}	Main discharge point at100 cm deep

MP_S	Main discharge point at surface
NF	Nanofiltration
NS	Chemically Activated Nut Shell
PB	Pyrolyzed and Chemically Activated Bagasse
PCA	Principal Component Analysis
PNS	Pyrolyzed Chemically Activated Nut Shell
PP	Potato Peel powder
RMG	Readymade Garments
RO	Reverse Osmosis
SEM	Scanning Electron Microscopy
SS	Suspended Solids
TDS	Total Dissolved Solids
TIED	Tannery Industrial Estate Dhaka
UF	Ultrafiltration
USP_{50}	Upstream point at 50 cm deep
USP_{100}	Upstream point at 100 cm deep
USP_S	Upstream point at surface
USEPA	United States Environmental Protection Agency
XRD	X-Ray Diffraction
ZPV	Zeta Potential Value

Chapter 1

Introduction

1.1. Background of the study

Water is one of the most precious natural resources in this earth. It is said that water is the "Life blood of biosphere" as it is the main component for functioning of all living cell. In this century it is appropriate to say that fresh and clean water is essential for existence of life. Bangladesh is a riverine country having 238 major rivers with blessings of nature [1]. In the developing countries, there is a common phenomenon to build up industries near the water bodies and discharge untreated effluents to the surface water and abuses of environment and natural resources. Globally water consumption increases significantly because of massive growth of civilization and industrialization, and hence discharge of huge wastewater to the environment with several pollutants, for instance heavy metals, dyes, hydrocarbons, phenols, detergents and other pollutants [2]. Wastewater from leather, textile, paper, plastic, cosmetic, and printing industries are the sources of some of these pollutants [3,4]. In nature, surface water is not pure as it dissolves different elements and compounds easily which degrade the water quality and adversely affects human health and livelihood besides hampering the availability of fresh water for agriculture, fisheries and public [5,6]. The rate of dumping of synthetic chemicals and waste into the aquatic environment is also growing day by day [7]. Therefore, surface water pollution is one of the most alarming threats for mankind today, and it is significant to apply intellectual power not only at technological development but also towards the protection of natural life support system.

Leather is a traditional export item of Bangladesh which plays a vital role for socio-economic development. Leather sector is the second-biggest foreign exchange earning sector of Bangladesh just after the readymade garments (RMG) sector. EPB (Export Promotion Bureau) announced that Bangladesh obtained US $1.019 billion in the economic year of 2018–2019 from leather and leather products sector. Due to COVID-19 pandemic situation, export earnings decreased to US$ 0.797 billion in the fiscal year of 2019-2020 and increased to US$ 0.941 billion in 2020-2021 [8]. The sector earned US$ 1.25 billion in fiscal year of 2021-2022 with more than 32% growth from previous year since after pandemic. The leather and leather products industries have a noteworthy position in the economy of our nation in terms of value addition and employs approximately 850,000 people directly or indirectly [9]. Bangladeshi leather is exclusively well known to the entire world for its eminent quality and covered exports around 0.6% of the total global market [10 ,11].

In spite of the socio-economic importance leather sector generate huge pollution to the environment. It is estimated that almost 85,000 tons of raw hides/skins are to be processed in

Bangladesh every year that produce huge quantity of solid and liquid wastes [10]. Around 156 tanneries had shifted from Hazaribagh, Dhaka to Tannery Industrial Estate Dhaka (TIED), Hamayetpur, (outskirt of Dhaka city) Savar on the bank of Dhaleshwari river with Central Effluent Treatment Plant (CETP) facility, though it is yet to be functioned accurately for controlling the pollution load of discharged wastewater [12,13].

Leather is a unique commodity through which rural farmer is connected with fashionable world. From ancient time leather tanning process was performed to meet the local demand like, cloths, footwear, water bag, drums, and musical instruments. It is a natural material which contain various complementary properties over synthetics, e.g., strength, aesthetic appeal, feel, breathability. Over the time, with increasing demand of leather and leather products encouraged the establishment of enterprise of modern commercial tanneries. In leather processing putrescible raw hides and skins are converted to non-putrescible leather through tanning process that protects it from microbial degradation, moisture, heat and other environmental effects. Different mechanical and chemical treatments are used to transform raw hides/skins into leather. Various chemicals; such as acids, alkalis, surfactants, biocides, dye stuffs, fat liquors, binders, cross linkers, handle modifiers, fixing agents, salts of sodium, ammonium and chromium are consumed during chemical process. Leather tanning process requires plenty of water and almost 30-35 liters water is required for 1 kg of hide processing [14]. Chrome tanning is the most familiar technique in leather processing, about 80-90% of tanneries use basic chromium sulfate (BCS) to enhance quality of leather as chromium cross links between the collagen fibers poses high mechanical properties, breathability, dyeing properties and better hydrothermal stability [15–17]. During chrome tanning, only 55-70% chromium is attached with pickle pelt and the rest is discharged with wastewater. In addition, spent chrome liquor contain approximate 2000-5000 mg/L of chromium [18,19]. Moreover, presently almost 100,000 types of dyes are commercially produced and 1.6 million tons of dyes are consumed yearly, among them 10-15% are discharged into water bodies during use [20,21]. Dye contaminated post tanning wastewater discharges a huge quantity of suspended solid, BOD and COD, which decreases dissolve oxygen of surface water and also protect sunlight penetration that reduce photosynthesis and increase turbidity of water [22,23]. The existence of dyes in wastewater enhances the potential danger of bioaccumulation, pollutes aquatic system and jeopardizes the whole environment [24]. It is very urgent to save water of this earth for future generation as well as for whole bio-network. Various physical, biological and chemical methods are generally used to remove Cr(III) and dye from tannery effluents [25–28].

Different treatment techniques have implied to lessen the intensity Cr(III) and colour imparting materials from the industrial effluents such as, chemical precipitation [29] coagulation [30], adsorption [31–33], membrane filtration [34], ion exchange [35], biological treatment [36], photo catalytic degradation [37], reverse osmosis and electro dialysis [38,39], nano filtration [40]. Adsorption is very potential method to minimize heavy metals and dyes from industrial effluents due to its operational simplicity, cost effectiveness, environment compatibility and easy recycling process [41–45]. Activated carbon is produced through heating at high temperature in absence of oxygen. Raw materials are obtained from agricultural and animal wastes or by-products such as straws of crops, seed husks, bagasse, fruit stones, nutshell and feces are used [46,47]. Due to having huge surface area and high cation exchange capacity, the activated carbon can efficiently remove organic and inorganic pollutants [48].

Different biological treatment methods are claimed more effective and economical compare to other physical and chemical treatment method [49,50]. However, these methods have some shortcomings like, large space, high capital investment, types and concentration, pH, temperature, salinity, structure of the compounds, incomplete metal removal, generation of toxic sludge or other waste byproducts which need to safe disposal [51,52]. In biodegradation process, microbial biomass and its activity are the key factor for the removal of pollutant, however, huge concentration of metals viz. Cr, Cu, Cd, Pb, As and Zn might have unfavorable effect on microbial growth and activity [53]. Adsorption exploits the biological materials to accumulate different metal and dyes from tannery effluents. Hence, developing agro-based adsorbents can be a solution to these problems which will be attractive as well as viable to apply.

1.2. Problem Statement

In conventional leather processing, chrome tanning produces spent chrome liquor containing significant amount of chromium with other organic and inorganic pollutants. Unused chromium salts are generally discharged in the final effluents, causing grave risk to the environment. Moreover, currently thousands of dyes are commercially available for leather dyeing. Dyeing wastewater contain plenty of dyes which pollutes surface water along with significant troubles to the whole aquatic environment. In Bangladesh, most of the tanneries and other industries are located near the bank of the rivers. Unfortunately, industrial unit load

effluents into the environment with partial treatment or without treatment which cause severe pollution to surface water.

1.3. Objectives of the study:

The main purpose of the study is to assess surface water pollution and to explore the possibilities of using different agro wastes as adsorbents to remove Cr(III) and leather dyes. To accomplish the general objectives, the work comprised in the thesis has been structured according to the following specific objectives:

a) Specific objectives concerning assessment of surface water pollution at the vicinity area of tannery:
    - Four river, Dhaleshwari, Buriganga, Bhairab and Karnaphuli water samples were collected to assess few important physicochemical parameters along with heavy metal concentration to understand the present pollution load of the surface water.

b) Specific objectives regarding Cr(III) adsorption process using chemically treated activated pyrolyzed peanut shell (PNS), chemically activated peanut shell (NS) and chemically activated pyrolyzed bagasse (PB):
    - Optimization of the preparation method of chemically activated pyrolyzed and natural adsorbents.
    - Characterization of the prepared PNS, NS and PB.
    - Study of the adsorption capacity of prepared PNS, NS and PB using Cr-salt.
    - Study of the regeneration process of PNS, NS and PB.
    - Application of the PNS, NS and PB adsorbents on tannery effluents.

c) Specific objectives relating to leather dye adsorption process using potato peel powder (PP):
    - Preparation of the adsorbent, PP.
    - Characterization of the prepared PP.
    - Study of the adsorption capacity of prepared PP to remove C.I.Acid Red 73 leather dye from tannery effluents.
    - Study of the regeneration process of PP.
    - Application of the PP as adsorbent on dye contaminated tannery effluents.

1.4. Thesis outlines

This document is divided into five chapters-

Chapter 1 contains background of the study, problem statement, objective of the study and thesis outlines.

Chapter 2 provides literature review of studies conducted by other researchers and to which this study has been referred. It includes background on the theory of the topics involve, as well as information on their usage and applications. This chapter emphasizes the benefits of employing adsorption process and low-cost materials in terms of cost, time and efficiency and demonstrates the applications of using it on wastewater.

Chapter 3 comprises a description of the methodology employed to achieve the objectives of the thesis. It focuses over the experiments that were carried out. It includes procedures, methods, equipment, apparatus and other significant information that were used to accomplish the experiments.

Chapter 4 describes the results that were attained during the experiments. It analyses the obtained results of different water quality parameter, represents favorable and unfavorable conditions for the best experiment results. The chapter also features on obtaining best possible conditions for the most efficient adsorption as well as to find out the fitness of experimental data with different Isotherm and Kinetics.

Finally, Chapter 5 attributes a conclusion to the thesis. It illuminates the outcomes that were obtained from the research followed by the references.

1.5. Review of literature

1.5.1. A brief description on leather manufacture

Leather manufacture involves a series of chemical processes and operations from preservation to finishing with the goal of transforming quickly degradable, highly putrescible raw hides and skins into stable and nonputrescible leather. Although different tanneries use different methods, there are some common processes in leather making. The main operations in leather making process are beam house processes, tanning, post-tanning and finishing. Each operation comprises a number of sub operations as describe bellow:

1.5.1.1. Beam house processes

1.5.1.1.1. Soaking- Soaking is the first beam house process. Hides and skins are soaked and washed in slightly alkaline condition with wetting agents to take out dirt and surplus salt and to restore the hide condition, as soon as it was slaughtered.

1.5.1.1.2. Green fleshing- The washed hides are placed over a beam and is scrubbed to remove any remaining flesh and is washed again.

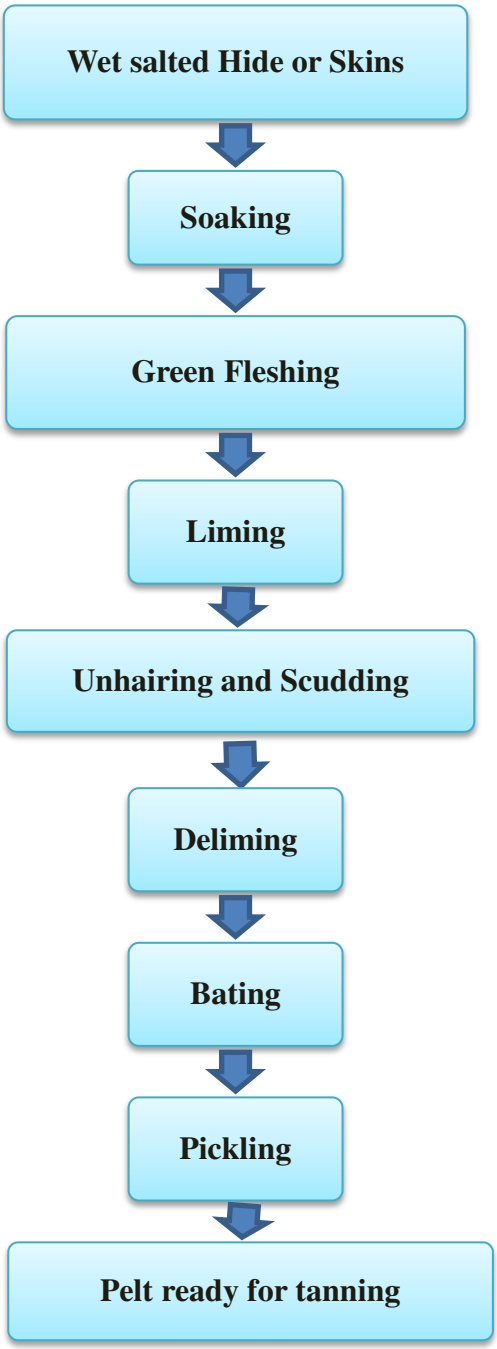

Scheme 1.1 Sequence of typical operations in the beam house.

1.5.1.1.3. Liming- Liming is done to loosen epidermis, adipose tissue and hair before tanning. Suspensions of calcium hydroxide, along with sharpening agents such as sodium sulphide, sodium hydrosulphide or dimethylamine, are added which speed up the liming process to remove hair.

1.5.1.1.4. Unhairing and Scudding- The remaining hair if any are removed by scrapping loosen hair from grain side. Scudding or squeezing of the lime pelt is carried out mechanically to press out partially degraded proteins, fats, hair roots etc.

1.5.1.1.5. Deliming- Limed pelt are then washed with various weak acids or buffer salts and water to reduce pH of the pelt from about 11.5 to about 8.5. Conventionally ammonium sulphate, ammonium chloride, sodium bisulphite, boric acid and lactic acid are widely used.

1.5.1.1.6. Bating- Bating is done by using specific types of enzymes to remove all residuals, partially degrade proteins and interfibrillary materials from the pelt for cleaning the fibers to receive the tanning agents readily and produce the desired properties to the finished leather.

1.5.1.1.7. Pickling- Pickling is the final operation prior to tanning is conducted to adjust the collagen to the condition required by the chrome or other tanning agents. Pickling reduces the pH of the pelt to between 2.0-2.5 through the action of HCL or H_2SO_4 acid, moreover, NaCl or Na_2SO_4 is added with pickle liquor to reduce swelling.

1.5.1.2. Tanning

In tanning process pelt is converted into leather through chemical cross-links between adjacent collagen molecules. Conventionally three types of tanning agents are widely used for leather tanning such as, mineral tanning, vegetable tanning, oil tanning, aldehydic tanning agents and the syntans.

1.5.1.2.1. Mineral tanning

1.5.1.2.1.1. Chrome tanning- After pickling at lower pH, chromium (III) salts are added to pickle pelt and for fixation of chromium (III) salts with collagen the pH is slowly increase by addition of base. In chrome tanning, chromium ions cross-link among free carboxyl groups covalently in collagen. It makes the leather bacteria defiant and hydrothermally stable. Chrome salts are stable at pH 2-4, but at higher pH precipitations will take place. This can be shown the following formulae:

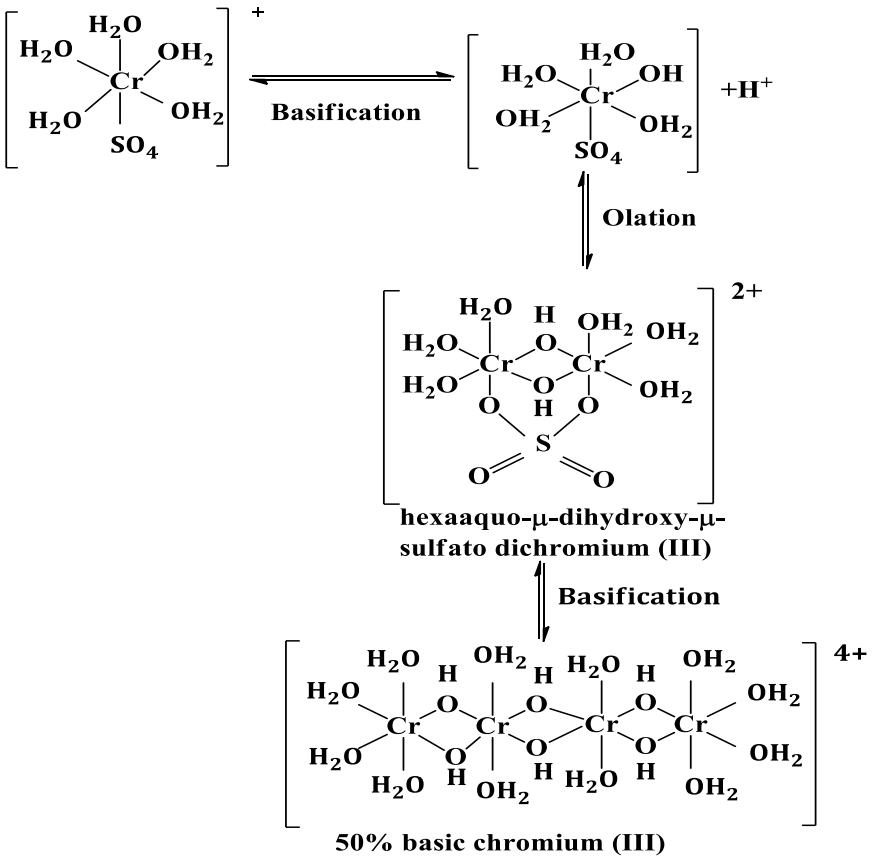

Scheme 1.2 Structure of basic chromium (III) complex [54]

1.5.1.2.1.2. Aluminum tanning - Aluminum salts, generally potash alum is used for white gloving leather. This process was known as 'tawing'. For thousands of years, it has been employed in the production of leather. It produces semi-aluminum leather when combined with conventional vegetable tanning. Aluminum (III) is more frequently used in leather tanning is for coloring because it precipitates as hydroxide, allowing colour to adhere with oxide. The range of stability is determined on the type of bonding; however, aluminum (III) is stable at pH 4 and the interaction is significantly more electrostatic.

1.5.1.2.1.3. Titanium tanning- Ti (IV) salts exhibit a comparable affinity towards collagen as aluminum (III) which interacts with collagen carboxyl in a way that is electrovalent rather than covalent. Moreover, one difference is that Ti (IV) salts have better filling effect resulting softer leather, due to the polymeric nature.

1.5.1.2.1.4. Zirconium tanning- The chemistry of Zirconium complexes is quite comparable to Cr(III) rather than Ti (IV), but tanning reaction is electrovalent and yielding slightly higher shrinkage temperature.

1.5.1.2.1.5. Iron tanning- As iron (III) has oxidizing power, iron (II) is preferred for leather tanning. The application is limited, because the lack of complexation with collagen carboxyl,

and hence iron tanned leather showed lower shrinkage temperature compare to chrome tanned leather.

1.5.1.2.2. Vegetable tanning

Vegetable tannins are polyphenolic compounds such as hydrolysable that are the products of pyrogallols and condensed are the derivatives of catechols. Phenolic groups of vegetable tannin form hydrogen bond with peptide link of the protein chains. Phenolic hydroxyls of vegetable tannins are capable to react with collagen, at the basic group of side chains and at the partially charged peptide links through hydrogen bonding.

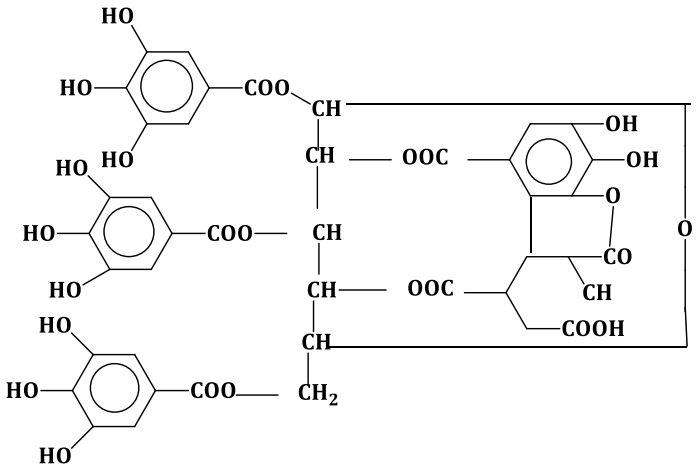

Scheme 1.3 Chebulinic acid (Hydrolysable tannins) [54]

1.5.1.2.3. Oil tanning

Oil tanning is generally performed through in situ oxidation of unsaturated oil, for example cod liver oil. Though oil tanning resists microbial attack still the shrinkage temperature is not increased appreciably beyond the value of raw pelt. This tanning method is applied to produce chamois leather,

1.5.1.2.4. Aldehydes and aldehydic tanning agents

1.5.1.2.4.1. Formaldehyde – Formaldehyde tanning yields white leather with plumpness and hydrophilicity. The leather making by formaldehyde tanning shows the shrinkage temperature up to 80^{o}C. Notably, due to toxicity hazard, the limit on the permissible concentration in the atmosphere of the workplace has obligatory a prohibition on its use as a reagent for leather production.

1.5.1.2.4.2. Glutaraldehyde –Glutaraldehyde tanned become plumpy and hydrophilic as like formaldehyde with same shrinkage temperature. On the other hand, the colour is striking,

with a prominent yellow hue that appears to be fairly orange. Due to the hazardous nature of glutaraldehyde, its utilization will have to be phased out.

1.5.1.2.5. Syntans

Syntan is the short form of synthetic tanning agents; usually they are aromatic, as hydroxy and sulfonate derivatives. Syntans are generally used in combination of other tanning agents to modify their action. Synthetic tanning materials are one of the most important and versatile leather auxiliaries that are needed for good quality leather. The characteristic of syntan is depending to the properties of monomeric precursors such as, phenol, toluene, cresol, naphthol, resorcinol, dihydroxy diphenyl sulfone etc. Syntans can be classified into major three groups according to their chemical constitution and main application – Auxiliary syntan, combination syntan and replacement syntan.

1.5.1.3. Basification

The basification processes extend the chrome tanning materials more astringent and quickens the tanning action. If tanning is incomplete or the pH is below 3.0, then more bicarbonate is applied to raise final pH to 3.0-3.5. Then wet blue leather is piled in a damp state for 2-3 days to complete the tanning process

1.5.1.4. Sammying and setting

After tanning, the leather is sammed to remove excess moisture before being processed mechanically. To stretch out the leather, the setting out process is carried out. Machines exists which combine the sammying and setting action. After sammying and setting, wet blue leather is sorted into different grades for further processing.

1.5.1.5. Shaving or splitting

To gain desired thickness shaving is carried out by the shaving machine. In case of thick pelt, it is splitted into layers of required thickness. The layer having the grain side makes the quality leather.

1.5.1.6. Trimming

Trimming is the operation of removing unwanted parts (rags or flags) from the wetblue in order to protect it from damage caused by different machinery during subsequent leather making operations and to keep the leather in shape.

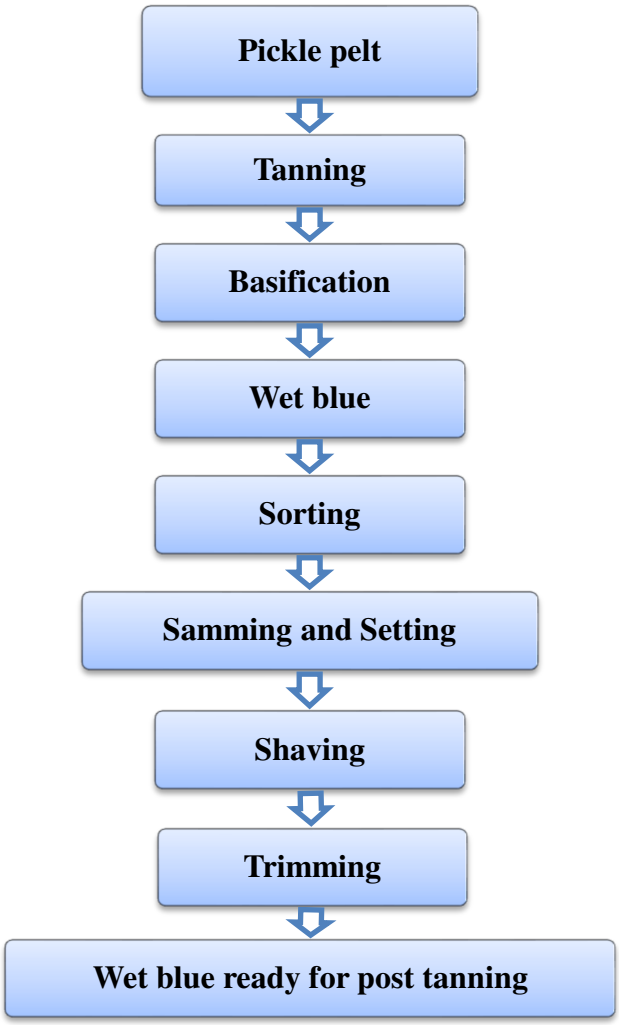

Scheme 1.4 Sequence of typical operations in the Tanning.

1.5.1.7. Post-tanning:

Post- tanning operation involves neutralization and washing, retanning, dyeing, fat liquoring and fixation mostly done in a same vessel. To enhance special property such as water vapor permeability, water resistance, flame retardancy, abrasion resistance, anti-electrostatic etc. different operations may also be carried out by adding some special chemicals in post-tanning operation.

1.5.1.7.1. Neutralization - In this operation wet blue leather is brought to suitable pH for the process of retanning, dyeing and fatliquoring. pH is raised up to 4.8-6.5 using dilute solutions of mild alkali like, sodium formate, sodium bicarbonate or ammonium bicarbonate, based on the type of products.

1.5.1.7.2. Retanning- -Retanning with a wide variety of chemicals such as vegetable tanning agents, syntans, mineral tanning agents gives the required feel and body to the leather and

adjust the dyeing properties according to final product or customer demand.

1.5.1.7.3. Dyeing - Dyeing is done in drum with selected water-based acid, basic and direct dyestuffs to develop appropriate colour to the whole leather surface as fashion market demand. A variety of dyeing auxiliaries, syntans or surface-active agents are generally applied to enhance the desired evenness and depth of shade.

Scheme 1.5 Sequence of typical operations in post tanning.

1.5.1.7.4. Fatliquoring- Fatliquoring restores the fat content that was previously removed during beam house operations from naturally occurs raw hides and skins. The fat liquor utilized might be of animal or vegetable origin or it could be made synthetically using mineral oil. This method restricts the fibers to stick together and brittleness when the leather dried out.

1.5.1.7.5. Fixing - To avoid bleeding of the dyes and fat liquors, the retanned, dyed and fat liquored leather is frequently fixed with formic aid and washed before being piled to allow the fatty matters to migrate into the inside of the leather.

1.5.1.7.6. Drying -The leather is then hanged on racks in a drying room with warm air to remove moisture.

1.5.1.7.7. Staking - The leather is made soft and pliable by working mechanically in all direction over a hard-edge slating of creases. Staking machine could be jaw-type or vibration staking.

1.5.1.7.8. Toggling - The leather is stretched out to full size on the toggle frame and clamps until thoroughly dry. After drying leather is known as crust which is saleable product.

1.5.1.8. Finishing

Finishing is the most important and last operation in leather processing. The overall aim of finishing is to improve the aesthetic value of the final leather. It also provides the required attributes in terms of colour, gloss, adhesion, fastness to light, heat and perspiration, water vapour permeability and water resistance as needed for the final application. The leather finishing techniques and the composition of different finishing seasons are changing gradually with the development of science and technology in different industrial fields.

1.5.1.8.1. Staining coat- This coat is generally containing anionic dye and dye penetrating agent. If the depth and brilliance of colour is to be improved then one more coat is applied with cationic dye solution.

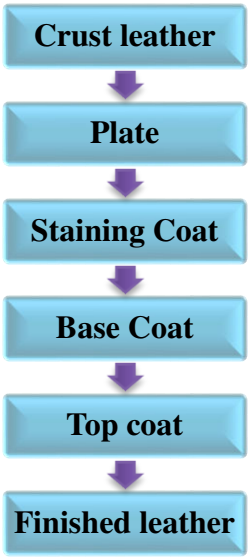

Scheme 1.6 Sequence of typical operations in leather finishing

1.5.1.8.2. Base coat-The base coat has traditionally been applied by padding, either by hand or machine. This coat contains casein and pigment which is much heavier, but depends on the type of end products. Base coat incorporates good flexing resistance, good adhesion, better scuff resistance etc.

1.5.1.8.3. Top coat- Top coat are the final coat in the finishing process. Except patent leather

the top coat should be sprayed in thin coats. However, to make sure sufficient film formation they should not be sprayed too dry.

1.5.2. Tannery effluents

A substance that is put into the environment and has a negative impact on the usefulness of resources is called pollutants. The substance that affects the stability of the natural environment is known as pollution. In leather production, soaking, liming, deliming, bating, pickling, tanning, dyeing and fatliquoring are the most water-intensive operations and wastewater generating process [55–57]. Various chemicals, such as strong acids and alkalis, surface active agents, wetting agents, basic chromium sulphate, organic and inorganic salts, vegetable tanning agents, bleaching agents, dye stuff, different fat liquor, syntans, finishing agents and salts of metal are employed during leather manufacturing [58–59]. Wastewater generated from tannery create heavy pollution with high content of salinity, organic and inorganic matter, dissolve and suspended solids, ammonia, organic nitrogen and specific pollutants like sulphide, chromium and a range of heavy metal salt residues [60].

1.5.2.1. Physicochemical parameters in tannery effluents

Tannery effluents can alter the physical, chemical and biological properties of aquatic environments. Other than chromium (Cr), tannery effluents contain some chemical contaminants, which are primarily caused by salts of Fe, Zn, Cu, Ca, Na and anions such as sulphate, nitrate, phosphate and parameters such as SS, TDS, BOD_5, COD, pH, Oil and grease [61].

1.5.2.1.1. Suspended Solids (SS) – The quantity of insoluble matter present in the wastewater is known as suspended solids. The insoluble materials cause different troubles when discharged from tannery; generally, they are made up of solids with two distinct properties such as- settle able solids and semi-colloidal solids. Settleable solids generate from all stages in beam house process with fine protein particles, residues from various chemicals and reagents which are being discharged from different effluents. Moreover, semi- colloidal solids are very fine solids, will not settle down in effluent for a considerable period of time. These are generally protein residues mostly produced from liming, vegetable tanning and retanning processes which will not directly cause sludge crisis. It takes a while for bacterial digestion to break them down and eventually settle.

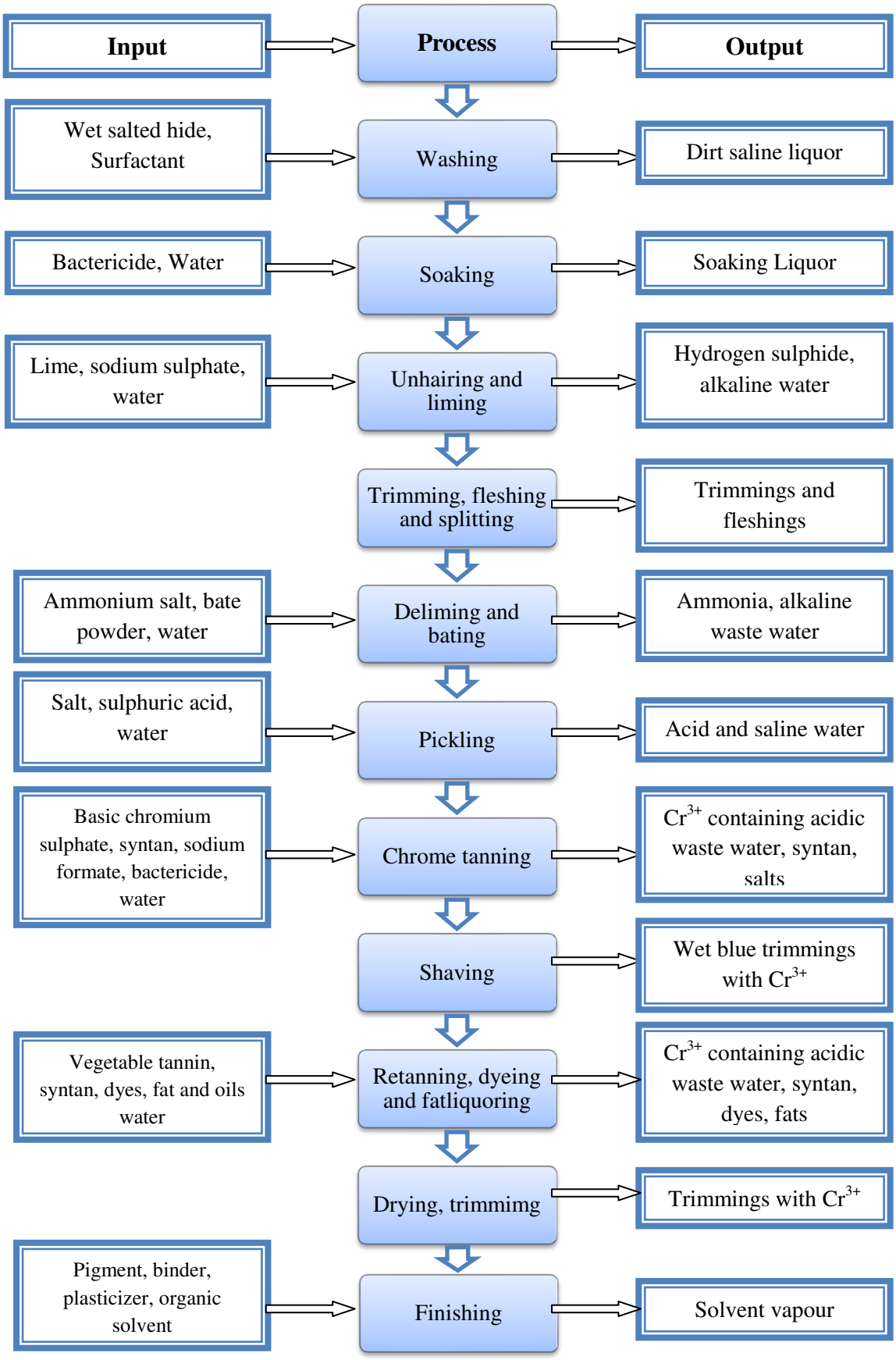

Scheme 1.7 Flow chart of tannery operations and environmental impact

1.5.2.1.2. Total dissolved solids (TDS) - TDS is the amount of all organic and inorganic

materials dissolved in wastewater; basically, it is everything present in water other than pure water and suspended solids. In the case of tannery wastewater, the major pertinent components are sulphates and chlorides.

1.5.2.1.3. Electrical conductivity (EC) - EC measures how well the liquid carries the electric current through it. When water is subjected to pollution, contamination due to metal ions increases the level of EC.

1.5.2.1.4. Biochemical Oxygen Demand (BOD_5) - BOD_5 is the amount of dissolve oxygen consumed by microorganisms to breakdown the organic materials in the wastewater over a 5-day period at 20°C. Many of tannery effluents take longer time to breakdown; usually, vegetable tanning wastewater, which is frequently stated to be up to 20 days. Moreover, chemicals, like retanning agents, fat liquors, dyes and residuals of keratinous substances need longer digestion period. This lengthy breakdown time indicates that, ecological impact is spread over as the wastewater components are carried greater distance before they broken down.

1.5.2.1.5. Chemical Oxygen Demand (COD) - COD is an indicator of water quality, which measures the amount of oxygen required to oxidize all of organic and inorganic compounds in a wastewater. Practically, COD value is influenced by the chemicals employed in various leather manufacturing processes and their biodegradability.

1.5.2.1.6. Nitrogen (N) – Numerous compounds in wastewater hold nitrogen as a part of their chemical structure. The important prevalent chemicals are ammonia generated by deliming agents and proteinaceous substances from liming process are the major sources of nitrogen.

1.5.2.1.7. Sulphides (S^{2-}) – The main sources of sulfide level in tannery effluents are the usages of Na_2S, NaHS and dissolved hair during liming.

1.5.2.1.8. Neutral salts (Chlorides, Cl^- and sulphates, SO_4^{2-}) - Generally huge amount of common salt are used to preserve raw hides and skins or in pickling process, which introduces sodium chloride into the system. They continue as a burden on the environment since they are extremely soluble and persistent which are unaffected by effluent management or nature. Moreover, sulphates are generating from H_2SO_4 or produce from the chemicals contain huge sulphate content. For instance, chrome tanning powder and several synthetic retanning agents both hold high level of sulphate.

1.5.2.1.9. pH - The standard pH value of industrial effluent is 6-9, and 6.5-8.5 according to DoE (1997) [62] and ECR (1997) [63], respectively. If the surface water pH deviates too far

from the recommended pH value, aquatic ecosystems (fish and plant life) may be at risk of losing their sustainability.

1.5.2.1.10. Oil and grease – During beam house operations, natural oil and grease are liberated from the hide or skin. However, due to poor uptake of synthetic fat liquor in fat liquoring process, some fatty substances may mix up with wastewater. These oil, grease and fatty maters agglomerate to form floated layer, which then bind other materials and create blockage problem particularly in effluent treatment plant.

1.5.2.2. Heavy metals

Heavy metals are the naturally occurring elements with their atomic number >20 and the density is higher than 5.0 g/cm^3 [64,65]. Heavy metals/metalloids viz. chromium, copper, zinc, arsenic, cadmium, mercury and lead are the major pollutants of water which can originate from both, natural (geologic parent material or rock outcropping) and anthropogenic such as agricultural sources, atmospheric deposition and industrial sources. These heavy metals are non-biodegradable, exist in the environment for long time and have tendency to enter in to the living tissue which causes serious damage to health like decrease body growth, harm of nervous system, different organ injure, cancer, as well as death at low concentrations [66–68]. Maximum contaminant level (MCL) for heavy metals established by USEPA are shown in **table-1.1** [66]**.**

Table 1.1 Maximum contaminant level (MCL) established by USEPA

Heavy metals	MCL (mg/L)
Arsenic	0.050
Cadmium	0.01
Chromium	0.05
Copper	0.25
Nickel	0.20
Zinc	0.80
Lead	0.006
Mercury	0.00003

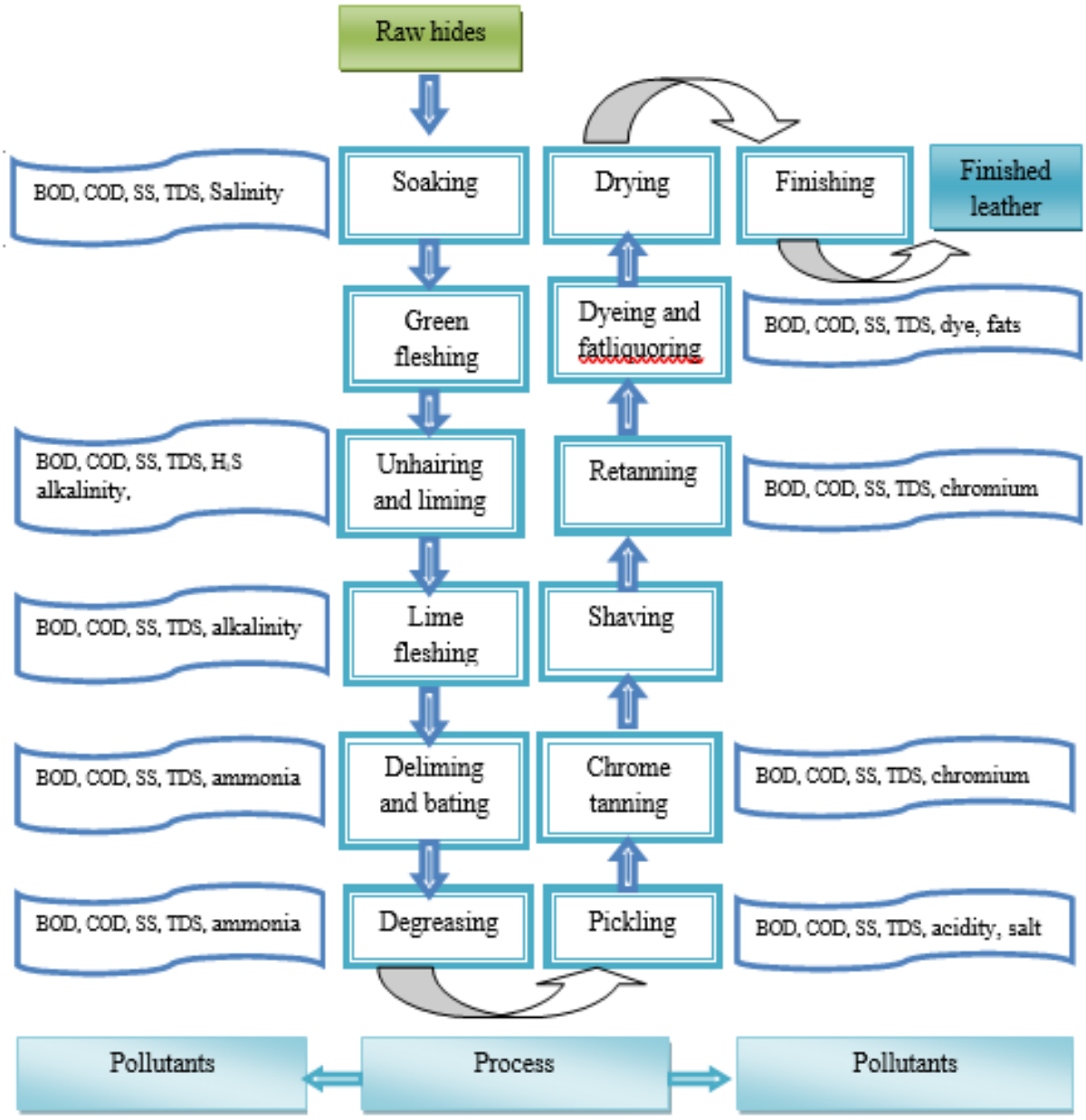

Scheme 1.8 Flow chart of tannery operations and pollutants [16]

1.5.2.2.1. Chromium

Chromium is the first-series transition element of group of VIB of periodic table which symbol is Cr. The name of the element chromium derived from the Greek word chrōma, meaning colour, as many of its compounds brightly coloured. It is silvery-gray, hard, brittle and lustrous metal which takes a high polish, resists tarnishing with melting point at 1907^{o}C, boiling point at 2672^{o}C and density of 7.19 g/cm^{3} at 20^{o}C [69]. Chromium is the 21st most plentiful mineral in the Earth's crust almost 100-140 mg/kg [70,71].

General use of chromium and its salts are in leather tanning, pigment and paint, fungicides,

ceramic and glass industry, photography, catalysts manufacturing, chrome alloy and chromium metal production, chrome plating and in corrosion control. It can subsist in oxidation states of +2 to +6, but the most prevalent forms are 0, +2, +3 and +6 [72]. Three oxidation states are - Cr(0) which occurs as metallic form, Cr(III) as chromic compounds and Cr(VI) as soluble CrO_4^{2-} and $Cr_2O_7^{2-}$ compounds found in nature [73]. Pure Cr metal is extremely prone to combining with oxygen and form a thin defensive oxide surface coat which protects underlying metal from oxidation [71, 74]. The valency state of chromium and its compounds, affects the properties of chromium, which define its toxicity and environmental impact. Only hexavalent chromium compounds are biologically active and known to be skin irritants, mutagenic and carcinogenic, but these hazardous properties do not exist in trivalent compounds or metallic chromium [75–77]. Hexavalent chromium is 1,000 times more hazardous compare to Cr(III), because of its higher water solubility and mobility [78,79]. However, high concentration of chromium (III) ions can affect remarkably on the ecosystem [80–81].

1.5.2.2.1.1. Chromium(III)

Chromium is present in the environment naturally as trivalent chromium. The uses of Cr(III) are - leather tanning, dye manufacturing, wood preserving, making alloys and brick lining for high temperature industrial furnaces. Trace amounts of Cr(III) is required as essential micronutrients to metabolize carbohydrate, proteins and fat properly in mammals and it is a co-factor for insulin action [82,83].

Different nonmetals, such as oxygen, chlorine, fluorine etc. and polyatomic anions like nitrate, sulfate, etc., can be combined with chromium to generate compounds, most of them are intensely colored.

In aqueous systems, Cr(III) can be present as $Cr^{3+,}$ $Cr(OH)^{2+}$, $Cr(OH)_2^{+}$, and $Cr(OH)_4^{-}$. In addition, the precipitated phase $Cr(OH)_3$ predominates between pH 6 and 12 [82]. Cr(III) generally forms soluble Cr^{3+} in the pH range 0 to 8 and in the Eh range from approximately-0.4 to 1.2 V. At pH greater than 4 to 7.5, Cr^{3+} dissolves to form soluble Cr(III) hydroxide cation and at a pH approximately 8.0, insoluble and amorphous $Cr(OH)_3$ forms, on the other hand at extreme reducing conditions, above pH 12.0 and below Eh 0.0, Cr^{3+} forms soluble anions which are shown in the following reactions [84,85]:

$$Cr^{3+} + H_2O \rightleftharpoons CrOH^{2+} + H^+$$

$$CrOH^{2+} + H_2O \rightleftharpoons Cr(OH)_2^{+} + H^+$$

$$Cr(OH)_2^{+} + H_2O \rightleftharpoons Cr(OH)_3 + H^+$$

$$Cr(OH)_3 + H_2O \rightleftharpoons Cr(OH)_4^{-} + H^+$$

Trivalent chromium is mainly originated in the tannery wastewater from the chrome tanning, retanning and dyeing processes in soluble form. After mixing with other tannery wastewater, chromium precipitates mainly as protein-chrome, which generates sludge. If discharged wastewater contains high chrome content then they might remain in the solution.

1.5.2.2.1.2. Chromium(VI)

Cr (VI) species primarily occur under oxidizing (Eh > 0) and alkaline conditions (pH > 6.0). In this condition Cr (VI) usually forms soluble chromate (CrO_4^{2-}), hydrogen chromate ($HCrO_4^-$), or ($Cr_2O_7^{2-}$) anions depending on the concentration and acidity. Above 6.5 pH, CrO_4^{2-} ions is the prevailing species, whereas at pH below 6.5, $HCrO_4^-$ ions dominates at lower concentrations (<0.03 mol/L).

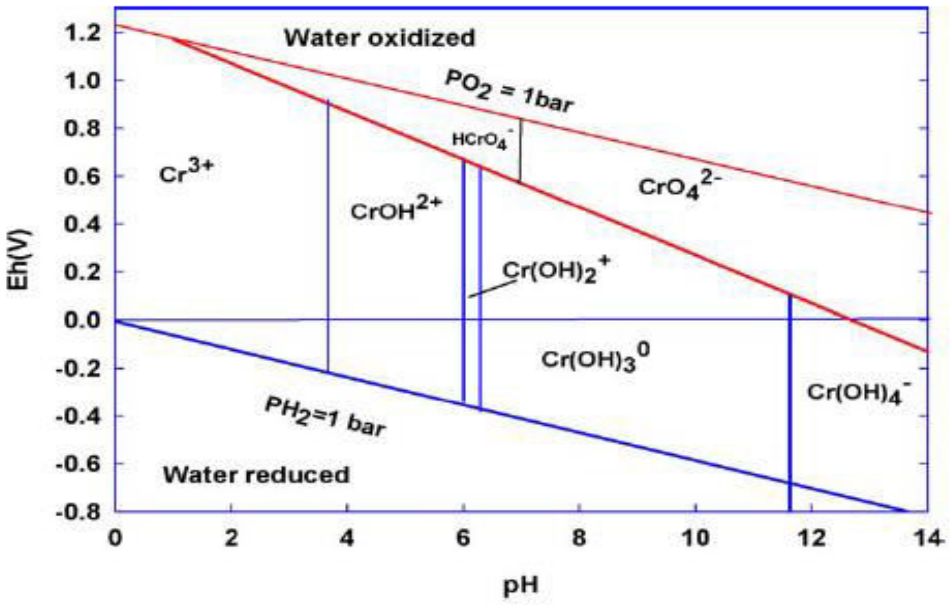

Figure 1.1 Eh-pH illustration of Cr-O-H_2O system [73].

Tannery effluents are likely to contain chromium in this form, and dichromates are toxic to fish life since they promptly penetrate through cell walls.

1.5.2.2.2. Nickel (Ni)

Nickel is a silvery-white, firm, pliable and ductile metal with melting point at 1453^{o}C and density of 8.91 g/cm^{3} at 20^{o}C. The most frequent oxidation state of nickel is +2, that forms compounds among anions like, carbonate, hydroxide, sulphide, sulfate, carboxylates and halides. It is mainly used to form alloys, metal finishing, batteries manufacturing, welding, as a catalyst and in the glass and ceramics industries [86]. Nickel is essential in little amount, however excess intake can lead to serious problems in lungs, kidneys, gastrointestinal distress, pulmonary fibrosis, and skin dermatitis [87].

1.5.2.2.3. Copper (Cu)

Copper is a ductile metal with very high electrical conductivity (59.6 x 10^{6} S/m), melting point at about 1083^{o}C and density of 8.93 g/cm^{3} at 20^{o}C. Other than small amount of metallic copper, copper can form a enormous range of compounds with oxidation states +1 and +2, either binary compounds (oxide, sulphide and halide) or coordination complexes with ligands (oxyanions complexes and organocopper complexes) [88]. Copper is extensively used in industrial processes (leather and textile dyeing, petroleum, paper, copper/brass-plating and rayon manufacturing) and as fungicides [89,90]. As a result copper is massively present in wastewater mainly in soluble form as Cu(II), that can cross the food chain through bioaccumulation It is micronutrient for metabolism of human body but excess dosage may generate stomach and intestinal chaos, anemia, kidney and liver harm, thus carry severe toxicological concerns, even death [91,92].

1.5.2.2.4. Cadmium (Cd)

Cd is soft, ductile, malleable, bluish-white divalent metal with low melting point 321^{o}C and density of 8.65 g/cm^{3} at 20^{o}C. The main oxidation state of cadmium is +2, which occurs as a small component with zinc ores and hence it is a byproduct of zinc production. Cadmium is broadly used in battery production, pigment industry and for corrosion resistant plating. Excess exposure of Cd results in kidney dysfunction, carcinogenic and even causes of death [39, 93].

1.5.2.2.5. Lead (Pb)

Lead is a volatile, soft, supple and silvery metal which melting point is 327^{o}C and density of 11.34 g/cm^{3} at 20^{o}C which is the heaviest non-radioactive element among all of the stable element. Pb occurs in 0 and +2 oxidation states, but more common and reactive form of lead is Pb (II). General use of lead is as pigment, ceramics glazers, building materials, water pipes,

ammunition, paints, acid storage batteries, cosmetics (lipsticks, powder, mascara, etc.). Since, its ample appliance, humans are exposed to lead and have daily ingestion by food, drink and by breathing [94,95].

1.5.2.3. Leather Dyes

The coloured substances which have the affinity to the substrate e.g., leather, textile, papers and other materials are known as dye. The colour of the dye depends on the nature of chromophoric, auxochromic, bathochromic and hypsochromic groups. Some of the most significant chromophoric groups are azo (-N=N-), thio (>C=S), carbonyl (>C=O), nitroso (-N=O), azomethine (-CH=N-) and ethenyl (>C=C<) [96]. Leather dyes can be classified in relation to their chemical properties, extraction sources and usage. On the basis of chemical properties dyes can be –

1.5.2.3.1. Acid dyes– These dyes are metallic salts of organic-coloured acids containing sulfonic, nitro, nitroso, azo, triphenylmethane and carboxyl groups. They are dissolved in both water and alcoholic media and have attraction for amphoteric fibres and used for leather, nylon, paper, wool dyeing etc.

1.5.2.3.2. Basic dyes– these dyes are mainly chlorides or hydrochlorides derivatives (triarylmethane, cyanine, hemicyanine, diazahemicyanine, thiazine, oxazine, acridine) that impart colour to the substrate. These dyes are also water soluble and produce coloured cations in solutions which are mostly used in papers, pharmaceuticals and modified fibres.

1.5.2.3.3. Disperse dyes– These are significantly insoluble nonionic dyes which are being used for synthetic fibres such as nylon, acrylic, cellulose, cellulose acetate, polyester fiber dying.

1.5.2.3.4. Direct dyes– This type of dyes is polyazo compounds which are water soluble anionic dyes and show high affinity for cellulosic fibres in aqueous solution. These dyes are mainly used for dyeing of rayon, leather, paper, nylon etc.

1.5.2.3.5. Reactive dyes– These dyes impart brighter colour and usually used in cotton and other cellulosic fibers dyeing along with nylon and wool.

1.5.2.3.6. Solvent dyes– These dyes are normally nonpolar and hence insoluble in water, however soluble in solvent and are applied for plastics, lubricants, petrol, oils along with waxes.

1.5.2.3.7. Sulphur dyes– The dyestuffs of this group contain sulphur and dissolve in the

presence sodium sulphide and alkali and possess good washing fastness. In leather industry these dyes are mainly used in chamois leather dyeing which can be washed with soap and alkali.

There are 100,000 different dyes are commercially produced and 1.6 million tons of dyes are used in every year, among them 70% are azo dyes which is complex and harmful to the environment and mutagen [20, 97]. Leather and textile industry are two veteran consumers of dyes. Recently a major source of chromium and colour discharge into the surface water due to the incomplete exhaustion of chrome tanning, retanning agents and dyestuffs and is urgently needed to reduce the amount of chromium, residual dyes along with other pollutants.

1.5.3. Remediation techniques for pollution abatement of tannery effluents

At the earlier stages of modern industrialization, wastewater treatment started through some physical treatment like sedimentation, equalization to retain pH, reduction of TDS and TSS. Due to emergent situation various treatment processes has been incorporated to control the pollution level of industrial effluents.

Numerous researches have been investigated by many researchers on the treatment of tannery effluents for the remedy of high chromium and dye concentration. Sedimentation, chemical precipitation and electro-precipitation method, flocculation-coagulation, membrane filtration, oxidation, ion exchange process, liquid-liquid extraction, phytoremediation, infiltration percolation, and photocatalysis are some of the most popular techniques to remove chromium and dye from wastewater. The familiar methodologies used for the treatment of wastewater are discussed briefly-

1.5.3.1. Sedimentation: Sedimentation is a basic primary method for the abatement of pollution from wastewater. In this process suspended particles are separated from effluents by gravity settling. The wastewater remain with less velocity, hence particle in suspension stay stable in inert conditions and settle down by gravitational force [98,99].

1.5.3.2. Chemical Precipitation: Owing to the ease and cost effectiveness, chemical precipitation is recognized as one of the established technologies to remove toxic metals and pollutants from wastewater. The tiny suspended particles in the solution are made larger by the precipitating agent mainly hydroxide precipitant so that they can settle insoluble precipitates which are then removed from the solution by filtering or other suitable techniques [100–102]. The mechanism of chemical precipitation is shown by the following reaction-

$$M^{2+} + 2(OH)^{-} \Leftrightarrow M(OH)_2 \downarrow \quad (2.1)$$

where, M^{2+} and OH^- are the metal ions and the precipitants, respectively, and $M(OH)_2$ is the metal hydroxide.

1.5.3.3. Coagulation and flocculation: Coagulation and flocculation is very effective physicochemical method to remove heavy metal [103]. In this technique very small particles and colloids agglomerate into bigger particles, which help to reduces turbidity, natural organic matters, and other pollutants from wastewater [104]. Initially colloids are destabilized by neutralizing the forces and remain separated in coagulation, whereas, flocculation is the agglomeration of destabilized particles [102]. Coagulants such as, aluminium sulfate, ferric sulfate, polyaluminum chloride, polymeric ferric sulfate, and polyacrylamide are mostly used [105–106]. The major deficiency is the concentrated sludge that produced in massive [107] and may not so useful to azo, acid and basic dyes [108].

1.5.3.4. Membrane filtration: Since membrane filtration can remove suspended solid, organic and inorganic pollutants like heavy metals, it has drawn a significant consideration for inorganic effluents. Various forms of membrane filtration, including microfiltration (MF), ultrafiltration (UF), nanofiltration (NF), and reverse osmosis (RO), can be used to take out toxic metals and pollutants from industrial effluents according to the dimension of the particle that can be retained. The pore size of MF membrane cover a range of 0.05 to 10µm and 0.1 to 2 bar pressure whereas UF membrane pore size is 1 to 100 nm and operative pressure is 1 to 5 bar [109–111]. RO membranes are less porous 0.001 to 0.003 micron and operate with 10 to 20 bar pressure and NF filtration (pore size about to 0.0005 micron) can remove most of the inorganic and organic pollutants from wastewater [112–116].

1.5.3.5. Electrodialysis (ED): ED is another membrane process, where an electric field is used as driving force to separate the metal ions across charged membranes from one solution to other, where the anion migrate toward the anode and the cation toward the cathode, passage the anion-exchange and cation-exchanged membrane [66].

1.5.3.6. Oxidation: Oxidizing agents viz. chlorine, hydrogen peroxide, fenton's reagents, ozone is widely applied for the treatment of primarily treated wastewater. Oxidation is more popular method for the removal of pollutants as it needs very less quantity of oxidants and short reaction time. Chlorine is used as calcium hypochlorite and sodium hypochlorite for oxidation of dyes. Different dyes as for example acid, direct, reactive and metal complex dyes are readily decolorized by this process, however pH and catalyst have a crucial role in

this process. Dyes containing amino or substituted amino groups on a naphthalene ring are mainly prone to chlorine and decolorized more simply compare to other dyes [117]. Various metals for instance Fe, Cu, Ni and Cr are generated during decomposition of metal complex dye, which act as a catalyst and enhance decolourization process. Hydrogen peroxide (H_2O_2) has strong oxidizing and bleaching properties and applied for making peroxidase enzymes, that are used to remove dyes from wastewater. Moreover, ozonation is done by ozone produced from oxygen and showed very fruitful result to remove organic and inorganic pollutants [118].

Fenton's reagent is a mixture of hydrogen peroxide and an iron catalyst, which has more oxidizing power compare to hydrogen peroxide. It shows very attractive results to remove pollutants from industrial effluents. The process is too much pH dependent, which generate huge sludge also take longer time [119,120].

1.5.3.7. Ion exchange: Ion-exchange process is based on reversible substitution of ions from liquid to a solid matrix [113], and liberate new ions of a separate category but with same charge. The method is physical separation processes in which an insoluble matter (resin) takes ions from an electrolytic solution and releases chemically equivalent other ions without undergoing any chemical change [121]. Natural zeolites and silicate minerals are extensively used to reduce metal ions from effluents as because of easy availability and low cost. Moreover, synthetic resins are frequently used as they can almost entirely remove metal ions from solutions like high acidic resin with $-SO_3H$ groups and mild acid resin with –COOH groups [122]. Moreover, a starch-based polymer was develop to remove various dye from wastewater [123].

1.5.3.8. Biological treatment: Biological treatment is widely used removal technique applied for metal ion removal and decolouration of wastewater [124] as the process are cost effective and produce non-toxic end products. The process could be aerobic (in existence of O_2), anaerobic (in absence of O_2) or could be in combination of both. Microorganism such as, bacteria, fungi and yeast are commonly practiced to treat wastewater. Metal bearing bacteria like, *Bacillus cereus* [125] *Pseudomonas aeruginosa* [126] *Escherichia coli* [127] have possessed very remarkable biosorption performance to metal ions.

1.5.3.9. Adsorption: Adsorption is an effective purification and separation technique used for the reduction of pollution of industrial effluents [128]. The attachment of particles to the surface is known as adsorption. During adsorption various ions, atoms or molecules transfer from liquid to solid phase [129].

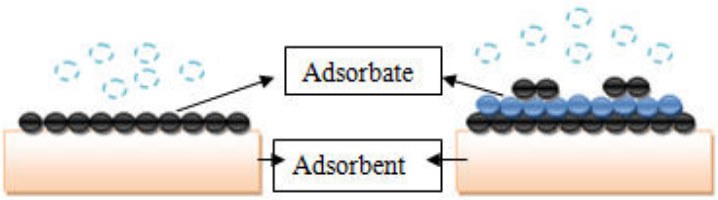

Figure 1.2 Monolayer and Multilayer Adsorption Process.

The substance that adsorbs is the adsorbate; the material on which adsorbate attach is adsorbent and desorption is the reverse process of adsorption [130]. The adsorption of pollutants on solids is because of increased free surface energy of the solids due to huge surface area [131]. Adsorption can be classified into the following categories on the bond formation and nature of chemical species that are getting interacted-

a) Physiosorption: Molecules adheres to the adsorbent surface through intermolecular attraction by Vander Walls or hydrogen bonds, is known as physical adsorption or physiosorption. Since, the bond nature is weak it could be easily reversible [132].

b) Chemisorption: In chemisorption, the molecules stick to the surface by forming a chemical bond generally by a covalent bond and coordination. The enthalpy of chemisorption is much higher than that of physiosorption and is complicated to separate chemisorbed species from the solid surface.

Adsorption is considered the most convenient, effective and economical technique for toxic substance removal from industrial wastewater. A brief explanation of different adsorbents, prepared from graphene and graphene-based materials, low-cost materials such as agricultural wastes, industrial by-products, natural mineral matters, and activated carbon, have been prepared and used to mitigate metal ions and coloring materials from effluents are presented below-

1.5.3.9.1. Graphene and graphene-based adsorbents

In recent year's graphene and graphene-based adsorbents have gained a lot of attention to remove heavy metals and dye from industrial effluents. Carbon atoms are organized in a hexagonal layer arranged one by one to form graphite and the Van der Waals force acts to bond two layers together [78]. This special form of carbon is known as graphite which is an allotropic form of carbon. When a single hexagonal layer is separated from graphite, then graphene is produced. Graphene oxide, a functionalized version of graphene, can be synthesized from graphite. Due to huge surface area, graphene-based materials are

recognized as adsorbents to eradicate toxic metals and dye from wastewater. Many researchers used different graphene-based materials, to reduce heavy metals and dye, some of them are described below-

Table 1.2 Adsorption capacity of heavy metal removal by graphene-based adsorbents

Name of the adsorbents	**Metal ions**	**Adsorption capacity (mg/g)**	**Ref.**
Graphene oxide polyamidoamine dendrimers (GO/PAMAMs)	Pb(II)	568.18	[133]
	Cd(II)	253.81	
	Cu(II)	68.68	
	Mn(II)	18.29	
Graphene oxide (GO)	Cu(II)	277.77	[134]
Functionalized Graphene oxide (GO-COOH)	Cu(II)	357.14	
Graphene oxide (GO)	Co(II)	21.28	[135]
Graphene oxide (GO)	Cr(VI)	1.222	[78]
Magnetic chitosan and graphene oxide-ionic liquid (MCGO-IL)	Cr(VI)	143.45	[136]
Chemically reduces graphene (CRG)	Cd(II)	6.32	[137]
Annealing reduces graphene (ARG)		0.499	
Graphene oxide (GO)		35.7	
Graphene oxide (GO) membranes	Cu(II)	72.6	[138]
	Cd(II)	83.8	
	Ni(II)	62.3	
Fe_3O_4/GO/Cu-ZEA	As (III)	50.51	[139]
Sodium Alginate/ Graphene oxide (SA/GO)	Mn(II)	18.11	[140]
$MnFe_2O_4$@TiO_2-rGO	Cu(II)	118.45	[141]
Graphene oxide (GO) aerogel	Cu(II)	29.59	[142]

Table 1.3 Adsorption capacity of dye removal by graphene-based adsorbents

Name of the adsorbents	**Dyes**	**Adsorption capacity (mg/g)**	**Ref.**
(ARGO)/Fe_3O_4 composite	Rhodamine 6G (Organic dye)	93.37	[143]
Graphene oxide (GO)	Basic Red 46	360.0	[144]
Thermally reduced graphene (TRG)	Methyl orange (MO)	89.3	[145]
Green reduces Graphene oxide (RGO)	Methylene Blue	276.06	[146]
Magnetic graphene oxide (MGO)	Methylene Blue (MB)	64.23	[147]
	Orange G (OG)	20.85	
G@SiO_2-AR	Methylene Blue	272.47	[148]
Graphene oxide (GO)	Methylene Blue	71.43	[149]
Fe_3O_4/chitosan/graphene	Methylene Blue	49.14	[150]
Fe_3O_4@GO@SA	Methylene Blue	317.0	[151]

1.5.3.9.2. Activated carbon (AC)

Activated carbons are the most common and commercial adsorbents applied for the abatement of hazardous materials from effluents because of its richness in micropores (< 2 nm) and mesopores (2-50nm) with high surface area and surface reactivity [152,153]. Development of activated carbons is possible by using any carbon containing-organic matters such as coconut shell, coconut fiber, saw dust, rice husk, banana peel, orange peel, palm fruits for metal ions sorption [154,155]. Numerous studies were reported in literature to remove metal ions and dyes by means of activated carbon prepared from various sources

R.V. Hemavathy et al [156] showed the Cu(II) ions adsorption through *Cassia fistula* seed biochar. HCl treated *Cassia fistula* biochar (HTCF), physically treated *Cassia fistula* biochar (PTCF) and H_2SO_4 treated *Cassia fistula* biochar (STCF) was applied to remove Cu^{2+} ions from aqueous solution. The effect of a variety of factors viz. pH, dose, temperature, time and concentration were investigated. It was observed from the data of Cu^{2+} ion adsorption

isotherm process followed Freundlich isotherm model. The maximum adsorption capacity of HTCF, PTCF and STCF were achieved 72.9, 115.4, and 303.5 mg/g respectively.

Table 1.4 Adsorption capacity of metal removal by activated carbon-based adsorbents

Metal	Activated carbon/ Bio-char	q_m (mg/g)	Parameters Studied	Equilibrium Isotherm	Ref.
Cr(III)	Peanut straw char	0.48	pH, Time, metal ion concentration	Langmuir, Freundlich	[157]
	Soyabean straw char	0.33			
	Canola straw char	0.28			
	Rice straw char	0.27			
Cr(VI)	Coffiee husk activated carbon	98.19%	pH, stirring speed, adsorbent dosage, metal ion concentration	Langmuir, Freundlich	[158]
Cr(VI)	Fruit peel of leechi activated carbon	50	Temperature, initial Cr(VI) concentration, time , pH	Langmuir, Freundlich, D-R	[159]
Cu(II)	*Ficus natalensis* fruits(FNF) activated carbon	161.29	pH, contact time, temperature, dosage, metal ion concentration	Langmuir, Freundlich	[160]
Pb(II)		1250			
Cr(VI)	Fleshed tannery waste activated carbon (FTWAC)	99%	pH, adsorbent dosage, contact time, and metal ion concentration	Langmuir, Freundlich	[161]
Co(II)	Activated carbon of waste potato peel	373-480	pH, contact time, metal ion concentration and temperature	Langmuir, Freundlich	[162]
Cr (total)	Biochar tea waste	68.2%	pH, adsorbent dosage, time, and metal ion concentration	-	[163]
Cr(III)	Activated carbon	40.29	temperature, particle size,	Freundlich,	[164]

	fabric cloth (ACF)		pH, and adsorbent dosage	Langmuir	
Cu(II)	Olive stones activated carbon	17.66	pH, and contact time,	Langmuir, Freundlich, R-P, Sips	[165]
Cd(II)		57.09			
Pb(II)		147.52			
Cd(II)	*Glebionis coronaria L. a*ctivated carbon	57.87	-	-	[166]
Co(II)		45.75			
Cd(II)	*Diplotaxis harra* biomass activated carbon	31.6	-	-	[167]
Co(II)		25.9			
Co(II)	Activated carbon of olive stones with oxygen containing functional group	16.20	-	Langmuir, Freundlich, R-P	[168]
Ni(II)		20.48			
Cu(II)		34.16			
Cd(II)	African palm fruit activated carbon	99.23%	Contact time, and temperature	-	[169]
Cu(II)		96.71%			
Ni(II)		95.34%			
Pb(II)		99.51%			
Pb(II)	Tire-derived activated carbon	322.5	pH, Contact time, and temperature	Langmuir, Freundlich, D-R, Temkin	[170]
Cu(II)		185.2			
Zn(II)		71.9			
Cr(VI)	Activated carbon from date seeds	44.05	pH, time, concentration, dosage, and temperature	Langmuir, Freundlich	[171]
Cr(VI)	Activated carbon from polysulfide rubber	8.92	pH, Contact time, adsorbent dosage	Langmuir	[172]

Table 1.5 Adsorption capacity of dye removal by activated carbon-based adsorbents

Dye	Activated carbon (AC)	q_m (mg/g)	Parameters Studied	Equilibrium Isotherm	Ref.
Congo Red	Date pits (modified with nitric acid)	105	pH, time, concentrations,	Langmuir, Freundlich, R-P	[153]
Mordant Black-11	Fleshed tannery waste activated carbon (FTWAC)	-	pH, adsorbent dosage, contact time, and dye concentration	Langmuir, Freundlich	[161]
Red azo dye		-			
Methylene Blue	Potato plant wastes AC	41.6-52.6	pH, adsorbent dosage, time, concentration and temperature	Langmuir, Freundlich	[173]
Malacite green		27-33.3			
DB38	Peanut shell microwave pyrolysis	110.6	pH, time,	Langmuir, Freundlich, R-P	[174]
RR141		284.5			
AR 97	Commercial AC	52.08	Dye concentration, time	Langmuir, Freundlich	[175]
AO 61		169.49			
ABr. 425		222.22			
Methylene Blue	El-Maghara mine coal nano- AC	29.50	-	Langmuir, Freundlich	[176]
Methylene Blue	Coconut shell AC nanofibers	166.7	Initial dye concentration	Langmuir,	[177]
Basic Blue 41	Filamentous algae AC	125	pH, time, initial dye concentration,	Langmuir, Freundlich	[178]
Remazol	Pomegranate	370.86	pH, time, initial	Langmuir,	[179]

Bbrilloiant Blue reactive dye	peel AC		dye concentration, and temperature	Freundlich, D-R, Temkin, Sips,	
Methylene Blue	Black olive stone AC	714	pH, initial dye concentration, and temperature	Langmuir, Freundlich	[180]
	Green olive stone AC	769			
Direct Blue 106	Pomegranate peel AC	54.05	pH, adsorbent dosages, initial dye concentration, and temperature	Langmuir, Freundlich, Temkin, D-R, Harkins-Jura	[181]
Direct Blue 78	AC	76.92	Adsorbent dosages, dye concentration, and salt effect	Langmuir, Freundlich, Temkin	[182]
Direct Red 31		111			
Direct Blue 2B	Mahgony sawdust AC	518	pH, time, dye concentration	Langmuir, Freundlich	[183]
Direct Green B		327.9			
Orange G dye	*Thespesia populnea* pods AC	9.129	Agitation, time, dye concentration, dosage	Langmuir, Freundlich	[184]

1.5.3.9.3. Low-cost adsorbents (LCAs)

These adsorbents are readily available in the form of industrial, agricultural, biological and residential waste or by-products, usable after renewal, effective over a wide range of pH, eco-friendly and inexpensive [185–187]. Several studies for the development, utilization, application of LCAs is adopted by many researchers and reported in literature to reduce pollutants from industrial wastewater. Some of the LCAs used in this purpose are discussed below-

X. Huang and co-workers [188] reported that NaOH modified fly ash (NaOH-FA) has good potential to reduce Pb^{2+} and Cd^{2+} from contaminated water. The authors observed that pseudo-second-order and Langmuir isotherm model were well fitted to explore adsorption processes, with maximum uptake capacity 126.55 and 56.31 mg/g for Pb^{2+} and Cd^{2+} in single arrangement at 298 K respectively. It was also observed that, when NaCl concentrations increased from 0 to 0.5 M in single and binary heavy metals, adsorption efficiency of adsorbent for Cd^{2+} decreased from 45.52 mg/g to 21.04 mg/g and 37.86 mg/g to 2.15 mg/g respectively. However, there was no significant change in the adsorption capacity for Pb(II) ether in single or binary solutions.

J. Antti Sirvio and M. Visanko [189] used lignin-rich wood nanofibers, sulfated wood nanofibers (SWNFs), sulfated sawdust nanofibers (SSDNFs) and sulfated cellulose nanofibres (SCNFs) to remove Pb^{2+} and Cu^{2+}. This study reported the effect of pH (3-5), heavy metal content (0.24-7.61 mmol/L) and adsorption time (0.5-24h). Adsorption capacity of SWNFs and SSDNFs were higher than SCNFs for both metals.

Ibrahim Hegazy and co-researchers [190] utilized olive pomace (OP) and seed husk of moringa (MSH) to remove Fe^{2+} and Mn^{2+} from solution. Batch adsorption studies were studied with the variation of adsorbent dosage, pH, time, and concentration. The pseudo-second-order kinetic model was obeyed by the adsorption kinetics of Fe^{2+} and Mn^{2+} and the Langmuir model was better fitted for both adsorbent. The adsorption capacity of OP for Fe^{2+} and Mn^{2+} was 10.406 and 10.460 mg/g and MSH was 10.28 and 11.641 mg/g for Fe^{2+} and Mn^{2+} correspondingly.

R.J. Nathan et al. [191] prepared biosorbent beads from banana, orange and potato peels (BP, OP and PP) and applied for the mitigation of metals from a cocktail mixture containing As^{5+}, Cd^{2+}, Cr^{6+}, Cu^{+2}, Hg^{2+}, Pb^{2+} and Ni^{+2} ions. This study investigated the impact of pH in the range (6.5-8.5) and results showed a noteworthy increase in the sorption capacity of the beads in case of As^{5+}, and Pb^{2+} adsorption, while it decreases significantly for Cd^{2+}, Cr^{6+}, Cu^{+2}, Hg^{2+}, and Ni^{+2} ions at higher pH >7. The adsorption capacity of BP beads was found effective for the concurrent removal of heavy metals from drinking water.

Banana, cucumber and potato peels (BP, CP and PP), respectively have been utilized as adsorbents to remove cationic (MB) and anionic (OG) dyes from wastewater by A. Stavrinou and co-investigator [192]. The biosorbents were characterized by ATR-FTIR, BET analysis, SEM, and XRD to realize adsorption mechanism. The authors observed that the biosorption of MB on BP and PP followed the Langmuir isotherm, but biosorption on CP obeyed the

Freundlich isotherm at low concentration and Langmuir model was followed at higher concentration. However, the biosorption of OG on BP, PP and CP was well fitted with the Langmuir model. The maximum adsorption capacity for MB was observed to be 211.9, 107.2 and 179.9 mg/g for BP, PP and CP at pH 6 and similarly for OG was experimented to 20.9, 23.6 and 40.5 mg/g at pH 2.

M. Rafatullah et al. [193] explored meranti sawdust to remove Cu^{2+}, Cr^{3+}, Ni^{2+} and Pb^{2+} ions from aqueous solutions. Surface morphology was investigated and characterized the adsorbent by SEM, BET surface area and average pore diameter, and FTIR. The effect of different factors - contact duration, concentration of metal ions, adsorbent dosage and temperature were performed. Maximum monolayer adsorption was observed 32.051, 37.878, 35.971 and 34.246 mg/g respectively.

G.F. Colho and co-workers [194] used chemically modified cashew nut shell (*Anacardium occidentale*) (CNS) to reduce Cd(II), Pb(II) and Cr(III) from solution. The adsorbent was characterized by FTIR, SEM, point of zero charge (PZC), thermo gravimetrical (TG) and porosimetry (BET) analysis. The adsorption kinetics was justified through pseudo-first-order, pseudo-second-order, Elovoch and intraparticle diffusion, however adsorption isotherm was linearized by Langmuir, Freundlich and Dubinin-Radushkevich. This study showed the impact of metal ions concentration, temperature, and desorption on removal efficiency. Maximum adsorption capacity was reported 47.505 mg/g by NaOH treated CNS for Cd(II), 27.129 mg/g by natural CNS for Pb(II), and 42.68 mg/g by NaOH treated CNS for Cr(III) adsorption.

K. Keya et al.[195] reported wheat bran (WB) and modified wheat bran (M-WB) to remove Cr^{6+} from aqueous solution. The study investigated the consequence of initial concentration of metal ions, contact time, and pH. The equilibrium data was very well explained by Freundlich model. The utmost adsorption capacities of WB and M-WB were 4.53 and 5.28 mg/g at pH 2 and 2.2 respectively.

S. Bamukyaye and W. Wanasolo [196] used egg shell and fish-scale to separate Cr^{6+} from tannery effluents. The consequences of adsorbent particle size, dosage, pH, contact duration, and metal concentration on Cr^{6+} removal were investigated. The maximum adsorption efficiency of egg shell and fish-scale for the separation of Cr^{6+} were 10.30 and 27.27 mg/g at pH 2 respectively.

H. Rezaei [197] explored *Spirulina sp.* for the biosorption of Cr^{6+} from aqueous solution. The author found that adsorption ability was increased with higher metal ion concentration. The impact of agitation duration, metal concentration, temperature, pH, and biomass dosage were investigated. The highest adsorption capacity of *Spirulina sp.* for Cr^{6+} was 90.91 mg/g at pH 5.

S, Gupta and B.V. Babu [198] applied sawdust as adsorbent to lessen Cr^{6+} from aqueous solution. The author utilized fresh sawdust to investigate the effect of metal concentration, pH, dosage, and contact duration and the maximum adsorption capability was obtained 41.5 mg/g at pH 1.

N. Itankar and Y. patil [199] utilized low cost bio-mass (modified sawdust) to remove Cr^{6+} from industrial wastewater. The outcome of the variation of adsorbent dosage, metal ions concentration and pH were investigated and the maximum adsorption efficiency was found to be 15.42 mg/g.

B. Nasernejad et al. [200] used carrot residue (CR) to the biosorption of Cr^{3+} Cu^{2+} and Zn^{2+} from industrial effluents. The adsorption isotherm was evaluated by Freundlich and Langmuir isotherm model. The highest adsorption capacity was acquired to be 45.09, 32.74 and 29.61 mg/g for Cr^{3+} Cu^{2+} and Zn^{2+} removal by CR.

E. Guechi and O. Hamdaoui [201] utilized potato peel to investigate Cu^{2+} removal capability from synthetic aqueous solution under different condition namely adsorbent dosage (0.25-1.5), pH (2-5), shaking rate (0-800 rpm), temperature (25-55^{o}C), ionic strength (0.25-5g/400ml), particle size (0.16-1.5mm), and Cu^{2+} concentration (25-300 mg/L). Adsorption isotherm was evaluated by Langmuir, Freundlich, Temkin and Elovich model and data was better fitted with both Langmuir and Freundlich model with a highest adsorption capability 84.74 mg/g at 25^{o}C.

R.A.K. Rao and F. Rehman [202] was conducted the experiment for adsorption of Cr^{6+} using fruits of Gulur (*Ficus glomerata*) from synthetic wastewater. Various effect of Cr^{6+} adsorption such as temperature, pH, initial Cr^{6+} concentration and duration were investigated. Moreover, surface morphology and active functional group was also studied by SEM and FTIR respectively. Adsorption equilibrium data was well fitted with Langmuir isotherm at 50^{o}C and exhaustive capacities were gained 5 and 23.1 mg/g respectively. Adsorption capacity of Cr^{6+}, Cr^{3+} by various adsorbents are shown in table 2.6, table 2.7 respectively, and adsorptive capacity of dye from various literatures is given in table 2.8.

Table 1.6 Aptitude of Cr^{6+} removal by various adsorbents

Title of the adsorbent	**pH**	**Adsorption capability (mg/g)**	**References**
Clarified sludge	3.0	26.31	[203]
Rice husk ash		25.64	
Activated alumina		25.57	
Fuller's earth		23.58	
Fly ash		23.86	
saw dust		20.70	
Neem bark		19.60	
Treated waste newspaper (TWNP)	3.0	59.88	[204]
Acrylonitrile grafted banana peels	3.0	6.17	[205]
Melaleuca diosmifolia leaf	2.0-10.0	62.50	[206]
Fertilizer industry waste	2.0	15.24	[207]
Alligator weed	1.0	88.11	[208]
Amine-fucntionalized modified rice straw	2.0	15.82	[209]
Raw dolomite	2.0	10.01	[210]
Modified coconut shells	2.0	~26	[211]
Mixed waste tea	2.0	94.34	[212]
Coffee ground		87.72	
Natural cactus (NC)	1.0-2.0	21.19	[213]
Dried cactus (DC)		2.63	
Palm oil fuel ash (POFA)	2.0	0.464	[214]
Wastw pomance of olive oil factory	2.0	18.69	[215]
Moringa stenopetala seed powder (MSSP)	2.0	9.709	[216]
Banana peel powder (BPP)	4.0	7.353	

Pistachio hull	2.0	116.3	[217]

Table 1.7 Adsorption ability of Cr^{3+} removal through different adsorbents

Name of the adsorbent	**pH**	**Capacity (mgg^{-1})**	**References**
Potato peel	4.0	38.46	[218]
Illitic clay	4.1	46.44	[219]
Vineyard pruning waste	4.2	12.453	[220]
Green mussel-lignin magnetic nanoparticles	5.0	44.56	[221]
Spirulina platensis biomass	6.0	30.7	[222]
Egg shell	5.0	200.25	[223]
Powdered marble		434.82	
Chitosan flakes	3.8	138.04	[224]
Padina gymnospora residue	6.2	31.52	[225]
Coconut shell fibre activated carbon	5.0	16.10	[164]
Fabric cloth activated carbon		40.29	
Passion-fruit shell biomass	3.0	27.93	[226]
Garden grass	~ 4.0	19.4	[227]
Cashew nutshell	3.5	13.93	[228]
Dry cow dung powder	3.0	19.31	[229]
Sugarcane pulp residue	5.0	15.85	[230]
Sugarcane biochar		3.43	
Glutaraldehyde treated *Cassia fistula*	5.0	95.41	[231]
Benzene treated *Cassia fistula*		85.71	
Marble waste powder	6.0	148.03	[232]
Sugar industrial waste	5.0	41.20	[233]

Yellow passion-fruit shell	5.0	85.1	[234]
Jackfruit peel modified by EDTA	4.0-5.0	41.67	[235]
Cellulose-g-poly(acrulamide-co-sulfonic acid) polymeric bio-adsorbent	6.0	274.69	[236]
Soybean meal waste	5.0	29.48	[237]
Eucalyptus bark	3.0	0.0262	[238]
EDTA modified attapulgite	3.0	131.37	[239]
Sewage sludge compost biomass	7.0	34.60	[240]
Fish scale waste	5.0	18.34	[241]

Table 1.8 Adsorption capacity of dye removal by various adsorbents

Title of the adsorbent	**Dye**	**pH**	**Capacity (mg/g)**	**References**
Potato peel waste biomass	Acid Blue113	2.0	11.71	[242]
	Acid black1	3.0	1.79	
Potato peel waste	Methylene blue	8.0	33.55	[243]
Chromium tanned leather waste	Acid red 357	3.0	148.2	[244]
HCHO treated potato peel (PP)	Methylene blue	8.0	47.62	[245]
H_2SO_4 treated potato peel (APP)	Methylene blue	12.0	41.60	
HCHO treated neem bark (NB)	Methylene blue	4.0	90.91	
H_2SO_4 treated neem bark (ANB)	Methylene blue	2.0	1,000.0	
Psyllium seed powder	Reactive orange 16	4.0	206.6	[246]
Walnut shell powder	Methylene blue	8.0	36.63	[247]
Giant reed	Reactive blue	3.0	3.94	[2]
	Reactive black	4.0	2.816	

Banana peels (BP)	Methylene blue	6.0	211.9	[192]
Cucumber peels (CP)			107.2	
Potato peels (PP)			179.9	
Banana peels (BP)	Orange G	2.0	20.9	
Cucumber peels (CP)			23.6	
Potato peels (PP)			40.5	
Corn stover hydrochar	Rhodamine B	~ 4.0	23.6 - 30.7	[248]
Date seeds	Methyl violet dye	6.5	59.5	[249]
Coconut coir dust	Methylene blue	6.0	29.50	[250]
Hazelnut shell	Crystal violet	10.0	181.82	[251]
Ageratum conyzoides leaf powder	Methylene blue	4.0	192.4	[252]
Modified rice bran	Reactive blue 4	6.1	185.19	[253]
Walnut shell	Malachite green	5.0	90.8	[254]
Jackfruit peel	Methylene blue	6.5	285.71	[255]
Rejected tea	Methylene blue	4.0- 8.0	156.0	[256]
Garlic peel	Direct Red 12B	2.0	37.96	[257]
Corn stalk	Direct Red 23	3.0	51.87	[258]
Wood apple shell	Methylene blue	2-10.0	95.2	[259]
	Crystal violet		129.87	
Magnetite/coir pith supported alginate beads	Malachite green	7.0	1.66	[260]

Chapter 2

Materials and Methods

2.1. Study area

In Bangladesh, about 156 tanneries are situated in the Tannery Industrial Estate, Dhaka (TIED), Hemayetpur, Savar on the bank of river Dhaleshwari. One tannery established at Jessore and one at Khulna on the bank of the river Bhairab, and two tanneries are at Chottogram near the river Karnaphuli. The other two tanneries are situated at Shafipur, Gazipur and Dhaka Export Processing Zone (DEPZ) and both of them have their own effluent treatment plant (ETP). Before shifting to TIED during 2017, all tanneries were there at Hazaribagh, Dhaka very near to the Buriganga river. In this study, water samples had been collected from Dhaleshwari, Buriganga, Bhairab, and Karnaphuli river to assess the pollution level of surface water.

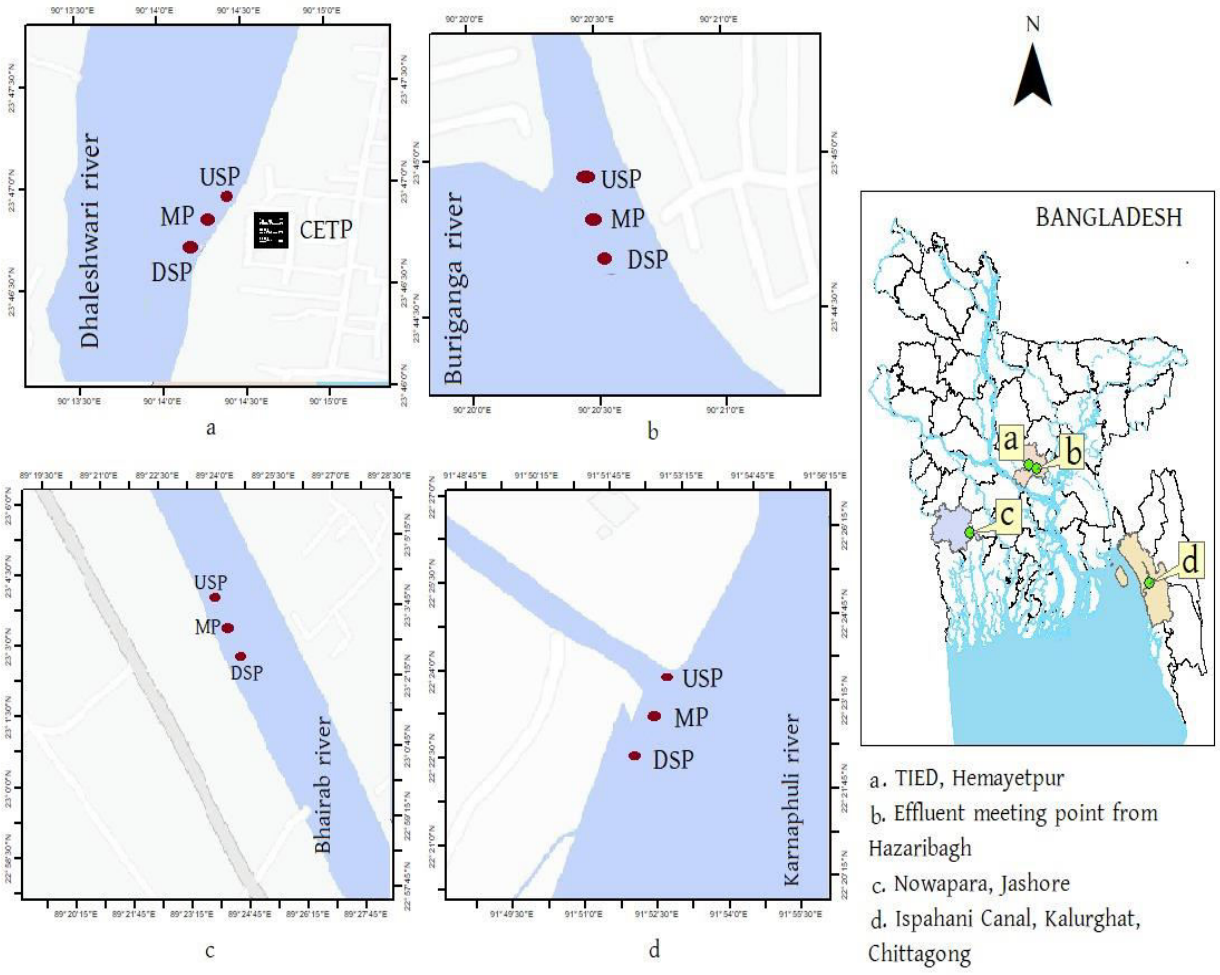

Figure 2.1 Location of a) Dhaleshwari b) Buriganga c) Bhairab and d) Karnaphuli river

According to Bangladesh Tanners Association (BTA), out of 156 tanneries at TIED around 130 tanneries were functional and produced wet blue, crust and finished leather. They discharged nearly 40,000 cubic meters of effluent per day against which the CETP had a

treatment capacity of only about 25,000 cubic meters. The tanneries at Chottogram and Khulna were also discharged effluents (treated and or untreated) to their nearby river, which tremendously polluted the surface water [13]. According to the local residents, Dhaleshwari river water had started to deteriorate after shifting of the tanneries at TIED. Besides tanneries a huge quantity of effluents from other miscellaneous industries also discharged to the river. During the sample collection there was moderate stream in the rivers.

Figure 2.2 Images of sample collecting area of Dhaleshwari river besides the TIED

2.2. Collection of river water samples

A total of 36 water samples were collected from three points, i.e., meeting point of discharged effluents from CETP to the river, 200 meter upstream and 200 meters downstream

of the meeting point of the river Dhaleshwari, Buriganga, Bhairab and Karnaphuli. Water sample had been collected in three layers from every point, i.e., surface, 50 cm deep and 100 cm deep from the surface. The samples are named as USP_S = Upstream point at surface, USP_{50} = Upstream point at 50 cm deep, USP_{100} = Upstream point at 100 cm deep, MP_S= Main discharge point at surface, MP_{50} = Main discharge point at 50 cm deep, MP_{100} = Main discharge point at 100 cm deep, DSP_S = Downstream point at surface, DSP_{50} = Downstream point at 50 cm deep, DSP_{100} = Downstream point at 100 cm deep. Water samples were collected during October-November 2020 and kept in non-transparent plastic bottles. Collected samples were carried to the laboratory with proper care and preserved in a refrigerator to prevent microbial decay of organic and inorganic materials. To assess the surface water pollution few important physicochemical parameters such as pH, Temperature, TDS, EC, NaCl content, BOD_5, COD along with heavy metal concentration, i.e., Cr, Ni, Cu, Cd, Pb, etc. were measured.

2.3. Collection of tannery effluent samples

In this study, chrome tanning, dyeing and tannery effluents were collected from a tannery at TIED, Hemayetpur, Savar Bangladesh. The effluents were collected during July 2021 and kept in non-transparent plastic bottles [2 liters capacity] and were brought to the laboratory with proper care.

2.4. Physico-chemical characteristics of river water, tanning and tannery effluents

In this study, pH was measured by HANNA Instrument (model-HI 98107) and mercury digital thermometer was used to assess the temperature. TDS, EC, and % NaCl of samples were investigated by HANNA Instrument (model- HI 2300) and BOD was assessed with HANNA Instrument (model-HI 98193). Moreover, official standard method (DIN 38409) was followed to determine the COD of the samples.

2.5. Heavy metals analysis of river water, tanning and tannery effluents

Heavy metals (Cr, Ni, Cu, Cd and Pb) of river water samples, tanning and tannery wastewater were measured by Inductively Coupled Plasma-Mass-Spectrometry, (ICP-MS–7900), Agilent Technologies International Japan Ltd. model no. - G8403A, through acid digestion.

2.6. Multivariate statistical analysis

In order to find out the correlation among the pollution parameters of studied water samples from four rivers of Bangladesh, Pearson correlation test were accomplished by using OriginPro software (OriginLab Corp., USA) version 2018 [261]. Multivariate statistical

analysis like Principal Component Analysis (PCA) [262] and Hierarchical Cluster Analysis (HCA) [263] were tested using same software.

2.7. Materials

Chromium (III) sulfate [$Cr_2(SO_4)_3.6H_2O$] as the source of Cr^{3+} was procured from Qualikems Fine Chem., India. Sulfuric acid (98%) and NaOH were bought from Merck, Germany. Commercial leather dye C.I. Acid Red 73 (AR73) was collected from a local tannery of TIED, Savar, Dhaka, Bangladesh. Peanut shells and bagasse were collected from the local market at Hazaribagh, and potato peel was arranged as kitchen waste from Dhaka, Bangladesh.

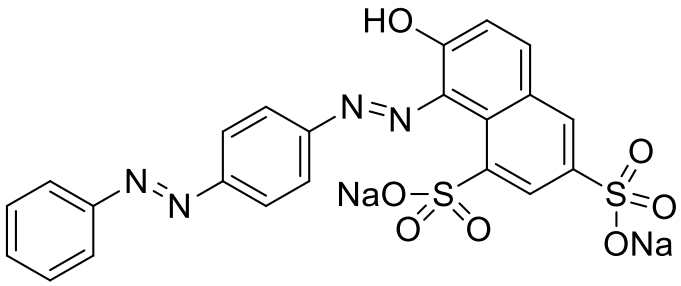

Figure 2.3 Molecular structure of C.I. Acid Red 73

Molecular formula of C.I. Acid Red 73 is $C_{22}H_{14}N_4Na_2O_7S_2$ and molecular weight is 556.490.

2.8. Development of adsorbents

2.8.1. Preparation of pyrolyzed and chemically activated nut shell (PNS)

Dried peanut shell was pyrolyzed at high temperature and chemically activated with NaOH. Finally, they were baked in an oven.

2.8.2. Preparation of chemically activated nut shell (NS)

Peanut shell was chemically activated with NaOH and baked in oven.

2.8.3. Preparation of pyrolyzed and chemically activated bagasse (PB)

Dried bagasse was pyrolyzed at high temperature and chemically activated with NaOH, followed by baking in oven.

2.8.4. Preparation of potato peel powder (PP)

Collected potato peel was washed, dried and grinded.

2.9. Characterization of PNS, NS, PB and PP

Fourier Transformed Infrared (FT-IR) Spectrophotometer (8400S Shimadzu, Japan) was utilized to study the chemical structure of PNS, NS, PB, and PP. The morphology and surface structure of PNS, NS, PB and PP were studied with Scanning Electron Microscope, SEM (JSM-6490LA, JEOL, USA) The Brunauer-Emmett-Teller (BET) surface area, pore volume, and pore size distribution of PNS, NS, PB and PP were analyzed with BET sorptometer (model no. BET-201-A, PMI, USA). X-ray diffraction of PNS, NS, PB and PP were performed on Multipurpose X-ray diffraction system (Ultima IV) with Cu Kα radiation (λ=0.154 nm, 40 kV, 1.64 mA) in the range 05-100^{o} to signify the crystallinity of the adsorbents. Zeta potential values of PNS, NS, PB and PP at a range of pH were assessed by Malvern Zetasizer Nano-ZS analyzer.

2.10. Adsorption study

By dissolving a specific amount of $Cr_2(SO_4)_3.6H_2O$ in deionized water, a stock-solution was prepared and the required solutions were then arranged by dilution with deionized water. Initial concentration of [$Cr_2(SO_4)_3.6H_2O$] solutions (32.06, 69.19, 135.43, 187.57, 271.74, 301.26, 363.47 mg/L) were determined by ICPMS and developed the calibration curve with UV-Visible Spectroscopy at 421 nm wavelength [264–266]. The amount of Cr^{3+} before and after adsorption for adsorbents (PNS, NS, PB and PP) from $Cr_2(SO_4)_3.6H_2O$ solutions were determined with UV-Visible Spectroscopy by the following calibration curve-

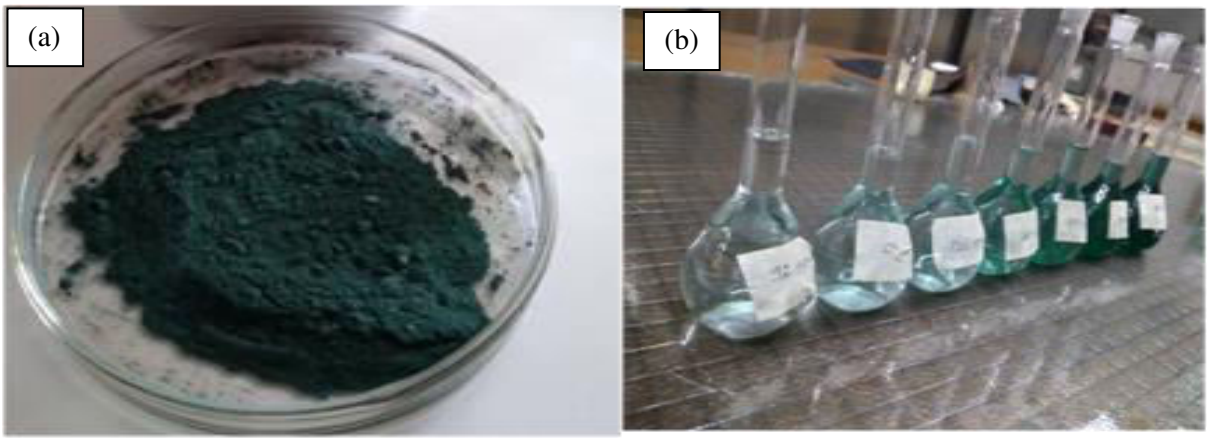

Figure 2.4 (a) $Cr_2(SO_4)_3.6H_2O$ powder (b) $Cr_2(SO_4)_3.6H_2O$ solution at different concentration

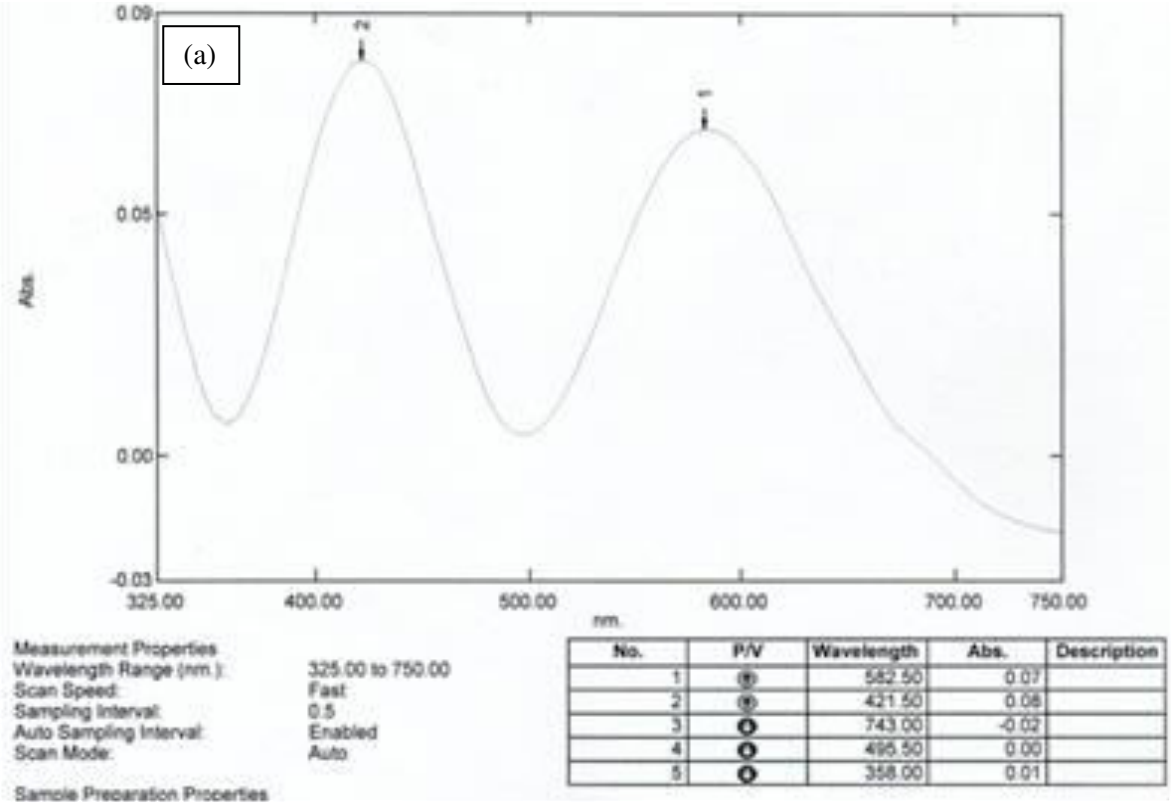

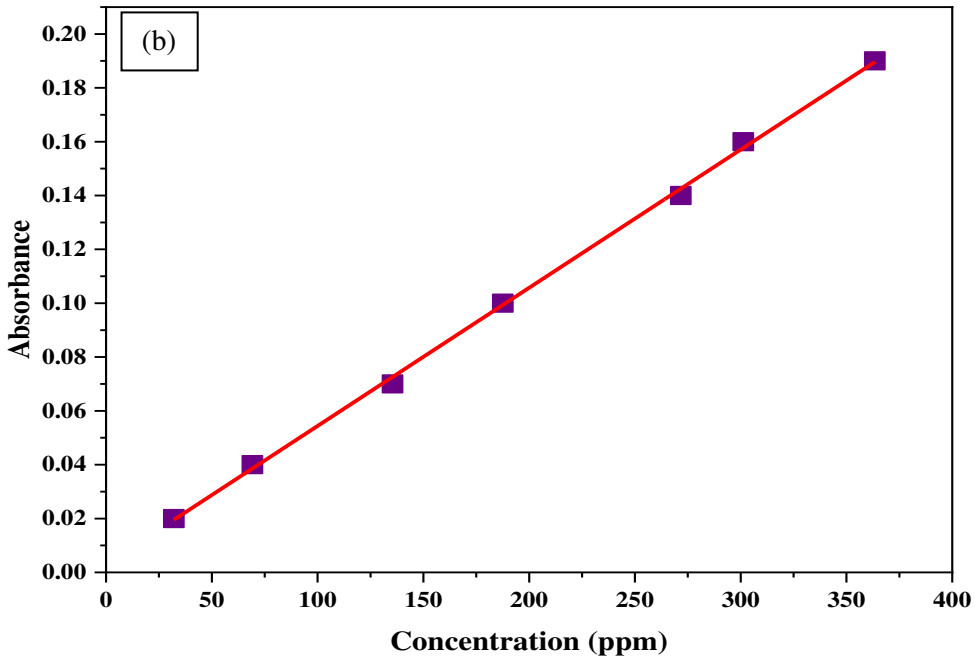

Figure 2.5 (a) UV-Vis spectra of $Cr_2(SO_4)_3.6H_2O$ solution and (b) Calibration Curve at 421 nm Wavelength

In this study batch experiments were carried out using a series of conical flasks in an orbital shaker with 25 mL of [$Cr_2(SO_4)_3.6H_2O$] and C.I. Acid Red 73 solution and fixed adsorbent doses were added to the solutions respectively. Experiments were conducted at different pH, adsorbent dosage, contact duration, initial Cr(III) and dye concentration, and temperature for

Cr^{3+} and dye adsorption respectively. Every batch experiment was run at a constant speed of shaker (160 rpm). The samples were filtered with Whattman filter paper and the concentration of filtrate was examined by UV-Visible spectroscopy. After optimization with batch experiment, the real samples (chrome tanning and tannery effluent) were analyzed with developed adsorbent (PNS, NS and PB) to remove Cr^{3+} and dyeing effluents were studied with PP to lessen leather dye. To compute adsorption capacity following equation was used-

$$q = \frac{(C_0 - C_f) \times V}{w} \tag{2.1}$$

where, q = adsorption capacity

C_0= initial concentration of Cr(III) or dye (ppm)

C_f= final concentration of Cr(III) or dye (ppm)

V= volume (L) of the $Cr_2(SO_4)_3$ or dye solution and

W = mass (g) of the adsorbent.

The equilibrium adsorption capacity q_e (mg/g) was deliberated by the following equation-

$$q_e = \frac{(C_0 - C_e) \times V}{w} \tag{2.2}$$

where, C_e= concentration of Cr^{3+} or dye (ppm) at equilibrium and % of removal was calculated with the following equation-

$$\%\ of\ removal = \frac{(C_0 - C_t) \times 100}{C_0} \tag{2.3}$$

C_t = concentration of Cr(III) or dye (ppm) at time, t

In this work, effect of pH on adsorption capacity was determined and was plotted against to pH. Adsorption capacity was found maximum at pH 5 for $Cr_2(SO_4)_3.6H_2O$ solutions. In case of anionic leather dye maximum adsorption capability was obtained at lower pH.

To find out the optimum dosage of adsorbent, the adsorption capacity and % of Cr(III) removal were plotted against adsorbents dosage. The point at which the adsorption capacity and % of removal intersects each other were considered as optimum dosage for Cr(III) removal and similarly optimum dosage for dye removal was also determined.

By using Langmuir model, theoretical utmost adsorption capacity q_m(mg/g) were calculated. For these, the adsorption capacities at different concentration were plotted against different period of time. When time increases, the adsorption capacity for a given concentration

increases with it, and after a while, it becomes nearly constant and is considered as equilibrium adsorption capacity (q_e). The concentrations at which the adsorption capacities became constant were considered as equilibrium concentration (C_e).

In order to realize the distribution of adsorbate on the adsorbent surface at equilibrium, experimental data was analyzed through Langmuir and Freundlich isotherm models [267, 268]. The theoretical highest adsorption capacity q_m(mg/g) was calculated by plotting C_e/q_e against C_e according to Langmuir model [198, 269]. The linear form of the Langmuir isotherm is stated as-

$$\frac{C_e}{q_e} = \frac{1}{q_m b} + \frac{1}{q_m} C_e \qquad (2.4)$$

where, C_e= concentration at equilibrium

q_e = adsorption capacity at equilibrium

q_m = maximum adsorption capacity and

b= Langmuir constant (L/mg)

Separation factor R_L is connected to Langmuir constant b, which represents the dimensionless equilibrium parameters and is calculated by using equation (5). $R_L > 1$ indicates unfavorable monolayer adsorption while $0 < R_L < 1$ indicates a favorable monolayer adsorption process [270]

$$R_L = \frac{1}{1 + C_m b} \qquad (2.5)$$

C_m= maximum initial adsorbate concentration.

Freundlich isotherm assumes multilayer adsorption with heterogeneous distribution [268, 271,272]. This isotherm relates the uptake capacity with equilibrium concentration commonly used isotherm for including adsorbents. This equation is outlined below-

$$lnq_e = lnk_F + \frac{1}{n} lnC_e \qquad (2.6)$$

where, k_F (L/g) and n are the Freundlich constants, k_F suggests multilayer adsorption capacity of adsorbent associated to bonding energy and 1/n represents adsorption intensity heterogeneity of the adsorbent sites [273]. The q_e is the adsorption capability and C_e is the adsorbate concentration in solution at equilibrium. k_F and n are designed from the graph lnq_e vs lnC_e where, n gives an assumption favorability of adsorption. Since n declines, adsorption

become more complicated (n=2-10 indicate good adsorption, n=1-2 difficult and n<1 indicate poor adsorption) [274].

Adsorption kinetics is noteworthy to evaluate the rate and performance of the adsorption process. In the present study, two kinetics models were utilized to describe adsorption processes. In 1998, Lagergren presented Pseudo-First-Order rate equation and in 1995 Ho and Mckay presented Pseudo-Second-Order equation to describe the kinetic process [190]. The linear appearance of Pseudo-First-Order rate equation is-

$$log(q_e - q_t) = logq_e - \frac{k_1}{2.303}t \quad (2.7)$$

here, q_e = equilibrium adsorption capacity

q_t = adsorption capacity at time, t

k_1= rate constant of pseudo-first-order kinetics (L/min)

Pseudo-first-order model was gained by plotting $\log(q_e-q_t)$ versus t, where a linear involvement between $\log(q_e-q_t)$ and t was observed.

The linear shape of Pseudo-Second-Order rate equation is-

$$\frac{t}{q_t} = \frac{1}{k_2 {q_e}^2} + \frac{1}{q_e}t \quad (2.8)$$

where, k_2= rate constant of Pseudo-Second-Order adsorption (g/mg min).

Pseudo-second-order model was attained via plotting t/q_t against time, t.

The change in Gibbs free energy (ΔG) indicates the assumption about adsorption process. Since, ΔG raises with increased temperature indicate physical adsorption and the process is favorable at low temperature [275]. In this research the changes in Gibbs free energy for adsorption on adsorbents at various temperature were calculated by equation [276] -

$$\Delta G = RTlnk_d \quad (2.9)$$

where, k_d is the distribution constant for the equilibrium sorption, R is the universal gas constant (8.314J $mol^{-1}K^{-1}$) and T is the absolute temperature (K). k_d was deliberated by using equation-

$$k_d = \frac{q_e}{C_e} \quad (2.10)$$

The average standard enthalpy changes ΔH and entropy change ΔS for the adsorption was designed by van't Hoff equation-

$$lnk_d = \frac{-\Delta H}{RT} + \frac{\Delta S}{R} \qquad (2.11)$$

lnk_d versus1/T was plotted to calculate ΔH and ΔS.

Regeneration capabilities of adsorbents provide constructive information about adsorption mechanism and commercial application of an adsorbent. So, in this work, regeneration was carried out for all the used adsorbents to remove chromium and dye.

To analyze the competence of all adsorbents with real sample (chrome tanning, dyeing and tannery effluents), the experiment was carried out by diluting the effluent samples, which is shown by **Figure 2.6.**

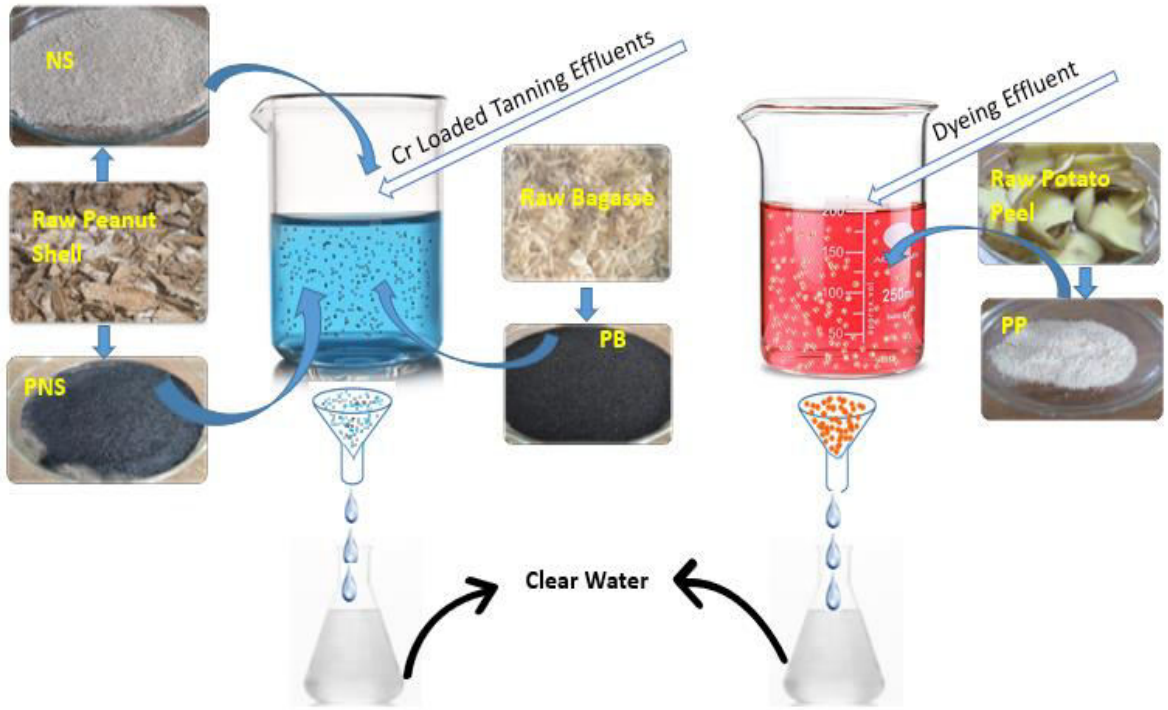

Figure 2.6 Schematic set up of an adsorption process

3.11. Safety precautions

As this research deals with water pollution in tannery effluents, Chromium and dye removal some precautionary measures were taken while performing the procedure. Proper PPE and protection were taken while handling the samples. All process was carried out in a hygienic and safe manner.

Chapter 3

Results and Discussion

3.1. Part 1: Assessment of Surface Water Pollution

Analysis of different physico-chemical characteristics including pH, temperature, TDS, EC, NaCl %, BOD, and COD along with heavy metals of the surface water samples collected from three layers at three locations of Dhaleshwari, Buriganga, Bhairab, and Karnaphuli river have been studied and their results are given below.

3.1.1. pH

The pH of the river water samples was shown in the **Table 3.1** and it ranged from 7.15 to 7.46 which indicated that Dhaleshwari, Buriganga, Bhairab, and Karnaphuli river water was near to neutral. According to DoE, and ECR (1997) the standard pH value of river water was 6.5-9.2, and 6.5-8.5 respectively [62-63]. The highest pH was 7.46 in the surface of Karnaphuli river at upstream point (USP_S) and the lowest was 7.15 in the surface of Buriganga at downstream point (DSP_S). The results showed (**Table 3.1, Figure 3.1**) that the pH of all samples was within the acceptable limit.

Table 3.1 pH of Dhaleshwari, Buriganga, Bhairab, and Karnaphuli river water samples

Sample	Dhaleshwari	Buriganga	Bhairab	Karnaphuli
USP_S	7.25	7.32	7.35	7.45
USP_{50}	7.23	7.28	7.33	7.29
USP_{100}	7.32	7.3	7.36	7.34
MP_S	7.4	7.35	7.41	7.42
MP_{50}	7.39	7.41	7.34	7.28
MP_{100}	7.37	7.38	7.29	7.39
DSP_S	7.38	7.15	7.36	7.41
DSP_{50}	7.39	7.3	7.37	7.37
DSP_{100}	7.36	7.19	7.27	7.39

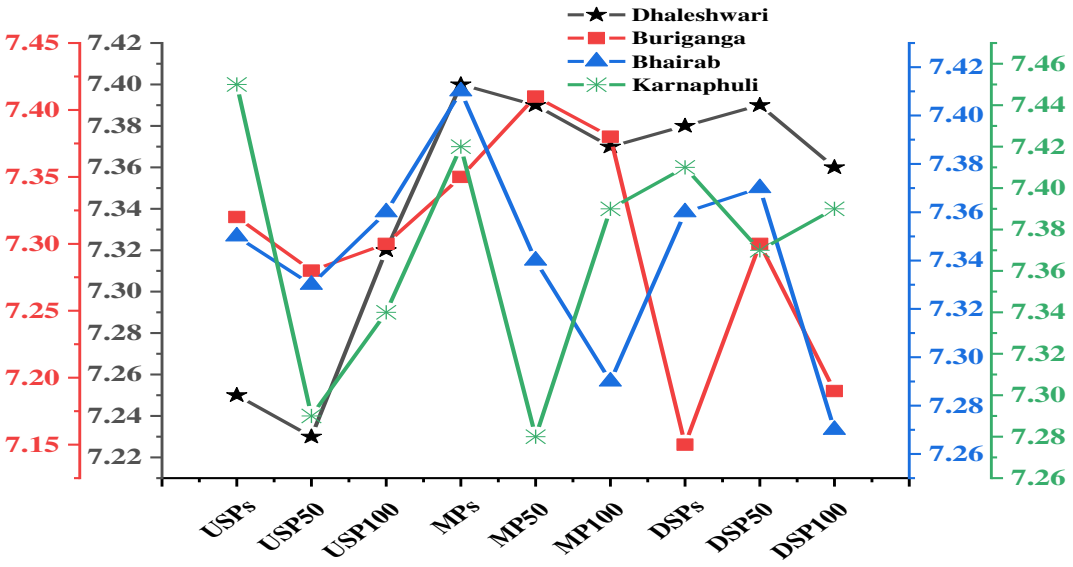

Figure 3.1 pH of Dhaleshwari, Buriganga, Bhairab and Karnaphuli river water samples

3.1.2. Temperature

The temperature was measured at the site using digital thermometer and it was recorded 26.8 - 28.1°C, 26.9 - 28.2°C, 24.9 - 26.6°C and 23.7 - 25.2°C in the samples of different layer of Dhaleshwari, Buriganga, Bhairab, and Karnaphuli river respectively. The DoE standard to uphold the aquatic life is within 20°C -30°C [62]. It was being observed from the **Table 3.2, Figure 3.2** that the temperature of all samples were within the DoE limit.

Table 3.2 Temperature (°C) of Dhaleshwari, Buriganga, Bhairab, and Karnaphuli river water

Sample	Dhaleshwari	Buriganga	Bhairab	Karnaphuli
USP_S	27.4	27.4	26.6	25.1
USP_{50}	27.8	27.9	25.4	24.8
USP_{100}	27.3	27.4	24.9	25
MP_S	28.1	27.7	26.3	25.2
MP_{50}	27.3	27.3	25.1	24.6
MP_{100}	26.8	27.6	25	23.7
DSP_S	27.3	28.2	25.6	25.1
DSP_{50}	27.3	26.9	26.2	24.7
DSP_{100}	26.9	27.4	24.9	23.8

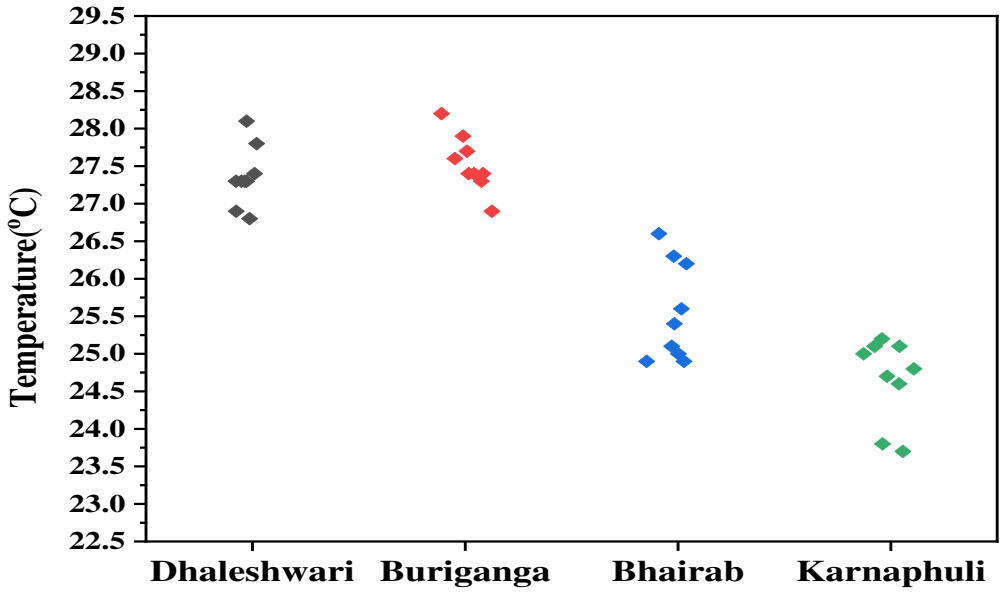

Figure 3.2 Temperature (°C) of Dhaleshwari, Buriganga, Bhairab, and Karnaphuli river water

3.1.3. Total Dissolved Solids (TDS)

TDS refer to the quantity of organic and inorganic matters that have been dissolved in the liquid. A higher TDS value than the recommended limit is a sign of water contamination [277] .The DoE standard limit for TDS is 2100 mg/L.

Table 3.3 TDS (mg/L) value of Dhaleshwari, Buriganga, Bhairab and Karnaphuli river water samples

Sample	Dhaleshwari	Buriganga	Bhairab	Karnaphuli
USP_S	127	145.4	868	2246
USP_{50}	125	141.8	850	2335
USP_{100}	128	146.1	964	1765
MP_S	957	188.35	1327	3560
MP_{50}	601	144.9	1416	3468
MP_{100}	134	145.6	1392	3390
DSP_S	167	174.5	1407	2249
DSP_{50}	165	197	1390	2295
DSP_{100}	166	197.73	1399	2147

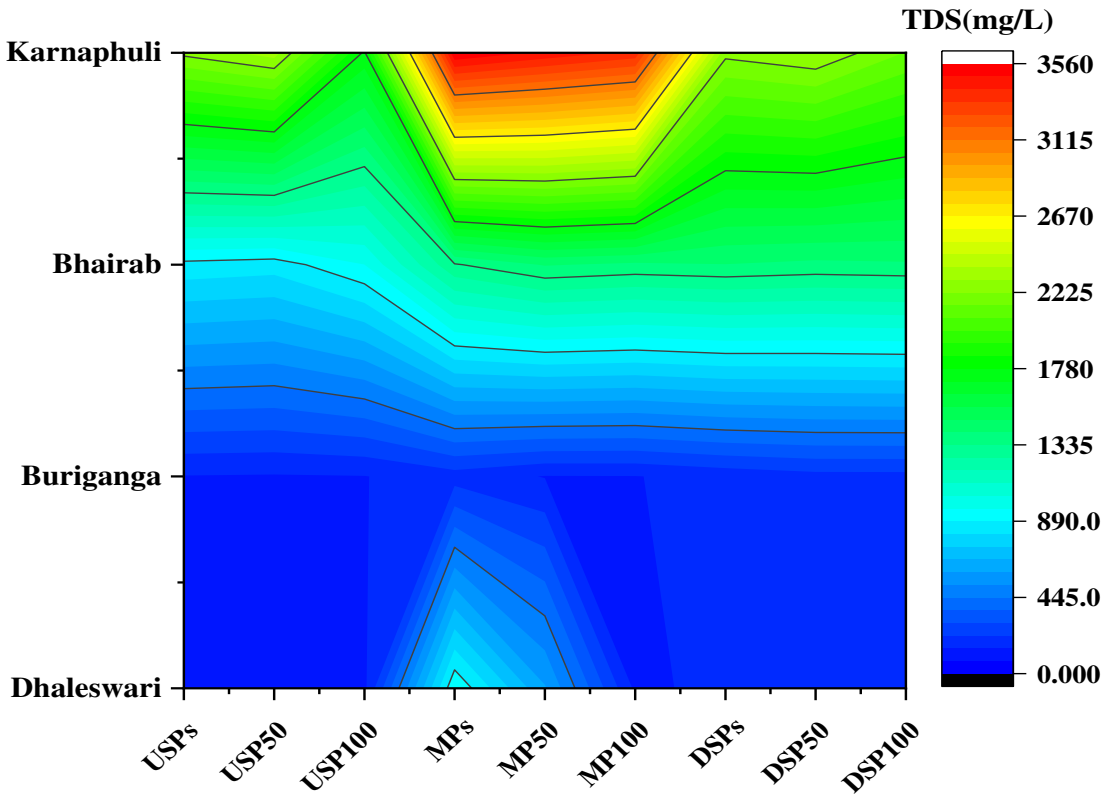

Figure 3.3 TDS value of Dhaleshwari, Buriganga, Bhairab and Karnaphuli river water samples

The results demonstrates that the TDS values of the samples from the river Dhaleshwari, Buriganga, Bhairab are within the limit whereas Karnaphuli river water samples have crossed the limit except the sample of USP_{100} (**Table 3.3, Figure 3.3**) which has good agreement with previous report [6], [61], [278].

3.1.4. Electrical Conductivity (EC)

EC measures how well a liquid carry electric current through it. When water is subjected to metal ion contamination the level of EC is increased. The DoE standard for EC is 1200 µS/cm [62]. The experimental data revealed (**Table 3.4, Figure 3.4**) that all samples of three sites of Bhairab and Karnaphuli crossed the allowable limit, indicating the poor condition of the river water which has good agreement with previous research [1] . Moreover, EC of all samples of Dhaleshwari and Buriganga river water were within the limit except MP_S of Dhaleshwari river which contained the highest EC value 1916 µS/cm and indicated that more metal ions are present in this layer. This might be due to the tannery wastewater which immediately mixed up with the water flow and getting diluted.

Table 3.4 EC (µS/cm) of Dhaleshwari, Buriganga, Bhairab and Karnaphuli river water sample

Sample	Dhaleshwari	Buriganga	Bhairab	Karnaphuli
USP_S	254	291.2	1717	1618
USP_{50}	249	283.8	1702	1682
USP_{100}	258	292.7	1929	1950
MP_S	1916	384.4	2627	4235
MP_{50}	734	290	2919	4130
MP_{100}	268	290	2856	3861
DSP_S	330	348	2810	2832
DSP_{50}	324	394	2792	2536
DSP_{100}	329	394	2763	2388
STD	1200	1200	1200	1200

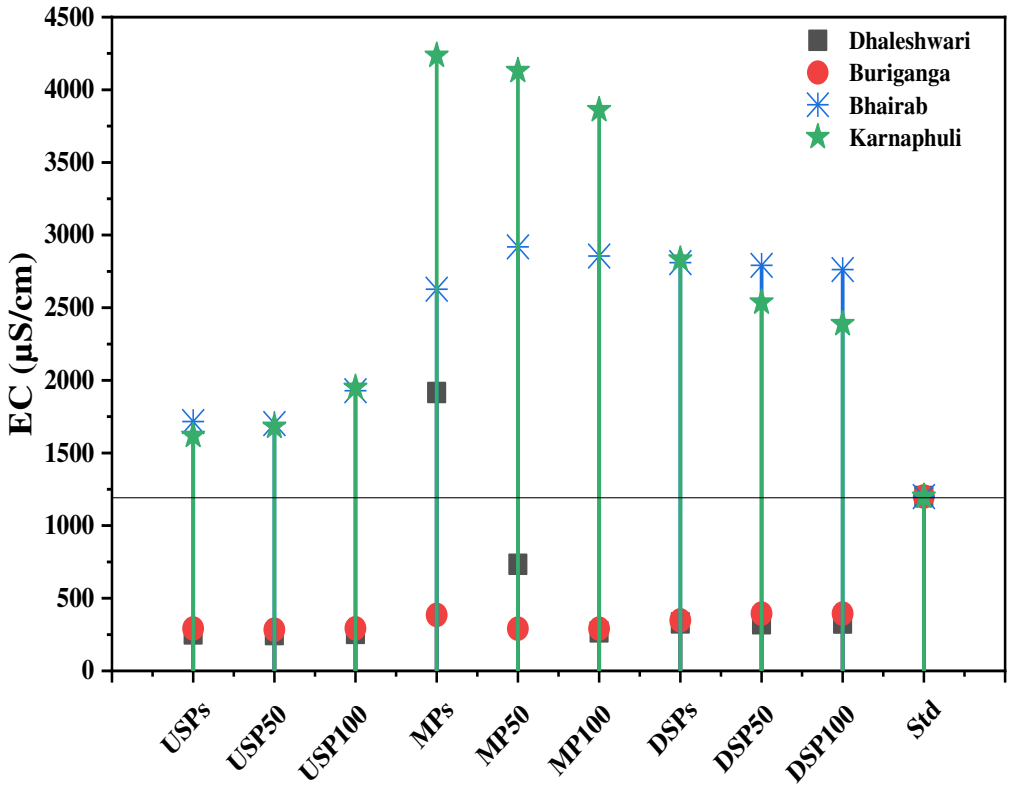

Figure 3.4 EC (µS/cm) of Dhaleshwari, Buriganga, Bhairab and Karnaphuli river water

3.1.5. NaCl %

Salinity refers to dissolved salt content in a water body. Freshwater salinity is usually less than 0.05% whereas, the average salinity of sea water is 3.5%, though it varies 3.2 to 3.7% due to rainfall, evaporation, river runoff and ice formation [278,279].

Table 3.5 NaCl% of Dhaleshwari, Buriganga, Bhairab and Karnaphuli river water samples

Sample	Dhaleshwari	Buriganga	Bhairab	Karnaphuli
USP_S	0.5	0.6	3.2	3.1
USP_{50}	0.5	0.6	3.1	3.8
USP_{100}	0.4	0.6	3.6	4.4
MP_S	3.7	0.7	4.8	7.3
MP_{50}	2.4	0.6	5.4	6.8
MP_{100}	0.5	0.6	5.1	6.7
DSP_S	0.7	0.7	5.2	6.8
DSP_{50}	0.6	0.8	5.1	5.8
DSP_{100}	0.7	0.8	5.4	5.3

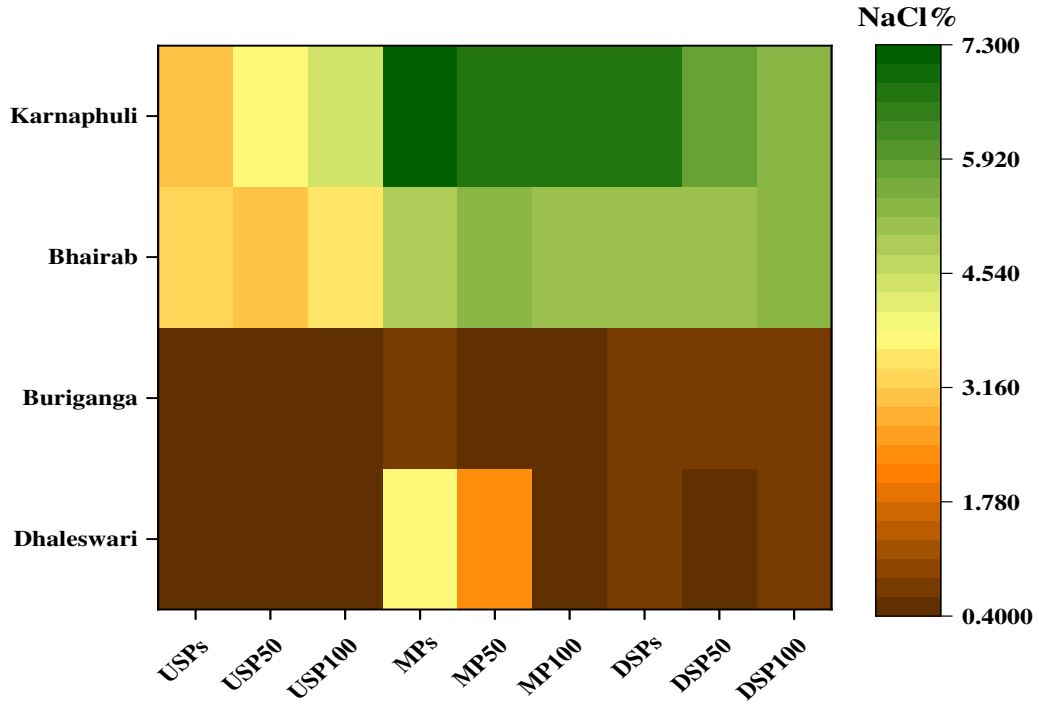

Figure 3.5 NaCl % of Dhaleshwari, Buriganga, Bhairab and Karnaphuli river water samples

Salinity between 0.1% - 2.5% is known as brackish water; Estuaries where fresh river water reach salty ocean water is instance of brackish water [281]. It is observed from the result (**Table 3.5, Figure 3.5**) that the salinity of Dhaleshwari river water was less compare to other three rivers, but the lower value of NaCl % was 0.4% and the highest value was 3.7% at main discharge point (surface), which was far ahead than fresh water salinity. It could be due to the mixing of different salts from leather processing industries along with other industries.

3.1.6. Biochemical oxygen demand (BOD_5)

BOD_5 is the measurement of the amount of dissolved oxygen consumed by microorganisms break down the organic matter in the effluent over a 05-day period at 20^{o}C. DoE, Bangladesh standard for BOD_5 is 50-250 mg/L [62]. The result showed (**Table 3.6, Figure 3.6**) that the range of BOD_5 value was 147-353 mg/L, 65-241 mg/L, 209-274 mg/L and 253-366 mg/L in Dhaleshwari, Buriganga, Bhairab and Karnaphuli river water respectively. BOD_5 value of Buriganga river water samples were within the DoE limit but Karnaphuli river water cross the limit. Whereas few sample of Dhaleshwari (USP_S, MP_S, DSP_{100}) and Bhairab (USP_{50}, $USP_{100,}$ MP_S, MP_{50}, $MP_{100,}$ DSP_{100}) having BOD_5 value within the standard limit.

Table 3.6 BOD_5 of Dhaleshwari, Buriganga, Bhairab and Karnaphuli river water samples

Sample	Dhaleshwari	Buriganga	Bhairab	Karnaphuli
USP_S	226	241	255	271
USP_{50}	258	76	248	253
USP_{100}	353	197	247	268
MP_S	192	224	209	326
MP_{50}	258	227	235	309
MP_{100}	262	186	247	284
DSP_S	319	90	253	366
DSP_{50}	348	78	274	357
DSP_{100}	147	65	244	317

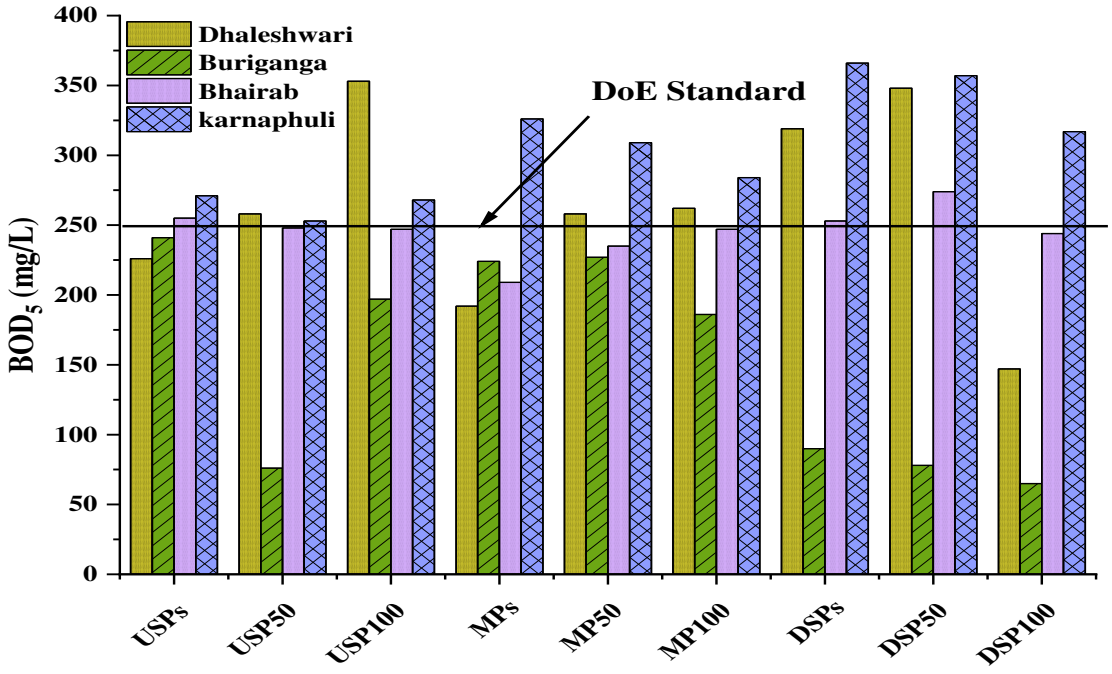

Figure 3.6 BOD_5 of Dhaleshwari, Buriganga, Bhairab and Karnaphuli river water samples

3.1.7. Chemical oxygen demand (COD)

COD is an indicator of water quality, which measures the quantity of oxygen essential to oxidize all organic and inorganic compounds in a particular water body. DoE standard for COD is 200-400 mg/L [62].

Table 3.7 COD value of Dhaleshwari, Buriganga, Bhairab and Karnaphuli river water

Sample	Dhaleshwari	Buriganga	Bhairab	Karnaphuli
USP_S	2780	2642	2843	3032
USP_{50}	2720	2520	2792	2928
USP_{100}	2650	2585	2595	2874
MP_S	4700	3470	3640	3740
MP_{50}	3940	3395	4056	3712
MP_{100}	3850	3287	3884	3667
DSP_S	3170	3540	3362	4506
DSP_{50}	2860	3260	3948	4212
DSP_{100}	2750	3250	2673	4304

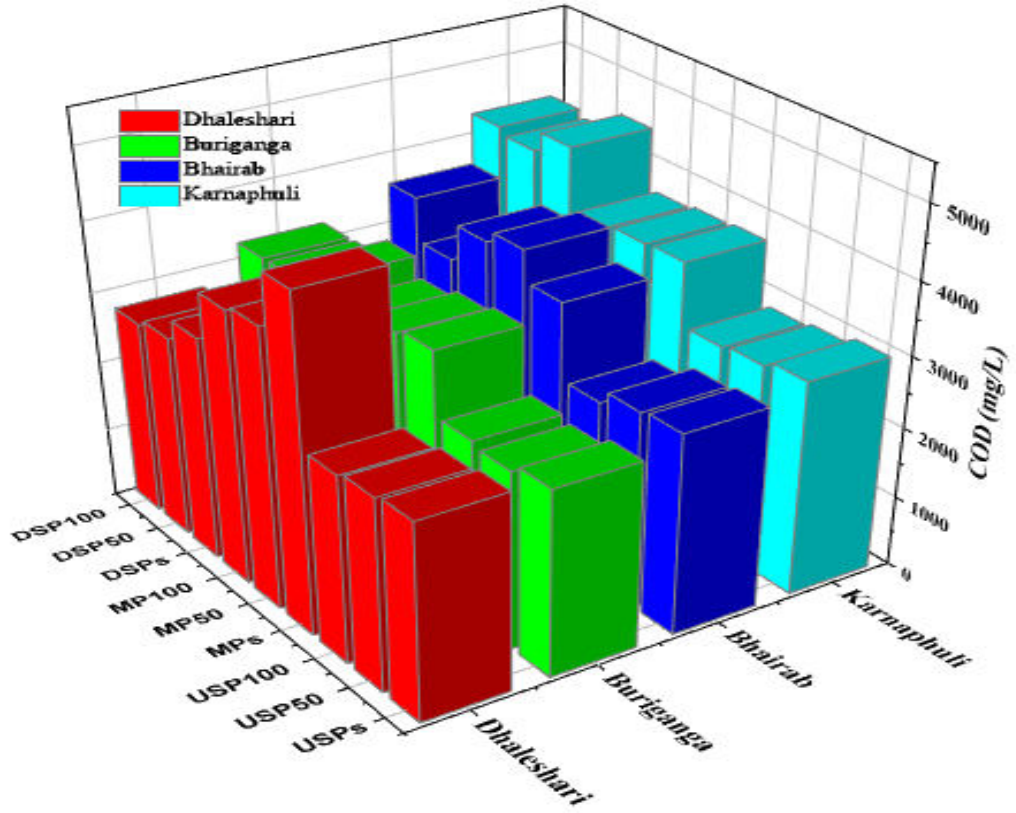

Figure 3.7 COD of Dhaleshwari, Buriganga, Bhairab and Karnaphuli river water samples

It has been revealed from the data (**Table 3.7, Figure 3.7**) that the range of COD value of Dhaleshwari, Buriganga, Bhairab and Karnaphuli river water samples are 2651-4703 mg/L, 2520-3540 mg/L, 2595-4056 mg/L and 2847-4506 mg/L accordingly which is very high compare to DoE standard which indicates more pollution in the water samples.

3.1.8. Heavy metals

Heavy metals for example Cr, Ni, Cu, Cd, and Pb are usually discharged from tanneries. Cr, Ni, Cu, Cd, and Pb concentration of experimented samples are showed in **Table 3.8**. The highest and lowest mean value of Cr concentration was found to be 10.2 mg/L in MP of Buriganga and 1.65 mg/L in DSP of Dhaleshwari, which has good agreement with previous data [282]. According to ECR'97 the permissible concentration of Cr, Cd, Cu, Pb, Ni, is 0.5mg/L, is 0.5mg/L, 0.5mg/L, 0.1mg/L, 1.0mg/L, respectively. Whereas measured Cr concentration of all samples was higher than permissible limit. On the other hand, Ni concentration was not detected in all samples of Bhairab and at DSP of Karnaphuli river water, but the average concentration of Ni at UPS, MP and DSP of Dhaleshwari river had crossed the limit.

Table 3.8 Heavy metal concentration of Dhaleshwari, Buriganga, Bhairab, and Karnaphuli river water samples

River	Sampling point	Heavy metals concentration (mg/l)				
		Cr	Ni	Cu	Cd	Pb
Dhaleshwari	USP	1.82±0.7	2.80±3.3	1.89±1.7	3.46±1.0	8.33± 2.9
	MP	8.64±4.4	0.96±1.0	2.13±0.9	2.48±0.9	8.59± 6.0
	DSP	1.65±0.9	0.77±0.3	7.79±2.0	2.82±1.3	9.03±5.0
Buriganga	USP	3.16±1.7	0.35±0.3	2.35±1.9	3.44±1.3	9.07±2.0
	MP	10.2±3.4	ND	3.49±3.2	3.40±0.4	7.84±6.8
	DSP	2.87±0.5	0.38±0.7	2.70±0.2	3.43±0.8	17.6±9.4
Bhirab	USP	5.94±0.7	ND	0.74±0.4	0.09±0.1	5.75±1.2
	MP	7.25±0.8	ND	0.62±0.2	2.77±1.2	6.02±1.3
	DSP	6.80±0.9	ND	0.93±0.5	0.06±0.0	5.37±1.2
Karnaphuli	USP	7.67±0.4	0.001±0	0.49±0.0	0.46±0.1	3.12±-.2
	MP	9.63±0.7	0.001±0	0.84±0.1	0.30±0.1	3.48±0.3
	DSP	8.94±0.1	ND	1.29±0.3	0.31±0.0	2.81±0.2
ECR'97 Limit (mg/l)		2.0	1.0	0.5	0.5	0.1

All values were presented as Mean ± SD of triplicate measurement. ND = Not detected, USP = Upstream point; MP = Meeting point; DSP = Downstream point

Besides, the mean concentration of Cu at USP of Karnaphuli was within the standard limit, while rest mean values of Dhaleshwari, Buriganga, and Bhairab were out of the limit. In addition, the highest and the lowest Cu concentration was observed 7.79 (mg/L) in DSP of Dhaleshwari and 0.49 (mg/L) in USP 7.23 (mg/L) of Karnaphuli river water sample respectively. Heavy metal Cd concentration of the collected samples of Dhaleshwari, Buriganga and Karnaphuli river water was higher than ECR'97 limit except USP and DSP of Bhairab river. Moreover, all mean values of collected samples of Dhaleshwari, Buriganga, Bhairab, and Karnaphuli river water contained more Pb concentration than tolerance limit.

3.1.9. Correlation analysis

A statistical study was performed to understand the correlation between analyzed metals and water pollution parameters.

Table 3.9 Correlation Matrix between heavy metals and water pollution parameters of Dhaleshwari, Buriganga, Bhairab, and Karnaphuli river of Bangladesh

	Cr	**Ni**	**Cu**	**Cd**	**Pb**	**BOD**	**COD**	**TDS**	**EC**	**NaCl**	**pH**
Cr	1										
Ni	-0.572	1									
Cu	-0.481	0.227	1								
Cd	-0.490	0.490	0.512	1							
Pb	-0.594*	0.287	0.435	**0.721****	1						
BOD	0.377	0.057	-0.139	-0.597*	**-0.864****	1					
COD	0.666*	-0.292	-0.224	-0.208	-0.215	0.275	1				
TDS	0.618*	-0.462	-0.550	**-0.776****	**-0.715****	0.588*	0.445	1			
EC	0.600*	-0.505	-0.601*	-0.769**	-0.678*	0.531	0.493	0.915**	1		
NaCl	0.631*	-0.520	-0.614*	**-0.807****	**-0.716****	0.579*	0.558	**0.921****	**0.984****	1	
pH	0.668*	-0.389	0.068	-0.435	**-0.725****	0.687*	0.436	0.404	0.376	0.426	1

*Correlation is significant at the 0.05% level (2-tailed)

** Correlation is significant at the 0.01% level (2-tailed)

Table 3.9 represents the Pearson correlation coefficient matrix for five heavy metals and six water pollution parameters of four river water samples associated to tannery effluent. These data revealed a significant correlation between electtric conductivity (EC) and NaCl (r=0.984), and TDS and NaCl (r=0.921). Again heavy metal Pb and BOD showed strong negative correlation (r=-0.864). Amog the heavy metals Cd, and Pb resulted significant correlation (r=0.721) and Cr, and Pb showed strong negative correlation coefficient. In this study, Ni did not shown any considerable correlation at 0.05% level but COD showed significant correlation only to Cr(III).

3.1.10 Multivariate statistical analysis

The calculated principal components (PCs) loading, percentage of variance, cumulative percentage of principal components analysis of heavy metals and parameters of water

pollution from four river water samples were displayed in **Table 3.10**. Eigen value>1 showed three principal components (PCs) representing 83.42% of variance.

Table 3.10 Variance loadings in different principal components (PCs) of heavy metals and water pollution parameters of studied water.

Parameters	PC1	PC2	PC3	PC4	PC5	PC6
Cr(III)	**0.311**	-0.026	**0.403**	0.096	**-0.471**	0.052
Ni	-0.217	0.282	**-0.418**	**0.640**	-0.063	-0.070
Cu	-0.226	**0.465**	0.273	-0.234	**0.602**	0.089
Cd	**-0.330**	0.046	0.251	0.305	-0.098	**0.790**
Pb	**-0.335**	-0.301	0.220	0.106	0.293	-0.252
BOD	0.272	**0.516**	-0.270	0.165	0.080	-0.067
COD	0.220	-0.045	**0.510**	**0.600**	0.239	-0.288
TDS	**0.358**	-0.120	-0.137	0.029	0.258	0.366
EC	**0.360**	-0.193	-0.110	0.051	0.299	0.266
NaCl	**0.373**	-0.162	-0.083	0.075	0.269	0.060
pH	0.255	**0.514**	0.326	-0.163	-0.157	-0.012
Eigenvalue	6.429	1.481	1.267	0.830	0.549	0.205
% of variance	58.44%	13.46%	11.52%	7.55%	4.99%	1.87%
Cumulative %	58.44%	71.90%	83.42%	90.97%	95.96%	97.82%

In PC1, % NaCl variance load was significant and revealed the salinity influence in tannery effluent used in curing, and pickling process. As NaCl increased the electrolyte content in wastewater, electric conductivity (EC) represented second most variance loadings in PC1. BOD, and pH displayed substantial loading in PC2 with 13.46% variance representing protenous source of pollution from tannery. In PC3, 11.52% variance mostly influenced by COD, followed by Ni. By considering only heavy metals in variance loadings Pb and Cd in PC1, Cu in PC2, and Ni, Cr in PC3 were prominents pollutants.

The minimal loadings of Cr(III) in PCs of tannery effluents is a good sign revealed proper treatment before discharging. But the effluents can be mixed with other industrial wastewater heavily thus reflecting the heavy presence of Pb, Cd, Cu, and Ni as all the sampling spot not olny comprised with tannery but also other industrial parks.

3.1.11. Principal Component Analysis (PCA)

Score plot of PC1 against PC2 of Dhaleshwari, Buriganga, Bhirab, and Karnaphuli river water pollution were also presented in **Figure 3.8,** which revealed that both the Dhaleshwari, and Buriganga river water displaying negative score in PC1 with nearly simiar values while the Karnaphuli, and Bhirab river scoring positively in that factor. However, PC2 represented all the rivers separately where the Buriganga, and Bhirab negativey scored but the Dhaleshwari, and Karnaphuli showed positive score.

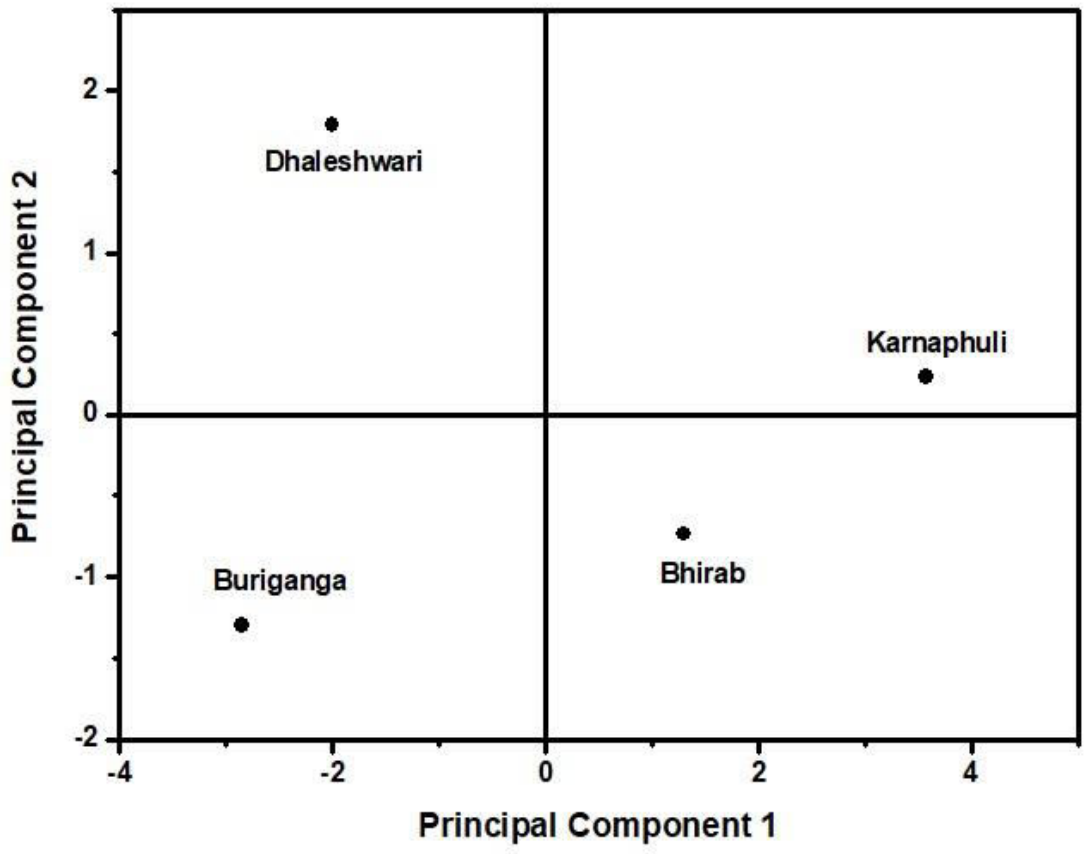

Figure 3.8 Score plot of PCA of four river water connected to tannery effluents.

3.1.12. Hierarchical cluster analysis

Hierarchical cluster analysis report was showed in **Figure 3.9** displaying two clusters of studied rivers. Dhaleshwari, and Buriganga showed one cluster, while Karnaphuli, and Bhirab were another. The distance of two cluster revealed that Bhirab and Karnaphuli, rivers

are more polluted than Dhaleshwari, and Buriganga. A previous study confirmed the hydrogeological connection between Dhaleshwari, and Buriganga river along with the pollution flow from previous one to last one [283]

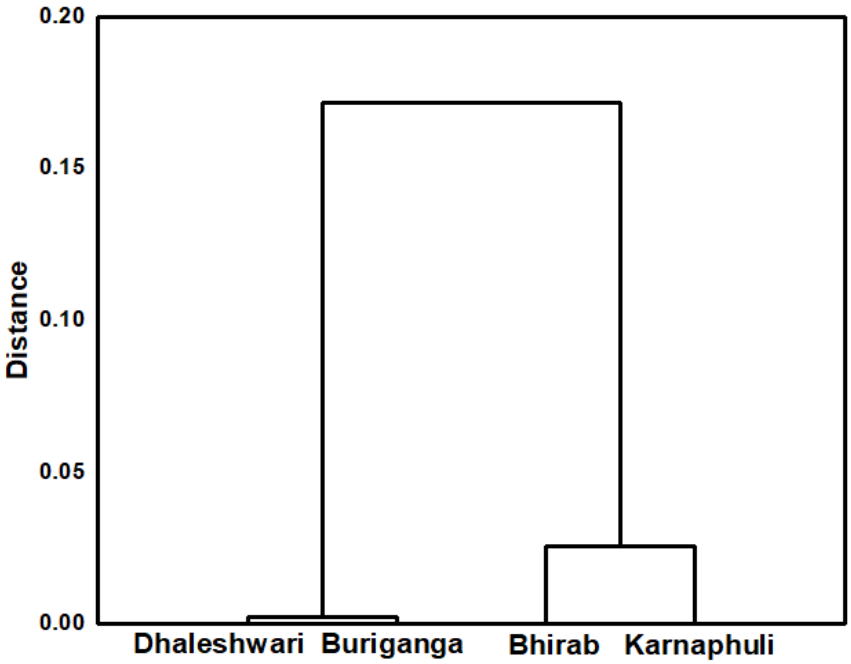

Figure 3.9 Hierarchical cluster analysis (HCA) of four river water connected to tannery effluents.

3.2. Part 2: Preparation, Characterization and Application of Adsorbents to Remove Cr(III) From Aqueous Solution and Tannery Effluents .

3.2.1. Chemically Activated Pyrolyzed Peanut Shell (PNS)

3.2.1.1. Preparation of PNS

In a tube furnace, dried peanut shells were pyrolyzed at 500 ±10 ºC for two hours, and they were subsequently chemically activated using analytical grade NaOH. Pyrolysis, also referred to as carbonization, is the process used to make charcoal, which is the chemical decomposition of the fiber caused by heating in the absence of oxygen [284]. A 25% NaOH was added with pyrolyzed peanut shell for chemical activation with stirring and left for 24 hours. The following day, the products was washed away by distilled water before being dried in air oven at 110-115ºC. Carbonization process generally enhance the amount of carbon and create an preliminary porosity and chemical activation is to enlarge pores [285]. Finally, NaOH activated dried pyrolyzed peanut shell (PNS) were pulverized and employed as an adsorbent.

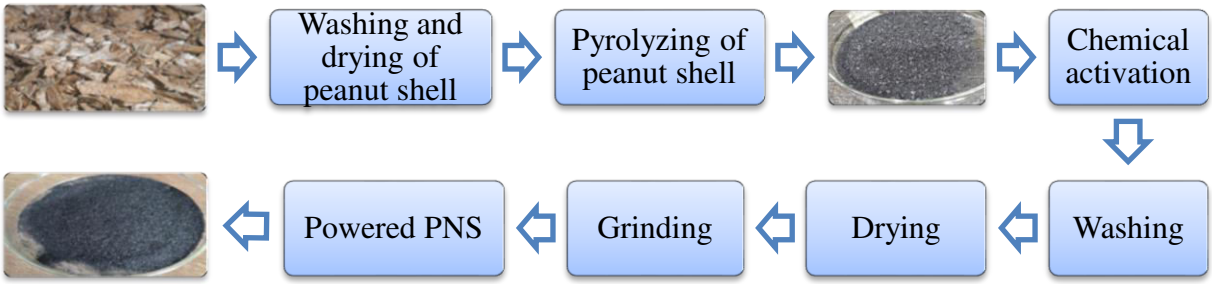

Flow chart 3.1 Flow diagram of PNS preparation

3.2.1.2. Characterization of PNS

3.2.1.2.1. Elemental analysis of PNS

In order to analyze the elements before and after adsorption of Cr(III) in to PNS, EDX analysis was performed. EDX analysis presented in **Figure 3.10** indicated that the chemical compositions of PNS are mainly C, N, O, P, S, K, Ca. Moreover, chromium was incorporated after adsorption. During the measurement of EDX different areas were focused and the corresponding peaks are shown.

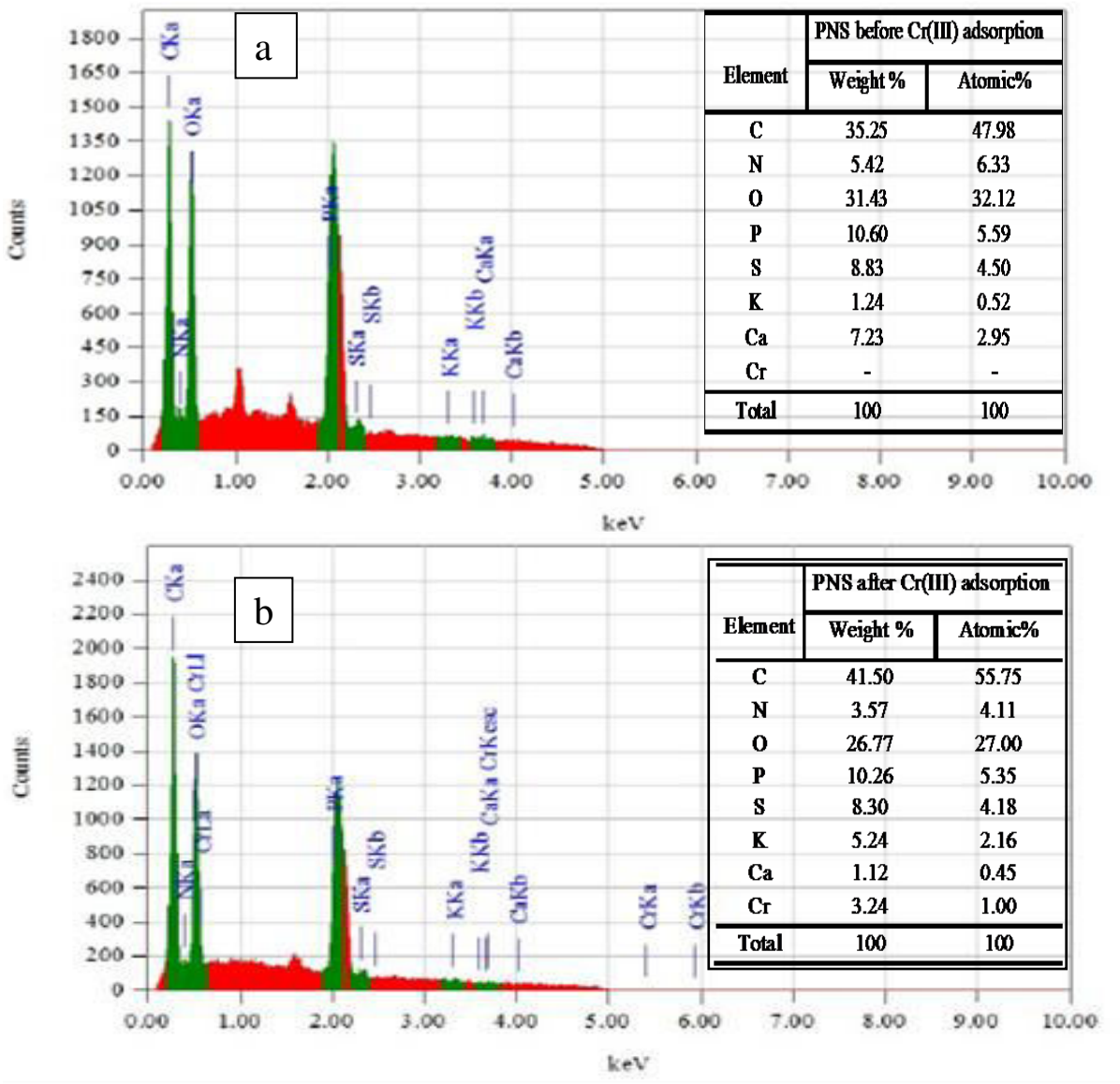

Element	PNS before Cr(III) adsorption	
	Weight %	Atomic%
C	35.25	47.98
N	5.42	6.33
O	31.43	32.12
P	10.60	5.59
S	8.83	4.50
K	1.24	0.52
Ca	7.23	2.95
Cr	-	-
Total	100	100

Element	PNS after Cr(III) adsorption	
	Weight %	Atomic%
C	41.50	55.75
N	3.57	4.11
O	26.77	27.00
P	10.26	5.35
S	8.30	4.18
K	5.24	2.16
Ca	1.12	0.45
Cr	3.24	1.00
Total	100	100

Figure 3.10 Energy dispersive X-ray (EDX) spectrum of PNS (a) before and (b) after Cr(III) adsorption.

In spectrum (a), the quantity of C, N, O, P, S, K, Ca and Cr were 47.98, 6.33, 32.12, 5.59, 4.50, 0.52, 2.95, and 0.00 measured in atomic % respectively, while in spectrum (b), the values were 55.75, 4.11, 27.00, 5.35, 4.18, 2.16, 0.45, and 1.00 respectively, which signify Cr(III) adsorption on to PNS.

3.2.1.2.2. FTIR analysis of PNS

The FTIR analysis is vital to recognize the distinctive functional groups, which are liable for adsorption of metal ions. It is well recognized that peanut shell contains lignin, cellulose and hemicelluloses. PNS experiences various modification throughout the chemical activation and Cr(III) ion adsorption processes. FTIR spectroscopy was utilized to evaluate the vibrational changes in PNS after chemical activation and adsorption processes. It is observed

from the **Figure 3.11** that some functional groups moved to a different frequency level or disappeared after activation and adsorption [286].

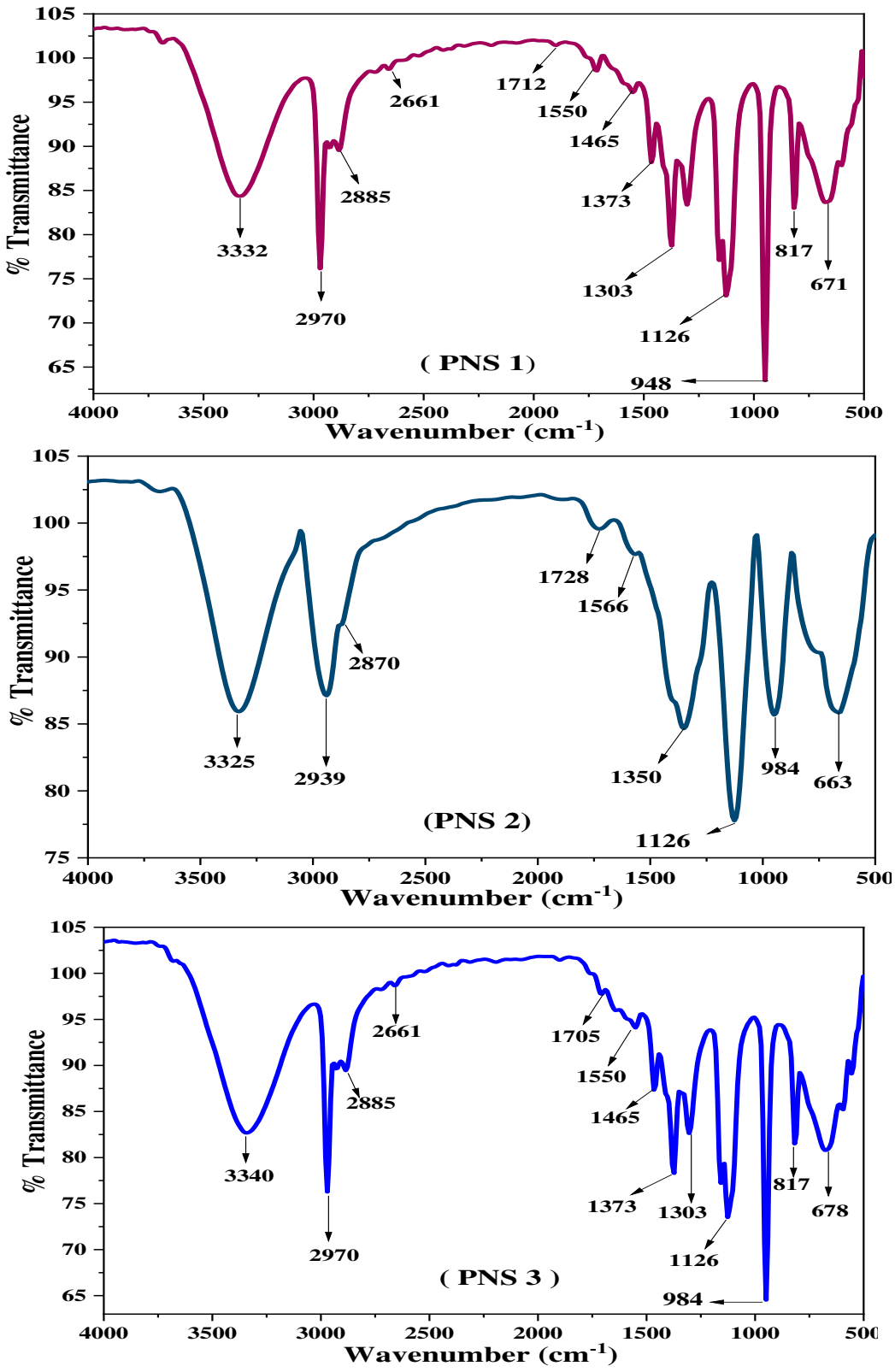

Figure 3.11 FTIR spectra of PNS-1 (pyrolyzed nutshell), PNS-2 (NaOH activated pyrolyzed nutshell), and PNS-3 (Cr^{3+}loaded NaOH activated pyrolyzed nutshell).

In the FTIR spectra of PNS-1, PNS-2, and PNS-3, the existence of –OH groups led to the observation of broad peaks at 3332, 3325, and 3340 cm^{-1} correspondingly. The band at 1712, 1728 and 1705 cm^{-1} indicating that –C=O groups were also exist in IR spectra. C-H stretching vibrations were observed at 2970 cm^{-1}, 2885 cm^{-1} in PNS-1; 2939 cm^{-1} and 2870 cm^{-1} in PNS-2 and 2970 cm^{-1} and 2885 cm^{-1} in PNS-3 Moreover, the peak between 1100 and 1300 cm^{-1} represents C-O (alcoholic, esters) groups of the adsorbent.

3.2.1.2.3. Scanning electron microscopic (SEM) analysis of PNS

Surface morphology of NaOH activated PNS was studied through SEM. The SEM image of activated PNS is shown in **Figure 3.12** demonstrates that it has cavities, an uneven, heterogeneous, and lamellar features that facilitate the adsorption process in aqueous solutions [194]. The quick volatilization of organic components in the biomass caused the well-defined porosity structure, which was advantageous for the attachment of metal ions [287].

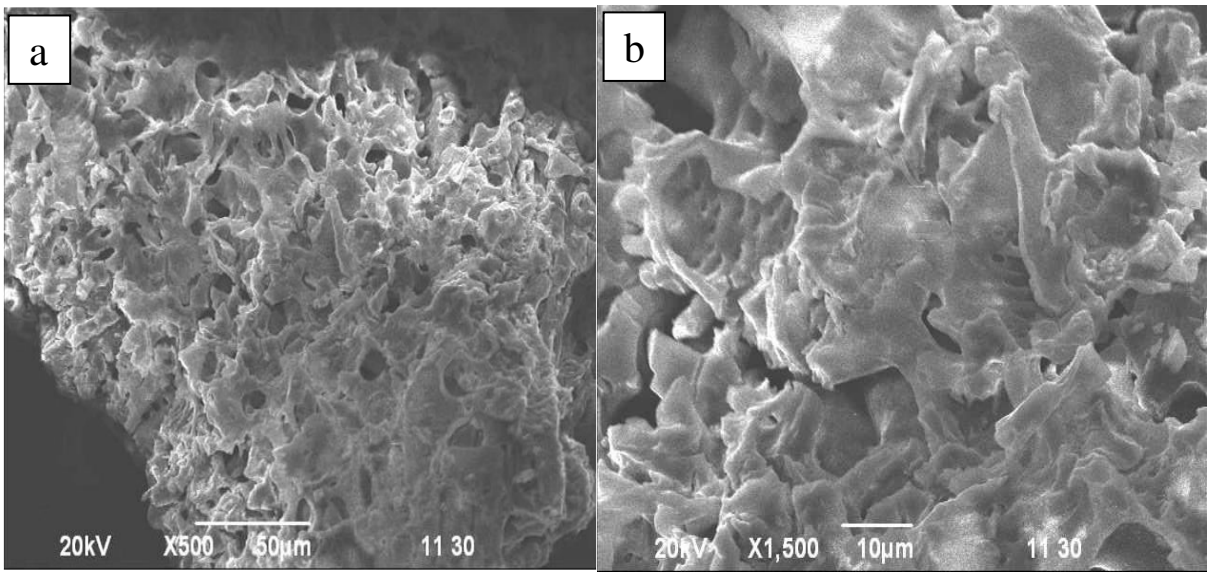

Figure 3.12 SEM images of PNS (a) 500x, and (b) 1500x magnification

3.2.1.2.4. X-Ray Diffraction (XRD) analysis of PNS

The X-ray diffraction pattern showed no clearly defined peak associated with the crystalline phase. It demonstrates a characteristic peak of carbonaceous compound. A bulge in the range of 2θ = 20 - 30° and a peak at 2θ = 22.8° were observed from the **Figure 3.13** because of amorphous nature with a high degree of disorder of PNS. The broad and weak peaks observed in XRD pattern of PNS indicates the existence of amorphous carbon [288].

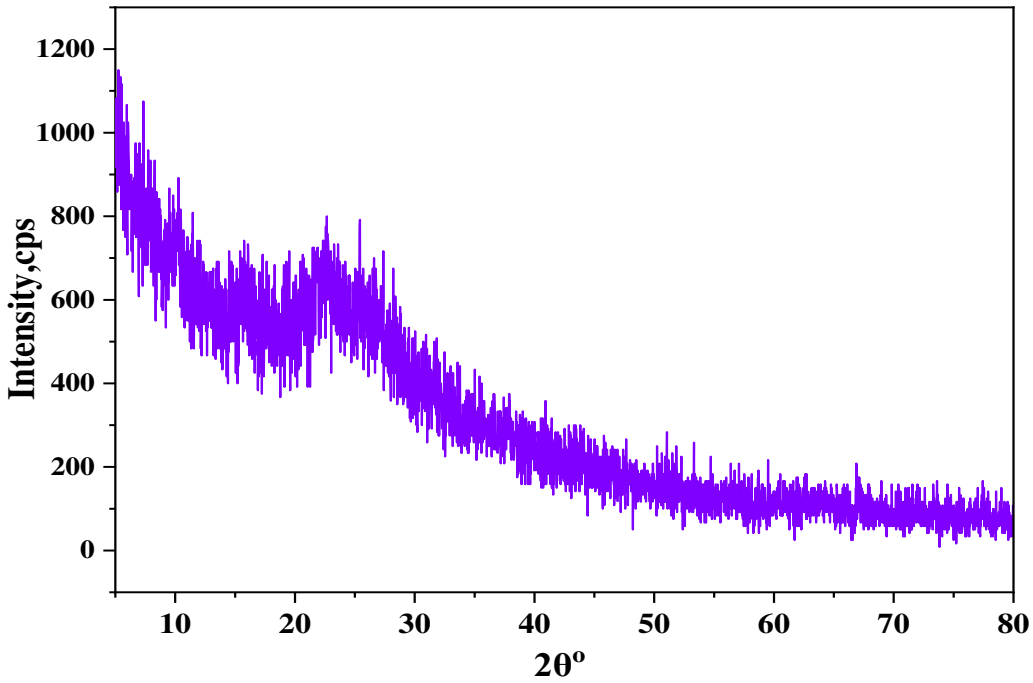

Figure 3.13 XRD analysis of PNS

3.2.1.2.5. Brunauer-Emmett-Teller (BET) analysis of PNS

Surface area, pore volume, and pore diameter of PNS were analyzed through nitrogen gas sorption system are presented in **Table 3.11**. Chemically activated PNS had low surface area of 3.68 m^2/g may be due to the breakdown of cell walls [289]. Pore sizes are classified as reported by IUPAC, which are micropores (diameter, d < 20 Å), mesopores (20 Å < d < 500 Å), and macropores (d > 500 Å) [193]. Barrett-Joiner-Halenda (BJH) method was followed to find out the average pore diameter was 89.41 Å, which signify that PNS consists of mesopores.

Table 3.11 BET surface area and porosity of PNS

Sl. No.	Parameter	Result
01.	BET Specific Surface Area using multi-point analysis (m^2/g)	3.68
02.	Total Pore Volume (cc/g)	0.0082
03.	Skeletal density (g/cc)	1.6863
04.	Porosity based on skeletal density (per gram of sample)	0.0137
05.	Average Pore Diameter, (Å)	89.41

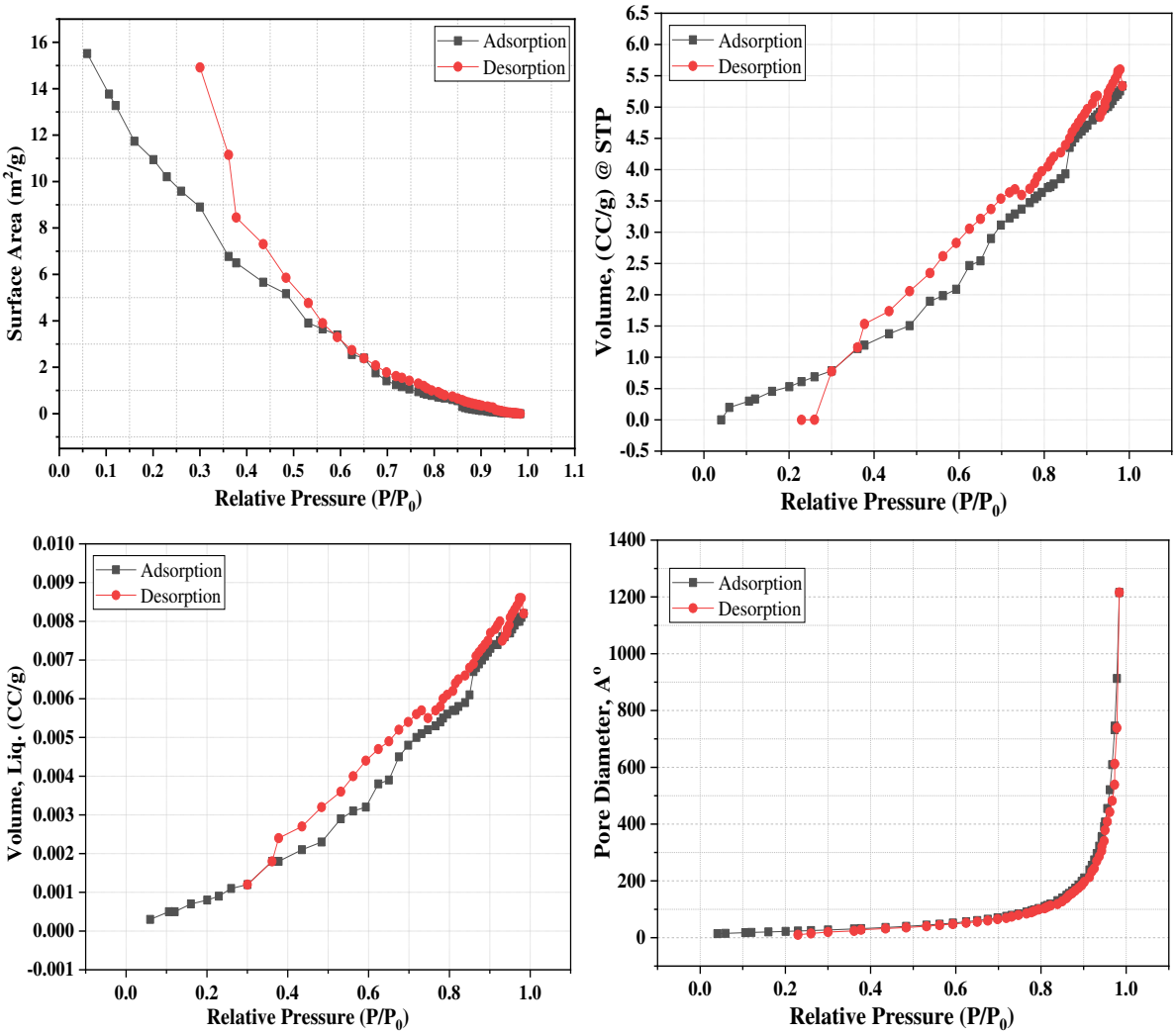

Figure 3.14 Adsorption and desorption isotherms of BET to PNS

3.2.1.2.6. Zeta potential value of PNS

Zeta potential value (ZPV) of PNS was also studied as a function of pH. The sample was prepared by dispersing PNS in deionized water to analyze the ZPV of PNS. The study was performed at 3.0-5.0 pH range. The **Table 3.12** and **Figure 3.15** signify that ZPV of PNS was positive (9.87 mV) at 3.0 pH, while the values were negative (-11.7 to -22.8 mV) with an increase of pH from 3.5 to 5.0.

Table 3.12 pH vs Zeta potential value of PNS

pH	3.0	3.5	4.0	4.5	5.0
ZPV (mV)	9.87	-11.7	-12.4	-18.8	-22.8

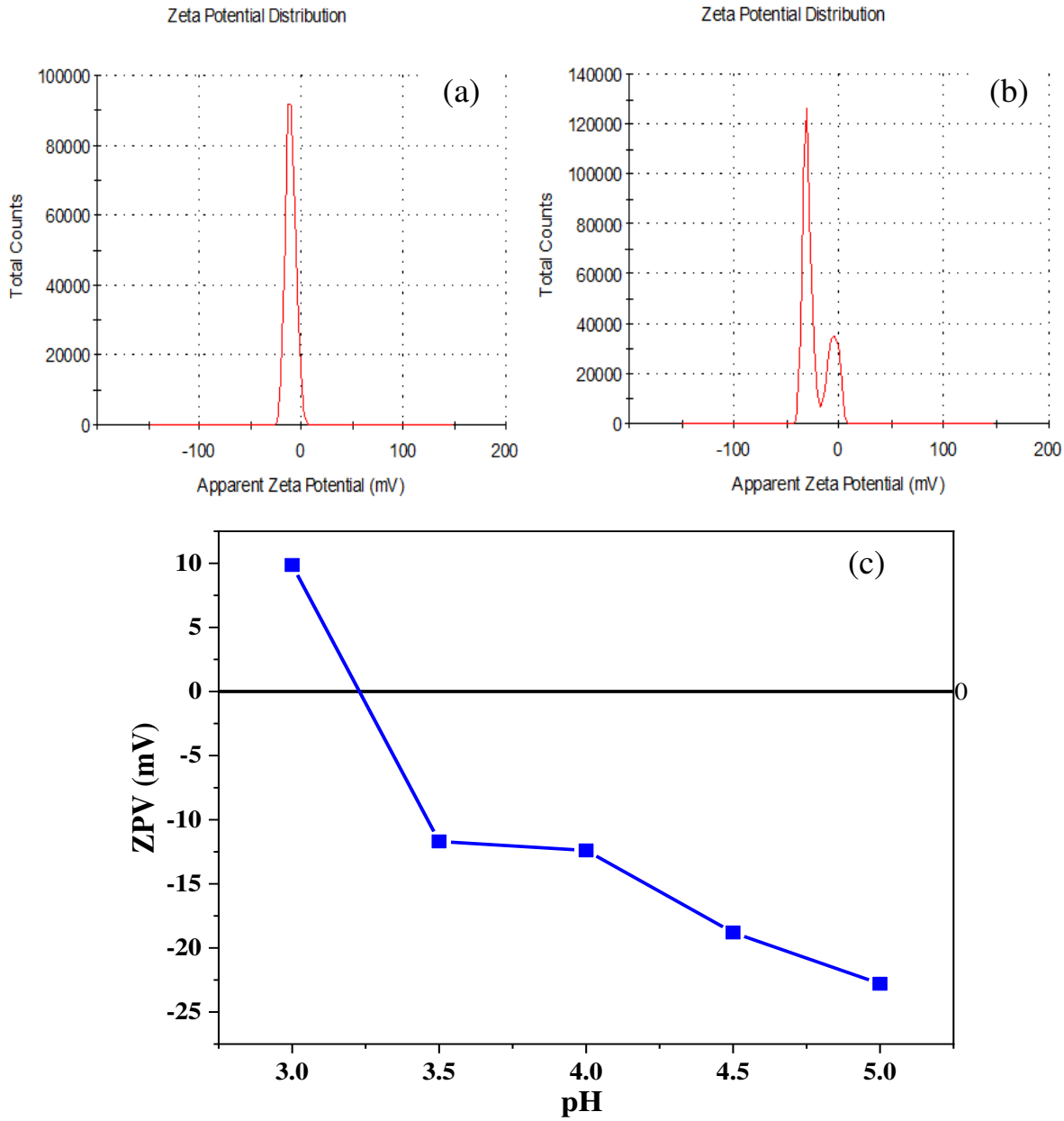

Figure 3.15 ZPV of PNS (a) at pH 3.5 (- 10.2 mV), (b) at pH 5.0 (-22.8 mV), and (c) ZPV of PNS at different pH

3.2.1.3. Adsorption of Cr^{3+} ions on PNS

3.2.1.3.1. Calibration curve of $Cr_2(SO_4)_3.6H_2O$ solution

A calibration curve was develop using 32.06, 69.19, 135.43, 187.57, 271.74, 301.26, and 363.47 ppm $Cr_2(SO_4)_3.6H_2O$ solutions by spectrophotometric method. Unknown concentration was determined before and after Cr^{3+} ions adsorption with respect to this calibration curve. After then adsorption capacity or % of removal was calculated through equation (2.1), or (2.2) and (2.3) respectively.

Table 3.13 Concentration vs absorbance data of $Cr_2(SO_4)_3.6H_2O$ salt solution

Concentration (ppm)	32.059	69.197	135.43	187.57	271.74	301.26	363.47
Absorbance	0.02	0.04	0.07	0.1	0.14	0.16	0.19

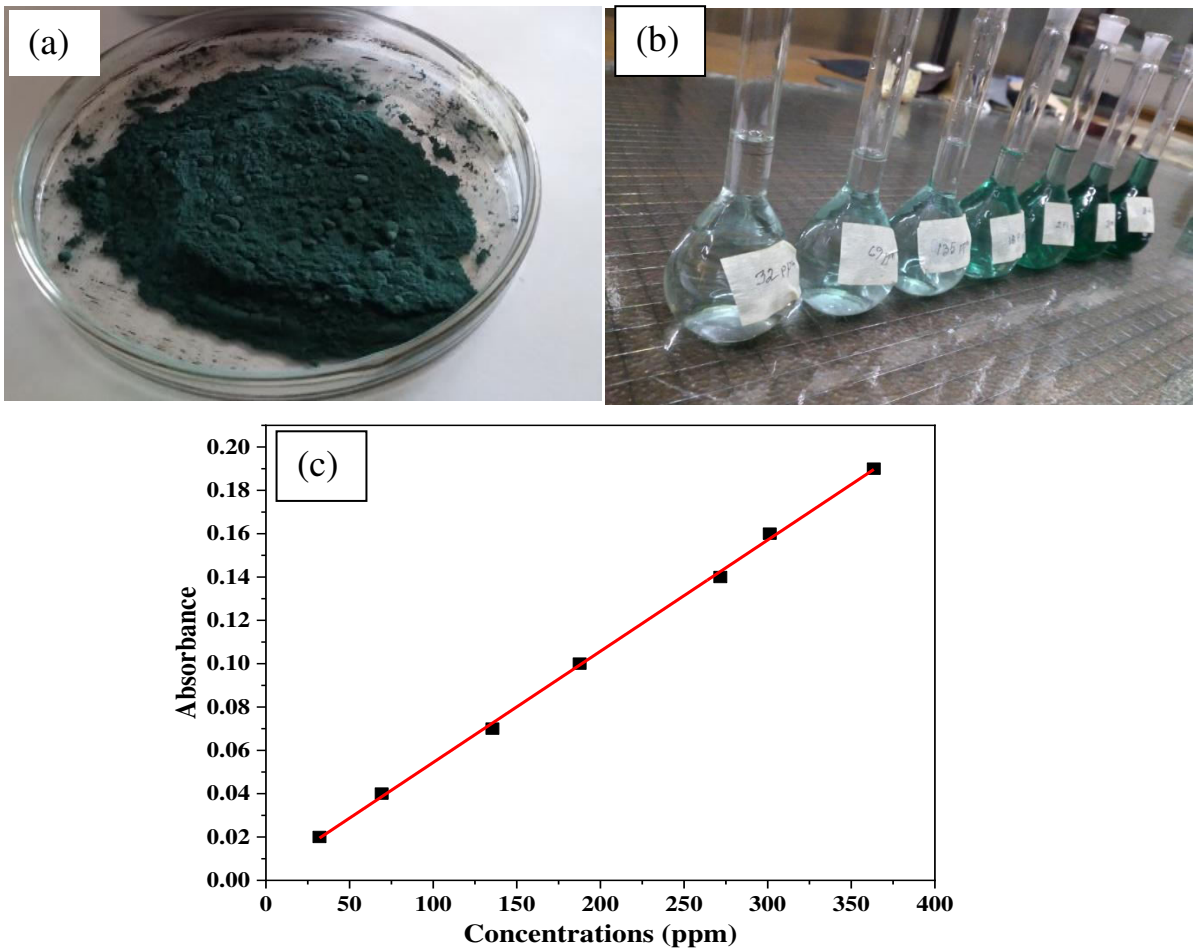

Figure 3.16 (a) $Cr_2(SO_4)_3.6H_2O$ powder (b) $Cr_2(SO_4)_3.6H_2O$ solution at different conc. and (c) calibration Curve of $Cr_2(SO_4)_3.6H_2O$ salt solution

3.2.1.3.2. Effect of pH on adsorption capacity of PNS for Cr^{3+} ions adsorption

The pH of metal ions solutions is a significant parameter to control the adsorption process as it disassociates the groups present on the surface hence change the surface charge of adsorbent. The effect of pH for Cr^{3+} ions adsorption by PNS was investigated with 256.53 ppm solution of $Cr_2(SO4)_3.6H_2O$ by varying it in the range of 3.0 to 5.0. In batch experiment 25 mL solutions were taken in each conical flask and put 63 mg PNS and then shaken in a orbital shaker at 160 rpm for 4 hours. After filtering the mixtures any change in Cr(III) ions concentrations were determined by UV-Vis spectroscopy. It is evident from the **Table 3.14**

and **Figure 3.17** that adsorption capacity of PNS was enhanced at higher pH of the solution and the maximum capacity was 69.72 mg/g at pH 5.

Table 3.14 pH v/s adsorption capacity data of PNS for Cr^{3+} adsorption

pH	3.0	3.5	4.0	4.5	5.0
Adsorption Capacity (mg/g)	53.09	51.32	56.13	60.1	69.72

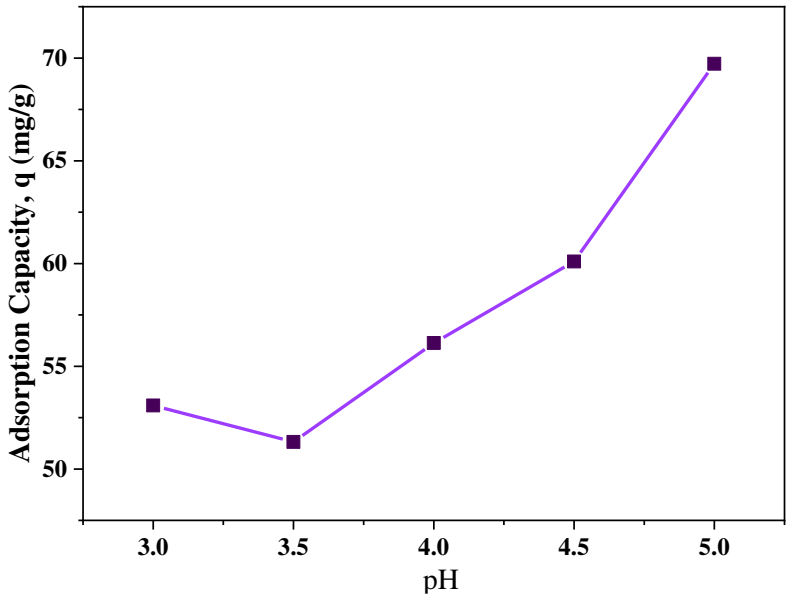

Figure 3.17 Effect of Cr-salt solution pH on adsorption capacity of PNS for Cr^{3+} ions adsorption

It is speculated that ion exchange (which was evident from EDX analysis **Figure 3.10)** and H-bonding may be the principle mechanism to remove of heavy metals [290]. At lower pH value (3.0) the adsorption capabilities observed to be less, because of the feisty adsorption of same positive charge of H^+ and metal ions with similar adsorption site. While, at pH 4.0 – 5.0, the lesser number of protons and more negative charges ensuing more Cr^{3+} adsorption. The surface negativity of PNS was increased with higher pH which was noticed from the ZPV (**Figure 3.15).**

$$—ROH \underset{\text{At Lower pH}}{\overset{\text{At Higher pH}}{\rightleftharpoons}} —R\bar{O} + H^+$$

In the research, all batch experiments were controlled at 5.0 pH to acquire highest adsorption capacity in addition to eliminate precipitation of Cr(III) [291]. Additionally, at pH >6 Cr(III) can be precipitated from the aqueous solution as $Cr(OH)_3$ [292]. The results agreed with

previous literature [237] and Cr speciation (**Figure 1.1**), it was observed that at pH >3 ionic species such as $CrOH^{2+}$, $Cr(OH)_2^{+}$ and bioadsorbent showed higher affinity to these species than for free Cr(III) ion.

3.2.1.3.3. Effect of adsorbent dosage on adsorption capacity and % removal

Effect of adsorbent dosage on Cr(III) adsorption was studied with different the dosage (1.5 - 4.0 g/L) to find out the optimum dose. The batch experiments were conducted for 4 hours with 240.57 ppm initial concentration at optimum pH 5.0. It is showed that (**Table 3.15, Figure 3.18)** % of Cr(III) removal was increased 46.86 to 87.53 % whereas adsorption capacity was decreased 75.16 to 52.65 mg/g with the increase of PNS dosage.

Table 3.15 Dosage v/s adsorption capacity and % removal data of PNS

Dosage (g/L)	1.5	2	2.5	3	3.5	4
Adsorption Capacity (mg/g)	75.16	65.51	58.83	56.57	52.99	52.64
Removal (%)	46.86	54.46	61.62	70.55	77.09	87.53

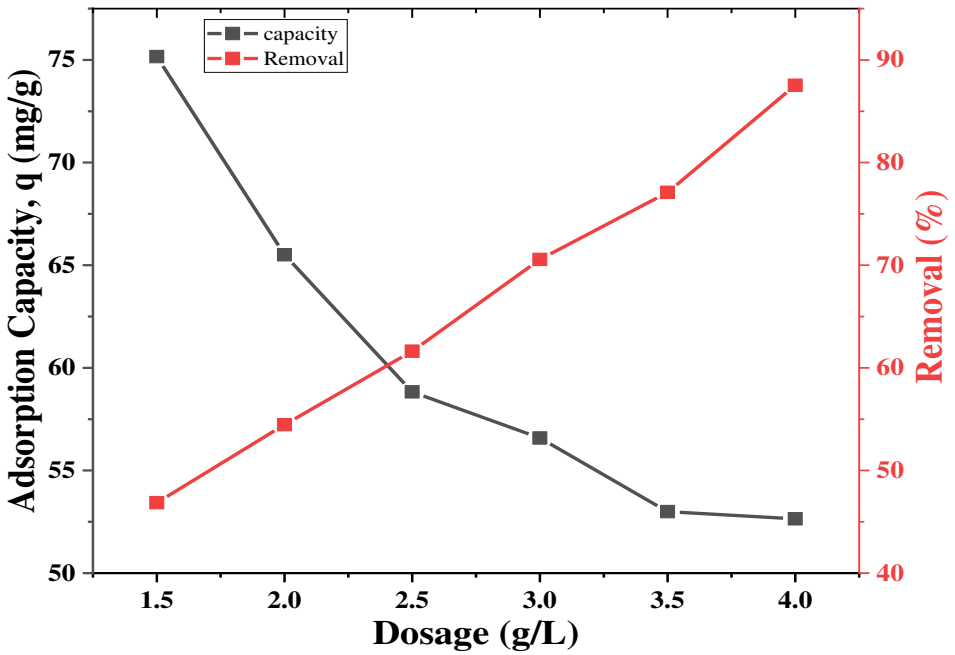

Figure 3.18 Effect of PNS dosage on adsorption capacity and % removal of Cr^{3+}

The availability of more adsorption sites is thought to boost the % removal of Cr(III), but more unsaturated sites lessen the adsorption capacity with higher adsorbent dosage [159]. It was observed that 2.37 g/L dose provides the best % removal also best adsorption capacity. However, for simplification 2.5 g/L dose were continued all over the study.

3.2.1.3.4. Effect of Cr^{3+} ions concentrations and contact time on adsorption capacity of PNS for Cr $^{3+}$adsorption

To explore the effect of Cr^{3+} ions concentrations and contact time on adsorption capacity of PNS, 25 mL solutions of five different concentrations (125.93, 196.97, 278.86, 330.55, and 370.11ppm) were taken in conical flasks and then 63 mg (2.5 g/L) PNS was added to each solution. The experiments were accomplished at 5.0 pH by several time intervals ranging from 5-600 minutes with constant shaking speed 160 rpm. The findings (**Table 3.16, Figure 3.19)** revealed that adsorption capacity increased with increasing duration until it reached at equilibrium and after then, there was no significant increase in adsorption capacity.

Table 3.16 Time vs adsorption capacity data of PNS for Cr $^{3+}$ ions adsorption

Time (min)	Adsorption capacity(mg/g)				
	125.93ppm	**196.97ppm**	**278.86ppm**	**330.55ppm**	**370.11ppm**
0	0	0	0	0	0
5	13.84	7.595	44.25	42.88	37.56
15	21.36	26.079	45.66	44.65	41.021
30	24.9	35.619	52.07	49.79	53.344
60	26.17	40.007	56.55	54.02	61.278
120	29.63	44.396	62.88	63.05	66.005
240	29.79	45.154	64.14	67.444	74.784
360	34.1	47.857	65.49	71.32	77.231
480	37.14	49.46	67.94	73.603	78.498
600	37.14	53.512	68.53	74.111	79.004

It was observed that adsorption capacity reached at equilibrium nearly 480 minutes, and the adsorption capacity was increased with higher Cr^{3+} ion concentration. At lower initial concentration, 125.93 ppm, equilibrium adsorption capacity was 37.22 mg/g while at 196.97, 278.86, 330.55, and 370.11 ppm concentration, adsorption capacity was 53.51, 68.53, 74.11, 79.00 mg/g correspondingly. The utmost adsorption capacity 79.00 mg/g was attained at 370.11 ppm solution.

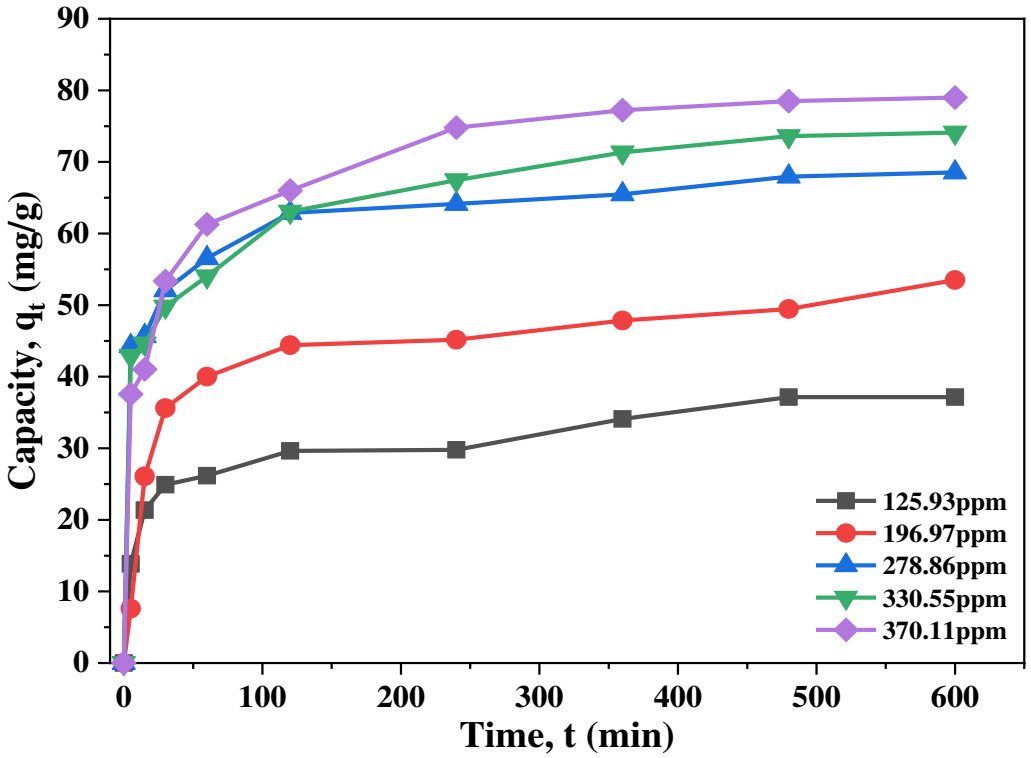

Figure 3.19 Effect of Cr^{3+} ions concentrations and contact time

The explanation is because initially there were more active sites available, but after certain time these sites got saturated [203]. Moreover, the equilibrium adsorption capacity was increased with higher Cr^{3+} ion concentration. It is caused in the gradient of concentration between the Cr(III) ion in bulk solution and adsorbent surface, which causes mass transfer among aqueous and solid phase [218].

3.2.1.4. Adsorption isotherms

To understand the affiliation among the quantity of adsorbate adsorbed on the adsorbent, normally analyze the experimental data with Langmuir and Freundlich isotherm. In Langmuir isotherm, the adsorbate is assumed to be absorbed on the adsorbent in a monolayer on well-defined with no intermolecular interactions. However, Freundlich isotherm deduces multilayer adsorption also signify non-uniform distribution.

3.2.1.4.1. Langmuir isotherm for Cr^{3+} adsorption

The Langmuir isotherm model was exercised by equation (3.4) plotting C_e/q_e versus C_e (**Table 3.17, Figure 3.20**). A linear connection among C_e/q_e and C_e was observed with acceptable regression factor (R^2=0.999). Maximum adsorption capacity q_m (theoretical), was calculated from the slope and found 104.82 mg/g. The separation factor R_L provides information of qualitative measure of the favorability, R_L >1 indicates unfavorable adsorption

while 0< R_L<1 indicates favorable process. In this study, R_L was calculated by equation (3.5) and the value was 0.138 indicates favorable monolayer adsorption process [293] .

Table 3.17 C_e vs C_e/q_e data of PNS at different concentration

Initial concentration (ppm)	125.93	196.97	278.86	330.55	370.11
Equilibrium concentration (C_e)	32.34	62.12	107.636	145.07	172.298
C_e/q_e	0.87	1.161	1.576	1.971	2.195

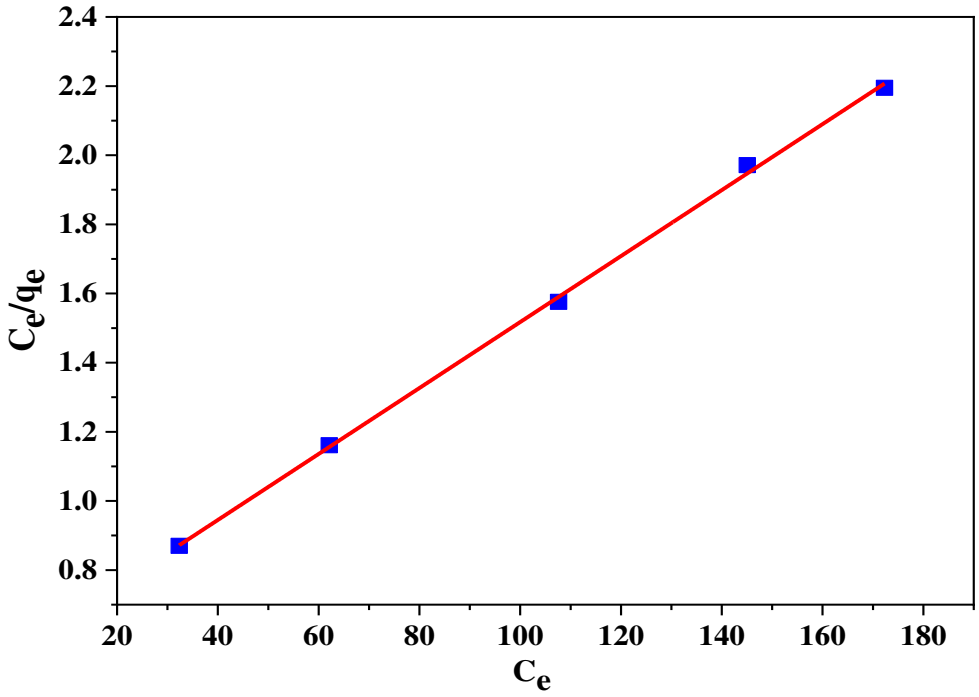

Figure 3.20 C_e vs C_e/q_e of PNS at different concentration for Cr^{3+} adsorption

3.2.1.4.2. Freundlich isotherm for Cr^{3+} adsorption

The experimental data was justified for multilayer adsorption mechanism through Freundlich isotherm equation (3.6) by plotting a graph of $\ln C_e$ versus $\ln q_e$ (**Table 3.18, Figure 3.21**) and linear connection was observed with good regression coefficient, R^2= 0.986. From the slope n was calculated and found to be 2.225 which showed good adsorption process [208].

Table 3.18 $\ln C_e$ vs $\ln q_e$ data of PNS at different concentration

Initial concentration (ppm)	125.93	196.97	278.86	330.55	370.11
$\ln C_e$	3.476	4.129	4.678	4.977	5.149
$\ln q_e$	3.615	3.979	4.218	4.298	4.363

Usually since n declines, adsorption becomes more complicated (n= 2-10 denotes good adsorption, n = 1-2 difficult adsorption and n<1 poor adsorption) [294].

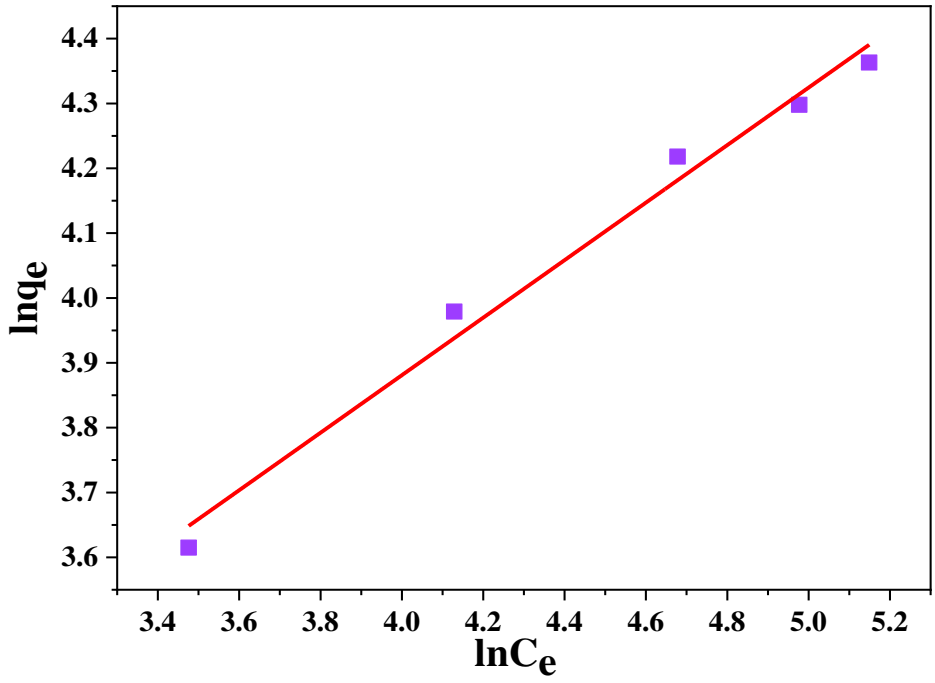

Figure 3.21 lnC_e vs lnq_e of PNS at different concentration for Cr^{3+} adsorption

3.2.1.4.3. Explanation on isotherms for Cr^{3+} adsorption

The values of various parameters of two models signify (**Table 3.19**) that the adsorption of Cr^{3+} on PNS obeyed both Langmuir and Freundlich isotherm but preferably the Langmuir model.

Table 3.19 Theoretical values of q_m, b, R_L, n, k_F and R^2 of adsorbent PNS

Isotherm model	q_m (mgg^{-1})	b (Lmg^{-1})	R^2	R_L	n	k_F
Langmuir isotherm	104.82	0.1239	0.999	0.138	-	-
Freundlich isotherm	-	-	0.986	-	2.225	8.221

3.2.1.5. Adsorption kinetics for Cr^{3+}adsorption

The adsorption kinetics is important to investigate how quickly ions move from liquid phase to solid phase and how long it takes to reach equilibrium. In this research, two kinetic models (Pseudo-First-Order and Pseudo-Second-Order) were applied to illustrate adsorption process.

3.2.1.5.1. Pseudo-first-order kinetic for Cr^{3+}adsorption

The Pseudo-First-Order kinetic equation (3.7) was introduced by Lagergren in 1898 to justify the adsorption process. Pseudo-First-Order isotherm was obtained by plotting a graph with $\log(q_e-q_t)$ against t (**Table 3.20, Figure 3.22**) where a linear relationship was observed in between $\log(q_e-q_t)$ and t.

Table 3.20 Time, t(min) and $\log(q_e-q_t)$ data of PNS at different concentration

Time, t(min)	$\log(q_e-q_t)$ at 125.93ppm	$\log(q_e-q_t)$ at 196.97ppm	$\log(q_e-q_t)$ at 278.86ppm	$\log(q_e-q_t)$ at 330.55ppm	$\log(q_e-q_t)$ at 370.11ppm
5	1.367	1.662	1.375	1.487	1.612
15	1.198	1.438	1.348	1.461	1.573
30	1.088	1.253	1.201	1.376	1.401
60	1.04	1.13	1.057	1.292	1.236
120	0.876	0.959	0.708	1.023	1.096
240	0.866	0.922	0.579	0.789	0.569
360	0.483	0.752	0.389	0.358	0.103
480	-	0.608	-	-	-

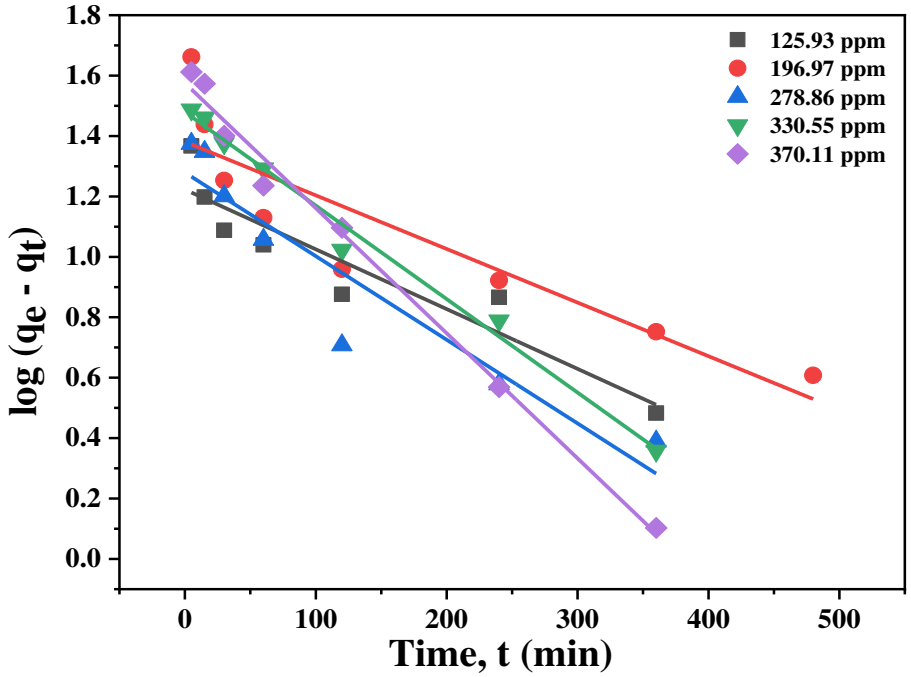

Figure 3.22 Pseudo-First-Order kinetics for Cr^{3+} adsorption on PNS

3.2.1.5.2. Pseudo-second-order reaction kinetic for Cr^{3+} adsorption

In 1999 Ho and Mckay validate Pseudo-Second-Order rate reaction (3.8). Pseudo-Second-Order model was prevailed with a graph by putting t/q_t versus t (**Figure 3.23**).

Table 3.21 Time, t(min) and t/q_t data of PNS at different concentration

Time, t(min)	t/q_t at 125.93ppm	t/q_t at 196.97ppm	t/q_t at 278.86ppm	t/q_t at 330.55ppm	t/q_t at 370.11ppm
5	0.361	0.658	0.112	0.117	0.133
15	0.702	0.575	0.328	0.336	0.365
30	1.204	0.842	0.576	0.603	0.562
60	2.292	1.499	1.061	1.111	0.979
120	4.049	2.702	1.908	1.903	1.818
240	8.056	5.315	3.74	3.539	3.209
360	10.557	7.522	5.497	5.048	4.661
480	-	9.704	-	-	-

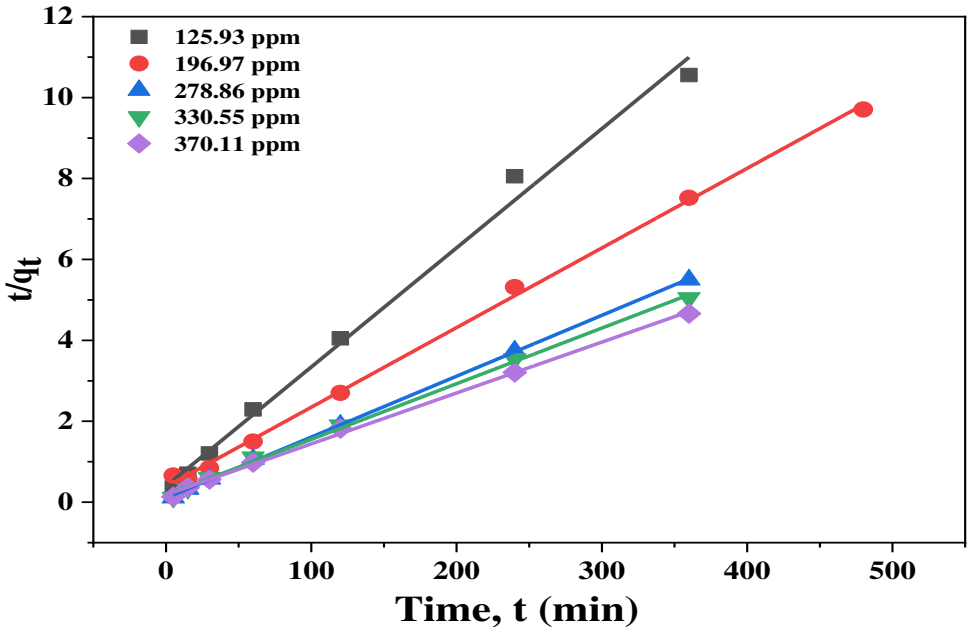

Figure 3.23 Pseudo-Second-Order kinetic for Cr^{3+} adsorption on PNS

3.2.1.5.3. Explanation on kinetics for Cr^{3+} adsorption

The kinetic models' parameters are deliberated from the slop and intercept of each linear plot are summarized in **Table 3.22.** The linear fitting results of two models suggest that in case of Pseudo-Second-Order model the theoretical q_e values agreed well with the experimental q_e. It was also found that correlation coefficient (R^2) value of Pseudo-Second-Order kinetic model was also superior to Pseudo-First-Order kinetic model.

Table 3.22 Pseudo-First-Order and Pseudo-Second-Order kinetics parameter

Model	Parameters	125.93ppm	196.97ppm	278.86ppm	330.55ppm	370.11ppm
Pseudo-First-Order	q_e^* (mg g^{-1})	37.14	49.46	67.94	73.603	78.498
	k_1(1/min)	0.00456	0.0041	0.00637	0.00712	0.00953
	R^2	0.875	0.805	0.894	0.989	0.990
	q_e^{**} (mgg^{-1})	16.71	24.048	19.02	30.14	37.60
Pseudo-Second-Order	k_2 (g/mg min)	0.00128	0.00078	0.00162	0.00087	0.00078
	R^2	0.989	0.995	0.999	0.998	0.998
	q_e^{**} (mg g^{-1})	36.82	53.276	68.12	74.68	80.52

*** Experimental, **Theoretical**

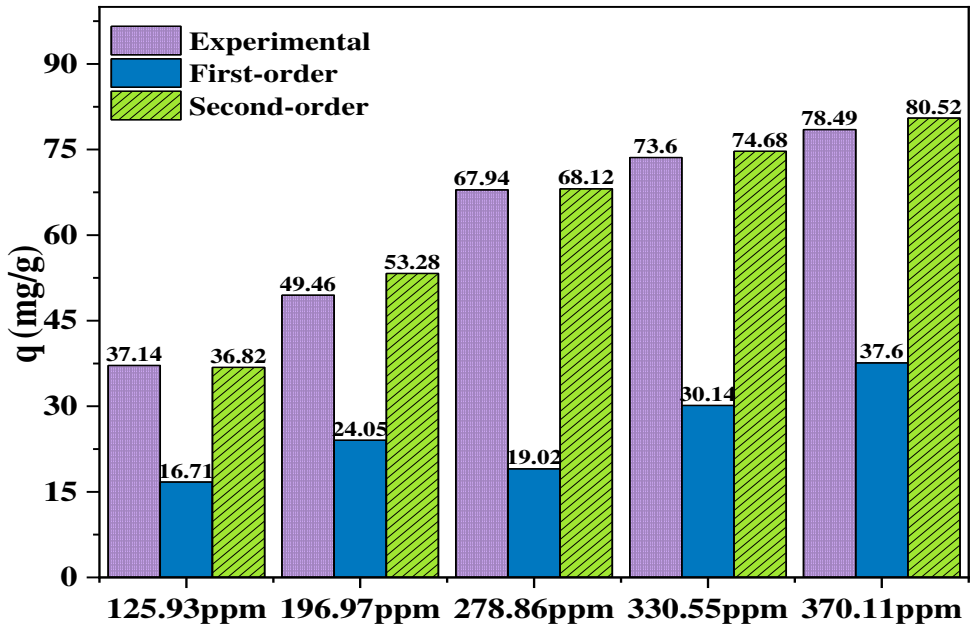

Figure 3.24 Comparison between experimental and calculated adsorption capacity of PNS

It is evident from the **Figure 3.24** that the calculated adsorption capacities were justified with the experimental values in case of Pseudo-Second-Order kinetic. Hence, it is comprehensible that Pseudo-Second-Order model was better fitted for Cr^{3+} adsorption on PNS compared to earlier model.

3.2.1.6. Thermodynamic analysis for Cr^{3+} adsorption

To recognize endothermic/exothermic nature of the adsorption process for Cr^{3+} adsorption on PNS was studied at different temperature. Batch experiments were performed at a series of temperatures to find out thermodynamic parameters, e.g., Gibbs free energy (ΔG), enthalpy (ΔH), and entropy (ΔS) by using equations (3.9), (3.10) and (3.11).

Table 3.23 Temperature, time and adsorption capacity data of PNS for Cr^{3+}ions adsorption

Time, t (min)	Adsorption Capacity (mg/g)			
	293K	308K	323K	338K
120	31.06	28.44	23.97	32.08
240	41.36	46.00	36.38	41.62
360	51.07	48.54	45.33	43.64
480	50.56	48.62	45.24	44.31
600	51.15	48.37	46.00	43.72

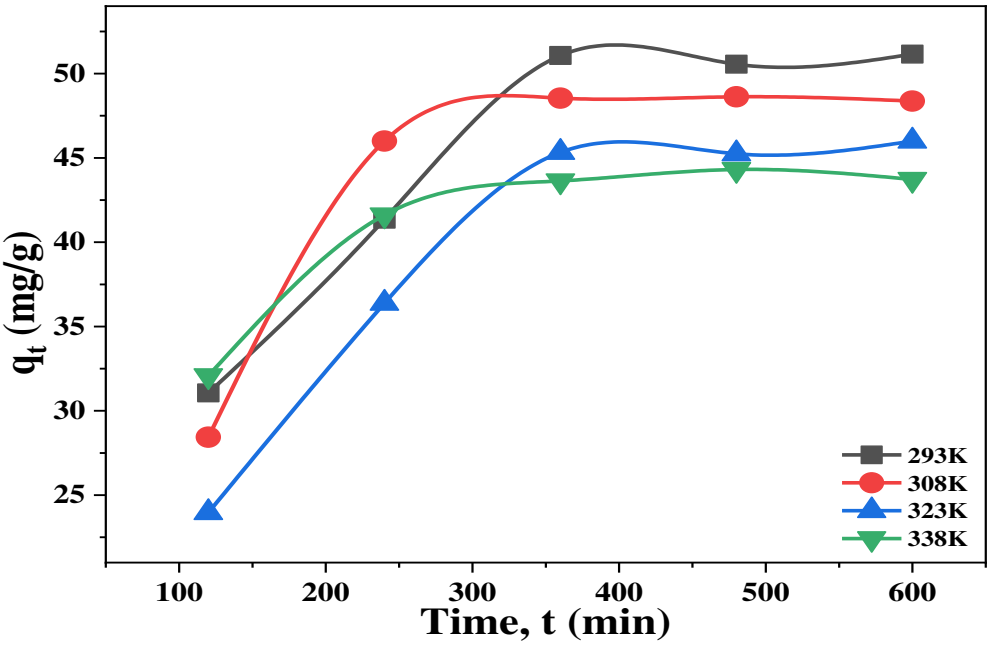

Figure 3.25 Temperature, time vs adsorption capacity data for Cr^{3+} ions adsorption

For this study, 63mg PNS was added in to 25 mL (151.03 ppm) of $Cr_2(SO4)_3.6H_2O$ solution at 5.0 pH for each experiment. The batch experiments were than shaken in a orbital shaker at 293K, 308K, 323K and 338K temperature for different time period ranging from 120-600 minutes. The impact of temperature and contact duration on adsorption capacity of PNS were studied and showed in **Table 3.23** and **Figure 3.25.**

With increased temperature, the adsorption capacity of PNS was declined. This is due to the fact as temperature rises, the kinetic energy increases and releases of the adsorbate from PNS. At 293K temperature the equilibrium adsorption capacity was 51.07 mgg^{-1}, which decreased to 48.54, 45.33, and 43.64 mgg^{-1} at 308K, 323K and 338K respectively.

Table 3.24 van't Hoff equation 1/T vs lnk_d data of PNS

1/T	0.0034	0.0032	0.003	0.0029
lnk_d	0.827	0.525	0.208	0.061

A straight line was acquired through a graph by plotting 1/T versus lnk_d (**Table 3.24, Figure 3.26**). The standard enthalpy (ΔH), and entropy (ΔS) was obtained from the slope and intercept and were -12.799 kJ/mol and -0.0366 kJ/mol (**Table 3.25**) respectively.

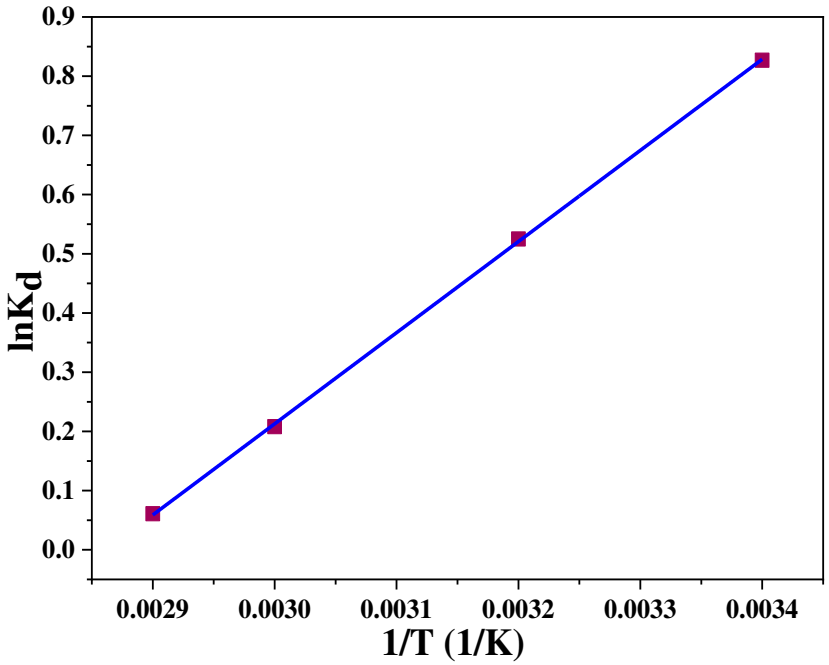

Figure 3.26 van't Hoff equation 1/T vs lnk_d plot of PNS for Cr^{3+} adsorption

Table 3.25 Thermodynamic parameters of PNS for Cr^{3+} adsorption

T(K)	ΔG (kJ/mol)	ΔH (kJ/mol)	ΔS (kJ/mol K)	R^2
293	-2.0156	- 12.799	- 0.0366	0.999
308	-1.345			
323	-0.559			
338	-0.171			

At the temperatures of 293K, 308K, 323K and 338K, the values of ΔG for Cr^{3+} adsorption on PNS were calculated to be -2.015, -1.345, -0.559 and -0.171 kJ/mole, correspondingly. The negative ΔG exposed that adsorption of Cr^{3+} on PNS was spontaneous and negative value of ΔH suggested exothermic in nature. Moreover, the negative ΔS exposed less randomness at the solid/solute interface throughout the adsorption of Cr^{3+} on PNS [295].

3.2.1.7. Plausible mechanism for Cr^{3+} adsorption on PNS

Sorption mechanism express the electrostatic interaction within oppositely ionized particles by means of various bond formations such as H-bonding, van der Waals force, dipole-dipole induction, ion-exchange and so on. Previous studies showed that functional groups like carboxyl, hydroxyl, methoxy, and phenolic groups exist in pyrolyzed peanut shell might bind and remove metallic ions and other contaminants from effluents [294-295]. In this study it is assumed that PNS contains hydroxyl group cellulose which is supposed to form hexa-coordinate complexes through arresting Cr^{3+} ions from solution (**Scheme 3.1**).

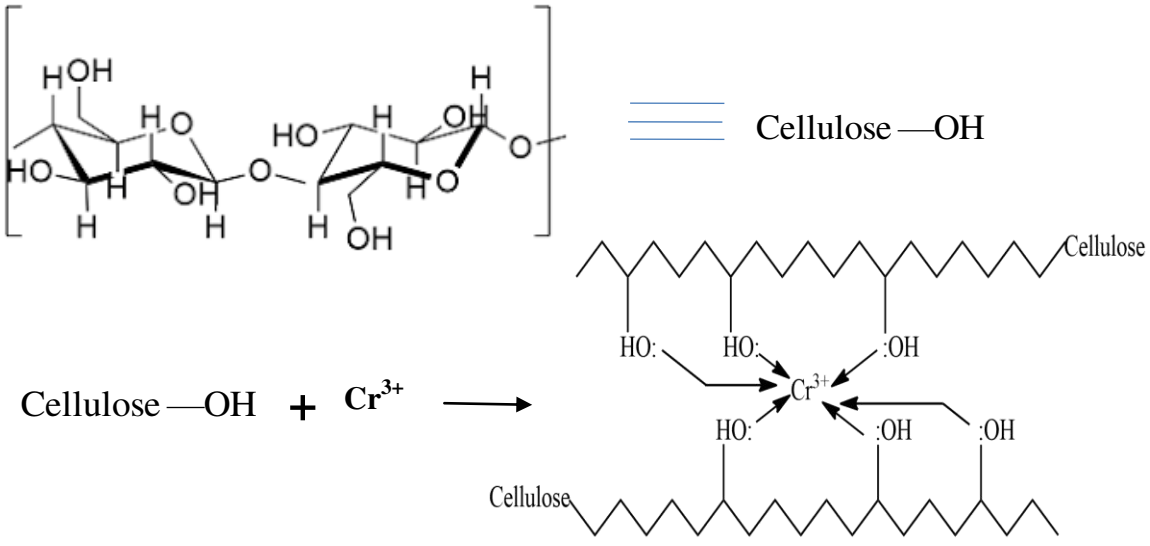

Scheme 3.1 Plausible mechanisms of Cr^{3+} adsorption on PNS

3.2.1.8. Regeneration of used PNS

The prospect of re-using PNS as adsorbent was investigated. Cr^{3+} laden PNS was regenerated using 1.0 M H_2SO_4 and NaOH solution four times which was shown in the **Flow chart 3.2.**

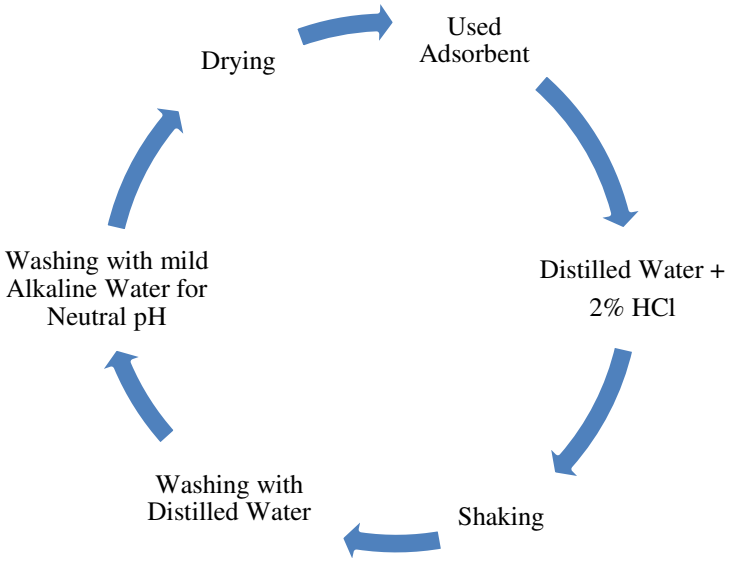

Flow chart 3.2 Flow diagram of regeneration of used PNS

Experimental pH, adsorbent dose and other parameters were at optimum level. The findings of regeneration trials are presented in **Figure 3.27** which demonstrates that adsorption capacity steadily dropped from 48.41 to 15.48 mg/g. It is clear that regenerated PNS can be reused to remove Cr^{3+} from aqueous solution.

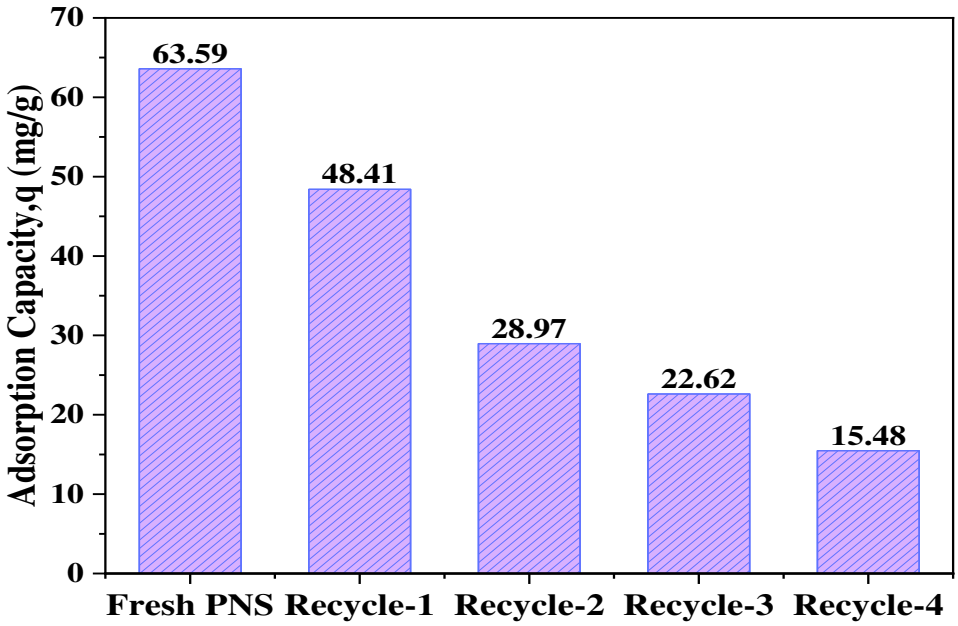

Figure 3.27 Adsorption capacities of regenerated PNS

3.2.1.9. Application of PNS on real sample (Tanning wastewater and tannery wastewater) for alleviation of pollution load

3.2.1.9.1. Application of PNS on tanning wastewater

After assessing the capabilities of PNS in removing Cr^{3+} from prepared $Cr_2(SO_4)_3.6H_2O$ solution by various batch experiments, the performance to remove chromium ions from real sample (Chrome tanning effluent) was verified. To observe the adsorption of Cr ions from concentrated Chrome tanning effluent, 15 g of PNS was added to 500 mL of Chrome tanning effluent and agitated at room temperature for 4 h at pH 5.0. The concentration of chromium before and after adsorption was analyzed by ICP-MS and other water quality parameter such as pH, TDS, EC, NaCl %, BOD_5, and COD were also tested, however the outcomes are showed in **Table 3.26.**

Table 3.26 Quality parameters of chrome tanning effluents before and after adsorption.

Parameters	**Before adsorption**	**After adsorption**	**% of removal**	**DoE/ECR Standard**
Cr (ppm)	3276.64	1092.74	66.63	2.0
Adsorption Capacity (mg/g)	-	72.79	-	-
pH	4.6	5.4	-	6.5-9.2
TDS (ppm)	11723	3803	67.56	2100
EC (µS/cm)	10637	3421	67.83	1200
NaCl (%)	8.5	3.63	57.29	
BOD_5 (ppm)	3273	1207	63.12	≤100
COD (ppm)	9632	3569	62.95	200-400

3.2.1.9.2. Application of PNS on tannery wastewater

To examine the performance of PNS with tannery effluent, 5 g of adsorbent PNS was applied to 500 mL of tannery effluent and shaken at room temperature for 4 hours at pH 5.0. The concentration of chromium before and after adsorption was determined by ICP-MS. Moreover, different water quality parameter like pH, TDS, EC, NaCl %, BOD_5, and COD were also tested, and the data are showed in **Table 3.27.**

Table 3.27 Quality parameters of tannery effluents before and after adsorption.

Parameters	Before adsorption	After adsorption	% of removal	DoE /ECR Standard
Cr (ppm)	423.28	68.58	83.79	2.0
Adsorption Capacity (mg/g)	-	35.47	-	-
pH	5.5	6.3	-	6.5-9.2
TDS (ppm)	7791	2576	66.94	2100
EC (µS/cm)	5348	1519	71.59	1200
NaCl (%)	4.2	1.5	64.28	-
BOD_5 (ppm)	2207	578	73.81	≤100
COD (ppm)	4278	1286	69.93	200-400

3.2.1.9.3. Discussion on real sample analysis

Obtained results indicate (**Table 3.26**, **Table 3.27**) that after adsorption, the % of chromium removal was 66.63% and 83.79% but the adsorption capability was 72.79 and 35.47 mg/g in case of Chrome tanning effluents and tannery effluents respectively. In case of tannery effluent, adsorption capacity was much lower compare to prepared solution that could be due to the existence of different matrices or ions that were being used in leather manufacturing which decrease the capacity of the PNS [298]. On the other hand, after adsorption by PNS the water quality parameters (pH, TDS, EC, NaCl %, BOD_5, and COD) of collected Chrome tanning and tannery effluents were also reduced significantly.

3.2.2. Chemically activated peanut shell (NS)

3.2.2.1. Preparation of NS

Collected peanut shells were washed and dried initially and then chemically activated with analytical grade NaOH (25%) with stirring and left for 24 hours. The products were then cleaned with distilled water and dried in an air oven at 110-115 ^{O}C. The activated dried peanut shell (NS) were powdered and employed in the research.

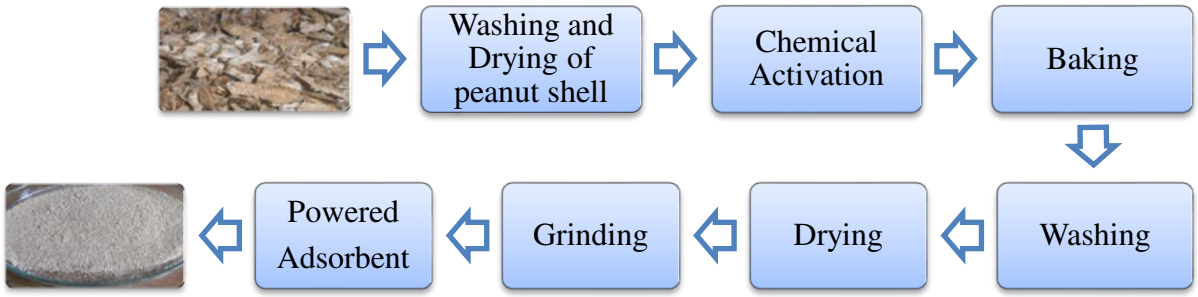

Flow chart 3.3 Flow diagram of NS preparation

3.2.2.2. Characterization of NS

3.2.2.2.1. Elemental analysis of NS

In order to analyze the elements of adsorbent NS before and after Cr^{3+} adsorption, EDX analysis was conceded**. Figure 3.28** revealed that the chemical composition of NS before and after Cr(III) adsorption were mainly carbon, oxygen, phosphorus, sulfur, potassium, and calcium.

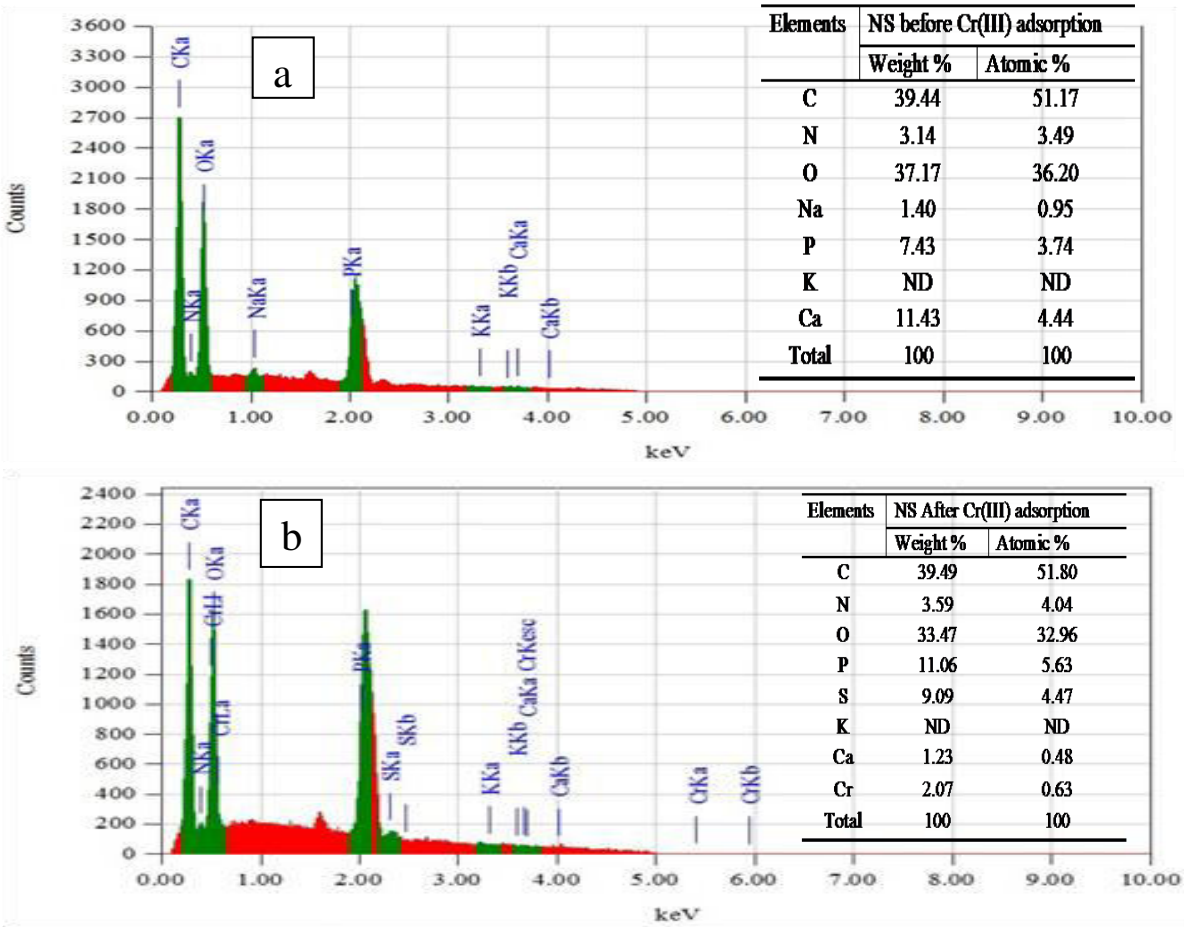

Elements	NS before Cr(III) adsorption	
	Weight %	Atomic %
C	39.44	51.17
N	3.14	3.49
O	37.17	36.20
Na	1.40	0.95
P	7.43	3.74
K	ND	ND
Ca	11.43	4.44
Total	100	100

Elements	NS After Cr(III) adsorption	
	Weight %	Atomic %
C	39.49	51.80
N	3.59	4.04
O	33.47	32.96
P	11.06	5.63
S	9.09	4.47
K	ND	ND
Ca	1.23	0.48
Cr	2.07	0.63
Total	100	100

Figure 3.28 Energy dispersive X-ray (EDX) spectrum of NS (a) before and (b) after Cr(III) adsorption.

Moreover, chromium was included after adsorption process. In spectrum (a), the quantity of Cr was 0.00, while in spectrum (b), the values was 2.07 in weight % and 0.63 was in atomic %, which imply Cr(III) adsorption on to NS.

3.2.2.2.2. FTIR analysis of NS

The FTIR spectral analysis is very important for identification of the distinctive functional groups, which are accountable for adsorption of metal ions.

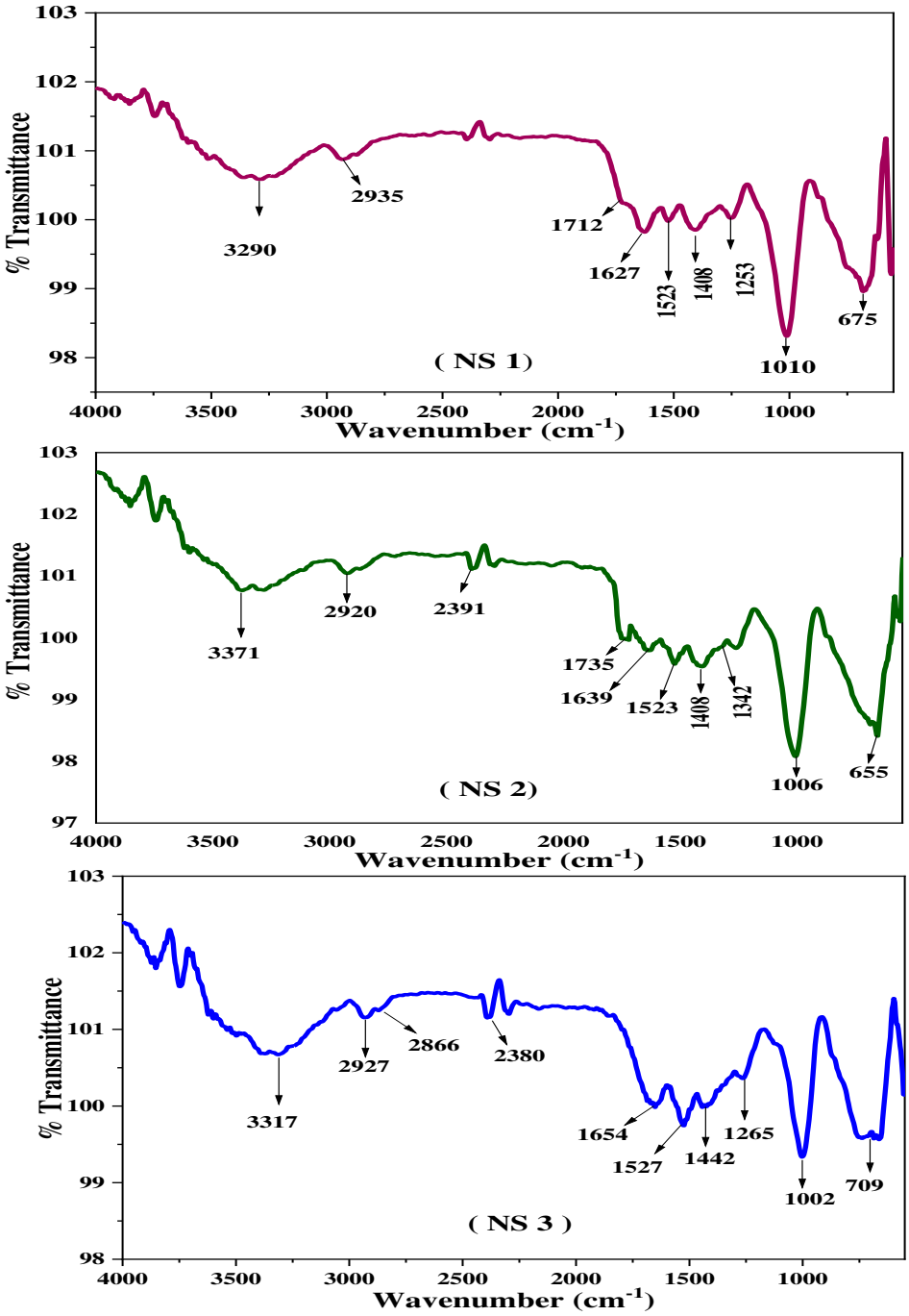

Figure 3.29 FTIR spectra of NS-1 (Dried nutshell), NS-2 (NaOH activated nutshell), and NS-3 (Cr(III) loaded NaOH activated nutshell).

Generally peanut shell is composed of lignin, cellulose and hemicelluloses. FTIR spectroscopy was utilized to assess the vibrational changes in NS after chemical activation and adsorption processes. **Figure 3.29** shows that after activation and adsorption, several functional groups migrated to a new frequency level or disappeared [286]. In the FTIR spectra of NS-1, NS-2, and NS-3, the existence of –OH groups led to the observation of broad peaks at 3290, 3371, and 3317 cm^{-1} respectively. Peaks at 1712, and 1735 cm^{-1} indicating that –C=O groups were also exist in IR spectra. C-H stretching vibrations were observed at 2935 cm^{-1} in NS-1; 2920 cm^{-1} in NS-2 and 2927 cm^{-1} and 2866 cm^{-1} in NS-3.

3.2.2.2.3. Scanning Electron Microscopic (SEM) of NS

Surface morphology of NaOH activated NS was investigated by means of SEM at the magnification power (500 x and 1500 x). The SEM image of activated NS shown in **Figure 3.30** demonstrates that it has cavities, rough, heterogeneous structure, and lamellar features which make possible the adsorption of metal ions [179].

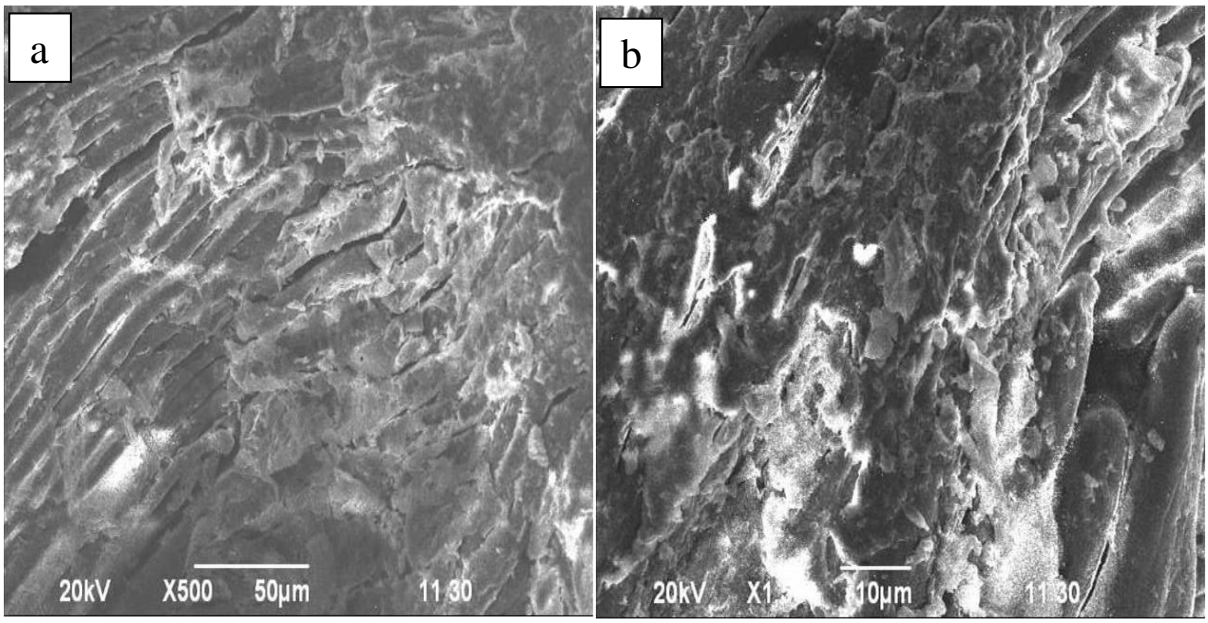

Figure 3.30 SEM images of NS (a) 500x, and (b) 1500x magnification

3.2.2.2.4. X-Ray diffraction (XRD) analysis of NS

There was no distinct peak associated with the crystalline phase in the XRD pattern. It illustrates a characteristic peak of carbonaceous compound. A bump in the range of $2\theta = 20 - 30°$ and a peak at $2\theta = 22.11°$ was perceived (**Figure 3.31**) because of amorphous structure with a high degree of disorder of NS. The broad and weak peaks in the XRD pattern of NS suggests the existence of amorphous carbon [288].

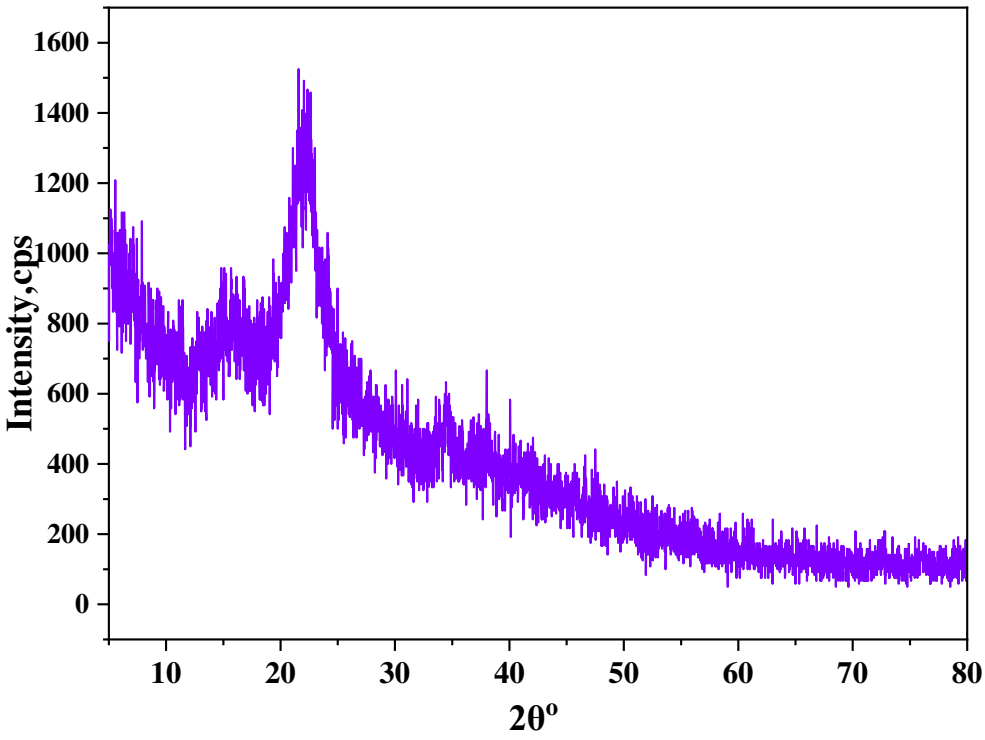

Figure 3.31 XRD analysis of NS

3.2.2.2.5. Brunauer-Emmett-Teller (BET) analysis of NS

Surface area, pore volume, and pore diameter of NS were investigated by nitrogen gas sorption system are presented in **Table 3.28**. Chemically activated NS had low surface area of 10.14 m^2/g may be because of the breakdown of cell walls [289]. Average pore diameter of NS was calculated following Barrett-Joiner-Halenda (BJH) method and the value was 57.54 Å, which indicate that NS consists of mesopores [193].

Table 3.28 BET surface area and porosity of NS

Sl. No.	Parameter	Result
01.	BET Specific Surface Area using multi-point analysis (m^2/g)	10.14
02.	Total Pore Volume (cc/g)	0.0146
03.	Skeletal density (g/cc)	0.7711
04.	Porosity based on skeletal density (per gram of sample)	0.0111
05.	Average Pore Diameter, (Å)	57.54

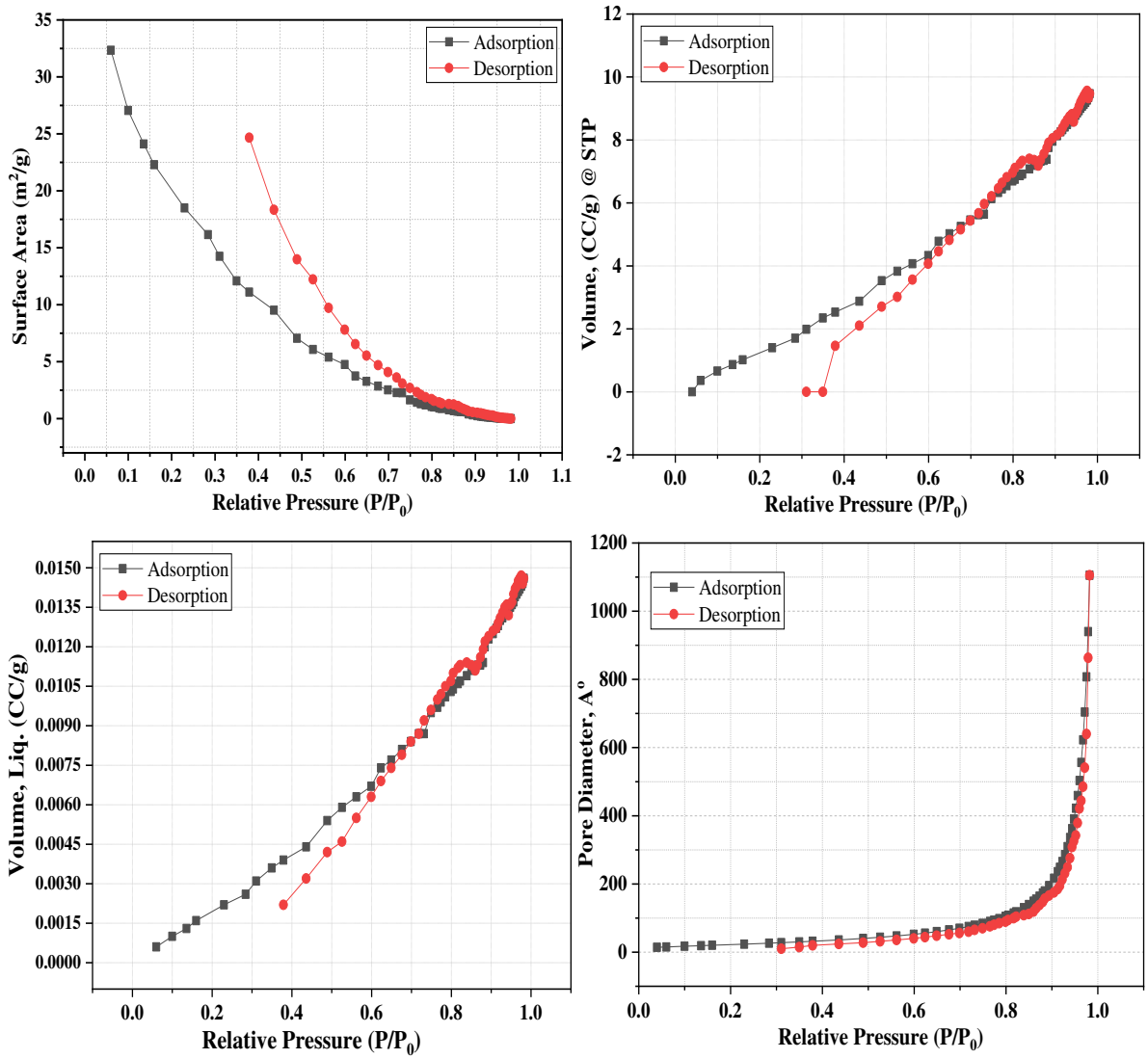

Figure 3.32 Adsorption and desorption isotherms of BET to NS

3.2.2.2.6. Zeta potential value of NS

Zeta potential value (ZPV) was investigated for adsorbent NS by dispersing in deionized water with the pH range of 3.0-5.0. The results revealed (**Table 3.29** and **Figure 3.33**) that that ZPV of NS was positive (7.08 mV) at 3.0 pH and (3.82 mV) at 3.5 pH, while the values were negative (-3.74 to -18.2 mV) at pH 4.0 to 5.0.

Table. 3.29 pH vs Zeta potential data of NS

pH	3	3.5	4	4.5	5
ZPV (mV)	7.08	3.82	-3.74	-10.3	-18.2

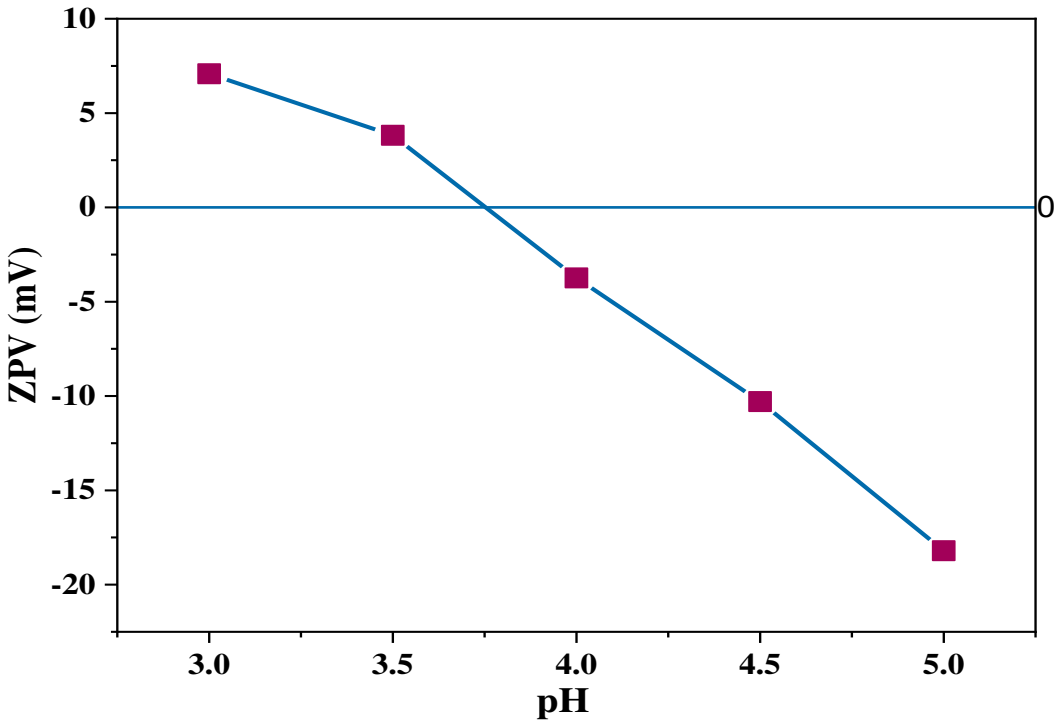

Figure 3.33 ZPV of NS at different pH

3.2.1.3. Adsorption Cr(III) ions on NS

3.2.2.3.1. Effect of pH on adsorption capacity of NS for Cr^{3+} adsorption

The pH of metal ions solutions is a vital factor to control the adsorption process as it disassociates the groups present on the surface hence change the surface charge of adsorbent. The impact of pH on Cr^{3+} ions adsorption through NS was analyzed with 256.53 ppm solution of $Cr_2(SO4)_3.6H_2O$ by varying it in the range of 3.0 to 5.0. In the experiment 63 mg NS were added in each solution (25 mL) and the mixtures were shaken at 160 rpm for 4 hours. After filtering the solutions any change in Cr(III) ions concentrations were determined by UV-Vis spectroscopy. It is evident from the **Table 3.30** and **Figure 3.34** that adsorption capacity of NS was raised at higher pH of solution and the highest capacity was 57.82 mg/g at pH 5.0.

Table 3.30 pH v/s adsorption capacity data of NS for Cr^{3+} adsorption

pH	3	3.5	4	4.5	5
Adsorption Capacity (mg/g)	31.82	40.77	45.92	48.53	57.82

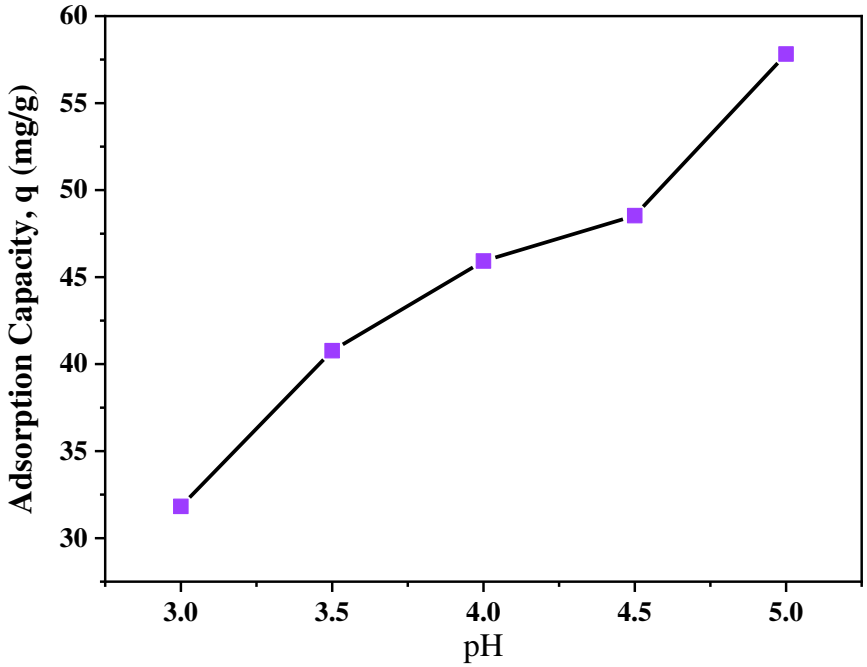

Figure 3.34 Effect of pH for Cr^{3+} ions adsorption

It is assumed that the ion exchange (which was evident from the EDX analysis **Figure 3.28)** and hydrogen bonding could be the principle mechanism to remove heavy metals [290]. At 3.0 pH the adsorption capabilities was low, because of the same positive charge of H^+ and metal ions with similar adsorption site. While, at pH 4.0 – 5.0, the smaller amount of protons and more negative charges ensuing more Cr(III) adsorption. The surface negativity of NS was enhanced at higher pH (**Figure 3.34).**

$$—ROH \underset{\text{At Lower pH}}{\overset{\text{At Higher pH}}{\rightleftharpoons}} —R\bar{O} + H^+$$

In this research, batch experiments were performed at 5.0 pH to acquire highest adsorption capacity in addition to avoid precipitation [291]. Moreover, at pH >6 Cr^{3+} can be precipitated from the aqueous solution as $Cr(OH)_3$ [292]. The results agreed with previous literature [237] and Cr speciation (**Figure 1.1**).

3.2.2.3.2. Effect of adsorbent dosage on adsorption capacity and % of removal

Impact of adsorbent dosage on Cr^{3+} adsorption was analyzed by applying different dosage from 1.5 to 4.0 g/L to find out optimum dose. The batch experiments were conducted with 240.57 ppm initial concentration for 4 hours at optimum pH 5.0. It is observed from **Table 3.31,** and **Figure 3.35,** that removal % of Cr^{3+} was increased 44.56 to 74.18 % whereas adsorption capacity was decreased 71.46to 44.61 mg/g with the increase of PNS dosage.

Table 3.31 Dosage v/s adsorption capacity and % removal data of NS

Dosage (g/L)	1.5	2	2.5	3	3.5	4
Adsorption Capacity (mg/g)	71.46	58.81	54.35	50.77	48.07	44.61
Removal (%)	44.56	48.89	56.94	63.304	69.96	74.18

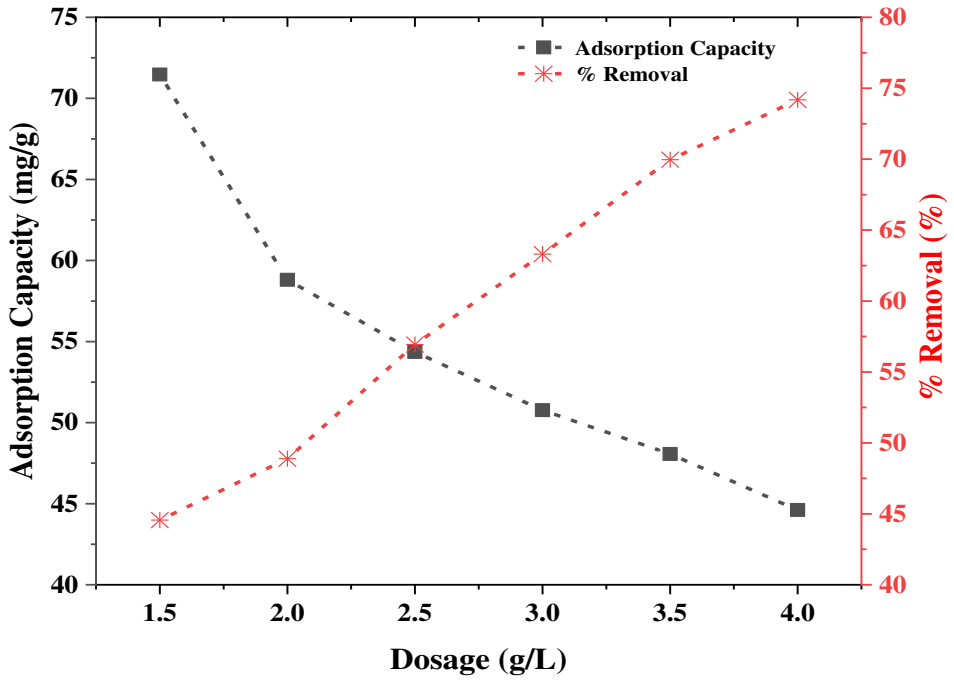

Figure 3.35 Effect of NS Dosage on adsorption capacity and % removal

The availability of more adsorption sites is responsible to enhance the % removal of Cr^{3+}, but more unsaturated sites reduces adsorption capability with increased adsorbent dosage [299]. It was evident that at dose 2.5 g/L showed the best % removal also best adsorption capacity and were maintain all over the study.

3.2.2.3.3. Effect of Cr^{3+} ions concentrations and contact time

To investigate the effect of Cr^{3+} ions concentrations and contact time on adsorption capacity of NS, 25 mL solutions of five different concentrations (125.93, 175.28, 196.97, 240.57, 278.86 ppm) were taken in conical flasks and 63 mg (2.5 g/L) NS was added in to conical flask each. The study was executed at 5.0 pH by several time intervals ranging from 5-600 minutes at 160 rpm shaking speed. The outcome (**Table 3.32, Figure 3.36)** revealed that adsorption capacity increased with increasing duration until it reached at equilibrium and after then, there was no remarkable increase in adsorption capacity.

Table 3.32 Time vs adsorption capacity data of NS for Cr^{3+} ions adsorption

Time (min)	125.93 ppm	175.28 ppm	196.97 ppm	240.57 ppm	278.86 ppm
0	0	0	0	0	0
5	16.88	13.079	16.63	16.46	20.42
15	23.89	17.642	16.965	18.988	21.61
30	25.32	18.063	20.59	30.976	22.37
60	27.18	21.273	22.95	31.059	22.54
120	30.22	27.519	27.26	31.817	24.56
240	31.06	30.134	29.71	35.365	32.58
360	31.82	37.563	40.345	39.837	41.36
480	32.41	39.33	40.936	44.059	47.52
600	32.83	39.587	41.442	44.309	47.61

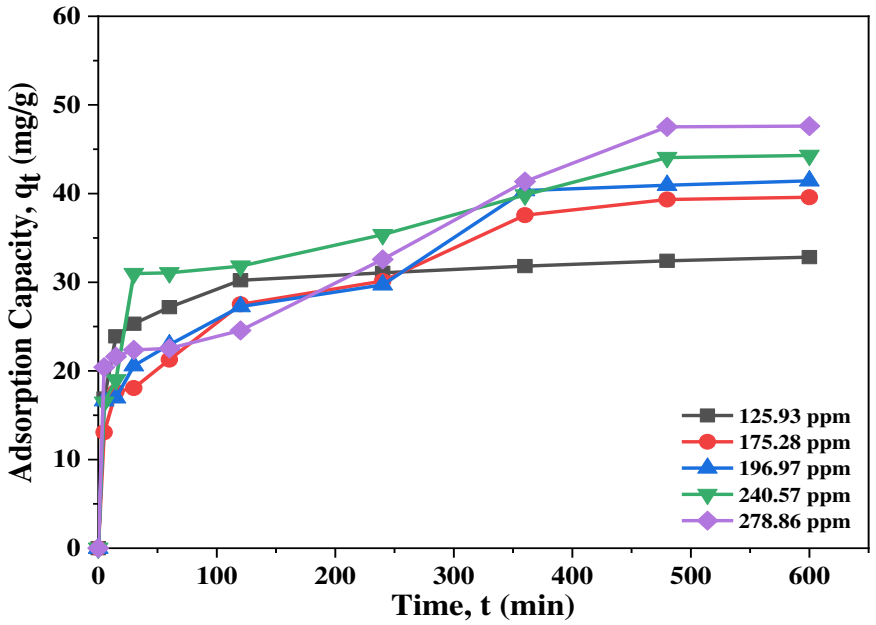

Figure 3.36 Effect of Cr^{3+} ions concentrations and contact time on adsorption capacity of NS

It was found that approximately after 360 minutes adsorption capacity reached at equilibrium condition. It was also showed that adsorption capacity was enhanced with higher metal ion concentration. At an initial Cr^{3+} concentration of 125.93 ppm, the adsorption capacity was

31.82 mg/g whereas at 175.28, 196.97, 240.57, and 278.86 ppm concentration, adsorption capacity were 39.33, 40.93, 44.06, and 47.52 mg/g respectively. The obtained top most adsorption capacity was 47.52 mg/g in case of 278.86 ppm concentration.

Since, initially there were more active sites available, but after certain time these sites got saturated [141], [203]. Moreover, the equilibrium adsorption capacity was also enhanced with more Cr^{3+} ion concentration. It is due to the gradient of concentration between the Cr^{3+} ion in bulk solution and adsorbent surface, which causes mass transfer within aqueous and solid phase [218].

3.2.2.4. Adsorption isotherms for Cr^{3+} adsorption on NS

Langmuir and Freundlich isotherms are generally used to justify the correlation between the quantity of adsorbate adsorbed on the adsorbent surface. In Langmuir isotherm, the adsorbate is assumed to be absorbed on the adsorbent in a monolayer on well-defined with no intermolecular interactions. However, Freundlich isotherm exposes multilayer adsorption also suggests non-uniform distribution.

3.2.2.4.1. Langmuir isotherm

The Langmuir isotherm model was exercised by equation (3.4) plotting C_e/q_e versus C_e (**Table 3.33, Figure 3.37**). A linear relation within C_e/q_e and C_e was observed with acceptable regression factor (R^2=0.997). Maximum adsorption capacity q_m (theoretical), was calculated from the slope and found 58.24 mg/g. The separation factor R_L provides information of qualitative measure of the favorability, R_L >1indicates unfavorable adsorption while 0< R_L<1 indicates favorable process. In this study, R_L was calculated by equation (3.5) and the value was 0.1211 which approving monolayer adsorption process [293] .

Table 3.33 C_e vs C_e/q_e data of NS at different concentration for Cr^{3+} adsorption

Initial concentration (ppm)	125.93	175.28	196.97	240.57	278.86
Equilibrium concentration (C_e)	45.73	76.16	93.81	129.54	159.11
C_e/q_e	1.437	1.936	2.292	2.940	3.346

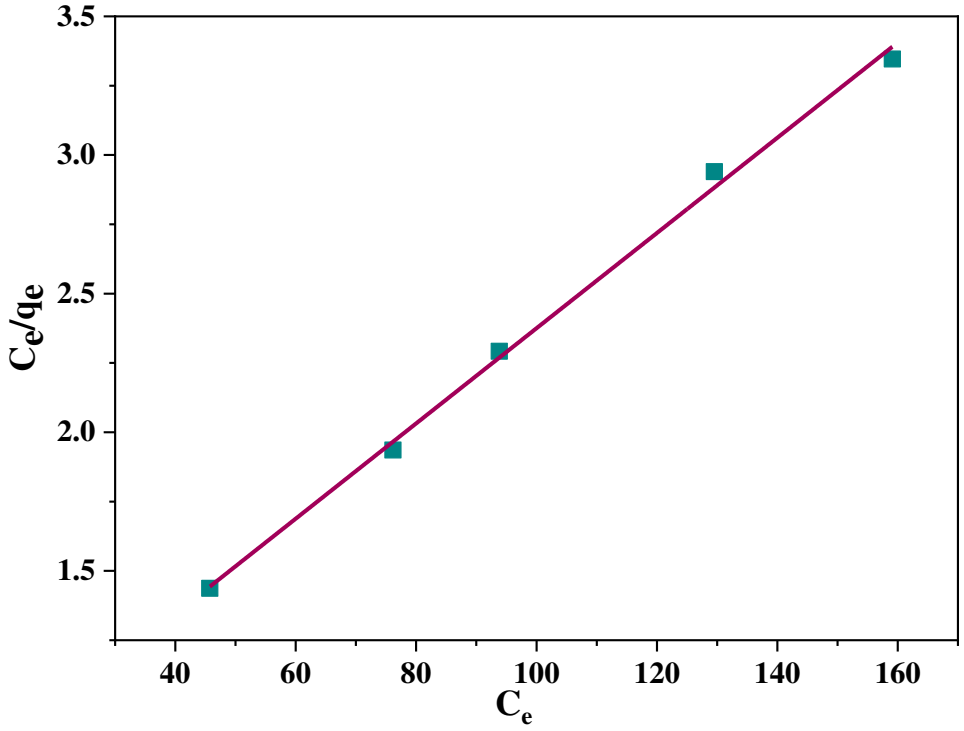

Figure 3.37 Langmuir isotherm for Cr^{3+} adsorption on NS

3.2.2.4.2. Freundlich isotherm

Freundlich isotherm equation (3.6) was implied to justify multilayer adsorption mechanism by plotting a graph of lnC_e versus lnq_e (**Table 3.34, Figure 3.38**) and linear relationship was observed with good regression coefficient, R^2= 0.978. From the slope n was calculated and found to be 3.24 which expressed good adsorption process [208]. Usually since n decreases, adsorption becomes more difficult (n= 2-10 denotes good adsorption, n= 1-2 difficult adsorption and n<1 poor adsorption) [294].

Table 3.34 lnC_e vs lnq_e data of NS at different concentration for Cr^{3+} ions adsorption

Initial concentration (ppm)	125.93	175.28	196.97	240.57	278.86
lnC_e	3.823	4.333	4.541	4.864	5.069
lnq_e	3.46	3.672	3.712	3.786	3.861

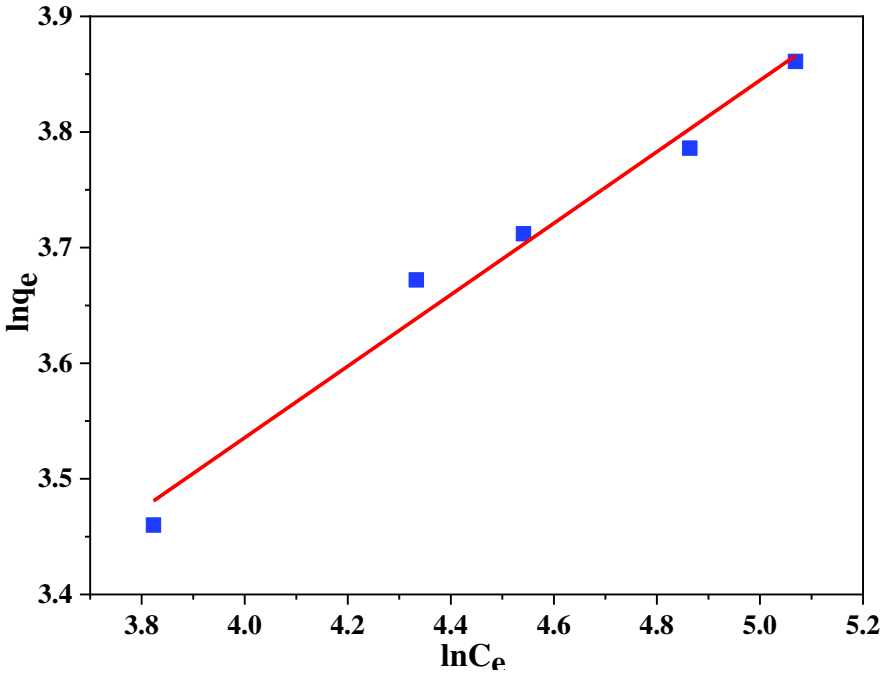

Figure 3.38 Freundlich isotherm for Cr^{3+} adsorption on NS

3.2.2.4.3. Rationalization on isotherms for Cr^{3+}adsorption

The results of different parameters of two isotherm models signify (**Table 3.35**) that adsorption of Cr^{3+}on NS obeyed both isotherm but preferably Langmuir model.

Table 3.35 Values of q_m, b, R_L, n, k_F and R^2 of adsorbent NS

Parameters	q_m (mg/g)	b (Lmg^{-1})	R^2	R_L	n	k_F
Langmuir isotherm	58.24	0.026	0.997	0.1211	-	-
Freundlich isotherm	-	-	0.978	-	3.24	9.966

3.2.2.5. Adsorption kinetics for Cr^{3+} adsorption on NS

The adsorption kinetics is significant to explore how quickly ions travel from liquid to solid phase and how long it takes to accomplish equilibrium condition. In this study, Pseudo-First-Order and Pseudo-Second-Order kinetic models were used to justify the adsorption process.

3.2.2.5.1. Pseudo-first-order kinetic for Cr^{3+} adsorption

The Pseudo-First-Order kinetic equation (3.7) was introduced by Lagergren in 1898 to illustrate the adsorption process. The model was obtained by plotting a graph with $\log(q_e-q_t)$

against t (**Table 3.36, Figure 3.39**) where a linear affiliation was observed among $\log(q_e-q_t)$ and t.

Table 3.36 Time, t(min) and $\log(q_e-q_t)$ data of NS at different concentration

Time, t(min)	$\log(q_e-q_t)$ at 125.93 ppm	$\log(q_e-q_t)$ at 175.28 ppm	$\log(q_e-q_t)$ at 196.97 ppm	$\log(q_e-q_t)$ at 240.57 ppm	$\log(q_e-q_t)$ at 278.86 ppm
5	1.174	1.419	1.386	1.441	1.433
15	0.899	1.336	1.379	1.399	1.413
30	0.813	1.328	1.308	1.117	1.400
60	0.666	1.257	1.255	1.114	1.398
120	0.204	1.072	1.136	1.087	1.361
240	-0.119	0.964	1.027	0.939	1.174
360	-	0.248	-0.228	0.626	0.789

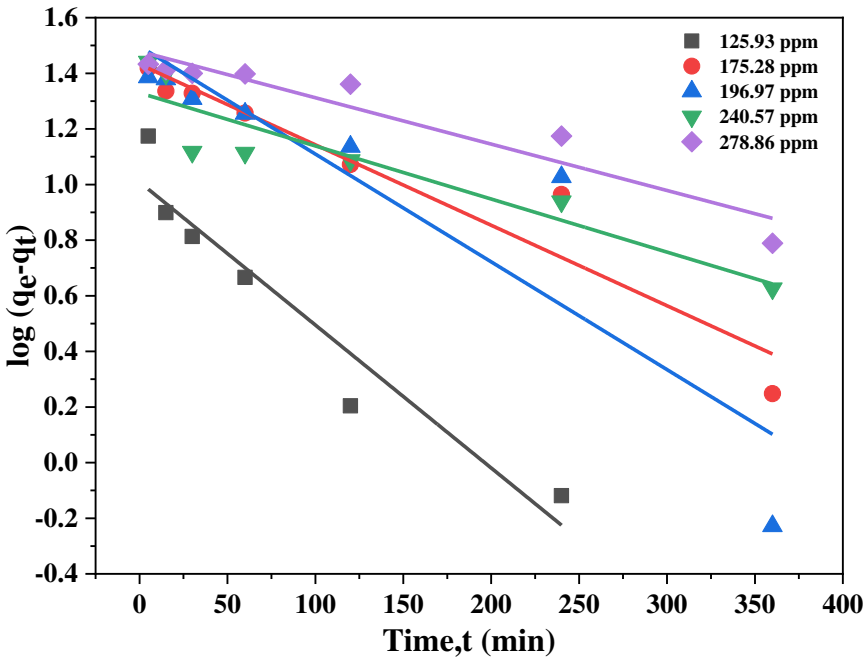

Figure 3.39 Pseudo-First-Order kinetic for Cr^{3+} adsorption on NS

3.2.2.5.2. Pseudo-second-order kinetic for Cr $^{3+}$ adsorption

In 1999 Ho and Mckay authenticated Pseudo-Second-Order rate reaction (3.8), and the model was gained with a graph by plotting t/q_t versus t (**Figure 3.40**).

Table 3.37 Time, t(min) and t/q_t data of NS at different concentration

Time, t(min)	t/q_t at 125.93 ppm	t/q_t at 175.28 ppm	t/q_t at 196.97 ppm	t/q_t at 240.57 ppm	t/q_t at 278.86 ppm
5	0.296	0.382	0.301	0.304	0.245
15	0.628	0.851	0.884	0.789	0.694
30	1.185	1.661	1.457	0.968	1.341
60	2.208	2.82	2.614	1.932	2.662
120	3.971	4.361	4.344	3.772	4.886
240	7.727	7.964	8.078	6.786	7.366
360	11.314	9.584	8.923	9.037	8.704
480	-	12.203	-	10.894	10.1

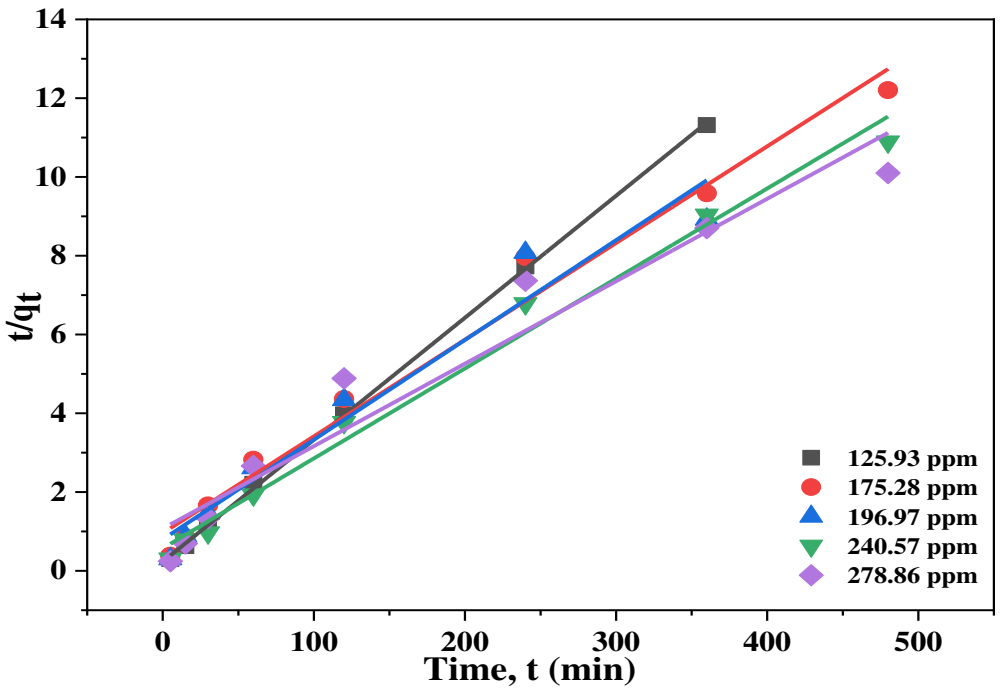

Figure 3.40 Pseudo-Second-Order kinetics for Cr^{3+} adsorption on NS

3.2.2.5.3. Clarification on kinetics for Cr^{3+} adsorption on NS

The kinetics parameters are calculated and expressed in **Table 3.38** from the slop and intercept of each linear plot**.**

Table 3.38 Kinetics parameter for Cr^{3+} adsorption on NS

Kinetics model	Parameters	125.93 ppm	175.28 ppm	196.97 ppm	240.57 ppm	278.86 ppm
Pseudo-First-Order	q_e^* (mg g^{-1})	31.82	39.33	40.94	44.06	47.52
	k_1(1/min)	0.0118	0.00645	0.0087	0.0044	0.0037
	R^2	0.923	0.924	0.822	0.861	0.914
	q_e^{**} (mgg^{-1})	10.21	27.05	31.41	21.33	30.13
Pseudo-Second-Order	k_2 (g/mg min)	0.0041	0.00063	0.00059	0.00091	0.0004
	R^2	0.999	0.980	0.955	0.987	0.942
	q_e^{**} (mg g^{-1})	32.36	40.82	42.55	43.86	47.85

* Experimental, **Theoretical

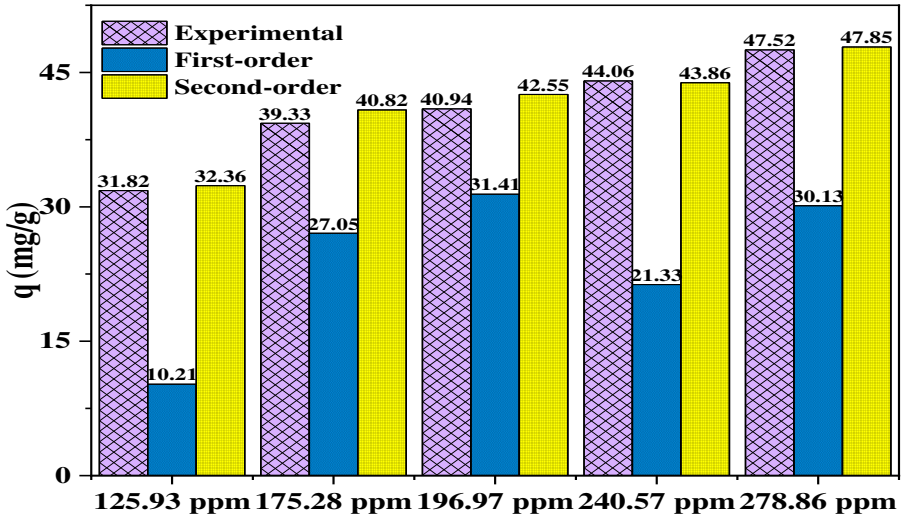

Figure 3.41 Comparison between experimental and calculated adsorption capacity

The linear fitting results of the two models signified that in case of pseudo-second-order model the theoretical q_e values approved with the experimental q_e values. It was also established that the correlation coefficient (R^2) value of pseudo-second-order kinetic model was better compare to Pseudo-first-order kinetic model. The results from the **Figure 3.41** prove that the calculated adsorption capacities were in good concurrence with the experimental values in case of Pseudo-second-order kinetics. Hence, it is logical that Pseudo-second-order model was well justified for Cr^{3+} adsorption on NS compared to previous model.

3.2.2.6. Thermodynamic analysis

To verify the adsorption nature of Cr^{3+} on NS in response to temperature whether the adsorption process either endothermic or exothermic was also studied at different temperature. Batch experiments were conducted at a range of temperatures to find out thermodynamic parameters, e.g., Gibbs free energy (ΔG), enthalpy (ΔH), and entropy (ΔS) using equations (2.9), (2.10) and (2.11).

Table 3.39 Temperature and time vs adsorption capacity data of NS for Cr^{3+} ions adsorption

Time, t (min)	Adsorption Capacity (mg/g)			
	293K	**308K**	**323K**	**338K**
60	21.36	17.05	17.64	19.24
120	28.36	25.33	24.23	21.69
240	36.46	33.35	30.05	28.87
360	41.62	39.76	37.73	36.04
480	41.53	39.59	37.56	35.79
600	41.69	39.67	37.48	35.54

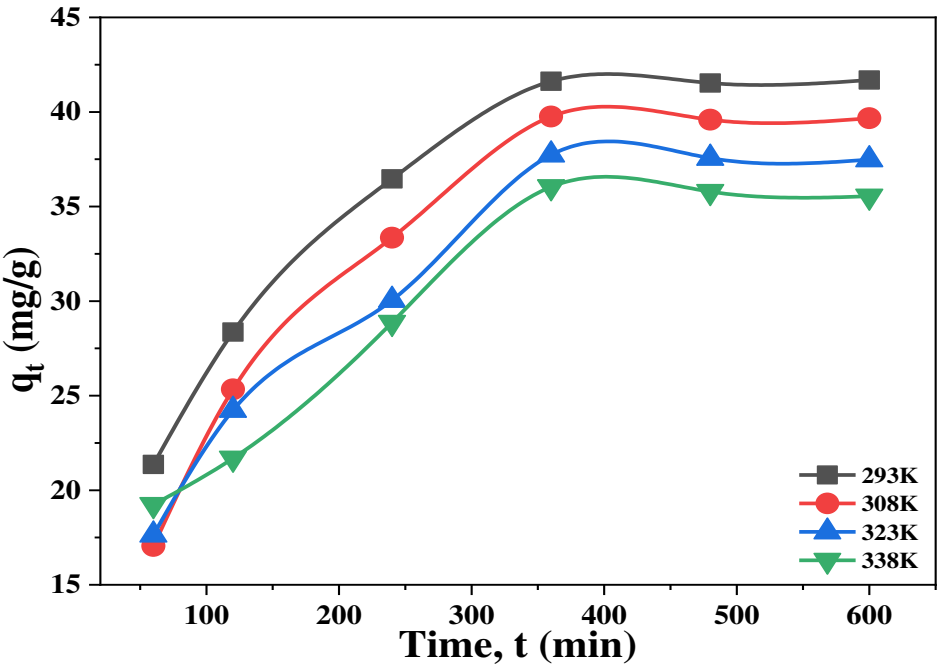

Figure 3.42 Temperature, time vs adsorption capacity data of NS

In this study, 63 mg (2.5 g/L) NS was added in to 25 mL (125.72 ppm) of $Cr_2(SO4)_3.6H_2O$ solution at 5.0 pH for each experiment. The batch experiments were than shaken in an orbital shaker at 293K, 308K, 323K and 338K temperature for different time period ranging from 60-600 min. The impact of temperature and contact duration on adsorption capacity of NS were analyzed and presented in **Table 3.39** and **Figure 3.42.**

With increased temperature, the adsorption capacity of NS was decreased [300]. Fact is that, when temperature raises, the kinetic energy increases and releases of the adsorbate from NS. At 293K temperature the equilibrium adsorption capacity was 41.62 mg/g which decreased to 39.76, 37.73, and 36.04 mg/g at 308K, 323K and 338K respectively.

Table 3.40 van't Hoff equation 1/T vs lnk_d data of NS for Cr^{3+} adsorption

1/T	0.0034	0.0032	0.003	0.0029
lnk_d	0.691	0.443	0.208	0.033

A straight line was obtained through a graph by plotting 1/T versus lnk_d (**Table 3.40, Figure 3.43**). The standard enthalpy (ΔH), and entropy (ΔS) was achieved from the slope and intercept and were - 10.699kJ/mol and - 0.031kJ/mol (**Table 3.41**) respectively.

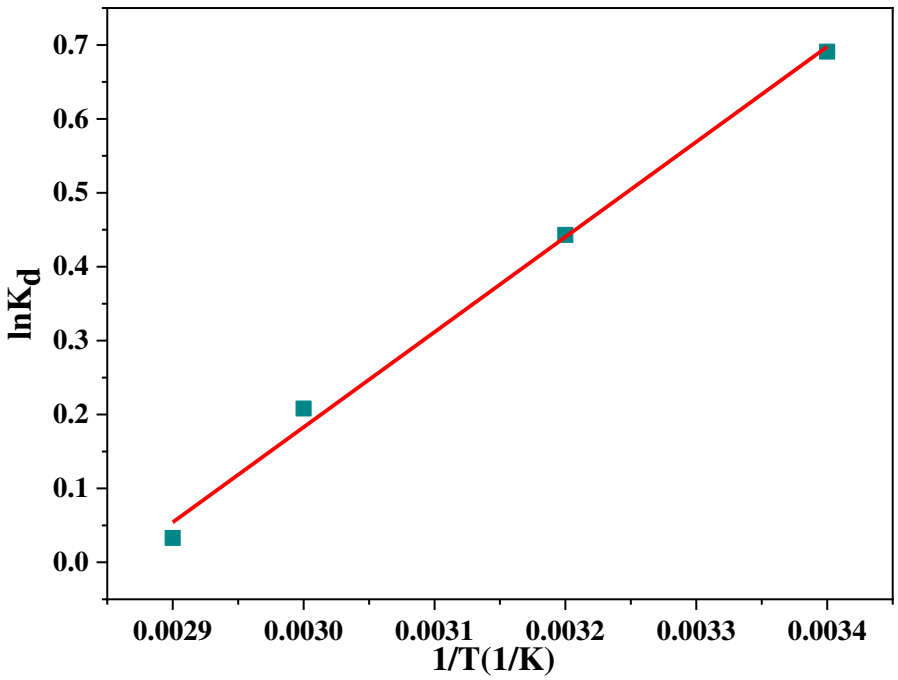

Figure 3.43 van't Hoff equation 1/T vs lnk_d plot of NS for Cr^{3+} adsorption

Table 3.41 Thermodynamic parameters of NS for Cr^{3+} adsorption

T(K)	ΔG (kJ/mol)	ΔH (kJ/mol)	ΔS (kJ/mol K)	R^2
293	-1.683	- 10.699	- 0.031	0.995
308	-1.134			
323	-0.559			
338	-0.093			

The values of ΔG for adsorption of Cr^{3+} on NS at the temperatures of 293K, 308K, 323K and 338K were found to be -1.683, -1.134, -0.559, and -0.093 kJ/mole, correspondingly. The negative ΔG suggests that adsorption of Cr^{3+} on NS was spontaneous and negative ΔH imply the exothermic nature of process. Moreover, the negative ΔS signify the reduction in randomness at the solid/solute interface during the adsorption of Cr^{3+} on NS [295].

3.2.2.7. Plausible mechanism for Cr^{3+} adsorption on NS

Sorption mechanism related with electrostatic interaction among oppositely charged particles through different bond formations for instance H-bonding, van der Waals force, dipole-dipole induction, and ion-exchange. It was proven from earlier investigation that the functional groups such as carboxyl, hydroxyl, methoxy, and phenolic groups exist in peanut shell could attach and remove Cr-ions and the other pollutants from wastewater [294, 295]. It is assumed that NS contains hydroxyl groups cellulose which are supposed to form hexa-coordinate complexes with Cr^{3+} ions from solution (**Scheme 3.2**).

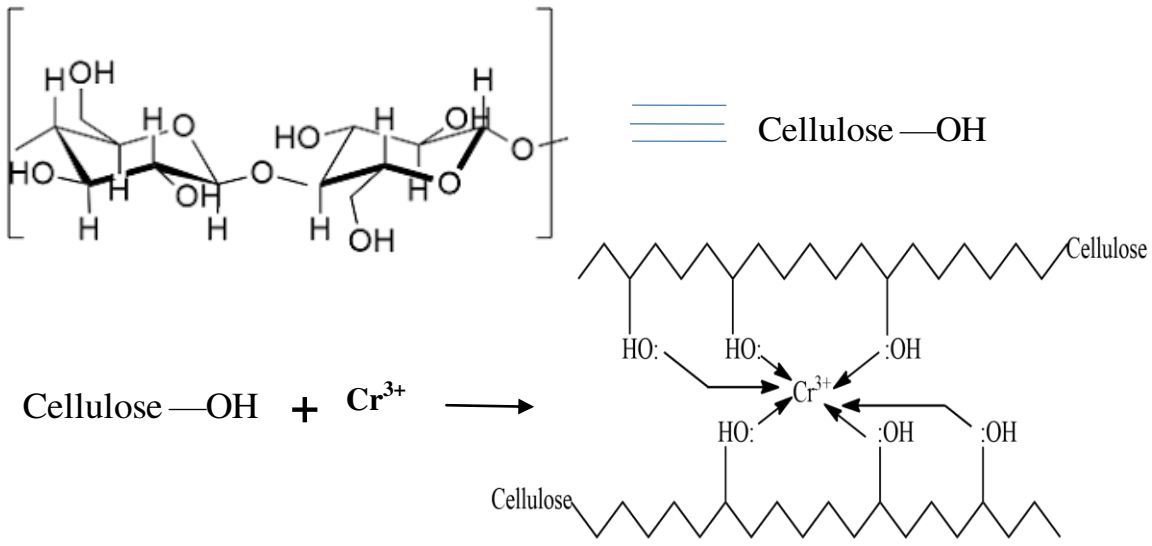

Scheme 3.2 Plausible mechanisms of Cr^{3+} adsorption on NS

3.2.2.8. Regeneration of used NS

The potentiality of re-using NS as adsorbent was investigated. Cr^{3+} loaded NS was regenerated using 1.0 M H_2SO_4 and NaOH solution which was shown in the **Flow chart 3.4.**

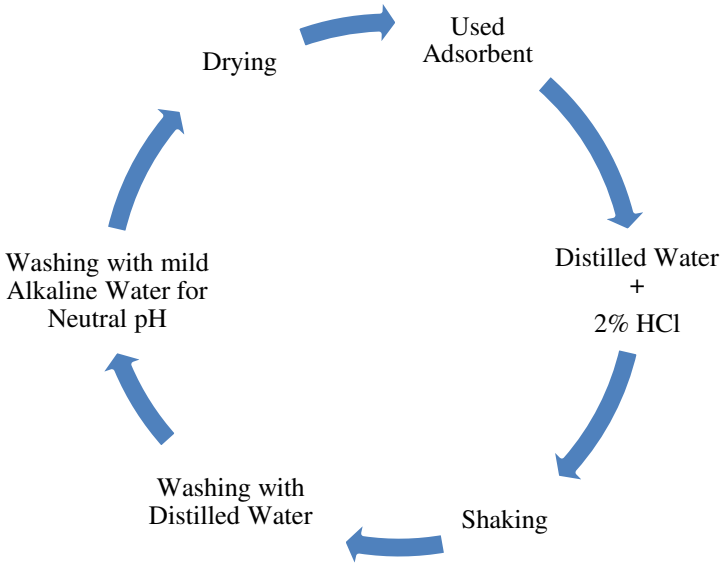

Flow chart 3.4 Flow diagram of regeneration of used NS

Experimental pH, adsorbent dose and other conditions were at optimum level. The consequences of regeneration studies are exposed in **Figure 3.44** which demonstrates that adsorption capacity gradually lowered from 34.92 to 17.46 mg/g. It is understandable that regenerated NS can be reused to lessen Cr^{3+} from aqueous solution.

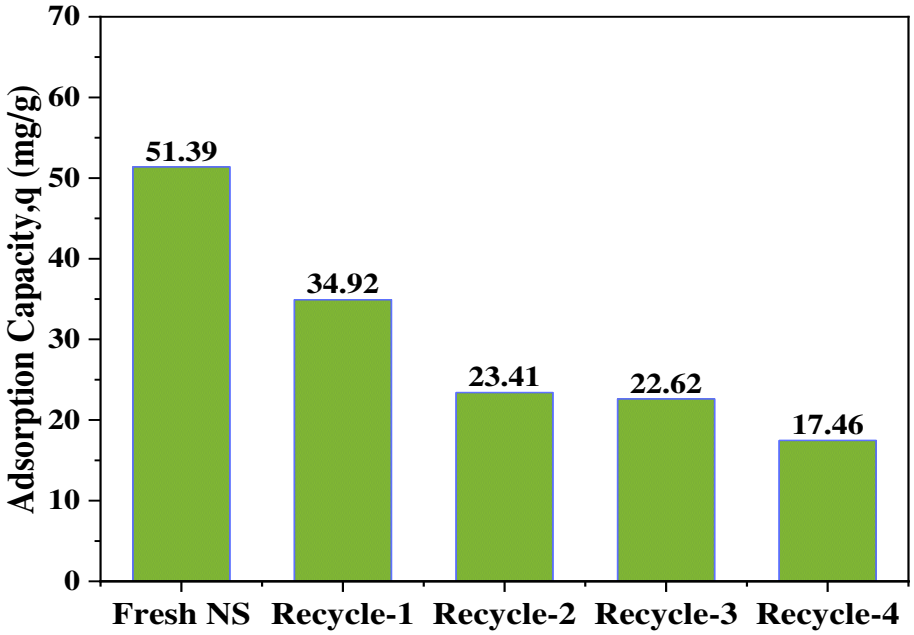

Figure 3.44 Adsorption capacities of regenerated NS

3.2.2.9. Application of NS on real sample (Tanning wastewater and tannery wastewater) for alleviation of pollution load

3.2.2.9.1. Application of NS on chrome tanning effluents

After justify the capabilities of NS in removing Cr(III) ions from prepared $Cr_2(SO_4)_3.6H_2O$ solution by different batch experiments, the performance to remove chromium ions from real sample (Chrome tanning effluent) was confirmed. To investigate the adsorption of Cr ions from concentrated Chrome tanning effluent, 15 g of NS was put to 500 mL of Chrome tanning effluent and shake at room temperature for 4 hours by maintaining pH 5.0. The amount of chromium before and after adsorption was analyzed by ICP-MS and other water quality parameter such as pH, TDS, EC, NaCl %, BOD_5, and COD were also tested, and the values are represented in **Table 3.42.**

Table 3.42 Quality parameters of chrome tanning effluents before and after adsorption.

Parameters	**Before adsorption**	**After adsorption**	**% of removal**	**DoE /ECR Standard**
Cr (ppm)	3276.64	1533.34	53.18	2.0
Adsorption Capacity (mg/g)	-	58.11	-	-
pH	4.6	5.1	-	6.5-9.2
TDS (ppm)	11723	4957	57.72	2100
EC (µS/cm)	10637	4145	61.03	1200
NaCl (%)	8.5	3.8	55.29	-
BOD_5 (ppm)	3273	1317	59.76	≤100
COD (ppm)	9632	3897	59.54	200-400

3.2.2.9.2. Application of NS on tannery effluents

To analyze the performance of NS with tannery effluent, 5 g of adsorbent NS was added to 500 mL of tannery effluent and shaken at room temperature at pH 5.0 for 4 hours. The concentration of chromium before and after adsorption was determined by ICP-MS. Moreover, different water quality parameter like pH, TDS, EC, NaCl %, BOD_5, and COD were also tested, and the results are showed in **Table 3.43.**

Table 3.43 Quality parameters of Tannery effluents before and after adsorption.

Parameters	Before adsorption	After adsorption	% of removal	DoE /ECR Standard
Cr (ppm)	423.28	106.23	74.84	2.0
Adsorption Capacity (mg/g)	-	31.71	-	-
pH	5.5	6.2	-	6.5-9.2
TDS (ppm)	7791	2724	65.04	2100
EC (µS/cm)	5348	1793	66.47	1200
NaCl (%)	4.2	1.6	61.90	-
BOD_5 (ppm)	2207	732	66.83	≤100
COD (ppm)	4278	1505	64.82	200-400

3.2.1.9.3. Discussion on real sample analysis

The experimented results indicate (**Table 3.42**, **Table 3.43**) that after adsorption, the % of chromium removal was 53.18 % and 74.84 % but the adsorption capability was 58.11 and 31.71 mg/g in case of Chrome tanning effluents and tannery effluents respectively. In case of tannery effluent, adsorption capacity was lower compare to prepared solution. This might be due to the interference of different matters or ions that were being used during leather manufacturing which decrease the capacity of the NS [298]. Moreover, after adsorption by NS, different water quality parameters of Chrome tanning and tannery effluents were also reduced significantly.

3.2.3. Chemically Activated Pyrolyzed Bagasse (PB)

3.2.3.1. Preparation of PB

In a tube furnace, sugarcane bagasse was pyrolyzed at 500 ±10 ^{o}C temperature for 2 hours, and they were consequently activated using analytical grade NaOH. Chemical activation was carried out by adding 25% NaOH with pyrolyzed bagasse and left for 24 hours. The next day, the products was rinsed by distilled water before being dried in air oven at 110-115 ^{O}C. Carbonization process usually enhanced the carbon content and create porosity and chemical activation is to extend pores [285]. The activated dried pyrolyzed bagasse (PB) were powdered and employed in this study.

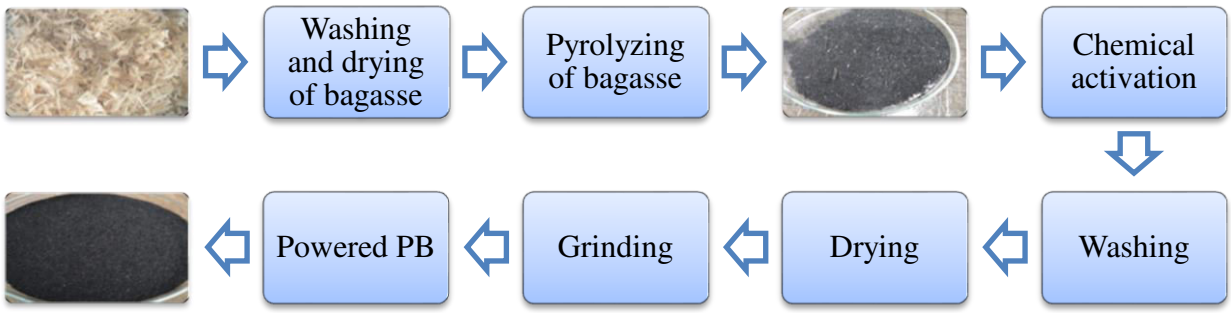

Flow chart 3.5 Flow diagram of PB preparation

3.2.3.2. Characterization of PB

3.2.3.2.1. Elemental analysis of PB

To explore the elements of adsorbent PB before and after Cr(III) adsorption, EDX analysis was conceded**. Figure 3.45** showed that the chemical composition of PB before and after Cr(III) adsorption were mainly carbon, oxygen, phosphorus, sulfur, potassium, calcium etc. However, chromium was added after adsorption process. In spectrum (a), the quantity of C, N, O, P, S, K, Ca and Cr were 58.80, 4.37, 18.87, 7.02, 4.95, 2.19, 3.80, and 0.00 measured in atomic % respectively, while in spectrum (b), the values were 59.31, 3.20, 25.03, 4.36, 4.33, ND, 1.45, and 2.32 respectively, which signify Cr(III) adsorption on to PB.

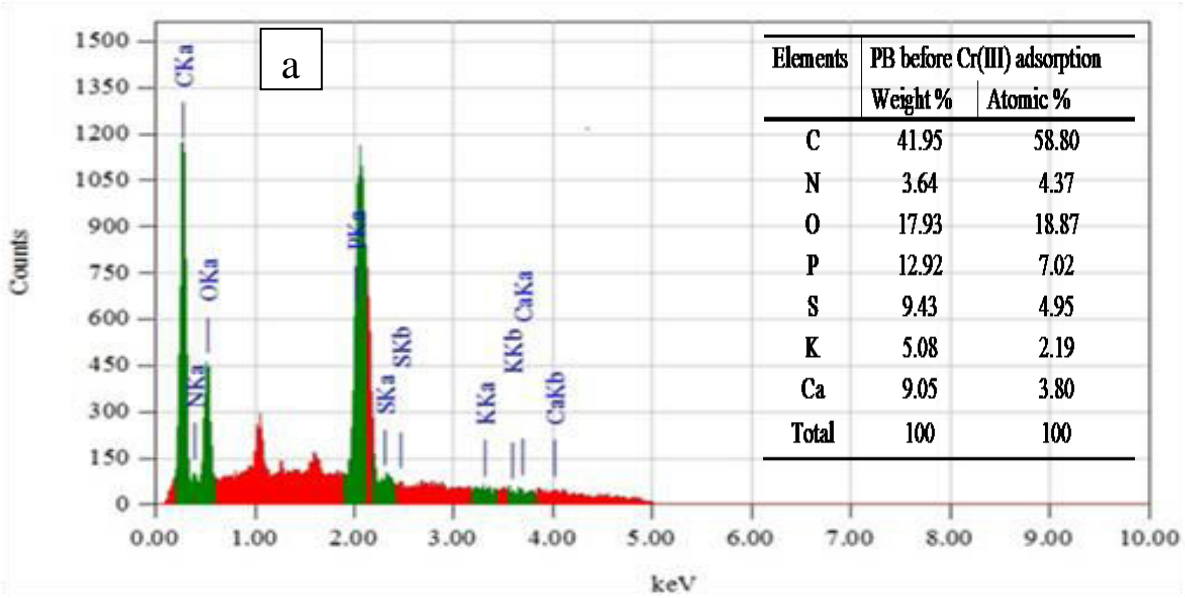

Elements	PB before Cr(III) adsorption	
	Weight %	Atomic %
C	41.95	58.80
N	3.64	4.37
O	17.93	18.87
P	12.92	7.02
S	9.43	4.95
K	5.08	2.19
Ca	9.05	3.80
Total	100	100

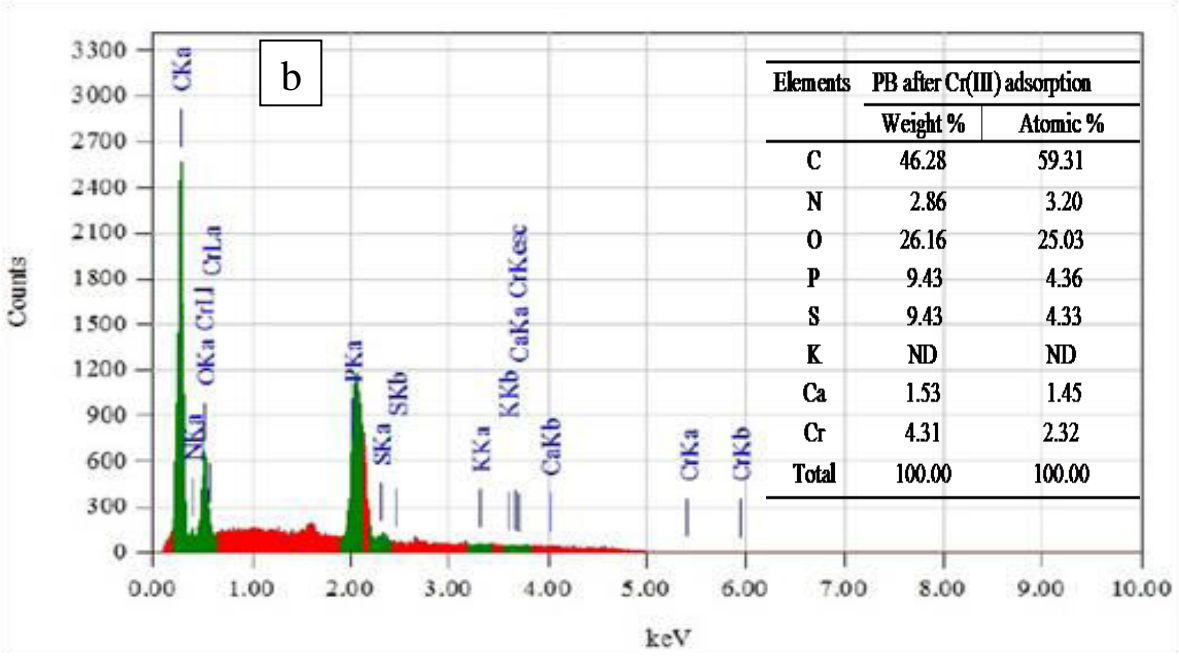

Elements	PB after Cr(III) adsorption	
	Weight %	Atomic %
C	46.28	59.31
N	2.86	3.20
O	26.16	25.03
P	9.43	4.36
S	9.43	4.33
K	ND	ND
Ca	1.53	1.45
Cr	4.31	2.32
Total	100.00	100.00

Figure 3.45 Energy dispersive X-ray (EDX) spectrum of PB (a) before and (b) after Cr(III) adsorption.

3.2.3.2.2. FTIR analysis of PB

The FTIR spectroscopy provides information of the functional groups present in PB faces a number of modification during the chemical activation and Cr(III) ion adsorption processes, shown in **Figure 3.46**.

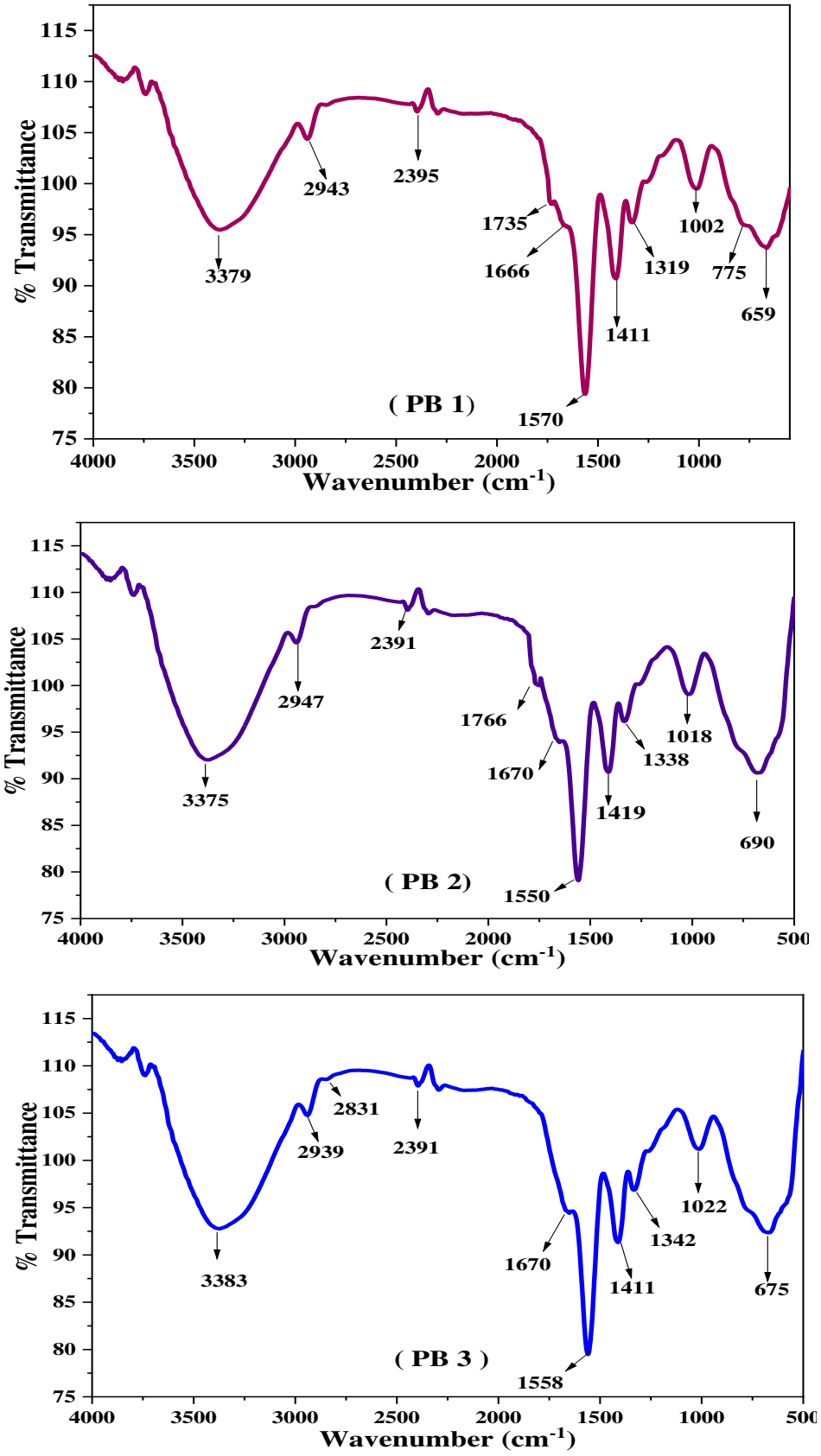

Figure 3.46 FTIR spectra of PB-1 (pyrolyzed bagasse), PB-2 (NaOH activated pyrolyzed bagasse), and PB-3 (Cr(III) loaded NaOH activated pyrolyzed bagasse).

It is also observed that the intensity of major bands present in PB after chemical activation was more and some functional groups shifted to different frequency level [284]. The FTIR spectra of PB-1, PB-2, and PB-3, the existence of –OH groups led to the observation of broad peaks at 3379, 3375, and 3383 cm^{-1} respectively. Peaks at 1735, 1766 and 1670 cm^{-1} demonstrating that –C=O groups were also available in the spectra. C-H stretching vibrations were seen at 2943 cm^{-1} in PB-1; 2947 cm^{-1} in PB-2 and 2939 cm^{-1} and 2831 cm^{-1} in PB-3. The peak at 1666 cm^{-1}, 1670 cm^{-1}, 1670 cm^{-1} represent alkene C=C and aromatic C=C (1600-1475 cm^{-1}) in PB-1, PB-2, and PB-3, region respectively [301]. Moreover, the peak between 1100 and 1300 cm^{-1} represents C-O (alcoholic, esters) groups of the adsorbent.

3.2.3.2.3. Scanning electron microscopic (SEM) analysis of PB

SEM was utilized to analyze the surface morphology of NaOH activated PB and the image is presented in the **Figure 3.47.** The figure illustrated that it has apertures, an rough, assorted structure, and lamellar texture which facilitate the adsorption process in aqueous solutions [194].

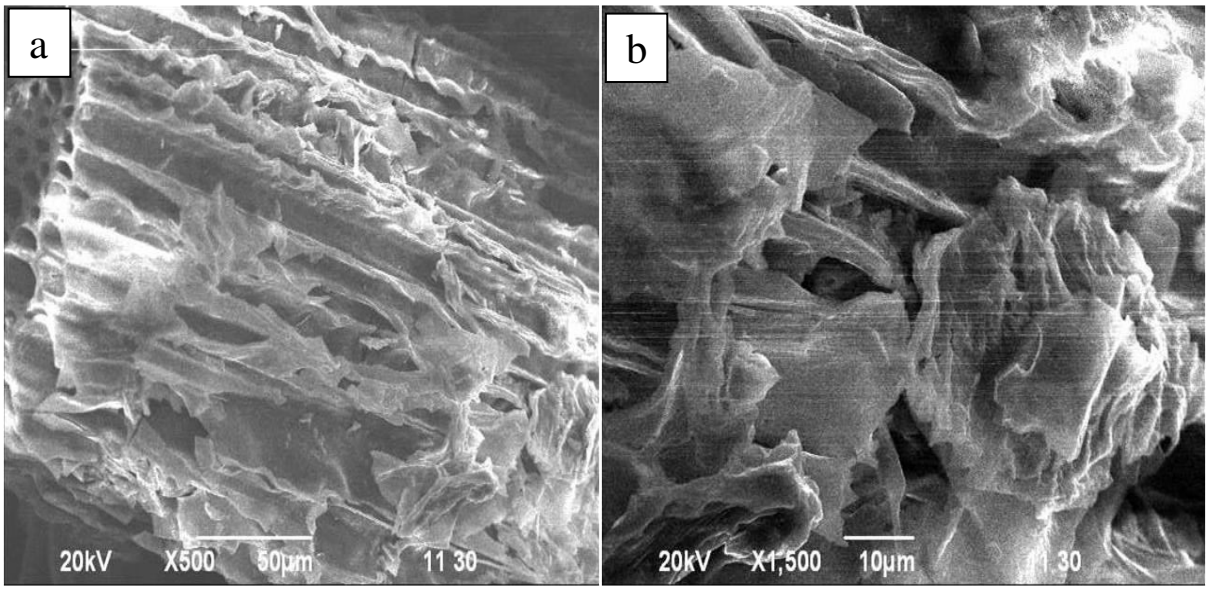

Figure 3.47 SEM image of PB (a) 500x, and (b) 1500x magnification

3.2.3.2.4. X-Ray diffraction (XRD) analysis of PB

There was no sharp peak associated with the crystalline phase in the XRD pattern. It displays a distinctive peak of carbonaceous components. Owing to the amorphous structure with a high level of disorder of PB, a hump in the range of $2\theta = 20 - 30°$ and a peak at $2\theta = 22.5°$ were observed (**Figure 3.48)**. The presence of amorphous carbon is indicated by the broad and weak peaks in the XRD pattern of PB [288].

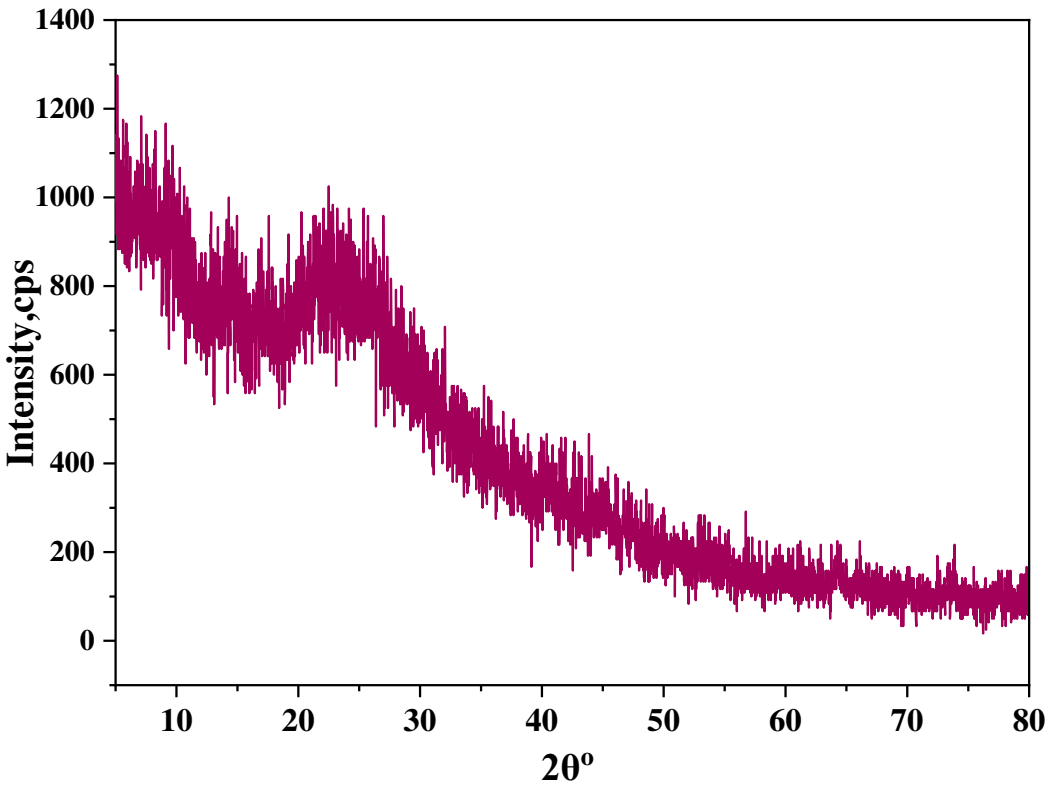

Figure 3.48 XRD analysis of PB

3.2.3.2.5. Brunauer-Emmett-Teller (BET) analysis of PB

Surface area, pore volume, and pore diameter of PB were analyzed by nitrogen gas sorption system are presented in **Table 3.44**. Chemically activated PB had low surface area of 3.68 m^2/g could be due to the breakdown of cell walls [289]. Barrett-Joiner-Halenda (BJH) method was followed to decide the average pore diameter, and it was 89.41 Å, which suggest that PB consists of mesopores [193].

Table 3.44 BET surface area and porosity of PB

Sl. No.	Parameter	Result
01.	BET Specific Surface Area using multi-point analysis (m^2/g)	5.72
02.	Total Pore Volume (cc/g)	0.0218
03.	Skeletal density (g/cc)	1.1950
04.	Porosity based on skeletal density (per gram of sample)	0.0254
05.	Average Pore Diameter, 4V/S (Å)	152.32

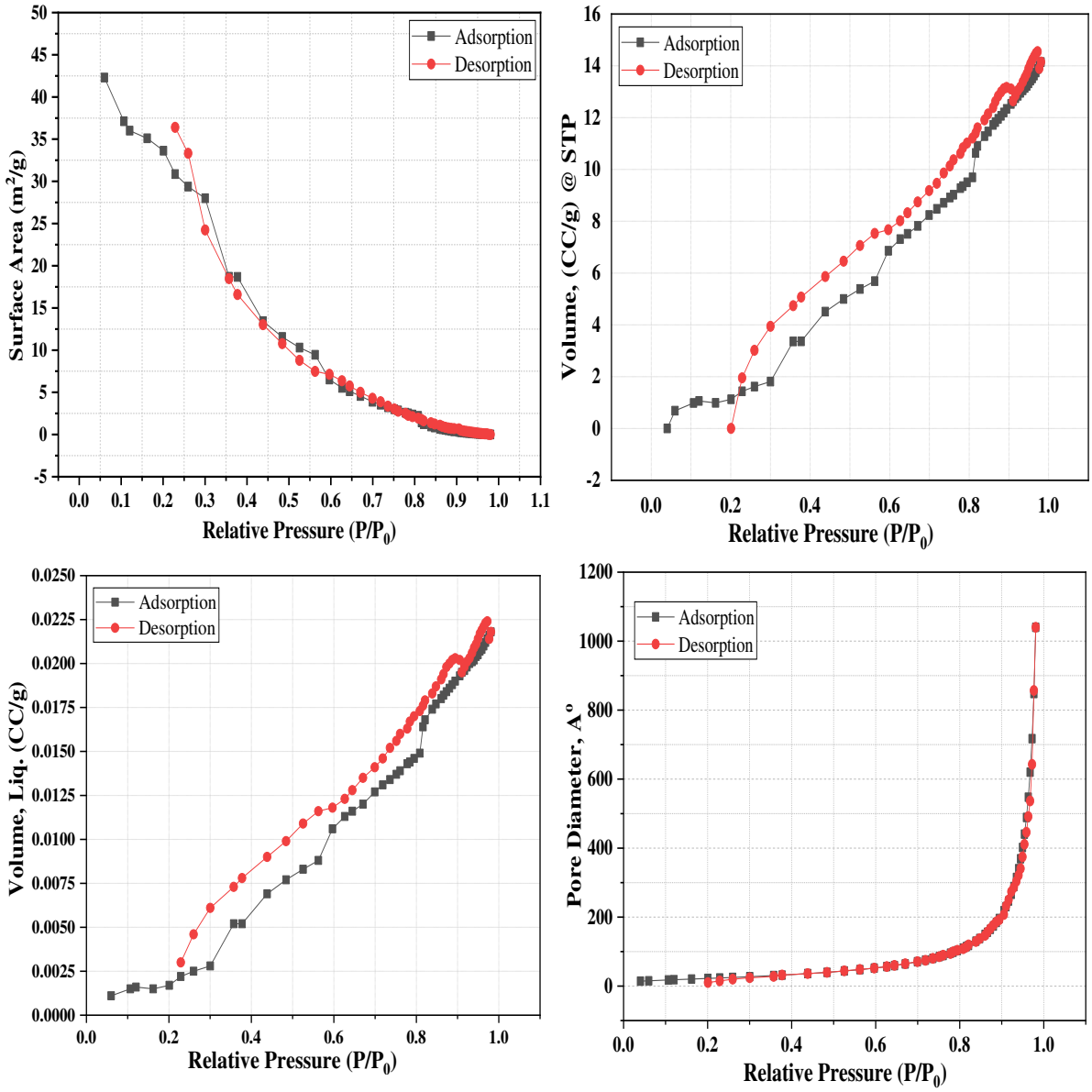

Figure 3.49 Adsorption and desorption isotherms of BET to PB

3.2.3.2.6. Zeta potential value of PB

Zeta potential value (ZPV) of PB was also investigated as a function of pH. PB sample was prepared by dispersing PB in deionized water to study the ZPV of PB. The experiment was controlled in the pH range of 3.0-5.0.

Table 3.45 pH vs Zeta potential data of PB

pH	3	3.5	4	4.5	5
Zeta potential value (mV)	17.1	12.6	2.31	-28.6	-31.5

From the **Table 3.45** and **Figure 3.50** signify that ZPV of PB was positive (17.7-2.3 mV) at 3.0 – 4.0 pH, while the values were negative (-28.6 to -31.5 mV) with an increase of pH from 4.5 to 5.0.

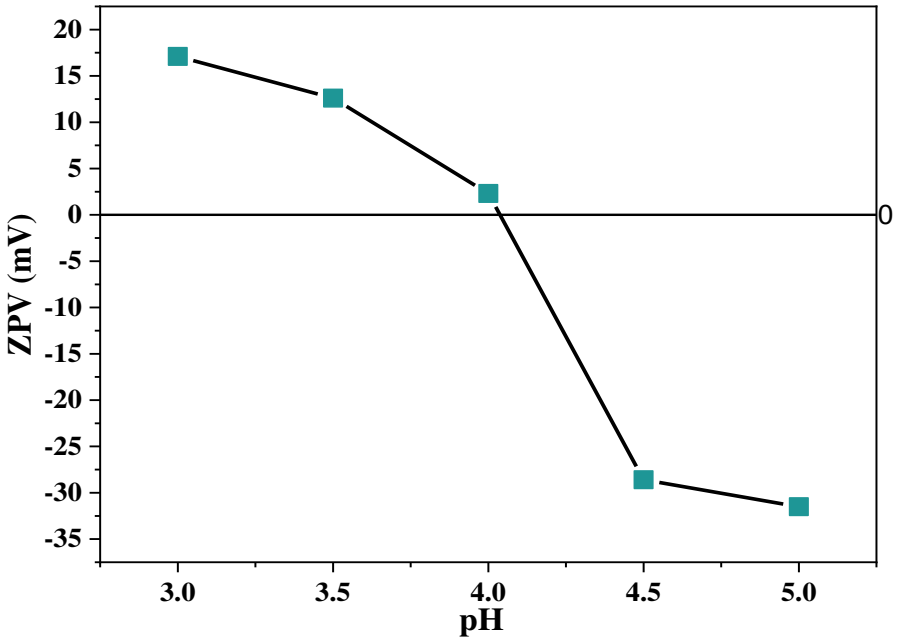

Figure 3.50 ZPV of PB at different pH

3.2.3.3. Adsorption Cr(III) ions on PB

3.2.3.3.1. Effect of pH on adsorption capacity of PB for Cr^{3+} ions adsorption

The impact of pH on Cr^{3+} ions adsorption by PB was studied with 280.78 ppm solution of $Cr_2(SO4)_3.6H_2O$ by varying it in the range of 3.0 to 5.0. In the experiment 63 mg PB were added in each solution (25 mL) and were shaken at 160 rpm for 4 hours. After filtering the mixtures the change in Cr^{3+} ions concentrations were determined by UV-Vis spectroscopy. It is comprehensible from the **Table 3.46** and **Figure 3.51** that adsorption capacity of PB was enhanced with higher pH of the solution and the best capacity was 60.94 mg/g at pH 5.

Table 3.46 pH v/s adsorption capacity data of PB for Cr^{3+} ions adsorption

pH	3	3.5	4	4.5	5
Adsorption Capacity (mg/g)	46.93	55.2	54.76	58.916	60.94

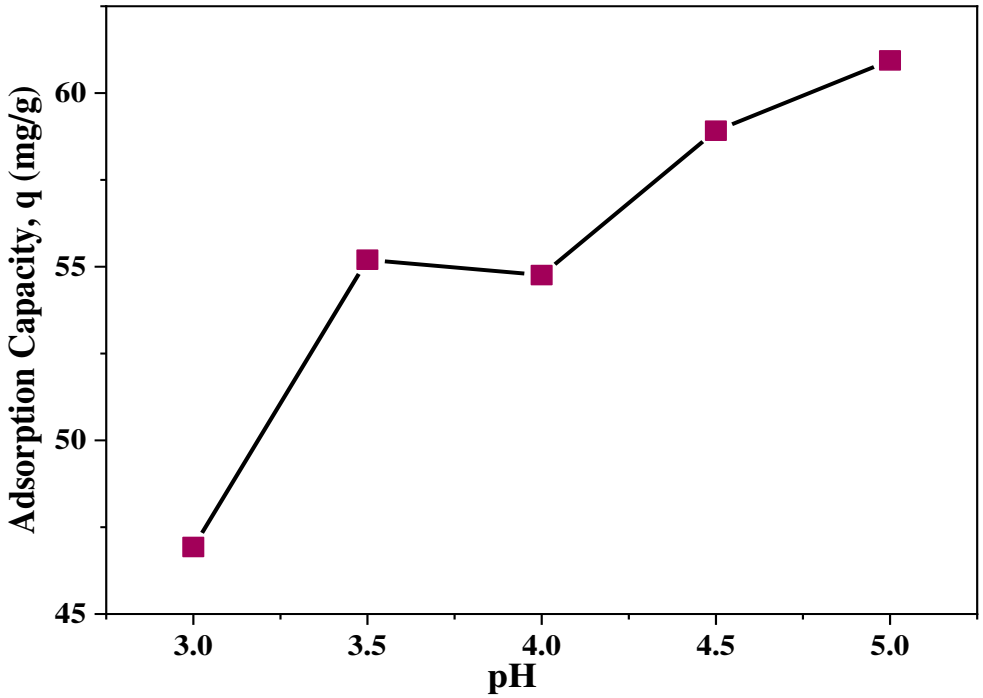

Figure 3.51 Effect of Cr-salt solution's pH on adsorption capacity of PB for Cr^{3+} ions adsorption

It is assumed that the ion exchange (which was evident from the EDX analysis **Figure 3.45)** and H-bonding might be the main mechanism for the removal of heavy metals [290]. At lower pH value (3.0) the adsorption efficiency was low, because of the feisty adsorption of same positive charge of H^+ and metal ions with similar adsorption site. While, at higher pH values (4.5 – 5.0), the lower number of protons and greater number of negative charges ensuing higher Cr(III) adsorption. According to the data from ZPV (**Figure 3.50),** the surface negativity of PB was increased as pH increased.

$$—ROH \underset{\text{At Lower pH}}{\overset{\text{At Higher pH}}{\rightleftharpoons}} —R\bar{O} + H^+$$

In this study, all batch experiments were conducted at 5.0 pH to acquire highest adsorption capacity in addition to avoid precipitation of Cr^{3+} [291]. Moreover, at pH >6 Cr^{3+} can be precipitated from the aqueous solution as $Cr(OH)_3$ [292]. The results agreed with previous literature [237] and Cr speciation (**Figure 1.1**), it was observed that at pH >3 ionic species such as $CrOH^{2+}$, $Cr(OH)_2^+$ and adsorbent showed higher affinity to these species than for free Cr(III) ion.

3.2.3.3.2. Effect of adsorbent dosage on adsorption capacity of PB for Cr^{3+} ions adsorption and % of removal

Effect of adsorbent dosage on Cr(III) adsorption was studied by changing the dosage from 1.5 to 4.0 g/L to find out the optimum dose. The batch experiments were conducted for 4 hours with 240.57 ppm initial concentration at optimum pH 5.0. It is showed that (**Table 3.47, Figure 3.52**) % of Cr(III) removal was raised 42.09 to 84.99% whereas adsorption capacity was reduced 66.32 to 50.89 mg/g with the increase of PB dosage.

Table 3.47 Dosage v/s adsorption capacity and % removal data of PB

Dosage (g/L)	1.5	2	2.5	3	3.5	4
Adsorption Capacity (mg/g)	66.32	61.26	59.08	54.09	52.02	50.89
Removal (%)	42.09	51.15	62.16	67.76	76.55	84.99

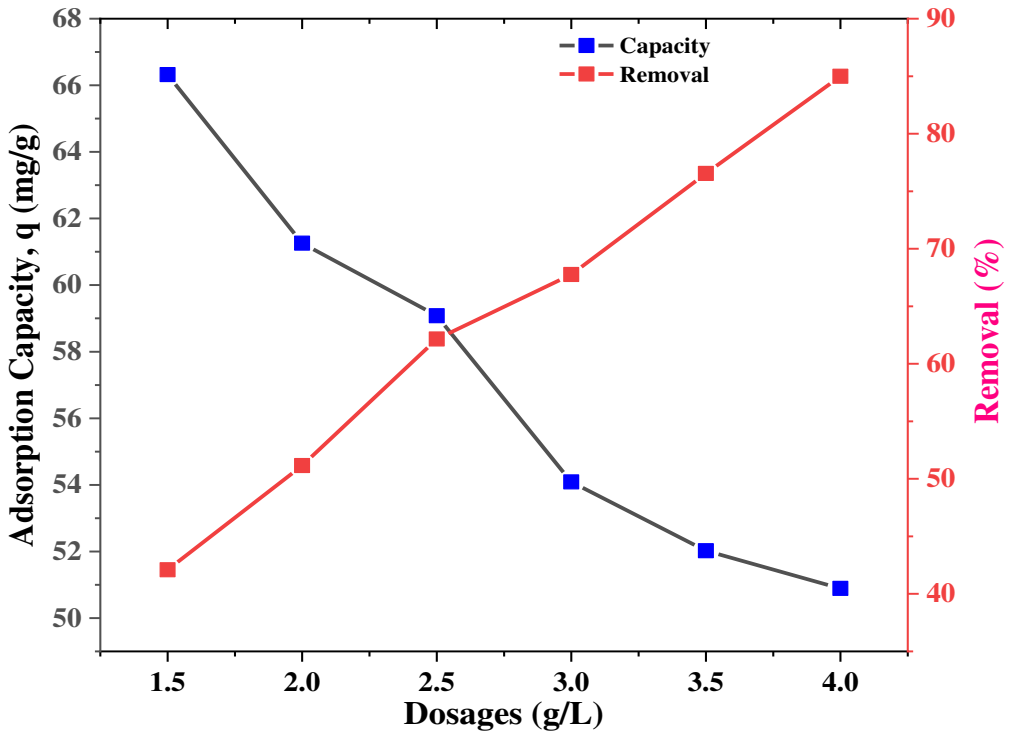

Figure 3.52 Effect of PB Dosage on adsorption capacity and % removal

The availability of more adsorption sites is responsible to enhanced the % removal of Cr(III), but additional unsaturated sites reduce the adsorption capacity with more adsorbent dosage [302]. It was also observed that at dose 2.5 g/L showed the best % removal also best adsorption capacity and employed all over the study.

3.2.3.3.3. Effect of Cr^{3+} concentrations and contact time on adsorption capacity of PB for Cr^{3+}adsorption

To evaluate the effect of Cr^{3+}ions concentrations and contact duration on adsorption efficiency of PB, 25 mL solutions of four different concentrations (125.93, 175.28, 196.97, and 240.57 ppm) were taken in conical flasks and then added 63 mg (2.5 g/L) PB in to each solution. The batch experiments were performed at 5.0 pH by specific time intervals ranging from 5-600 minutes with constant shaking speed 160 rpm.

Table 3.48 Time vs adsorption capacity data of PB for Cr^{3+} ions adsorption

Time (min)	Adsorption capacity (mg/g)			
	125.93 ppm	**175.28 ppm**	**196.97 ppm**	**240.57 ppm**
0	0	0	0	0
5	13.25	36.04	37.89	25.57
15	22.12	43.72	41.95	32.33
30	22.28	47.26	42.71	32.83
60	29.79	48.03	48.36	42.29
120	31.65	48.82	48.62	45.99
240	36.72	49.21	52.42	51.82
360	39.25	49.88	55.37	58.83
480	40.09	51.48	55.54	60.68
600	40.68	51.56	55.79	60.71

The results (**Table 3.48, Figure 3.53)** signify that adsorption capacity were increased with increasing duration until it reached at equilibrium. It was established that adsorption capacity reached at equilibrium almost after 480 minutes and the adsorption capacity was increased with higher metal ion concentration. At 125.93 ppm initial Cr^{3+} concentration, adsorption capacity was 40.09 mg/g while at 175.28, 196.97, and 240.57 ppm concentration, adsorption capacity was 51.489, 55.37, and 60.68 mg/g accordingly.

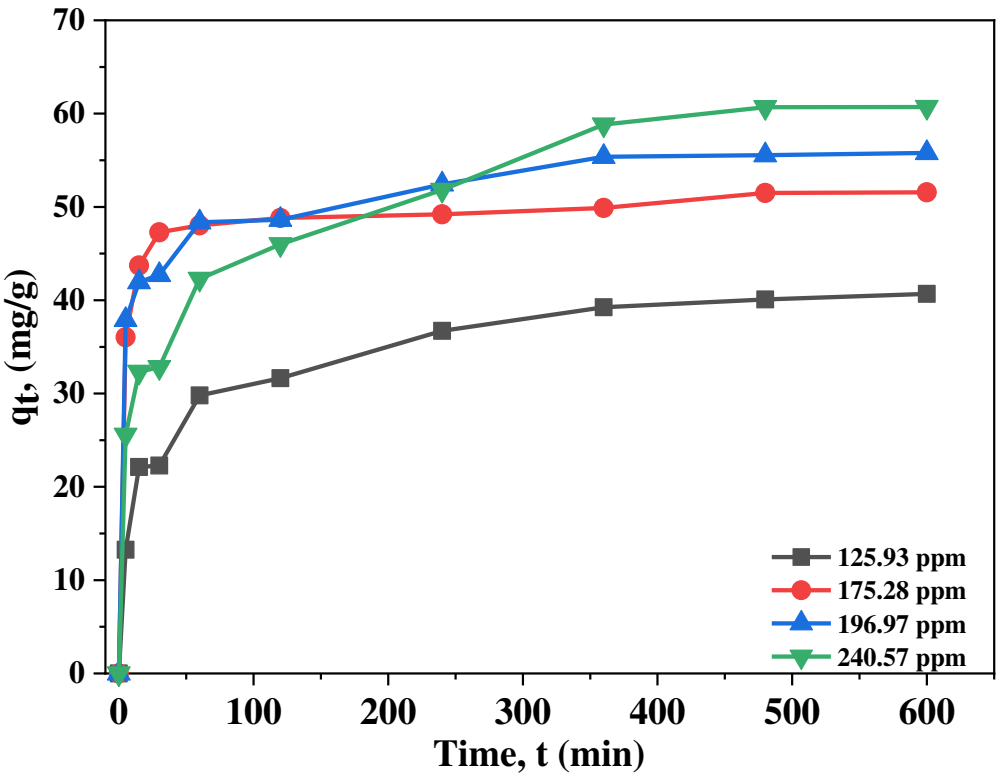

Figure 3.53 Effect of Cr^{3+} concentrations and contact time

The justification is because at starting time there were adequate active sites available, but after certain time these sites got saturated [203]. Moreover, the equilibrium adsorption capacity was increased with higher Cr^{3+} ion concentration. It is due to the gradient of concentration between the Cr(III) ion in bulk solution and adsorbent surface, which causes mass transfer within aqueous and solid phase [218].

3.2.3.4. Adsorption isotherms for Cr^{3+} adsorption on PB

To assess the relationship between the amount of adsorbate adsorbed on the adsorbent, frequently investigated by analyzing the experimental data with Langmuir and Freundlich isotherm. In the Langmuir isotherm, the adsorbate is implicit to be absorbed on the adsorbent in a monolayer on well-defined with no intermolecular interactions. However, Freundlich isotherm assumes multilayer also suggest non-uniform distribution.

3.2.3.4.1. Langmuir isotherm

The Langmuir isotherm model was analyzed by equation (3.4) plotting C_e/q_e versus C_e (**Table 3.49, Figure 3.54**). A linear link between C_e/q_e and C_e was observed with acceptable regression factor (R^2=0.999). Maximum adsorption capacity q_m (theoretical), was calculated from the slope and observed 74.63 mg/g. The separation factor R_L provides information of

qualitative measure of the favorability, R_L >1indicates unfavorable adsorption while 0< R_L<1indicates favorable process. In this study, R_L was calculated by equation (3.5) and the value was 0.0767 indicates favorable monolayer adsorption process [303] .

Table 3.49 C_e vs C_e/q_e data of PB at different concentration for Cr^{3+} adsorption

Initial concentration (ppm)	125.93	175.28	196.97	240.57
Equilibrium concentration (C_e)	24.894	45.526	57.438	87.648
C_e/q_e	0.599	0.884	1.037	1.444

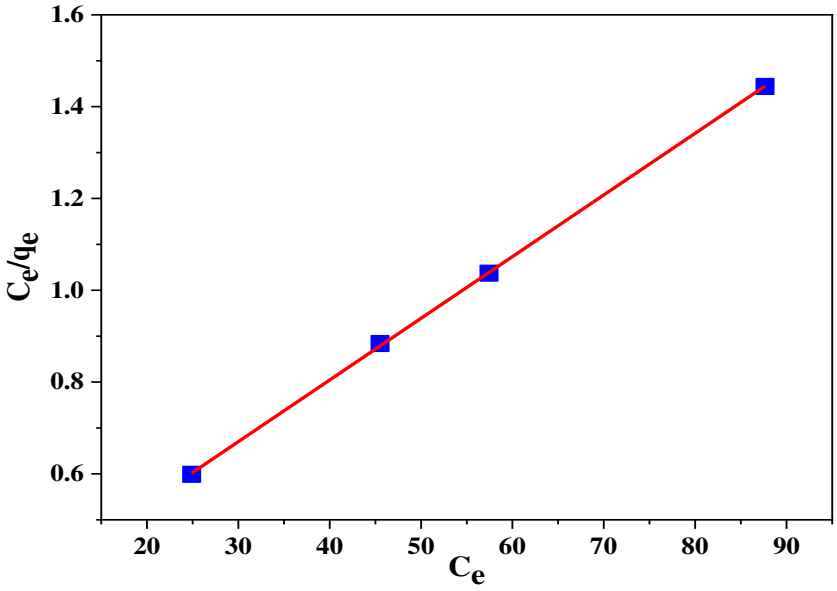

Figure 3.54 Langmuir isotherm for Cr^{3+} adsorption on PB

3.2.3.4.2. Freundlich isotherm

The experimental data was justified for multilayer adsorption mechanism through Freundlich isotherm equation (3.6) by plotting a graph of $\ln C_e$ versus $\ln q_e$ (**Table 3.50, Figure 3.55**) and linear connection was observed with good regression coefficient, R^2= 0.973. From the slope n was calculated and found to be 2.985 which showed good adsorption process [208].

Table 3.50 $\ln C_e$ vs $\ln q_e$ data of PB at different concentration

Initial concentration (ppm)	125.93	175.28	196.97	240.57
$\ln C_e$	3.215	3.818	4.051	4.473
$\ln q_e$	3.691	3.941	4.016	4.106

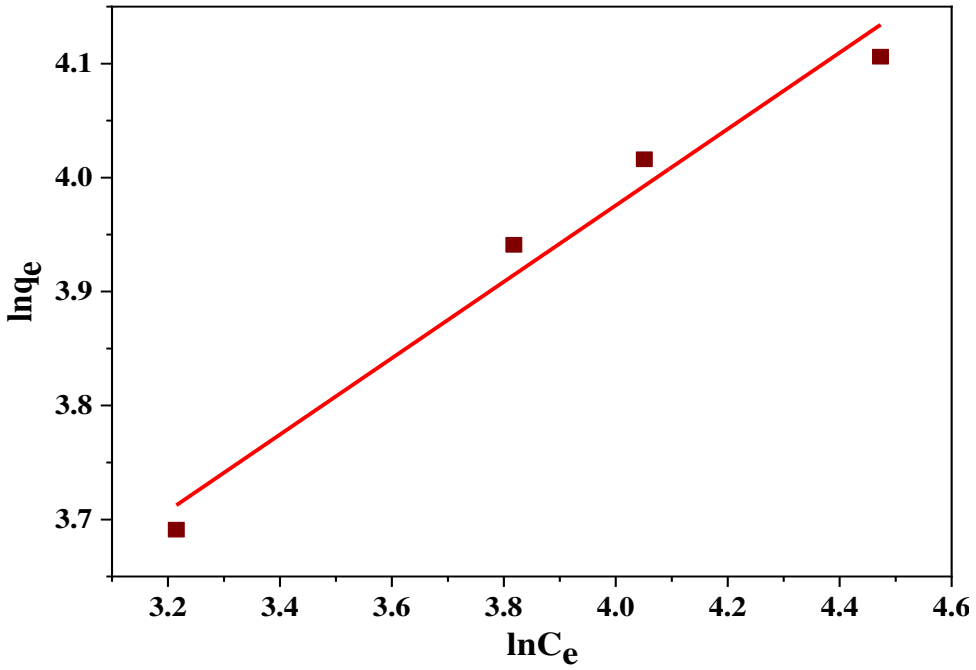

Figure 3.55 Freundlich adsorption isotherm for Cr^{3+}) adsorption on PB

3.2.3.4.3. Explanation on isotherms for Cr^{3+} adsorption

The results of different parameters of the models imply (**Table 3.51**) that adsorption of Cr^{3+} on PB comply both Langmuir and Freundlich isotherm but preferably the Langmuir model.

Table 3.51 Theoretical values of q_m, b, R_L, n, k_F and R^2 of adsorbent PB

Parameters	q_m (mg/g)	b (Lmg^{-1})	R^2	R_L	n	k_F
Langmuir isotherm	74.63	0.05	0.999	0.0767	-	-
Freundlich isotherm	-	-	0.973	-	2.985	13.94

3.2.3.5. Adsorption kinetics for Cr^{3+} adsorption on PB

The adsorption kinetics is significant to examine how rapidly ions move from aqueous to solid phase and how much time it takes to reach equilibrium. In the study, two kinetic models (Pseudo-First-Order and Pseudo-Second-Order) were analyzed to express the adsorption process.

3.2.3.5.1. Pseudo-first-order kinetics

To illustrate the adsorption, process the pseudo-first-order kinetic equation (3.7) was introduced by Lagergren in 1898. Pseudo-first-order kinetic model was obtained by plotting a

graph with $\log(q_e-q_t)$ against t (**Table 3.52, Figure 3.56**) where a linear affiliation was achieved in between $\log(q_e-q_t)$ and t.

Table 4.52 Time, t(min) and $\log(q_e-q_t)$ data of PB at different concentration

Time, t(min)	$\log(q_e-q_t)$ at 125.93 ppm	$\log(q_e-q_t)$ at 175.28 ppm	$\log(q_e-q_t)$ at 196.97 ppm	$\log(q_e-q_t)$ at 240.57 ppm
5	1.425	1.189	1.242	1.545
15	1.254	0.89	1.128	1.452
30	1.25	0.625	1.102	1.445
60	1.013	0.539	0.845	1.265
120	0.926	0.426	0.829	1.167
240	0.527	0.358	0.469	0.947
360	-0.076	0.205	-	0.268

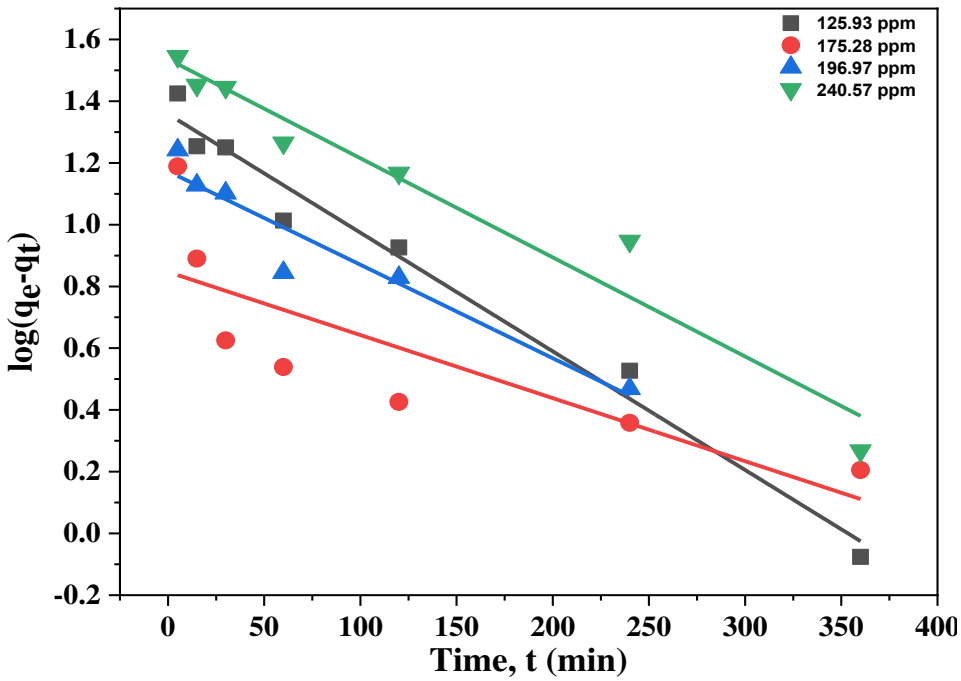

Figure 3.56 Pseudo-First-Order kinetics for Cr^{3+} adsorption on PB

3.2.3.5.2. Pseudo-second-order reaction kinetics

In 1999 Ho and Mckay presented pseudo-second-order rate reaction (3.8). The model was analyzed with a graph by plotting t/q_t versus t (**Figure 3.57**).

Table 3.53 Time, t (min) and t/q_t data of PB at different concentration

Time, t(min)	**t/q_t at 125.93 ppm**	**t/q_t at 175.28 ppm**	**t/q_t at 196.97 ppm**	**t/q_t at 240.57 ppm**
5	0.377	0.139	0.132	0.196
15	0.678	0.343	0.358	0.464
30	1.346	0.635	0.702	0.914
60	2.013	1.249	1.241	1.419
120	3.791	2.458	2.468	2.609
240	6.536	4.877	4.578	4.631
360	9.172	7.274	6.495	6.119
480	11.973	9.322	-	7.909

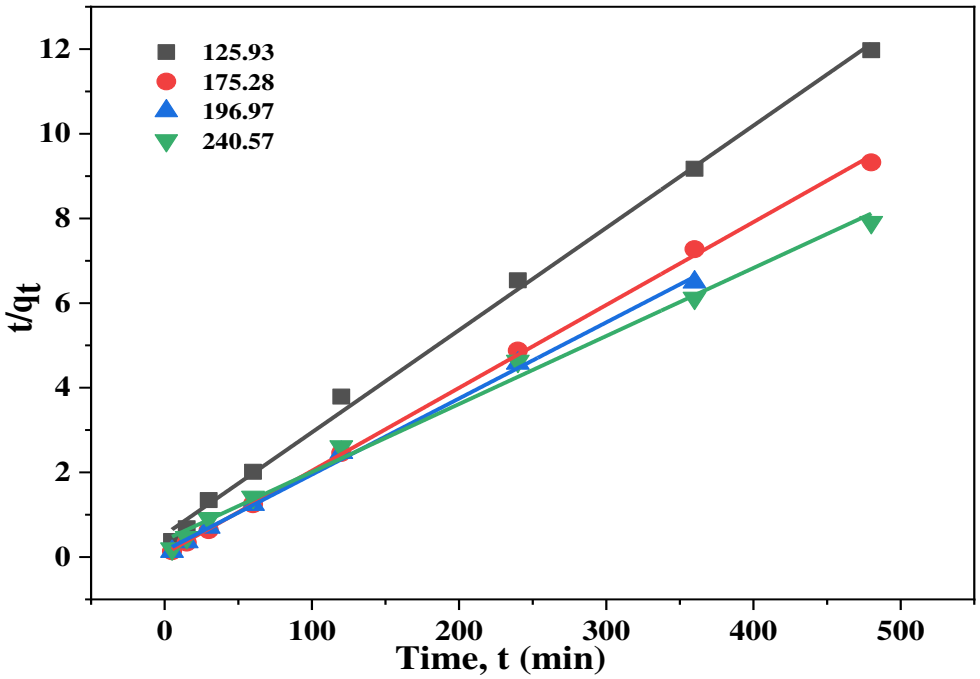

Figure 3.57 pseudo-second-order kinetics for Cr^{3+} adsorption on PB

3.2.3.5.3. Explanation on kinetics model

The kinetic models parameters are calculated from the slop and intercept of each linear plot are presented in **Table 3.54.**

Table 3.54 pseudo-first-order and pseudo-second-order kinetics parameters

Kinetics model	Parameters	125.93 ppm	175.28 ppm	196.97 ppm	240.57 ppm
Pseudo-first-order	q_e^* (mg g^{-1})	40.09	51.489	55.37	60.685
	k_1(1/min)	0.0089	0.0047	0.0069	0.0074
	R^2	0.978	0.662	0.924	0.853
	q_e^{**} (mgg^{-1})	22.86	7.01	14.89	34.36
Pseudo-second-order	k_2 (g/mg min)	0.00109	0.00478	0.00215	0.00064
	R^2	0.997	0.999	0.997	0.993
	q_e^{**} (mg g^{-1})	41.49	51.07	55.62	62.23

*Experimental, **Theoretical

The linear fitting results of the two models proposed that in case of pseudo-second-order model the theoretical q_e values matched better with the experimental q_e values. It was also found that the correlation coefficient, R^2 values (0.997, 0.999, 0.997, and 0.993) of pseudo-second-order kinetic model was better than that of pseudo-first-order kinetic (0.978, 0.662, 0.924, and 0.853) model.

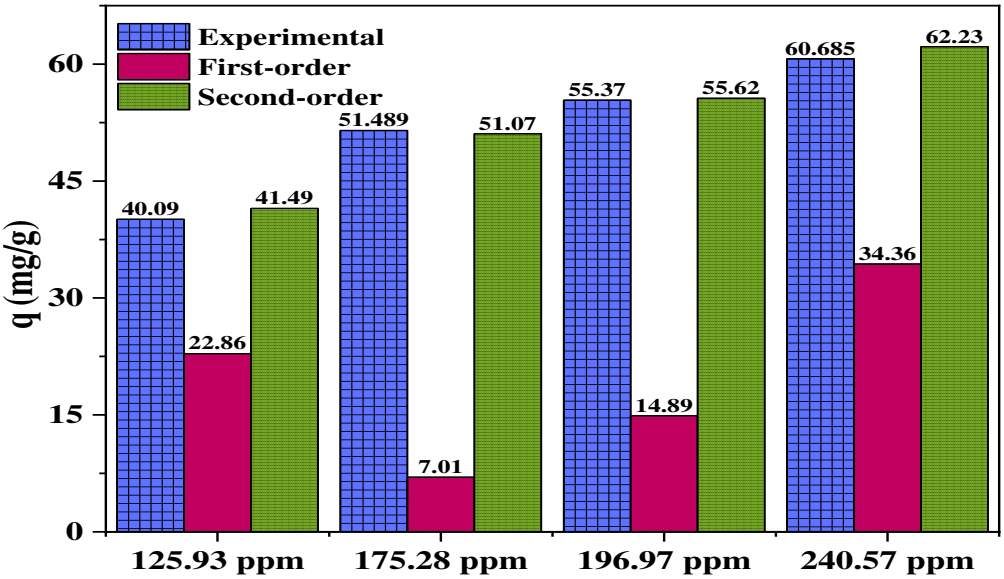

Figure 3.58 Comparison between experimental and calculated adsorption capacity

Figure 3.58 illustrated that the calculated adsorption capacities were in good agreement with the experimental values of pseudo-second-order kinetics. Therefore, it is logical that pseudo-second-order model was better fitted for Cr(III) adsorption on PB compared to the Pseudo-First-Order model.

3.2.3.6. Thermodynamic analysis for Cr^{3+} adsorption on PB

To understand the nature (endothermic or exothermic) of adsorption process of Cr(III) on PB was studied at different temperature. Batch experiments were attempted at various temperatures to assess thermodynamic parameters, e.g., Gibbs free energy (ΔG), enthalpy (ΔH), and entropy (ΔS) by the equations (3.9), (3.10) and (3.11). For this study, 63mg (2.5 g/L) PB was added in to 25 mL (149.75 ppm) of $Cr_2(SO4)_3.6H_2O$ solution at 5.0 pH for each experiment. The batch experiments were than shaken in an orbital shaker at 293K, 308K, 323K and 338K temperature for different time period ranging from 60-600 minutes. The impact of temperature and contact duration on adsorption capacity of PB were investigated and showed in **Table 3.55** and **Figure 3.59.**

Table 3.55 Temperature and time vs adsorption capacity data of PB for Cr^{3+}

Time (min)	Adsorption Capacity (mg/g)			
	293K	308K	323K	338K
0	0	0	0	0
60	39.69	24.65	27.18	20.68
120	42.04	29.29	27.26	29.79
240	47.18	47.27	41.27	37.39
360	51.65	49.21	46.85	44.57
480	51.49	49.79	46.59	44.06
600	51.83	49.29	46.34	44.73

The result showed that the adsorption capacity of PB was decreased at higher temperature. This might be happened as temperature rises, the kinetic energy increases and releases of the adsorbate from PB [304]. At 293K temperature the equilibrium adsorption capacity was 51.65 mg/g which decreased to 49.21 mg/g, 46.85 mg/g, and 44.57 mg/g at 308K, 323K and 338K correspondingly.

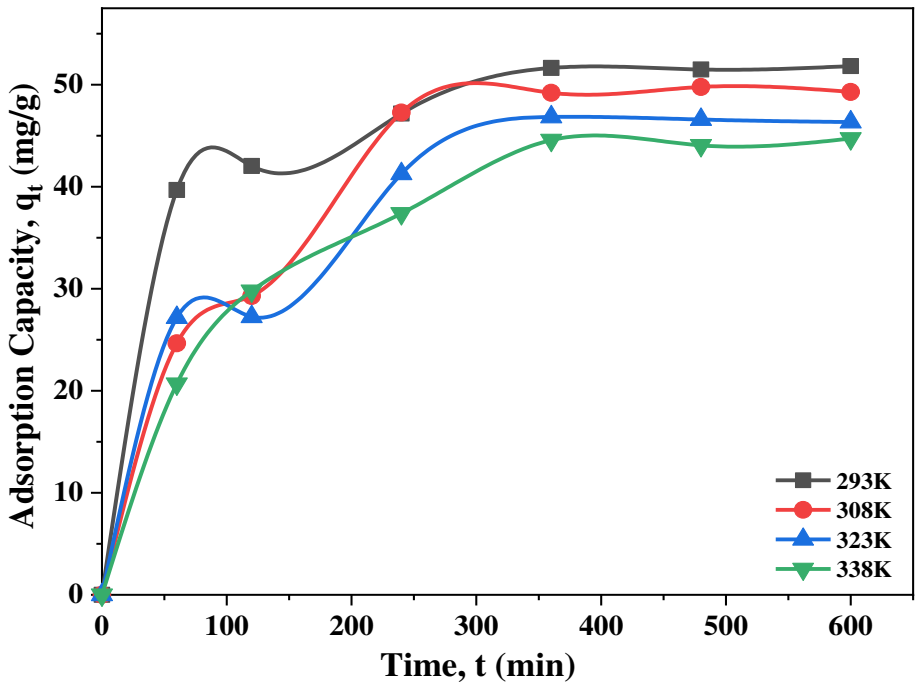

Figure 3.59 Effect of temperature and time of Cr^{3+} adsorption on PB

Table 3.56 Van't Hoff equation 1/T vs lnk_d data of PB for Cr^{3+} adsorption

1/T	0.0034	0.0032	0.003	0.0029
lnk_d	0.969	0.648	0.391	0.174

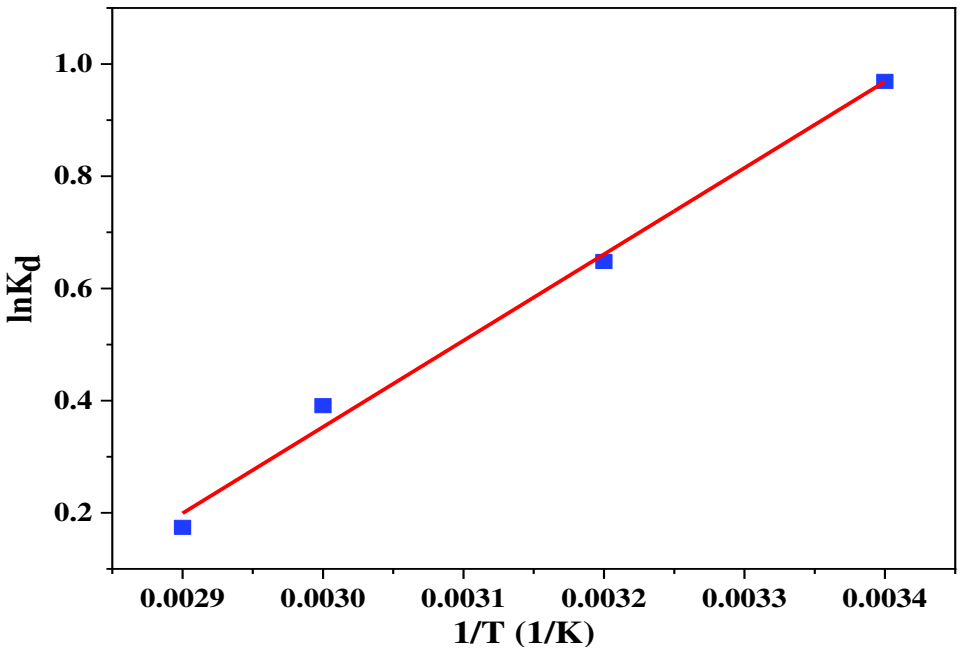

Figure 3.60 Thermodynamics of Cr^{3+} adsorption on PB

A straight line was attained through a graph by plotting 1/T versus $\ln k_d$ (**Table 3.56, Figure 3.60**). The standard enthalpy (ΔH), and entropy (ΔS) was obtained from the slope and intercept and were -12.797 kJ/mol and -0.0355 kJ/mol (**Table 3.57**) respectively.

Table 3.57 Thermodynamic parameters of PB for Cr^{3+} adsorption

T(K)	ΔG (kJ/mol)	ΔH (kJ/mol)	ΔS (kJ/mol K)	R^2
293	- 2.36	- 12.797	- 0.355	0.994
308	-1.659			
323	-1.05			
338	-0.489			

At the temperatures of 293K, 308K, 323K and 338K, the values of ΔG for adsorption of Cr^{3+} on PB were found to be -2.36, -1.659, -1.05 and -0.489kJ/mol, respectively. The negative ΔG suggest that adsorption of Cr^{3+}on PB was spontaneous and negative ΔH indicated exothermic in nature. Additionally the negative ΔS revealed less randomness at the solid/solute interface through the adsorption of Cr^{3+}on PB [295].

3.2.3.7. Plausible mechanism for Cr^{3+}adsorption on PB

Adsorption mechanism deals with the electrostatic interaction among oppositely ionized particles by dint of various bond formations like H-bonding, Van der Waals force, dipole-dipole induction, ion-exchange and so on.

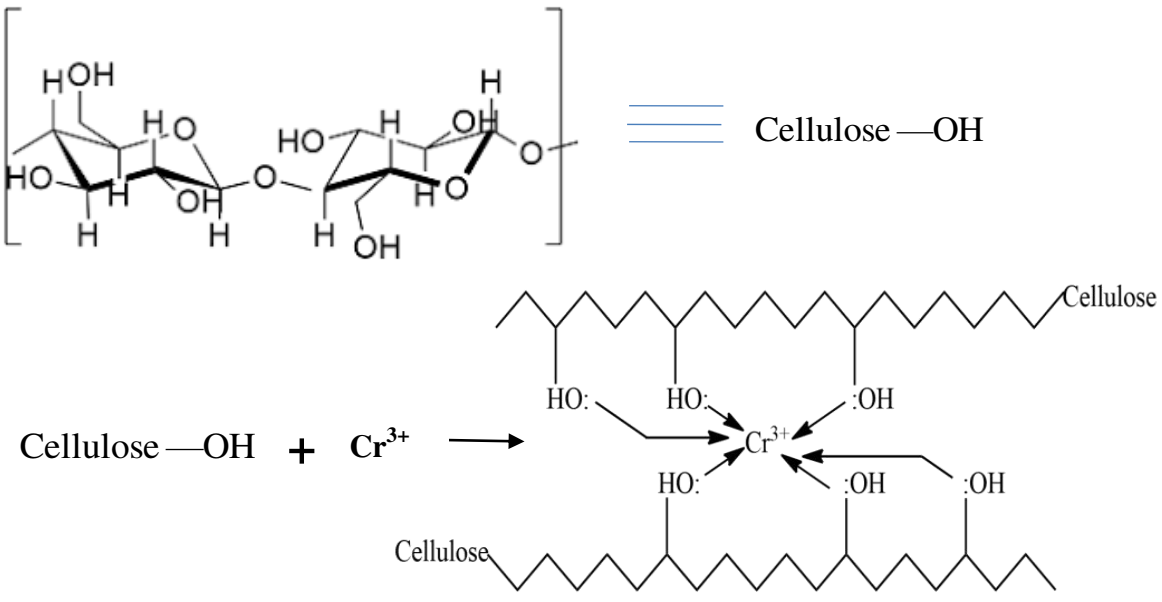

Scheme 3.3 Plausible mechanisms of Cr^{3+} adsorption on PB

It was exposed from earlier research that the functional groups like carboxyl, hydroxyl, methoxy, and phenolic groups present in pyrolyzed bagasse could attract and remove Cr^{3+} ions along with other impurities from effluents [296], [297]. In this study it is assumed that PB contains hydroxyl group cellulose which is believed to figure hexa-coordinate complexes with Cr^{3+} ions from the solution (**Scheme 3.3**).

3.2.3.8. Regeneration of used PB for Cr^{3+}adsorption

The probability of re-using PB as adsorbent was investigated. Cr^{3+} loaded PB was regenerated using 1.0 M H_2SO_4 and NaOH solution four times which was shown in the **Flow chart 3.6**.

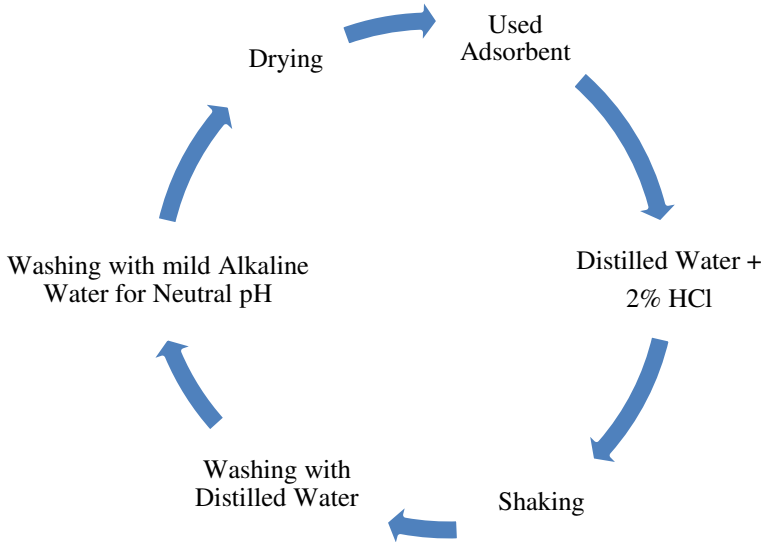

Flow chart 3.6 Flow diagram of regeneration of used PB

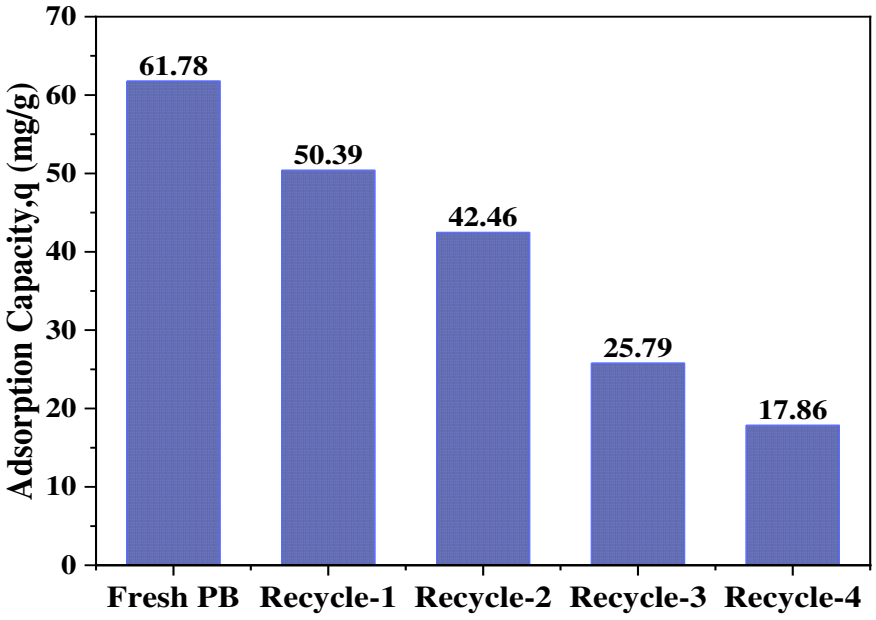

Figure 3.61 Adsorption capacities of regenerated PB

Experimental pH, adsorbent dose and other conditions were at optimum level. The results of regeneration studies are presented in **Figure 3.61** which shows that adsorption capacity step by step decreased from 50.39 mg/g to 17.86 mg/g. It is cleart that regenerated PB can be reused to remove Cr^{3+} from aqueous solution.

3.2.3.9. Application of PB on real sample (Tanning wastewater and tannery wastewater) for alleviation of pollution load

3.2.3.9.1. Application of PB on Chrome tanning wastewater

After evaluating the capabilities of PB to remove Cr^{3+} ions from $Cr_2(SO_4)_3.6H_2O$ solution through a number of batch experiments, the effectiveness in removing of chromium ions from real sample (tanning wastewater) was justified. In order to observe the adsorption of Cr ions from concentrated chrome tanning effluent, 15 g of PB was added to 500 mL of Chrome tanning effluent and shaken at room temperature for 4 hours duration at pH 5.0. The concentration of chromium before and after adsorption was analyzed by ICP-MS and other water quality parameter such as pH, TDS, EC, NaCl %, BOD_5, and COD were also tested, and the values are presented in **Table 3.58.**

Table 3.58 Quality parameters of Chrome tanning effluents before and after adsorption.

Parameters	**Before adsorption**	**After adsorption**	**% of removal**	**DoE/ECR Standard**
Cr(ppm)	3276.64	1103.19	66.33	2.0
Adsorption capacity (mg/g)	-	72.45	-	-
pH	4.6	5.2	-	6.5-9.2
TDS (ppm)	11723	3972	66.12	2100
EC (µS/cm)	10637	3834	63.96	1200
NaCl (%)	8.5	3.4	60.00	-
BOD_5 (ppm)	3273	1288	60.64	≤100
COD (ppm)	9632	3452	64.16	200-400

3.2.3.9.2. Application of PB on tannery wastewater

To investigate the performance of PB with tannery effluent, 5 g of adsorbent PB was added to 500 mL of tannery effluent by shaking at room temperature for 4 hours at pH 5.0. The concentration of chromium before and after adsorption was determined by ICP-MS. Moreover, water quality parameter such as pH, TDS, EC, NaCl %, BOD_5, and COD were also tested, and the results are showed in **Table 3.59.**

Table 3.59 Quality parameters of Tannery effluents before and after adsorption.

Parameters	**Before adsorption**	**After adsorption**	**% of removal**	**DoE/ECR Standard**
Cr (ppm)	423.28	72.46	82.88	2.0
Adsorption Capacity (mg/g)	-	35.04	-	-
pH	5.5	6.3	-	6.5-9.2
TDS (ppm)	7791	2583	66.85	2100
EC (µS/cm)	5348	1564	70.76	1200
NaCl (%)	4.2	1.5	64.29	-
BOD_5 (ppm)	2207	619	71.95	≤100
COD (ppm)	4278	1271	70.29	200-400

3.2.1.9.3. Discussion on real sample analysis

The results showed (**Table 3.58** and **Table 3.59**) that after adsorption, the % of chromium removal was 66.33 % and 82.88 % but the adsorption capacity was 72.45 and 35.04 mg/g in case of Chrome tanning effluents and tannery effluents correspondingly. In case of tannery effluent, adsorption capacity was much lower compare to prepared solution could be due to the interference of other matters or ions that are being incorporated in leather manufacturing which decrease the capacity of the PB [298]. However, after adsorption with PB the water quality parameters (pH, TDS, EC, NaCl %, BOD_5, and COD) of collected Chrome tanning and tannery effluents were also decreased notably.

3.3. Part 3: Preparation, Characterization and Application of Adsorbent to Remove Leather Dye C.I. Acid Red 73 (AR73) from aqueous solution and tannery effluents.

3.3.1. Preparation of potato peel powder (PP)

Collected potato peels were washed and cut into small pieces. After that, pieces potato peels were dried out in air oven at 60 ^{O}C for 48 hours. The dried peels were then powdered in a stainless grinding machine and preserved in an air tight bottle. Powdered potato peels (PP) were used as adsorbent in this study to remove dye from aqueous solution and tannery effluents.

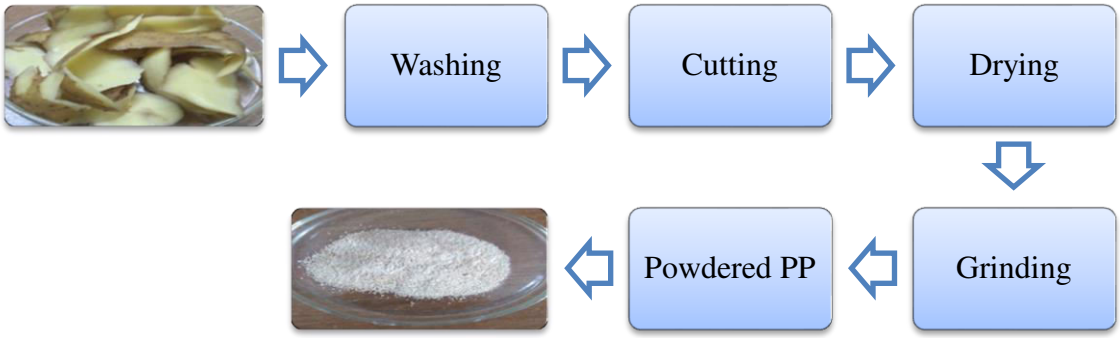

Flow chart 3.7 Flow diagram of PP preparation

3.3.2. Characterization of PP

3.3.2.1 Chemical composition of PP

Composition of potato peel [303 - 304] from the **Table 3.60** it is observed that the highest component was carbohydrate and protein and others are minor components.

Table 3.60 Proximate chemical composition of potato peel

Component	Dry weight (%)
Moisture	11.2
Carbohydrate	64.47 - 66.74
Protein	12.50 - 13.52
Fibre	8.71
Fat	2.20

3.3.2.2. Elemental analysis of PP

Dye laden EDX image of PP revealed an increase in elements composition after adsorption. The functional group of the adsorbent and the reactive groups of the adsorbate may be responsible for the change in elemental composition of dye loaded PP. There was a noticeable mass transfer of the C-group of the adsorbate onto the PP surface was observed whilst oxygen was consumed [252].

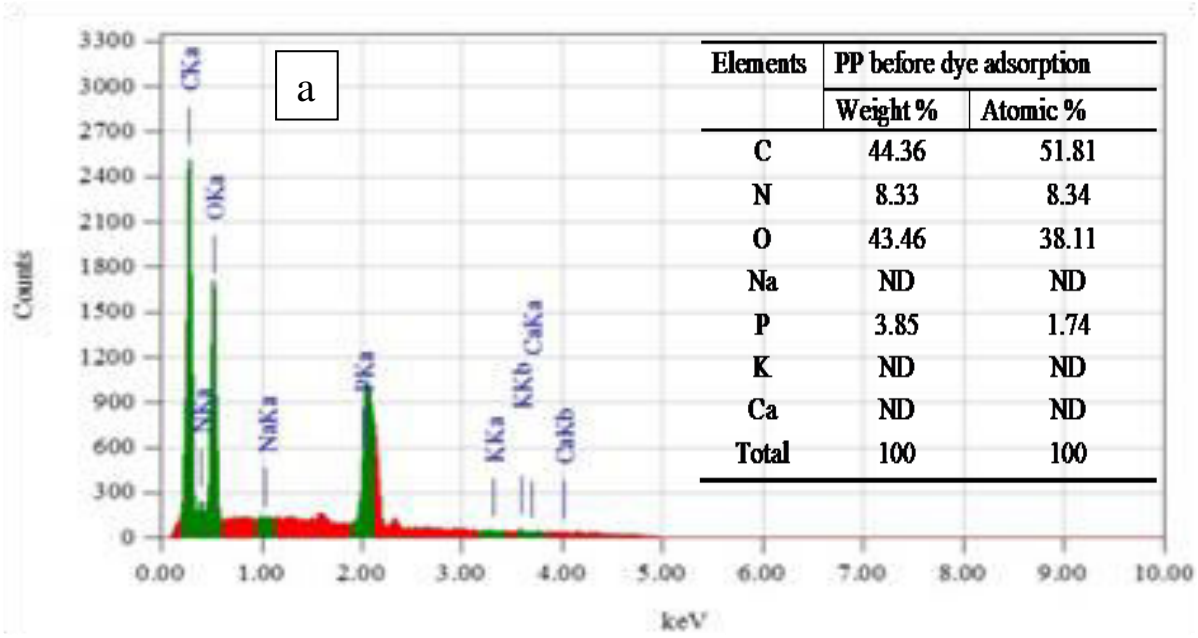

Elements	PP before dye adsorption	
	Weight %	Atomic %
C	44.36	51.81
N	8.33	8.34
O	43.46	38.11
Na	ND	ND
P	3.85	1.74
K	ND	ND
Ca	ND	ND
Total	100	100

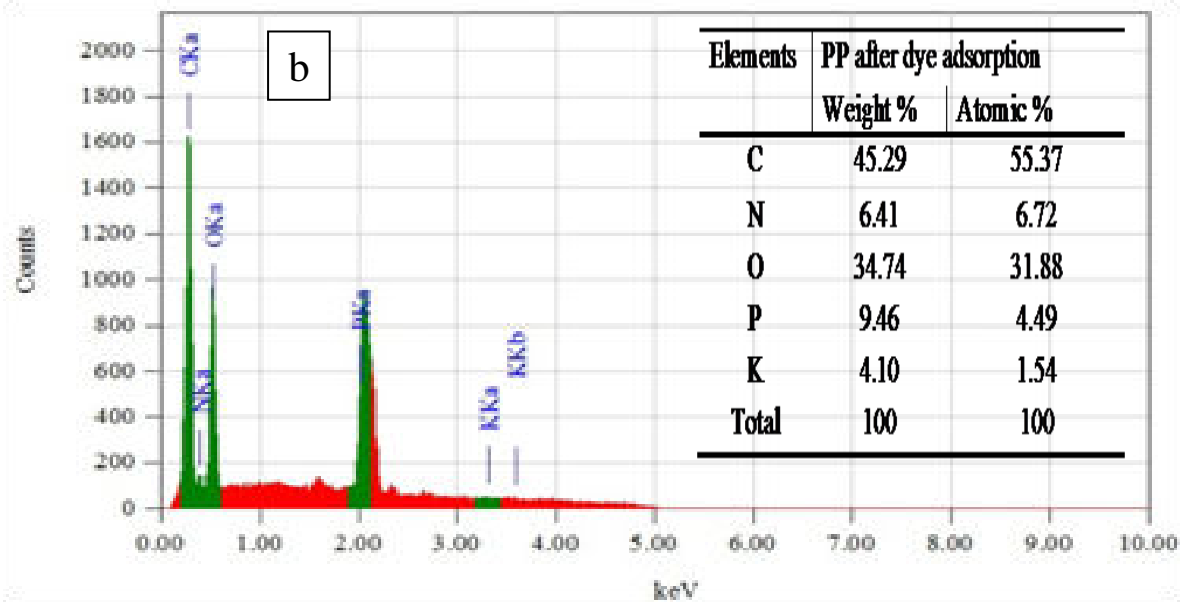

Elements	PP after dye adsorption	
	Weight %	Atomic %
C	45.29	55.37
N	6.41	6.72
O	34.74	31.88
P	9.46	4.49
K	4.10	1.54
Total	100	100

Figure 3.62 Energy dispersive X-ray (EDX) spectrum of PP (a) before and (b) after dye adsorption.

3.3.2.3. FTIR analysis of PP

The FTIR spectrum of PP in the range of 4000 to 600 cm^{-1} before and after dye adsorption is presented in **Figure 3.63**. The spectrum displays many peaks reflecting the complex nature of PP. The peak at 3321 cm^{-1} in PP-1 and 3360 cm^{-1} and PP-2, was due to OH stretching vibration which suggests the presence of alcohols and phenols [307]. The band at 2931 and 2920 cm^{-1} were attributed to the saturated aliphatic -CH groups. The peak associated to OH and COOH were detected at 1639, 1450, 1280 and 1072 cm^{-1} in case of PP-1, whereas, another significant peak was 1377 cm^{-1} of aliphatic C-H [300]. The FTIR spectrum of PP after dye adsorption exhibit changes due to may be complex bonding, hydrogen bonding or other electrostatic interaction. The intensity of the peaks after dye adsorption were relatively more compare to before dye adsorption [192, 201].

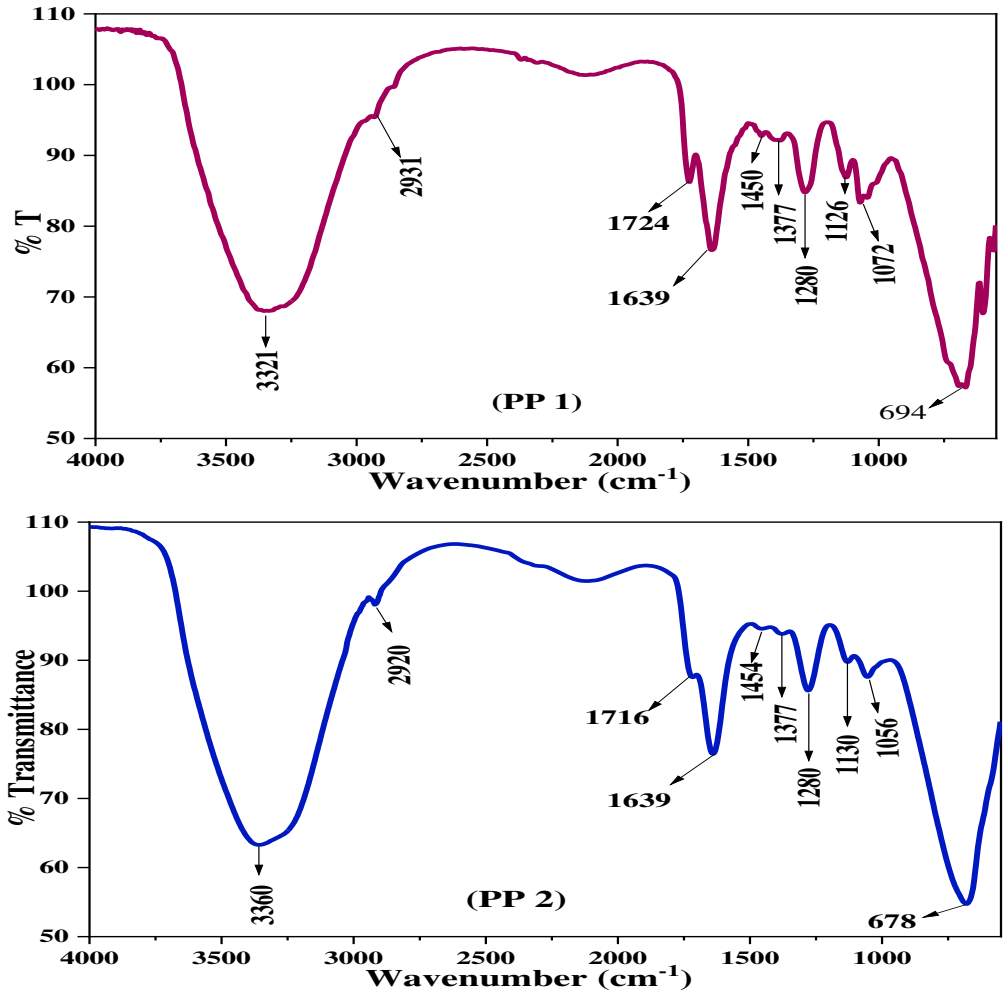

Figure 3.63 FTIR spectra of PP-1 (Potato peel powder before dye adsorption), PP-2 (Potato peel powder after dye adsorption)

3.3.2.4. Scanning Electron Microscopic (SEM) analysis of PP

Surface morphology of PP was showed through the SEM image (**Figure 4.64)** which has rough and porous structure that support the adsorption process for dye removal [201].

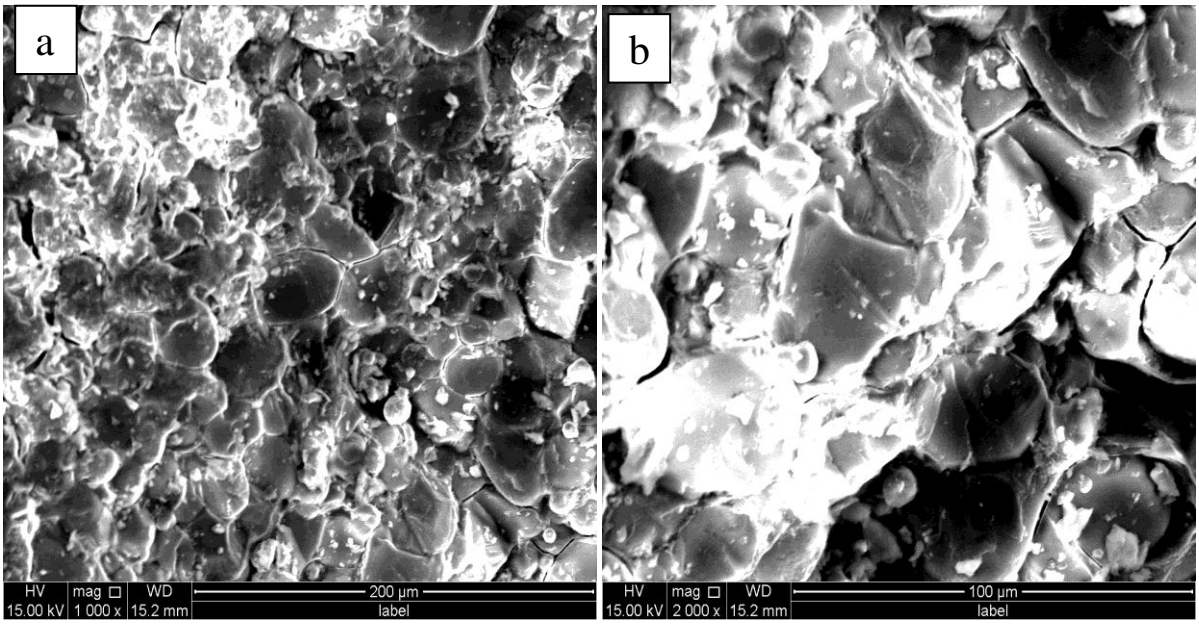

Figure 3.64 SEM images of PP (a) 1000x, and (b)2000x magnification

3.3.2.5. X-Ray diffraction (XRD) analysis of PP

There was no well-defined peak associated with the crystalline phase in the XRD pattern. It displays a typical peak of carbonaceous compound.

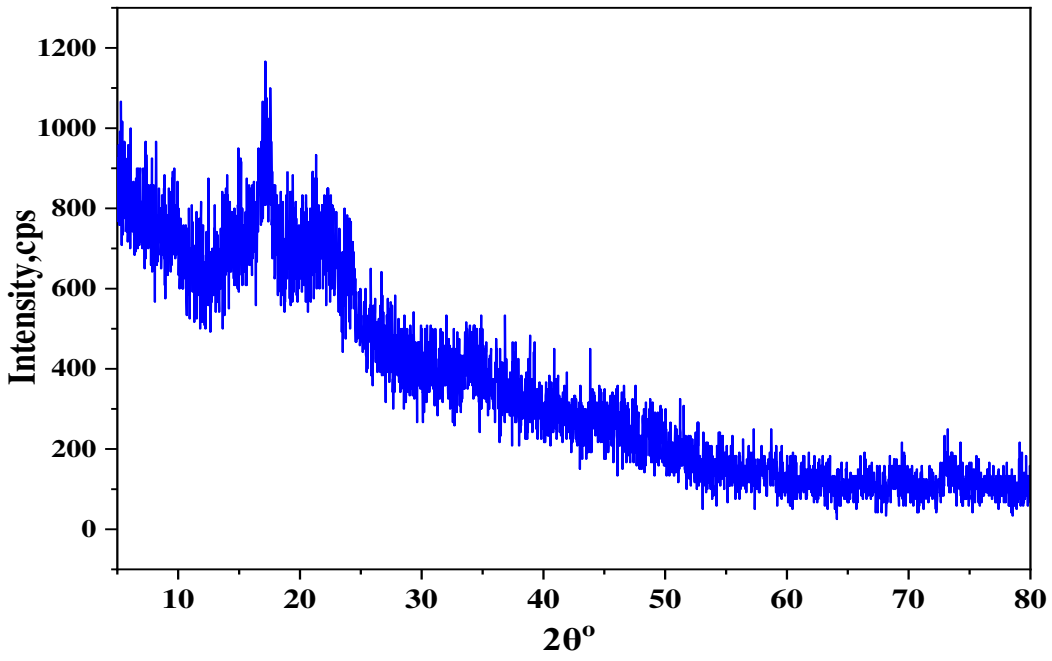

Figure 3.65 XRD analysis of PP

A hump in the range of 2θ = 15-25° and a peak at 2θ = 17.16° were observed (**Figure 3.65)** due to the amorphous structure with a high degree of disorder of PP. The presence of amorphous carbon is indicated by the broad and weak peaks in the XRD pattern of PP [288].

3.3.2.6. Brunauer-Emmett-Teller (BET) analysis of PP

Surface area, pore volume, and pore diameter of PP were analyzed by nitrogen gas sorption system are presented in **Table 3.61**. Powdered PP had low surface area of 2.00 m^2/g may be due to the breakdown of cell walls [287, 306]. Barrett-Joiner-Halenda (BJH) method was followed to compute the average pore diameter was 85.98Å, which suggest that PP consists of mesopores [193].

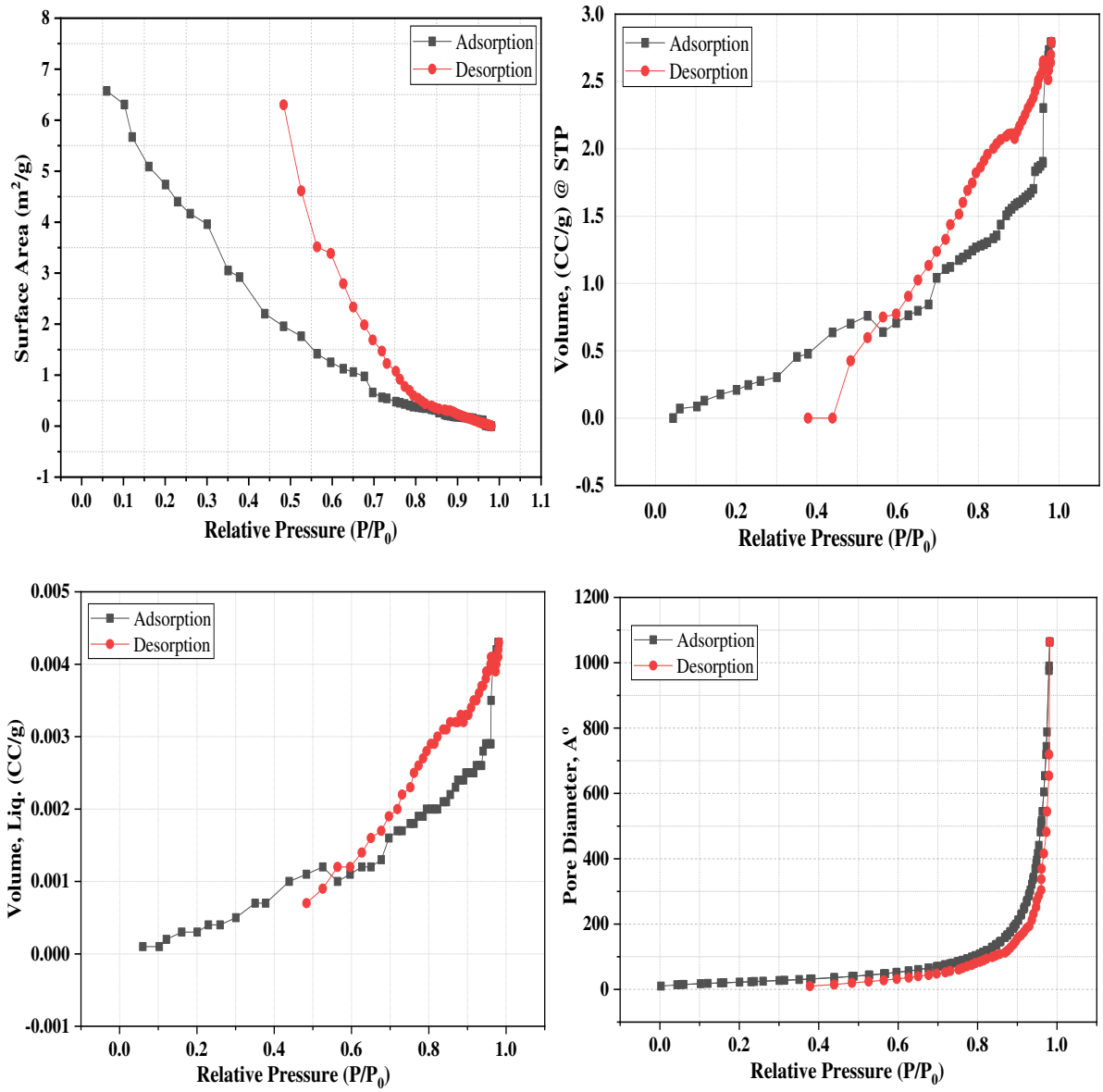

Figure 3.66 Adsorption and desorption isotherms of BET to PP

Table 3.61 BET surface area and porosity of PP

Sl. No.	Parameter	Result
01.	BET Specific Surface Area using multi-point analysis (m^2/g)	2.00
02.	Total Pore Volume (cc/g)	0.0043
03.	Skeletal density (g/cc)	1.8649
04.	Porosity based on skeletal density (per gram of sample)	0.0080
05.	Average Pore Diameter, 4V/S (Å)	85.98

3.3.2.7. Zeta potential value of PP

To investigate the role of pH of PP on Zeta potential value (ZPV) was examined. PP sample was prepared by dispersing PP in deionized water to analyze the ZPV. The study was performed in the pH range of 2.0-10.0.

Table 3.62 pH vs Zeta potential data of PP

pH	2	4	6	8	10
ZPV (mV)	0.597	0.264	-0.186	-0.306	-0.393

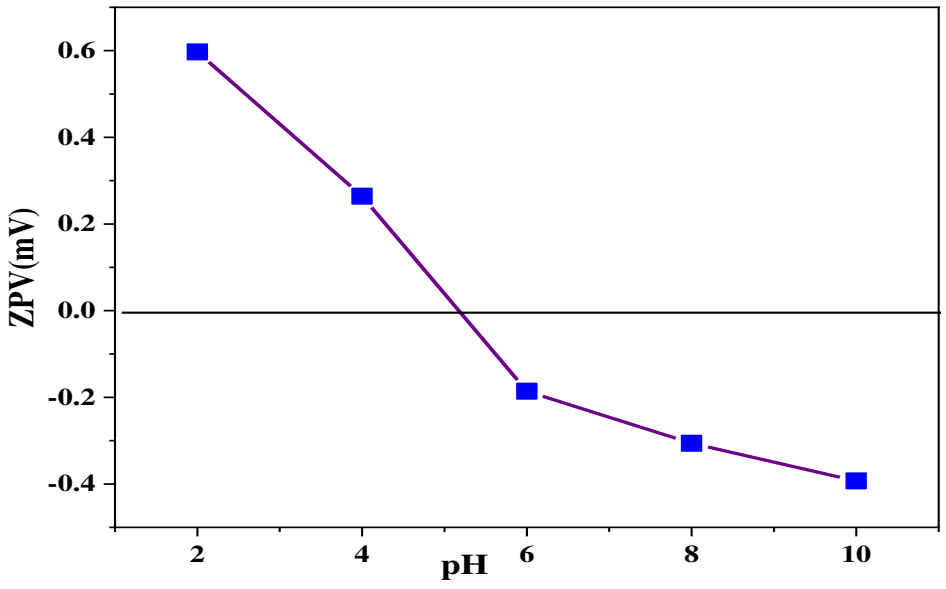

Figure 3.67 Zeta potential value of PP at different pH

From the **Table 3.62** and **Figure 3.67,** it is revealed that ZPV of PP was positive (0.264 mV) up to 4.0 pH, while with an increase of pH from 6.0 to 10.0, the values were negative (-0.186 to -0.393 mV).

3.3.3. Adsorption of leather dye C.I. Acid Red 73 (AR73) on PP

3.3.3.1. Calibration curve of dye AR73

A calibration curve was developed by using 5, 25, 50, 75, 100, 125, and 150 ppm dye solutions in UV-visible spectroscopy by spectrophotometric method (**Table 3.63** and **Figure 3.68**). Unknown concentration was measured before and after dye adsorption with reference to this calibration curve. After then adsorption capacity or % of removal was computed through the equation (3.1), or (3.2) and (3.3) respectively.

Table 3.63 Concentration vs absorbance data of dye (AR73) solutions

Conc. (ppm)	5	25	50	75	100	125	150
Absorbance	0.1914	0.6274	1.2083	1.734	2.2904	2.8633	3.3912

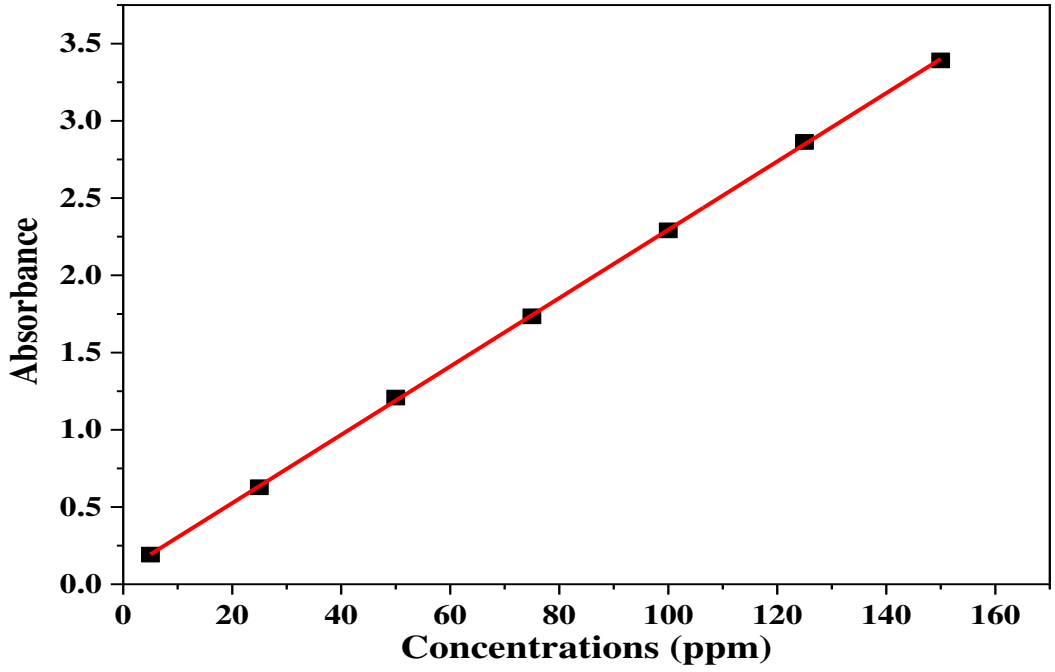

Figure 3.68 Calibration curve of dye (AR73) solutions

3.3.3.2. Effect of pH on adsorption capacity of PP for dye adsorption

The impact of pH on the adsorption of dye (AR73) on PP was studied with 150 ppm dye solution by varying it in the range of 2.0 to 7.0. In these experiment 50 mg PP were added in

each solution (25 mL) and then shaken at 160 rpm for 2 hours. After filtering the mixtures any change in dye concentrations were determined by UV-Vis spectroscopy. It is visible from the **Table 3.64** and **Figure 3.69** that adsorption capacity of PP was decreased with higher pH (2.0 to 7.0) and the utmost capacity was 74.99 mg/g at pH 2.0.

Table 3.64 pH v/s adsorption capacity data of PP for dye (AR73) adsorption

pH	2	3	4	5	6	7
Adsorption Capacity, q (mg/g)	74.99	71.38	49.78	33.92	35.89	34.2

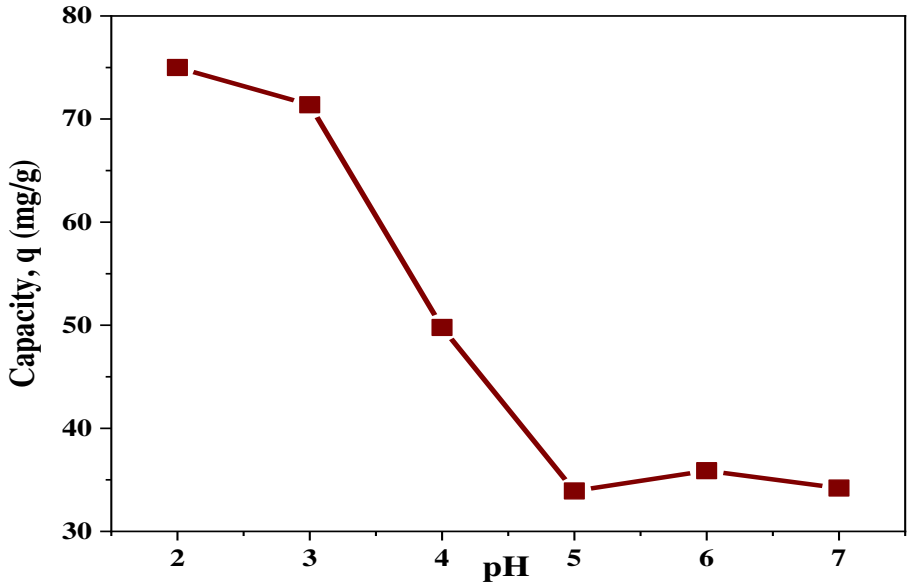

Figure 3.69 Effect of dye solution's pH on adsorption capacity of PP for dye adsorption

It is predictable that ion exchange and H-bonding may be the principle mechanism to remove dye [290]. At lower pH (2.0) the adsorption capacities found to be high due to the higher number of protons ensuing higher adsorption of anionic dye (AR73). On the other hand surface negativity of PP was increased with higher pH which was observed from the ZPV (**Figure 3.67**), hence anionic dye AR73 adsorption on pp was decreased [309].

$$\text{Dye—SO}_3\text{Na} \xrightarrow{\text{At Lower pH}} \text{Dye—SO}_3\text{H}$$

$$\text{Dye—SO}_3\text{H} \underset{\text{Lower pH}}{\overset{\text{Higher pH}}{\rightleftharpoons}} \text{Dye—SO}_3^-$$

In the study, all batch experiments were performed at pH 2.0 to achieved highest adsorption capacity.

3.3.3.3. Effect of adsorbent dosage on adsorption capacity of PP for dye (AR73) adsorption and % of removal

Effect of adsorbent dosage on dye (AR73) adsorption was analyzed by applying various dosage from 0.5 to 3.0 g/L to set the optimum dose. The batch experiments were run for 2 hours with 150 ppm initial concentration at optimum pH 2.0.

Table 3.65 Dosage v/s adsorption capacity and % removal data of PP

Dosage (g/L)	0.5	1	1.5	2	2.5	3
Adsorption Capacity (mg/g)	251.44	138.92	95.63	73.46	59.39	49.98
Removal (%)	83.81	92.61	95.63	97.95	98.99	99.96

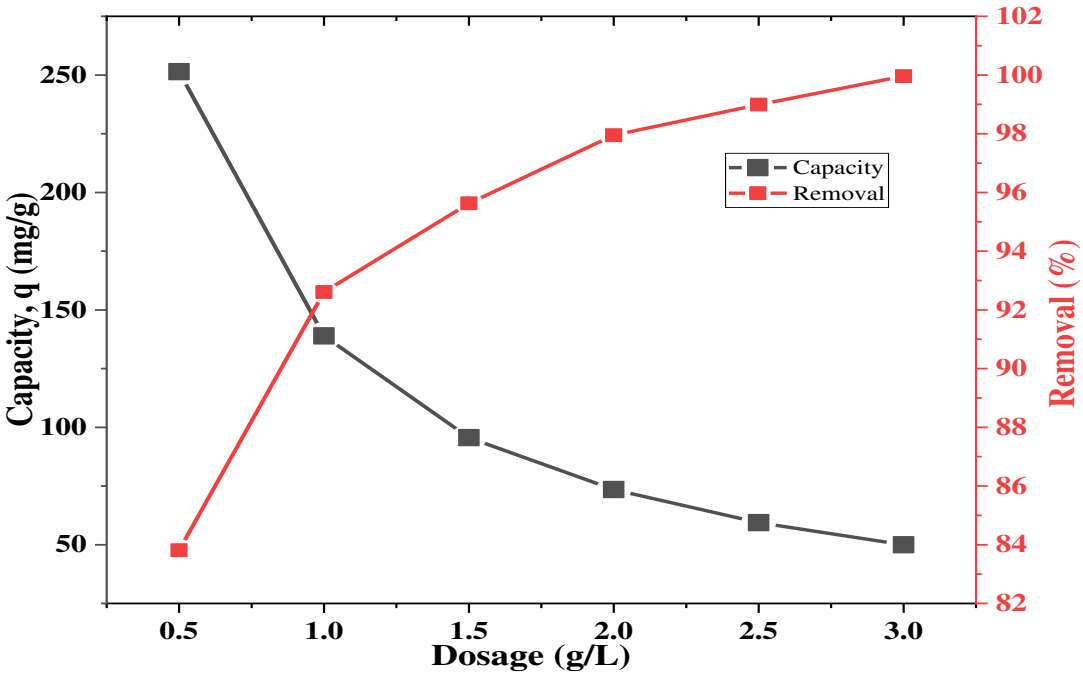

Figure 3.70 Effect of PP Dosage on adsorption capacity and % removal of dye

It is showed that (**Table 3.65, Figure 3.70**) % of dye removal was increased 83.81 to 99.96 % whereas adsorption capacity was decreased 251.44 to 49.98 mg/g with the increase of PP dosage. The availability of more adsorption sites is thought to improve the % removal of dye, but more unsaturated sites minimize the adsorption capacity with higher adsorbent dosage [159]. It was revealed that almost 1.00 g/L dose exhibits the best % removal also best adsorption capacity. However, for simplification 1.0 g/L dose were used all over the study.

3.3.3.4. Effect of dye concentrations and contact time on dye (AR73) adsorption

To search the impact of dye (AR73) concentrations and contact duration on adsorption capacity of PP, 20 mL solutions of four different concentrations (100, 150, 200, and 300, ppm) were taken in conical flasks and then 20 mg (1.0 g/L) PP was added to of each solution. The experiments were carried out at pH 2.0 by several time gaps ranging from 5-120 minutes with constant shaking speed 160 rpm.

Table 3.66 Time vs adsorption capacity data of PP for dye adsorption

Time (min)	Adsorption capacity (mg/g)			
	150 ppm	**200 ppm**	**250 ppm**	**300 ppm**
0	0	0	0	0
5	125.25	156.58	186.28	200.47
10	130.21	157.95	187.98	208.73
15	130.26	159.71	187.83	212.4
20	131.99	161.75	189.87	214.68
30	133.69	163.85	192.08	217.26
40	133.72	163.92	191.97	218.94
60	133.08	164.09	192.19	217.84
120	133.95	163.8	192.08	218.94

The findings (**Table 3.66, Figure 3.71)** revealed that adsorption capacity increased with increasing duration until it reached at equilibrium and after then, there was no significant increase in adsorption capacity. It was proven that adsorption capacity reached at equilibrium almost after 30 minutes, and adsorption capacity increased with higher dye concentration. In case of 150 ppm initial dye concentration, equilibrium adsorption capacity was 133.69 mg/g while at 200, 250, and 300 ppm concentration, adsorption capacity was 163.85, 192.08, and 217.26 mg/g correspondingly. The uppermost adsorption capacity 217.26 mg/g was attained with 300 ppm solution.

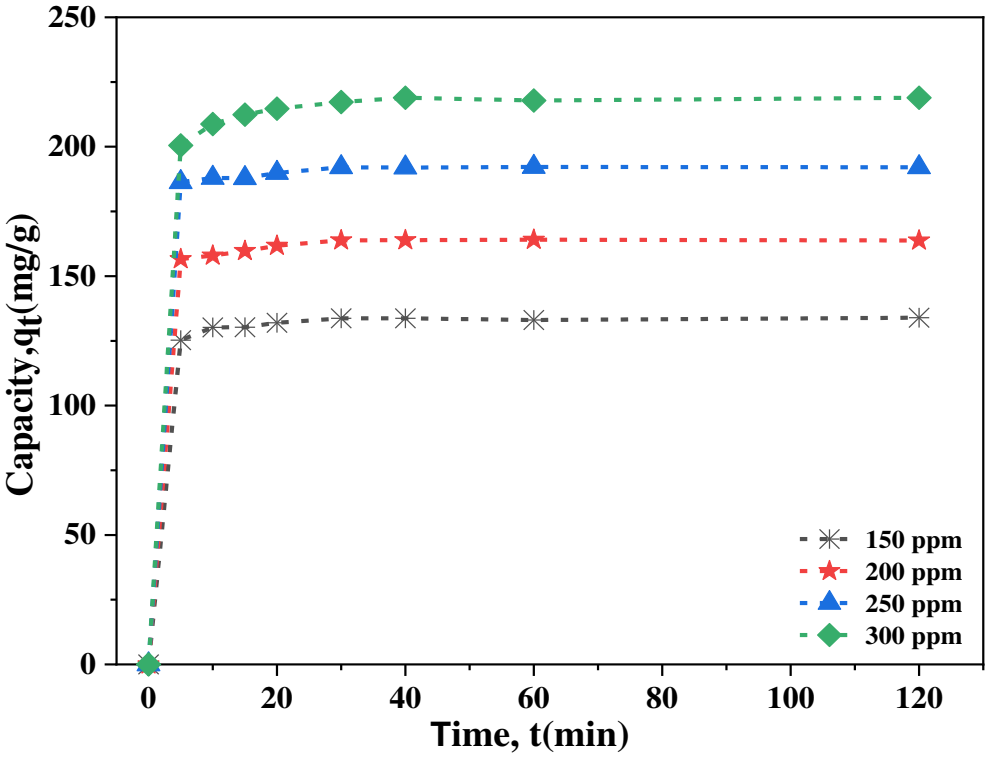

Figure 3.71 Effect of dye concentrations and contact time on adsorption capacity

The clarification is because initially there were more active sites available, but after certain time these sites got saturated [203]. Moreover, the equilibrium adsorption capacity was increased with higher dye concentration. It is because, the resistance to dye uptake decreased since the mass transfer driving force between the aqueous and solid phase increase [201, 308]

3.3.4. Adsorption isotherms for dye adsorption on PP

Adsorption isotherm tells the correlation within the number of adsorbates adsorbed on the adsorbent, commonly examined the experimental data with Langmuir and Freundlich isotherm. In Langmuir isotherm, the adsorbate is expected to be absorbed on the adsorbent in a monolayer on well-defined with no intermolecular interactions, however, Freundlich isotherm reflects multilayer adsorption with non-uniform distribution [311].

3.3.4.1. Langmuir isotherm for dye (AR73) adsorption

The Langmuir isotherm model was exercised by equation (3.4) plotting C_e/q_e versus C_e (**Table 3.67, Figure 3.72**). A linear link between C_e/q_e and C_e was observed with acceptable regression factor ($R^2 = 0.989$). Maximum adsorption capacity q_m (theoretical), was calculated from the slope and found 258.39 mg/g. The separation factor R_L provides information of qualitative measure of the favorability, R_L >1indicates unfavorable adsorption while 0<

R_L<1indicates favorable process. In this study, R_L was calculated by equation (3.5) and the value was 0.0565 indicates favorable monolayer adsorption process [293] .

Table 3.67 C_e vs C_e/q_e data of PP at different concentration for dye adsorption

Initial concentration (ppm)	150	200	250	300
Equilibrium concentration (C_e)	16.31	36.15	57.92	82.74
C_e/q_e	0.122	0.22	0.302	0.381

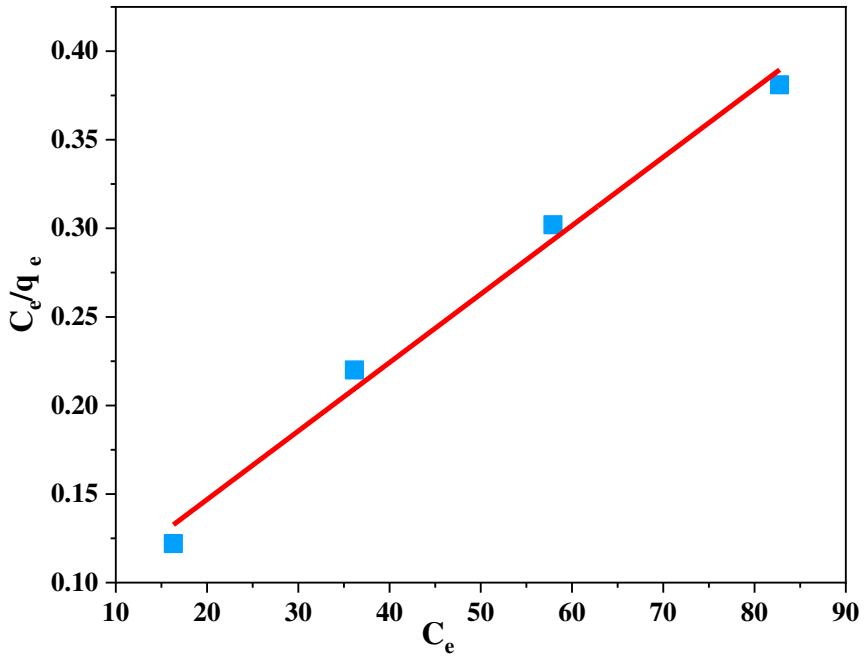

Figure 3.72 Langmuir isotherm for dye (AR73) adsorption on PP

3.3.4.2. Freundlich isotherm for dye (AR73) adsorption

The experimental data was justified for multilayer adsorption mechanism through Freundlich isotherm equation (3.6) by plotting a graph of $\ln C_e$ versus $\ln q_e$ (**Table 3.68, Figure 3.73**) and linear connection was observed with good regression coefficient, $R^2 = 0.993$. From the slope n was calculated and found to be 3.359 which showed good adsorption process [208]. Usually since n decreases, adsorption becomes more complicated (n = 2-10 denotes good adsorption, n = 1-2 difficult adsorption and n<1 poor adsorption) [294].

Table 3.68 lnC_e vs lnq_e data of PP at different concentration for dye adsorption

Initial concentration (ppm)	150	200	250	300
lnC_e	2.792	3.588	4.059	4.416
lnq_e	4.896	5.099	5.258	5.381

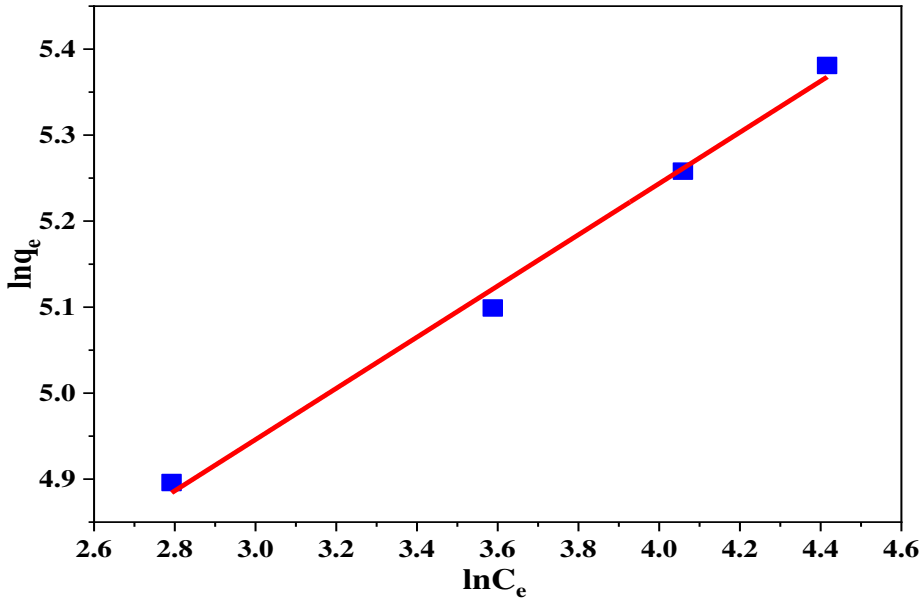

Figure 3.73 Freundlich adsorption isotherm for dye (AR73) adsorption on PP

3.3.4.3. Explanation on isotherms for dye adsorption

The values of various parameters of two models suggests (**Table 3.69**) that the adsorption of dye (AR73) on PP comply both Langmuir and Freundlich model but preferably the Freundlich model.

Table 3.69 Theoretical values of q_m, b, R_L, n, k_F and R^2 of adsorbent PP

Parameters	q_m (mg/g)	b (Lmg^{-1})	R^2	R_L	n	k_F
Langmuir isotherm	258.39	0.0556	0.989	0.0565	-	-
Freundlich isotherm	-	-	0.993	-	3.359	57.546

3.3.5. Adsorption kinetics for dye adsorption on PP

The adsorption kinetics is important to investigate how quickly ions move from aqueous to solid phase and how long it takes time to reach equilibrium position. In the study, two kinetic models (Pseudo-first-order and pseudo-second-order) were applied to justify the adsorption process.

3.3.5.1. Pseudo-First-Order reaction kinetics for dye adsorption on PP

The Pseudo-First-Order kinetic equation (3.7) was introduced by Lagergren in 1898 to illustrate the adsorption process. Pseudo-first-order kinetic model was obtained by plotting a graph with $\log(q_e-q_t)$ against t (**Table 3.70, Figure 3.74**) where a linear relationship was observed in between $\log(q_e-q_t)$ and t.

Table 3.70 Time, t(min) and $\log(q_e-q_t)$ data of PP at different concentration

Time, t(min)	$\log(q_e-q_t)$ at 150 ppm	$\log(q_e-q_t)$ at 200 ppm	$\log(q_e-q_t)$ at 250 ppm	$\log(q_e-q_t)$ at 300 ppm
5	0.926	0.862	0.763	1.225
10	0.542	0.771	0.613	0.931
15	0.535	0.617	0.628	0.687
20	0.23	0.322	0.344	0.412

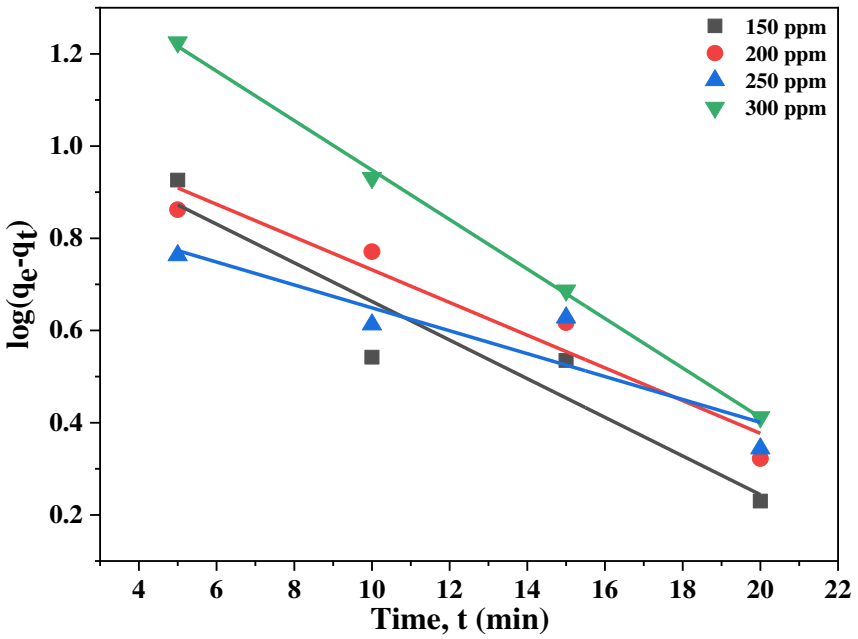

Figure 3.74 Pseudo-first-order kinetics for dye (AR73) adsorption on PP

3.3.5.2. Pseudo-second-order reaction kinetics for dye adsorption on PP

In 1999 Ho and Mckay established pseudo-second-order rate reaction (2.8) and the model was obtained with a graph by plotting t/q_t versus t (**Figure 3.75**).

Table 3.71 Time, t (min) and t/q_t data of PP at different concentration

Time, t(min)	t/q_t at 150 ppm	t/q_t at 200 ppm	t/q_t at 250 ppm	t/q_t at 300 ppm
5	0.0399	0.0319	0.0273	0.0249
10	0.0768	0.0633	0.0532	0.0479
15	0.1151	0.0939	0.0798	0.0706
20	0.1515	0.1236	0.1053	0.0932
30	0.2244	0.1831	0.1562	0.1381

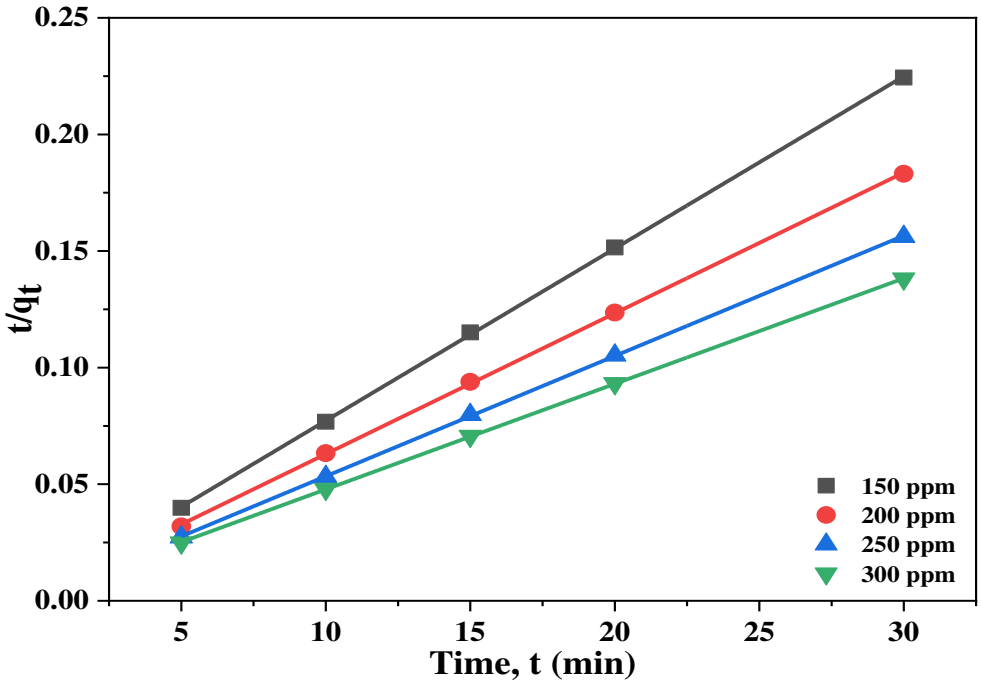

Figure 3.75 Pseudo-second-order kinetics for dye (AR73) adsorption on PP

3.3.5.3. Explanation on kinetics for dye adsorption on PP

Different parameters of kinetic models are computed from the slop and intercept of each linear plot are summarized in **Table 3.72.**

Table 3.72 Pseudo-First-Order and Pseudo-Second-Order kinetics parameters of dye adsorption on PP

Kinetics model	Parameters	150 ppm	200 ppm	250 ppm	300 ppm
Pseudo-First-Order	q_e^* (mg g^{-1})	133.69	163.85	192.08	217.26
	k_1(1/min)	0.0965	0.0815	0.0571	01234
	R^2	0.900	0.904	0.835	0.998
	q_e^{**} (mgg^{-1})	12.078	12.204	7.889	30.478
Pseudo-Second-Order	k_2 (g/mg min)	0.016	0.0138	0.015	0.0081
	R^2	0.999	0.999	0.999	0.999
	q_e^{**} (mg g^{-1})	135.14	166.67	192.31	222.22

* Experimental, ** Theoretical

The linear fitting results of the two models suggest that in case of pseudo-second-order model, the theoretical q_e values agreed well with the experimental q_e values. It was also found that the correlation coefficient (R^2) values of Pseudo-Second-Order kinetic model was better compare to pseudo-first-order-kinetic model.

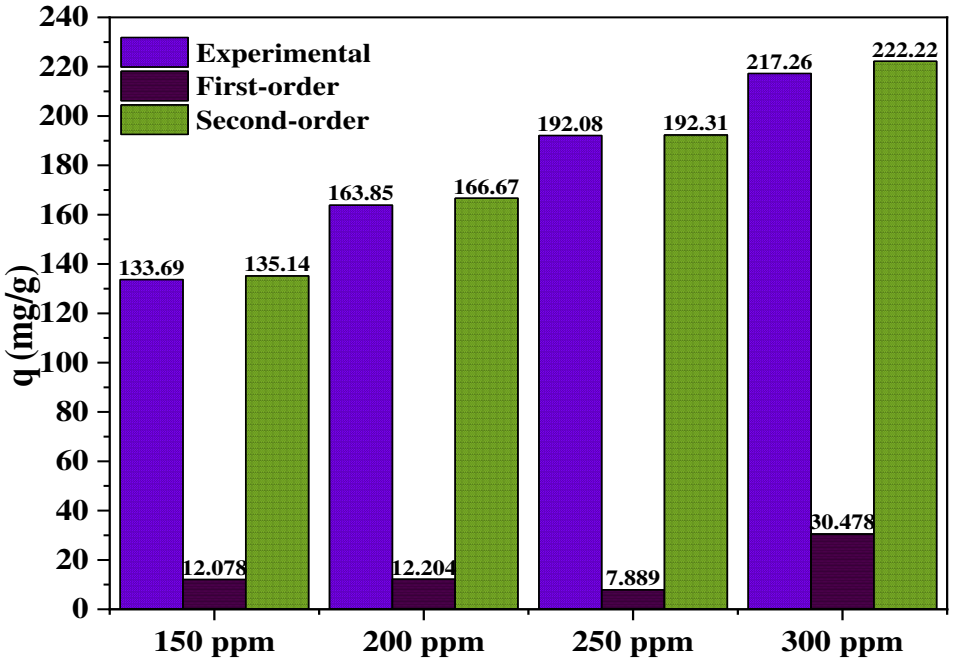

Figure 3.76 Comparison between experimental and calculated dye adsorption capacity of PP

The feasibility of the model is dependent on the closeness of the theoretical and experimental q_e value and the highness of regression coefficient (R^2). It is evident from the **Figure 3.76** that the calculated adsorption capacities were in good agreement with the experimental values in case of Pseudo-second-order kinetics. Hence, it is comprehensible that Pseudo-Second-Order model was better fitted for dye adsorption on PP compared to earlier model.

3.3.6. Thermodynamic analysis for dye (AR73) adsorption on PP

To verify endothermic or exothermic nature of the adsorption process of dye on PP was also studied at different temperature. Adsorption experiments were run at a series of temperatures to determine thermodynamic parameters, e.g., Gibbs free energy (ΔG), enthalpy (ΔH), and entropy (ΔS) by the equations (2.9), (2.10) and (2.11).

For this study, 20 mg PP was added in to 20 mL (150ppm) of dye solution at pH 2.0 for each experiment. The batch experiments were than shaken in an orbital shaker at 298K, 308K, 318K and 328K temperature at different time period ranging from 5-120 minutes. The impact of temperature and contact duration on dye adsorption capacity of PP were investigated and showed in **Table 3.73** and **Figure 3.77.** With increased temperature, the adsorption efficiency of PP was decreased [201].

Table 3.73 Temperature and time vs adsorption capacity data of PP

Time, t (min)	Adsorption Capacity (mg/g)			
	298K	**308K**	**318K**	**328K**
0	0	0	0	0
5	68.4	58.73	57.64	57.63
10	89.09	83.62	82.62	83.62
15	109.45	105.11	96.17	91.54
20	131.84	120.17	111	99.17
30	135.34	125.34	114.27	104.08
40	136.21	125.53	114.58	105.21
60	136.13	124.41	115.21	104.74
120	135.44	124.23	115	105.11

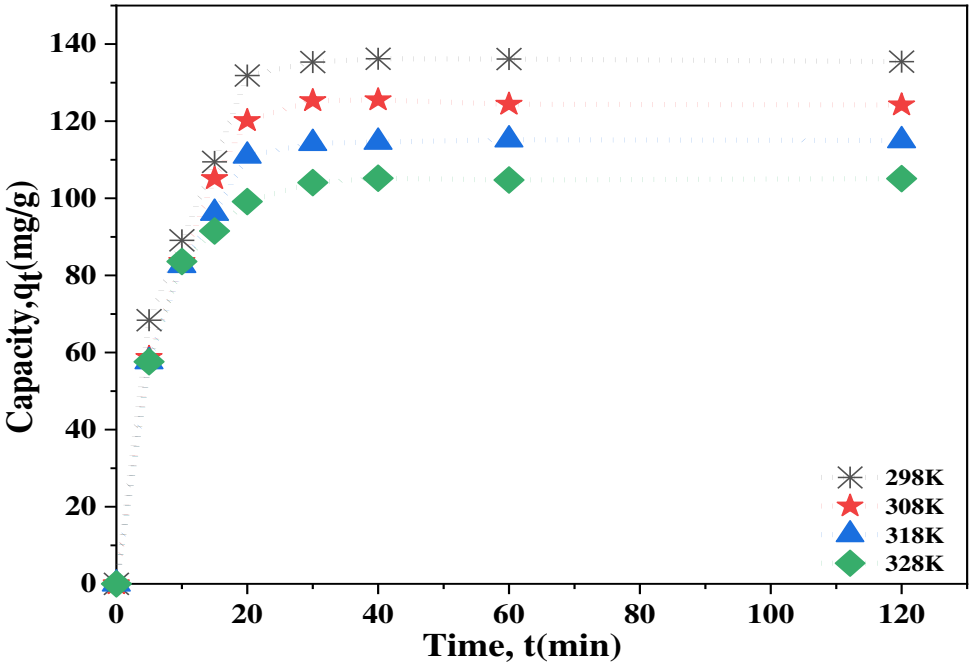

Figure 3.77 Effect of temperature and time of dye adsorption on PP

Table 3.74 van't Hoff equation 1/T vs lnk_d data of PP for dye adsorption

1/T	0.0034	0.0032	0.0031	0.003
lnk_d	2.223	1.626	1.163	0.818

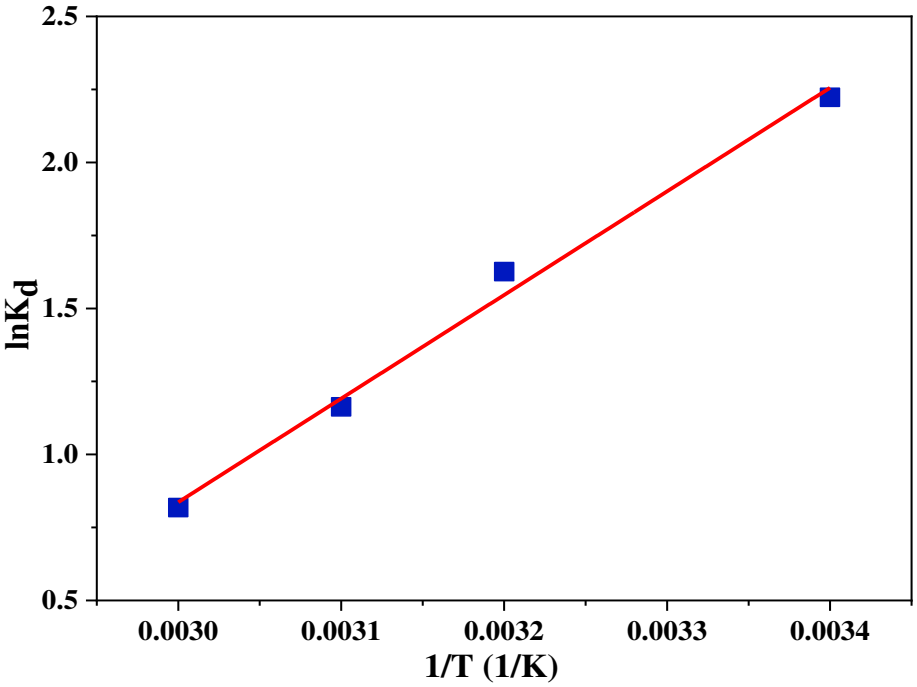

Figure 3.78 Thermodynamics of dye (AR73) adsorption on PP

Fact is that, when temperature raises, the kinetic energy increases and releases of the adsorbate from PP. At 298K temperature the equilibrium adsorption capacity was 135.34 mg/g which decreased to 125.34, 114.27, and 104.08 mg/g at 308K, 318K and 328K respectively.

Table 3.75 Thermodynamic parameters of PP for dye adsorption

T(K)	ΔG (kJ/mol)	ΔH (kJ/mol)	ΔS (kJ/mol K)	R^2
298	-5.503	- 29.498	- 0.0815	0.992
308	-4.102			
318	-3.074			
328	-2.231			

A straight line was acquired through a graph by plotting 1/T versus $\ln k_d$ (**Table 3.74, Figure 3.78**). The standard enthalpy (ΔH), and entropy (ΔS) was obtained from the slope and intercept and were - 29.498 kJ/mol and - 0.0815 kJ/mol (**Table 3.75**) respectively. The results of ΔG for adsorption of dye on PP at the temperatures of 293K, 308K, 323K and 338K were attained -5.503, -4.102, -3.074, and -2.231 kJ/mol, respectively. The negative ΔG exposed that adsorption of dye (AR73)) on PP was spontaneous and negative ΔH indicated exothermic in nature. Moreover the negative ΔS exposed the lessen in randomness at the solid/solute interface during the adsorption of dye on PP [295].

3.3.7. Plausible mechanism for dye adsorption on PP

Sorption mechanism express the electrostatic interaction between oppositely charged particles through different bond formations e.g., H-bonding, Van der Waals force, dipole-dipole induction, ion-exchange and so on. It was revealed from earlier investigation that the functional groups such as carboxyl, hydroxyl, and phenolic groups exist in bio- adsorbent could attach and remove dye along with other pollutants from dye effluents [295, 304]. It is assumed that PP contains hydroxyl and carboxyl groups which are supposed to form hydrogen bond (**Scheme 3.4**) with dye (AR73) which is prevail in this study [192].

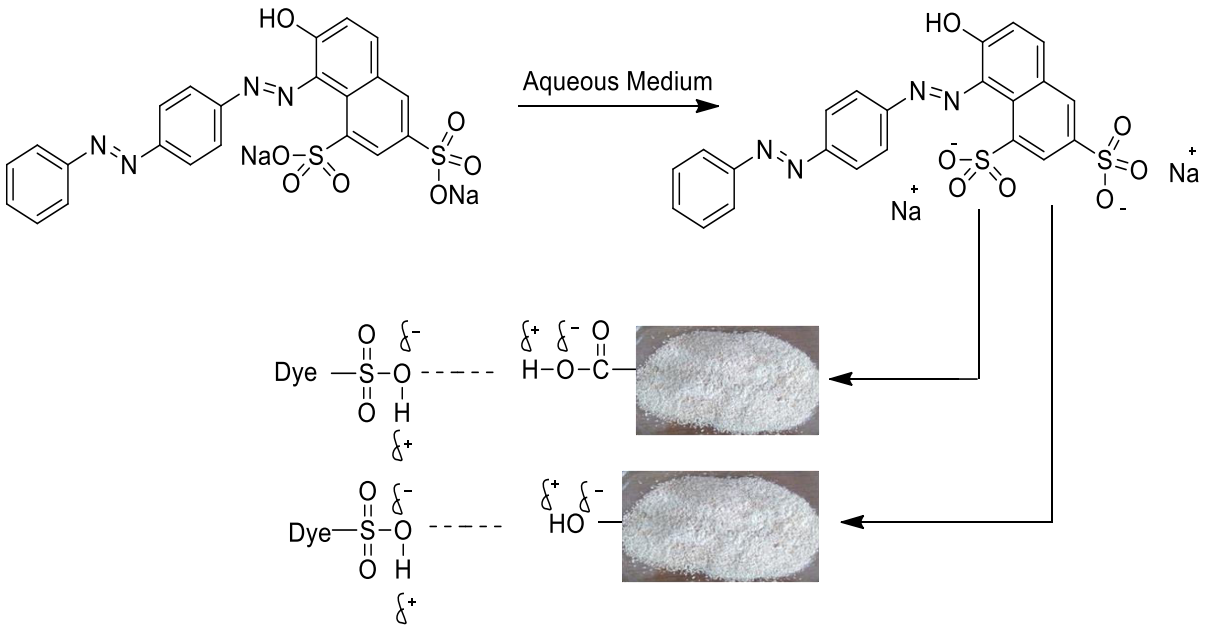

Scheme 3.4 Plausible mechanisms of dye (AR73) adsorption on PP

3.3.8. Regeneration of used PP for dye adsorption

The possibility of re-using PP as adsorbent was investigated. dye loaded PP was regenerated using1% NaOH and HCl solution thrice which was shown in the **Flow chart 3.8**.

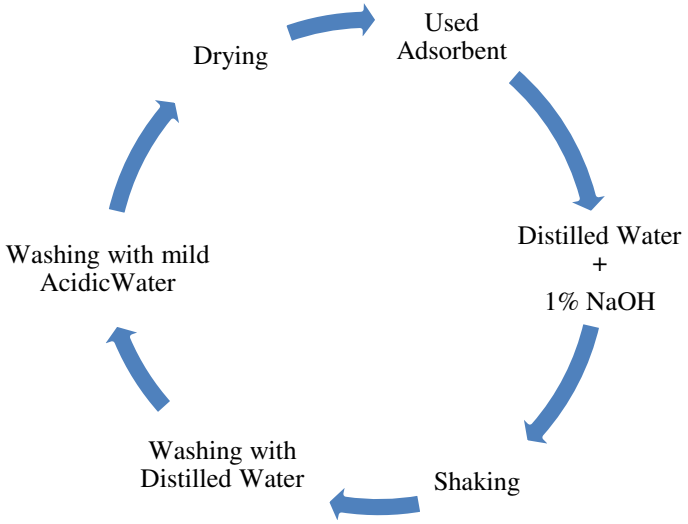

Flow chart 3.8 Flow diagram of regeneration of used PP

Experimental pH, adsorbent dose and other conditions were at optimum level. The results of regeneration studies are presented in **Figure 3.79** which shows that adsorption capacity gradually decreased from 86.73 to 37.49 mg/g. It is evident that regenerated PP can be reused to remove dye from aqueous solution.

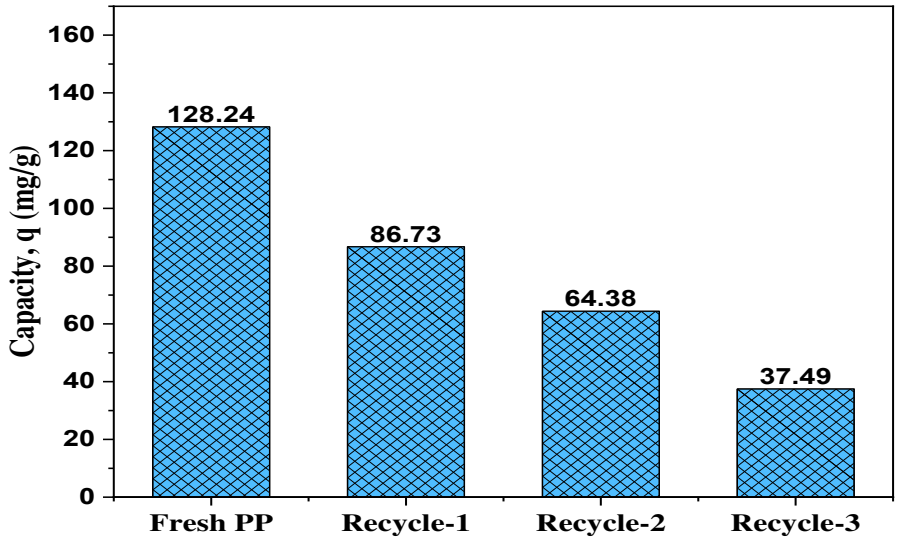

Figure 3.79 Adsorption capacities of regenerated PP

3.3.9. Application of PP on real sample (Dyeing wastewater) for alleviation of pollution load

After assessing the capabilities of PP in removing dye (AR73)) from aqueous solution by various batch experiments, the performance to remove dye from real sample (dye effluents) was verified. In order to observe the adsorption of dye from concentrated dye effluent, 250 mg (1.0g/L) of PP was added to 250 mL of dye wastewater and followed by shaking at room temperature for 2 hours at pH 2.8.

Table 3.76 Quality parameters of dye effluents before and after adsorption

Parameters	Before adsorption	After adsorption	% of removal	DoE Standard
Dye (PPM)	139.95	1.61	98.17	-
Adsorption Capacity (mg/g)	-	137.39	-	-
pH	5.5	5.2	-	6.5-9.2
TDS (ppm)	3,854	48	98.75	2100
EC (µS/cm)	1,709	97.3	94.31	1200
NaCl (%)	3.1	0.2	93.54	-
BOD_5 (ppm)	812	37	95.44	≤100
COD (ppm)	2164	286	86.78	200-400

The concentration of dye before and after adsorption was analyzed by UV-visible spectroscopy and other water quality parameter such as pH, TDS, EC, NaCl %, BOD_5, and COD were also tested, however the values are showed in **Table 3.76**.

3.3.10. Discussion on real sample analysis

Obtained results indicate (**Table 3.76**) that after adsorption, dye removal % was 98.17% but the adsorption capacity was 137.39 mg/g in case of dyeing effluents which is much lower than theoretical capacity (q_m, 258.39 mg/g). This is may be due to the presence of aggressive ions and other matters that were used in leather manufacturing which decrease the capacity of the PP [298]. On the other hand, after adsorption with PP the water quality parameters (pH, TDS, EC, NaCl %, BOD_5, and COD) of collected dyeing effluents were also reduced immensely and all values were within the standard limit except pH.

Chapter 4

Conclusions and Scope of Further Study

4.1. Conclusions

Water quality parameters had been determined for tannery effluent affected rivers of Bangladesh to evaluate the magnitude of surface water pollution. In the mitigation strategies, out of different remediation techniques adsorption had been applied by preparing various adsorbents from agro-based waste materials. The chemically activated pyrolyzed peanut shell and baggage and chemically activated peanut shell can be used as adsorbent to remove metal like chromium from tannery effluents. They could be regenerated and reused for several times. The natural potato peel could be the efficient adsorbent for the removal of leather dyes (anionic) from tannery effluents, however, further studies are warranted for their development as commercial adsorbent.

The following conclusions may be drawn from the present study

- This study found that important physicochemical parameter like TDS, EC, % NaCl and COD of Dhaleshwari, Buriganga, Bhairab and Karnaphuli river water were more than permissible limit set by national and international standards.
- A number of heavy metals such as Cr, Cu, Cd and Pb were observed greater than Bangladesh standard (ECR'97) which denoted the pollution level. It could be said that water of Dhaleshwari, Buriganga, Bhairab and Karnaphuli river were highly polluted as treated and or untreated tannery effluents discharged into the study area along with other industrial effluents.
- Chemically activated pyrolyzed peanut shell, chemically activated peanut shell, and chemically activated pyrolyzed bagasse had considerable adsorption capacity for the removal of chromium from aqueous solution and those could be used as competent adsorbents for the removal of chromium from tannery effluents.
- Potato peel powder showed significant adsorption capacity of anionic dyes from aqueous solution and leather dyeing effluent at lower pH, since the potato peel powder possessed positive surface charge at pH lower than pH_{zpc}.
- Al those adsorbents could be regenerated and reused for several time without losing too much capacity.
- The adsorption of Cr(III) was followed both the Langmuir and Freundlich isotherm models preferably Langmuir model by adsorbents pyrolyzed peanut shell, peanut shell, and pyrolyzed bagasse. However, potato peel powder was followed both the

Langmuir and Freundlich isotherm models preferably Freundlich model in case of dye adsorption.

- ❖ The pseudo-second-order kinetic model provided better correlation for all adsorbents compared to pseudo-first-order kinetic model.
- ❖ The value of Gibb's free energy and enthalpy change for all the prepared adsorbents were negative at different temperatures, which revealed the adsorption processes were physico-chemical and spontaneous at lower temperature.

4.2. Scope of Further Study

The following suggestions can be made for future study

- Adsorbents prepared from various agricultural by-products can be used for the removal of heavy metals and different anionic and cationic dyes since agricultural by-products are easily available and low cost.
- Composite can be prepared by mixing of agricultural by-products with different polymeric materials and adsorption capacity may studied for the reduction of pollution from tannery wastewater.
- The chemically activated pyrolyzed peanut shell, chemically activated peanut shell, and chemically activated pyrolyzed bagasse used for heavy metal removal are limited to lab scale, at present. Therefore, further research is required to scale up for a large-scale practical application.
- Potato peel powder showed significant adsorption capacity of anionic leather dye C.I. Acid Red 73 from aqueous solution and leather dyeing effluent, which could be tried for other dyes for leather and textile dyeing.

References:

[1] M. J. Uddin and Y. K. Jeong, "Urban river pollution in Bangladesh during last 40 years: potential public health and ecological risk, present policy, and future prospects toward smart water management," *Heliyon*, vol. 7, no. 2, p. e06107, 2021, doi: 10.1016/j.heliyon.2021.e06107.

[2] A. I. Alwared, A. J. Jaeel, and Z. Z. Ismail, "New application of eco-friendly biosorbent giant reed for removal of reactive dyes from water followed by sustainable path for recycling the dyes-loaded sludge in concrete mixes," *J. Mater. Cycles Waste Manag.*, vol. 22, no. 4, pp. 1036–1046, 2020, doi: 10.1007/s10163-020-00998-4.

[3] S. Liu, Y. Ding, P. Li, K. Diao, X. Tan, F. Lei, Y. Zhan, O. Li, B. Huang, and Z. Huang, "Adsorption of the anionic dye Congo red from aqueous solution onto natural zeolites modified with N,N-dimethyl dehydroabietylamine oxide," *Chem. Eng. J.*, vol. 248, pp. 135–144, 2014, doi: 10.1016/j.cej.2014.03.026.

[4] H. Zhang, H. Yang, B. Sarsenbekuly, M. Zhang, H. Jiang, W. Kang, and S. Aidarova., "The advances of organic chromium based polymer gels and their application in improved oil recovery," *Adv. Colloid Interface Sci.*, vol. 282, p. 102214, 2020, doi: 10.1016/j.cis.2020.102214.

[5] J. O. Ighalo, A. G. Adeniyi, J. A. Adeniran, and S. Ogunniyi, "A systematic literature analysis of the nature and regional distribution of water pollution sources in Nigeria," *J. Clean. Prod.*, vol. 283, no. xxxx, p. 124566, 2021, doi: 10.1016/j.jclepro.2020.124566.

[6] M. R. Uddin, M. M. Hossain, S. Akter, M. E. Ali, and M. A. Ahsan, "Assessment of some physicochemical parameters and determining the corrosive characteristics of the Karnaphuli estuarine water, Chittagong, Bangladesh," *Water Sci.*, vol. 34, no. 1, pp. 164–180, 2020, doi: 10.1080/11104929.2020.1803662.

[7] A. A. Alqadami *et al.*, *Efficient removal of toxic metal ions from wastewater using a recyclable nanocomposite: A study of adsorption parameters and interaction mechanism*, vol. 156. Elsevier Ltd, 2017. doi: 10.1016/j.jclepro.2017.04.085.

[8] B. Export Promotion Bureau, *Annual Report 2020-2021*. 2021.

[9] A. Rakib, "Export Trend of the Leather Industry of Bangladesh : Challenges to Sustainable Development," *BUFT J. Bus. Econ.*, vol. 1, pp. 163–187, 2020.

[10] H. L. Paul, A. P. M. Antunes, A. D. Covington, P. Evans, and P. S. Philips, "Bangladeshi leather industry: An overview of recent sustainable developments," *J. Soc. Leather Technol. Chem.*, vol. 97, no. 1, pp. 25–32, 2013.

[11] Asian Development Bank, "Developing the leather industry in Bangladesh," *ADB Briefs*, vol. NO. 102, no. 102, pp. 1–8, 2018, [Online]. Available: http://dx.doi.org/10.22617/BRF189645-2

[12] P. Brief, "The Leather Sector after the Tanning Industry Relocation : Issues and Challenges Prepared for : Prepared by : Research and Policy Integration for Development (RAPID) The Leather Sector after the Tanning Industry Relocation : Issues and Challenges □," no. May, 2019.

[13] M. M. Hasan, M. S. Ahmed, R. Adnan, and M. Shafiquzzaman, "Water quality indices to assess the spatiotemporal variations of Dhaleshwari river in central Bangladesh," *Environ. Sustain. Indic.*, vol. 8, no. September, 2020, doi:

10.1016/j.indic.2020.100068.

[14] K. Joseph and N. Nithya, “Material flows in the life cycle of leather,” *J. Clean. Prod.*, vol. 17, no. 7, pp. 676–682, 2009, doi: 10.1016/j.jclepro.2008.11.018.

[15] R. Aravindhan, B. Madhan, J. R. Rao, B. U. Nair, and T. Ramasami, “Bioaccumulation of Chromium from Tannery Wastewater: An Approach for Chrome Recovery and Reuse,” *Environ. Sci. Technol.*, vol. 38, no. 1, pp. 300–306, 2004, doi: 10.1021/es034427s.

[16] J. Buljan and I. Kráľ, “The framework for sustainable leather manufacture Second edition,” *United Nations*, p. 27, 2019, [Online]. Available: https://leatherpanel.org

[17] S. Ahmed, Fatema-Tuj-Zohra, M. S. H. Khan, and M. A. Hashem, “Chromium from tannery waste in poultry feed: A potential cradle to transport human food chain,” *Cogent Environ. Sci.*, vol. 3, no. 1, 2017, doi: 10.1080/23311843.2017.1312767.

[18] M. A. Hashem, M. Hasan, M. A. Momen, S. Payel, and M. S. Nur-A-Tomal, “Water hyacinth biochar for trivalent chromium adsorption from tannery wastewater,” *Environ. Sustain. Indic.*, vol. 5, no. February, p. 100022, 2020, doi: 10.1016/j.indic.2020.100022.

[19] C. R. China, M. M. Maguta, S. S. Nyandoro, A. Hilonga, S. V. Kanth, and K. N. Njau, “Alternative tanning technologies and their suitability in curbing environmental pollution from the leather industry: A comprehensive review,” *Chemosphere*, vol. 254, p. 126804, 2020, doi: 10.1016/j.chemosphere.2020.126804.

[20] S. Homaeigohar, “The nanosized dye adsorbents for water treatment,” *Nanomaterials*, vol. 10, no. 2, pp. 1–42, 2020, doi: 10.3390/nano10020295.

[21] S. M. A. Al Zumahi *et al.*, “Extraction, optical properties, and aging studies of natural pigments of various flower plants,” *Heliyon*, vol. 6, no. 9, p. e05104, 2020, doi: 10.1016/j.heliyon.2020.e05104.

[22] M. M. Mahdi, F. T. Zohra, and S. Ahmed, “Dyeing of Shoe Upper Leather with Extracted Dye from Acacia Nilotica Plant Bark-An Eco-Friendly Initiative,” *Prog. Color. Color. Coatings*, vol. 14, no. 4, pp. 241–258, 2021, doi: 10.30509/pccc.2020.166673.1074.

[23] M. Malakootian and M. R. Heidari, “Reactive orange 16 dye adsorption from aqueous solutions by psyllium seed powder as a low-cost biosorbent: kinetic and equilibrium studies,” *Appl. Water Sci.*, vol. 8, no. 7, pp. 1–9, 2018, doi: 10.1007/s13201-018-0851-2.

[24] Y. Tang, J. Zhao, Y. Zhang, J. Zhou, and B. Shi, “Conversion of tannery solid waste to an adsorbent for high-efficiency dye removal from tannery wastewater: A road to circular utilization,” *Chemosphere*, vol. 263, p. 127987, 2021, doi: 10.1016/j.chemosphere.2020.127987.

[25] R. Hao, D. Li, J. Zhang, and T. Jiao, “Green synthesis of iron nanoparticles using green tea and its removal of hexavalent chromium,” *Nanomaterials*, vol. 11, no. 3, pp. 1–13, 2021, doi: 10.3390/nano11030650.

[26] S. Chowdhury, R. Mishra, P. Saha, and P. Kushwaha, “Adsorption thermodynamics, kinetics and isosteric heat of adsorption of malachite green onto chemically modified rice husk,” *Desalination*, vol. 265, no. 1–3, pp. 159–168, 2011, doi: 10.1016/j.desal.2010.07.047.

[27] S. Ahmed, S. Aktar, S. Zaman, R. A. Jahan, and M. L. Bari, “Use of natural bio-

sorbent in removing dye, heavy metal and antibiotic-resistant bacteria from industrial wastewater," *Appl. Water Sci.*, vol. 10, no. 5, pp. 1–10, 2020, doi: 10.1007/s13201-020-01200-8.

[28] C. Lei, C. Wang, W. Chen, M. He, and B. Huang, "Polyaniline@magnetic chitosan nanomaterials for highly efficient simultaneous adsorption and in-situ chemical reduction of hexavalent chromium: Removal efficacy and mechanisms," *Sci. Total Environ.*, vol. 733, p. 139316, 2020, doi: 10.1016/j.scitotenv.2020.139316.

[29] M. Gheju and I. Balcu, "Removal of chromium from Cr(VI) polluted wastewaters by reduction with scrap iron and subsequent precipitation of resulted cations," *J. Hazard. Mater.*, vol. 196, pp. 131–138, 2011, doi: 10.1016/j.jhazmat.2011.09.002.

[30] S. Golbaz, A. J. Jafari, M. Rafiee, and R. R. Kalantary, "Separate and simultaneous removal of phenol, chromium, and cyanide from aqueous solution by coagulation/precipitation: Mechanisms and theory," *Chem. Eng. J.*, vol. 253, pp. 251–257, 2014, doi: 10.1016/j.cej.2014.05.074.

[31] A. Demirbas, "Heavy metal adsorption onto agro-based waste materials: A review," *J. Hazard. Mater.*, vol. 157, no. 2–3, pp. 220–229, 2008, doi: 10.1016/j.jhazmat.2008.01.024.

[32] X. Yang Y. Wan, Y. Zheng, F. He, Z. Yu, J. Huang, H. Wang, Y.S. Ok, Y. Jiang, and B. Gao, "Surface functional groups of carbon-based adsorbents and their roles in the removal of heavy metals from aqueous solutions: A critical review," *Chem. Eng. J.*, vol. 366, pp. 608–621, 2019, doi: 10.1016/j.cej.2019.02.119.

[33] K. C. G. Silva, T. N. Amaral, L. A. Junqueira, N. de Oliveira Leite, and J. V. de Resende, "Adsorption of protein on activated carbon used in the filtration of mucilage derived from Pereskia aculeata Miller," *South African J. Chem. Eng.*, vol. 23, pp. 42–49, 2017, doi: 10.1016/j.sajce.2017.01.003.

[34] Y. Zhang, J. Le Li, T. Cai, Z. L. Cheng, X. Li, and T. S. Chung, "Sulfonated hyperbranched polyglycerol grafted membranes with antifouling properties for sustainable osmotic power generation using municipal wastewater," *J. Memb. Sci.*, vol. 563, no. May, pp. 521–530, 2018, doi: 10.1016/j.memsci.2018.05.017.

[35] N. H. Shaidan, U. Eldemerdash, and S. Awad, "Removal of Ni(II) ions from aqueous solutions using fixed-bed ion exchange column technique," *J. Taiwan Inst. Chem. Eng.*, vol. 43, no. 1, pp. 40–45, 2012, doi: 10.1016/j.jtice.2011.06.006.

[36] A. Viancelli, W. Michelon, P. Rogovski, R. D. Cadamuro, E.B. de Souza,G. Fongaro, A. F. Camargo, F.S. Stefanski, B. Venturin, T. Scapini, C. Bonatto, K.P. Preczeski, N. Klanovicz, D. de Oliveira, and H. Treichel, "A review on alternative bioprocesses for removal of emerging contaminants," *Bioprocess Biosyst. Eng.*, vol. 43, no. 12, pp. 2117–2129, 2020, doi: 10.1007/s00449-020-02410-9.

[37] L. Suárez, C. Pulgarin, C. Roussel, and J. Kiwi, "Preparation, kinetics, mechanism and properties of semi-transparent photocatalytic stable films active in dye degradation," *Appl. Catal. A Gen.*, vol. 516, pp. 70–80, 2016, doi: 10.1016/j.apcata.2016.01.041.

[38] S. S. Ahluwalia and D. Goyal, "Microbial and plant derived biomass for removal of heavy metals from wastewater," *Bioresour. Technol.*, vol. 98, no. 12, pp. 2243–2257, 2007, doi: 10.1016/j.biortech.2005.12.006.

[39] F. Fu and Q. Wang, "Removal of heavy metal ions from wastewaters: A review," *J. Environ. Manage.*, vol. 92, no. 3, pp. 407–418, 2011, doi:

10.1016/j.jenvman.2010.11.011.

[40] P. G. Ingole, R. R. Pawar, M. I. Baig, J. D. Jeon, and H. K. Lee, "Thin film nanocomposite (TFN) hollow fiber membranes incorporated with functionalized acid-activated bentonite (ABn-NH) clay: Towards enhancement of water vapor permeance and selectivity," *J. Mater. Chem. A*, vol. 5, no. 39, pp. 20947–20958, 2017, doi: 10.1039/c7ta04945e.

[41] A. Naseer, A. Jamshaid, A. Hamid, N. Muhammad, M. Ghauri, and J. Iqbal, Sikander Rafiq, Shahzad khuram and Noor Samad Shah, "Lignin and lignin based materials for the removal of heavy metals from waste water - An overview," *Zeitschrift fur Phys. Chemie*, vol. 233, no. 3, pp. 315–345, 2019, doi: 10.1515/zpch-2018-1209.

[42] A. Bhattacharya, A. Gupta, A. Kaur, and D. Malik, "Alleviation of hexavalent chromium by using microorganisms: Insight into the strategies and complications," *Water Sci. Technol.*, vol. 79, no. 3, pp. 411–424, 2019, doi: 10.2166/wst.2019.060.

[43] Z. Velkova, G. Kirova, M. Stoytcheva, S. Kostadinova, K. Todorova, and V. Gochev, "Immobilized microbial biosorbents for heavy metals removal," *Eng. Life Sci.*, vol. 18, no. 12, pp. 871–881, 2018, doi: 10.1002/elsc.201800017.

[44] S. Amirnia, M. B. Ray, and A. Margaritis, "Heavy metals removal from aqueous solutions using Saccharomyces cerevisiae in a novel continuous bioreactor-biosorption system," *Chem. Eng. J.*, vol. 264, pp. 863–872, 2015, doi: 10.1016/j.cej.2014.12.016.

[45] R. Gusain, N. Kumar, and S. S. Ray, "Recent advances in carbon nanomaterial-based adsorbents for water purification," *Coord. Chem. Rev.*, vol. 405, p. 213111, 2020, doi: 10.1016/j.ccr.2019.213111.

[46] J. Hoslett, H. Ghazal, D. Ahmad, and H. Jouhara, "Removal of copper ions from aqueous solution using low temperature biochar derived from the pyrolysis of municipal solid waste," *Sci. Total Environ.*, vol. 673, pp. 777–789, 2019, doi: 10.1016/j.scitotenv.2019.04.085.

[47] G. Tan, W. Sun, Y. Xu, H. Wang, and N. Xu, "Sorption of mercury (II) and atrazine by biochar, modified biochars and biochar based activated carbon in aqueous solution," *Bioresour. Technol.*, vol. 211, no. Ii, pp. 727–735, 2016, doi: 10.1016/j.biortech.2016.03.147.

[48] J. Lehmann, "A handful of carbon," *Nature*, vol. 447, no. 7141, pp. 143–144, 2007, doi: 10.1038/447143a.

[49] A. B. dos Santos, F. J. Cervantes, and J. B. van Lier, "Review paper on current technologies for decolourisation of textile wastewaters: Perspectives for anaerobic biotechnology," *Bioresour. Technol.*, vol. 98, no. 12, pp. 2369–2385, 2007, doi: 10.1016/j.biortech.2006.11.013.

[50] I. M. Banat, P. Nigam, D. Singh, and R. Marchant, "Microbial decolorization of textile-dye-containing effluents: A review," *Bioresour. Technol.*, vol. 58, no. 3, pp. 217–227, 1996, doi: 10.1016/S0960-8524(96)00113-7.

[51] H. S. Lade, T. R. Waghmode, A. A. Kadam, and S. P. Govindwar, "Enhanced biodegradation and detoxification of disperse azo dye Rubine GFL and textile industry effluent by defined fungal-bacterial consortium," *Int. Biodeterior. Biodegrad.*, vol. 72, pp. 94–107, 2012, doi: 10.1016/j.ibiod.2012.06.001.

[52] F. Veglio' and F. Beolchini, "Removal of metals by biosorption: A review," *Hydrometallurgy*, vol. 44, no. 3, pp. 301–316, 1997, doi: 10.1016/s0304-

386x(96)00059-x.

[53] E. Bååth, “Thymidine incorporation into macromolecules of bacteria extracted from soil by homogenization-centrifugation,” *Soil Biol. Biochem.*, vol. 24, no. 11, pp. 1157–1165, 1992, doi: 10.1016/0038-0717(92)90066-7.

[54] T. Covington, *Tanning Chemistry. The Science of Leather*, vol. 10. Cambridge CB4 0WF, UK: The Royal Society of Chemistry, 2009.

[55] A. L. Tasca and M. Puccini, “Leather tanning: Life cycle assessment of retanning, fatliquoring and dyeing,” *J. Clean. Prod.*, vol. 226, pp. 720–729, 2019, doi: 10.1016/j.jclepro.2019.03.335.

[56] M. M. Uddin, M. J. Hasan, Y. Mahmud, F. T. Zohra, and S. Ahmed, “Evaluating suitability of glutaraldehyde tanning in conformity with physical properties of conventional chrome-tanned leather,” *Text. Leather Rev.*, vol. 3, no. 3, pp. 135–145, 2020, doi: 10.31881/TLR.2020.09.

[57] J. K. Kanagaraj, R. C. Panda, and M. V. K. Vinodh Kumar, “Trends and advancements in sustainable leather processing: Future directions and challenges-A review,” *J. Environ. Chem. Eng.*, vol. 8, no. 5, p. 104379, 2020, doi: 10.1016/j.jece.2020.104379.

[58] A. Shahriar, F.-T.- Zohra, A. B. M. W. Murad, and S. Ahmed, “Enhancement of Waterproofing Properties of Finished Upper Leather Produced from Bangladeshi Cow Hides,” *Eur. J. Eng. Res. Sci.*, vol. 4, no. 7, pp. 63–71, 2019, doi: 10.24018/ejers.2019.4.7.1426.

[59] S. Dixit, A. Yadav, P. D. Dwivedi, and M. Das, “Toxic hazards of leather industry and technologies to combat threat: A review,” *J. Clean. Prod.*, vol. 87, no. C, pp. 39–49, 2015, doi: 10.1016/j.jclepro.2014.10.017.

[60] Z. Song, C. J. Williams, and R. G. J. Edyvean, “Treatment of tannery wastewater by chemical coagulation,” *Desalination*, vol. 164, no. 3, pp. 249–259, 2004, doi: 10.1016/S0011-9164(04)00193-6.

[61] M. K. Ahmed, M. Das, M. M. Islam, M. S. Akter, S. Islam, and M. A. Al-Mansur, “Physico-chemical properties of tannery and textile effluents and surface water of river Buriganga and Karnatoli, Bangladesh,” *World Appl. Sci. J.*, vol. 12, no. 2, pp. 152–159, 2011.

[62] B. Department of Environment, *DoE (1997) Environment conservation rules, E.C.R-schedule 3, standards for water.*

[63] G. of the P. R. of Bangladesh., *ECR (1997). The Environment Conservation Rules,*.

[64] H. Ali, E. Khan, and I. Ilahi, “Environmental chemistry and ecotoxicology of hazardous heavy metals: Environmental persistence, toxicity, and bioaccumulation,” *J. Chem.*, vol. 2019, no. Cd, 2019, doi: 10.1155/2019/6730305.

[65] H. Ali and E. Khan, “What are heavy metals? Long-standing controversy over the scientific use of the term ‘heavy metals’–proposal of a comprehensive definition,” *Toxicol. Environ. Chem.*, vol. 100, no. 1, pp. 6–19, 2018, doi: 10.1080/02772248.2017.1413652.

[66] M. A. Barakat, “New trends in removing heavy metals from industrial wastewater,” *Arab. J. Chem.*, vol. 4, no. 4, pp. 361–377, 2011, doi: 10.1016/j.arabjc.2010.07.019.

[67] K.-J. Appenroth, “Soil Heavy Metals,” *Crossroads*, vol. 19, no. Im, pp. 1–18, 2010, doi: 10.1007/978-3-642-02436-8.

[68] Y. C. Sharma, V. Srivastava, V. K. Singh, S. N. Kaul, and C. H. Weng, "Nano-adsorbents for the removal of metallic pollutants from water and wastewater," *Environ. Technol.*, vol. 30, no. 6, pp. 583–609, 2009, doi: 10.1080/09593330902838080.

[69] J. D. Horn, *"Chromium, Physical and Chemical Properties," in Encyclopedia of Metalloproteins,*. 2013.

[70] J. Barnhart, "Chromium chemistry and implications for environment," *J. Soil Contam.*, vol. 6, no. 6, pp. 561–568, 2008.

[71] R. Saha, R. Nandi, and B. Saha, "Sources and toxicity of hexavalent chromium," *J. Coord. Chem.*, vol. 64, no. 10, pp. 1782–1806, 2011, doi: 10.1080/00958972.2011.583646.

[72] H. Oliveira, "Chromium as an Environmental Pollutant: Insights on Induced Plant Toxicity," *J. Bot.*, vol. 2012, pp. 1–8, 2012, doi: 10.1155/2012/375843.

[73] D. Mohan and C. U. Pittman, "Activated carbons and low cost adsorbents for remediation of tri- and hexavalent chromium from water," *J. Hazard. Mater.*, vol. 137, no. 2, pp. 762–811, 2006, doi: 10.1016/j.jhazmat.2006.06.060.

[74] W. E. Motzer, S. M. Testa, J. Guertin, and F.T. Stanin, *Independent Environmental Technical Evaluation Group, Chromium(VI) Hand Book,* 1st ed. New York,: CRC Press, 2005.

[75] A. Demirbaş, "Adsorption of Cr(III) and Cr(VI) ions from aqueous solutions on to modified lignin," *Energy Sources*, vol. 27, no. 15, pp. 1449–1455, 2005, doi: 10.1080/009083190523352.

[76] A. Bedemo, B. S. Chandravanshi, and F. Zewge, "Removal of trivalent chromium from aqueous solution using aluminum oxide hydroxide," *Springerplus*, vol. 5, no. 1, 2016, doi: 10.1186/s40064-016-2983-x.

[77] J. L. Gardea-Torresdey, K.J. Tiemann, V. Armendari,; L. Bess-Oberto, R.R. Chianelli, J. Rios, J.G. Parsons, and G. Gamez, "Characterization of Cr(VI) binding and reduction to Cr(III) by the agricultural byproducts of Avena monida (Oat) biomass," *J. Hazard. Mater.*, vol. 80, no. 1–3, pp. 175–188, 2000, doi: 10.1016/S0304-3894(00)00301-0.

[78] N. K. Mondal and S. Chakraborty, "Adsorption of Cr(VI) from aqueous solution on graphene oxide (GO) prepared from graphite: equilibrium, kinetic and thermodynamic studies," *Appl. Water Sci.*, vol. 10, no. 2, pp. 1–10, 2020, doi: 10.1007/s13201-020-1142-2.

[79] Y. Shi, R. Shan, L. Lu, H. Yuan, H. Jiang, Y. Zhang, Y. Chen, "High-efficiency removal of Cr(VI) by modified biochar derived from glue residue," *J. Clean. Prod.*, vol. 254, no. Vi, p. 119935, 2020, doi: 10.1016/j.jclepro.2019.119935.

[80] T. S. Anirudhan and P. G. Radhakrishnan, "Chromium(III) removal from water and wastewater using a carboxylate-functionalized cation exchanger prepared from a lignocellulosic residue," *J. Colloid Interface Sci.*, vol. 316, no. 2, pp. 268–276, 2007, doi: 10.1016/j.jcis.2007.08.051.

[81] S. Yang, L. Li, Z. Pei, C. Li, J. Lv, J. Xie, B. Wen, S. Zhang, "Adsorption kinetics, isotherms and thermodynamics of Cr(III) on graphene oxide," *Colloids Surfaces A Physicochem. Eng. Asp.*, vol. 457, no. 1, pp. 100–106, 2014, doi: 10.1016/j.colsurfa.2014.05.062.

[82] F. T. Stanin and M. Pirnie, *The Transport and Fate of Cr(VI) in the Environment*, vol. 73, no. 20. 2007.

[83] Hong Sun and Max Costa, "Handbook on the Toxicology of Metals (Fifth Edition)," vol. II, Specif, pp. 197–220, 2022.

[84] D. Rai, B. M. Sass, and D. A. Moore, "Chromium(III) Hydrolysis Constants and Solubility of Chromium(III) Hydroxide," *Inorg. Chem.*, vol. 26, no. 3, pp. 345–349, 1987, doi: 10.1021/ic00250a002.

[85] S. Krishnamurthy and M. M. Wilkens, "Environmental chemistry of chromium," *Northeast. Geol.*, vol. 16, no. 1, pp. 14–17, 1994.

[86] V. M. Nurchi and I. Villaescusa, "Agricultural biomasses as sorbents of some trace metals," *Coord. Chem. Rev.*, vol. 252, no. 10–11, pp. 1178–1188, 2008, doi: 10.1016/j.ccr.2007.09.023.

[87] C. E. Borba, R. Guirardello, E. A. Silva, M. T. Veit, and C. R. G. Tavares, "Removal of nickel(II) ions from aqueous solution by biosorption in a fixed bed column: Experimental and theoretical breakthrough curves," *Biochem. Eng. J.*, vol. 30, no. 2, pp. 184–191, 2006, doi: 10.1016/j.bej.2006.04.001.

[88] S. Karamat, R. S Rawat, T. L Tan, P.Lee, S. V. Springham, Anis-ur-Rehman, R. Chen, H. D. Sun,."Exciting dilute magnetic semiconductor: Copper-doped ZnO," *J. Supercond. Nov. Magn.*, vol. 26, no. 1, pp. 187–195, 2013, doi: 10.1007/s10948-012-1710-2.

[89] L. Trakal, R. Šigut, H. Šillerová, D. Faturíková, and M. Komárek, "Copper removal from aqueous solution using biochar: Effect of chemical activation," *Arab. J. Chem.*, vol. 7, no. 1, pp. 43–52, 2014, doi: 10.1016/j.arabjc.2013.08.001.

[90] S. Rao, Rifaqat Ali Khan; Ikram, "'Sorption studies of Cu(II) on gooseberry fruit (emblica officinalis) and its removal from electroplating wastewater,'" *Desalination*, vol. 277, no. 1–3, pp. 390–398, 2015.

[91] M. V. Subbaiah, Y. Vijaya, A. S. Reddy, G. Yuvaraja, and A. Krishnaiah, "Equilibrium, kinetic and thermodynamic studies on the biosorption of Cu(II) onto Trametes versicolor biomass," *Desalination*, vol. 276, no. 1–3, pp. 310–316, 2011, doi: 10.1016/j.desal.2011.03.067.

[92] A. T. Paulino, F. A. S. Minasse, M. R. Guilherme, A. V. Reis, E. C. Muniz, and J. Nozaki, "Novel adsorbent based on silkworm chrysalides for removal of heavy metals from wastewaters," *J. Colloid Interface Sci.*, vol. 301, no. 2, pp. 479–487, 2006, doi: 10.1016/j.jcis.2006.05.032.

[93] C. A. Dyer, "as Endocrine-Disrupting Chemicals," no. 1, pp. 111–133.

[94] P. B. Tchounwou, C. G. Yedjou, A. K. Patlolla, and D. J. Sutton, *Molecular, clinical and environmental toxicicology Volume 3: Environmental Toxicology*, vol. 101. 2012. doi: 10.1007/978-3-7643-8340-4.

[95] A. M. Florea and D. Büsselberg, "Occurrence, use and potential toxic effects of metals and metal compounds," *BioMetals*, vol. 19, no. 4, pp. 419–427, 2006, doi: 10.1007/s10534-005-4451-x.

[96] S. S. Dutta, *An Introduction To The Principles of Leather Manufacture*, Fourth Edi. Kolkata, India: Indian Leather Technologist's Association, 1999.

[97] J. Manzoor and M. Sharma, "Impact of textile dyes on human health and

environment," *Impact Text. Dye. Public Heal. Environ.*, no. April, pp. 162–169, 2019, doi: 10.4018/978-1-7998-0311-9.ch008.

[98] S. Samal, "Effect of shape and size of filler particle on the aggregation and sedimentation behavior of the polymer composite," *Powder Technol.*, vol. 366, pp. 43–51, 2020, doi: 10.1016/j.powtec.2020.02.054.

[99] A. Gottfried, A. D. Shepard, K. Hardiman, and M. E. Walsh, "Impact of recycling filter backwash water on organic removal in coagulation-sedimentation processes," *Water Res.*, vol. 42, no. 18, pp. 4683–4691, 2008, doi: 10.1016/j.watres.2008.08.011.

[100] A. Azimi, A. Azari, M. Rezakazemi, and M. Ansarpour, "Removal of Heavy Metals from Industrial Wastewaters: A Review," *ChemBioEng Rev.*, vol. 4, no. 1, pp. 37–59, 2017, doi: 10.1002/cben.201600010.

[101] S. K. Gunatilake, "Methods of Removing Heavy Metals from," *J. Multidiscip. Eng. Sci. Stud. Ind. Wastewater*, vol. 1, no. 1, pp. 13–18, 2015, [Online]. Available: www.jmess.org

[102] N. A. A. Qasem, R. H. Mohammed, and D. U. Lawal, "Removal of heavy metal ions from wastewater: a comprehensive and critical review," *npj Clean Water*, vol. 4, no. 1, 2021, doi: 10.1038/s41545-021-00127-0.

[103] D. Xu, B. Zhou, and R. Yuan, "Optimization of coagulation-flocculation treatment of wastewater containing Zn(II) and Cr(VI)," *IOP Conf. Ser. Earth Environ. Sci.*, vol. 227, no. 5, 2019, doi: 10.1088/1755-1315/227/5/052049.

[104] C. Zamora-Ledezma, D. Negrete-Bolagay, F. Figueroa, E. Zamora-Ledezma, M. Ni;Frank Alexis, V. H. Guerrero, "Heavy metal water pollution: A fresh look about hazards, novel and conventional remediation methods," *Environ. Technol. Innov.*, vol. 22, p. 101504, 2021, doi: 10.1016/j.eti.2021.101504.

[105] A. J. Hargreaves,P.W.J. Vale, L. Alibardi, C. Constantino, G. Dotro, E. Cartmell, P. Campo, "Coagulation–flocculation process with metal salts, synthetic polymers and biopolymers for the removal of trace metals (Cu, Pb, Ni, Zn) from municipal wastewater," *Clean Technol. Environ. Policy*, vol. 20, no. 2, pp. 393–402, 2018, doi: 10.1007/s10098-017-1481-3.

[106] F. M. Pang, S. P. Teng, T. T. Teng, and A. K. Mohd Omar, "Heavy metals removal by hydroxide precipitation and coagulation-flocculation methods from aqueous solutions," *Water Qual. Res. J. Canada*, vol. 44, no. 2, pp. 174–182, 2009, doi: 10.2166/wqrj.2009.019.

[107] F. I. Hai, K. Yamamoto, and K. Fukushi, "Hybrid treatment systems for dye wastewater," *Crit. Rev. Environ. Sci. Technol.*, vol. 37, no. 4, pp. 315–377, 2007, doi: 10.1080/10643380601174723.

[108] P. W. Wong, T. T. Teng, and N. A. R. Nik Norulaini, "Efficiency of the coagulation-flocculation method for the treatment of dye mixtures containing disperse and reactive dye," *Water Qual. Res. J. Canada*, vol. 42, no. 1, pp. 54–62, 2007, doi: 10.2166/wqrj.2007.008.

[109] K. J. Hwang, C. Y. Liao, and K. L. Tung, "Effect of membrane pore size on the particle fouling in membrane filtration," *Desalination*, vol. 234, no. 1–3, pp. 16–23, 2008, doi: 10.1016/j.desal.2007.09.065.

[110] N. K. R. A Basile, A Cassano, *Advances in Membrane Technologies for Water Treatment*. Cambridge: Woodhead Publishin, 2015.

[111] L. Fillaudeau, P. Blanpain-Avet, and G. Daufin, “Water, wastewater and waste management in brewing industries,” *J. Clean. Prod.*, vol. 14, no. 5, pp. 463–471, 2006, doi: 10.1016/j.jclepro.2005.01.002.

[112] Z. Yang and C. Y. Tang, *Novel membranes and membrane materials*. Elsevier B.V., 2018. doi: 10.1016/B978-0-444-63961-5.00007-9.

[113] H. Karimi-Maleh Y. Orooji, A. Ayati, S. Qanbari, B. Tanhaei, F. Karimi, M. Alizadeh, J. Rouhi, L. Fu, M. SillanpÃ¤Ã¤, *Recent advances in removal techniques of Cr(VI) toxic ion from aqueous solution: A comprehensive review*, vol. 329, no. Vi. 2021. doi: 10.1016/j.molliq.2020.115062.

[114] N. Al-Bastaki, “Removal of methyl orange dye and Na2so4 salt from synthetic waste water using reverse osmosis,” *Chem. Eng. Process. Process Intensif.*, vol. 43, no. 12, pp. 1561–1567, 2004, doi: 10.1016/j.cep.2004.03.001.

[115] R. Bouchareb, K. Derbal, Y. Özay, Z. Bilici, and N. Dizge, “Combined natural/chemical coagulation and membrane filtration for wood processing wastewater treatment,” *J. Water Process Eng.*, vol. 37, no. May, p. 101521, 2020, doi: 10.1016/j.jwpe.2020.101521.

[116] T. S. Y. Choong, T. G. Chuah, Y. Robiah, F. L. Gregory Koay, and I. Azni, “Arsenic toxicity, health hazards and removal techniques from water: an overview,” *Desalination*, vol. 217, no. 1–3, pp. 139–166, 2007, doi: 10.1016/j.desal.2007.01.015.

[117] T. Omura, “Design of chlorine-fast reactive dyes. Part 4: degradation of amino-containing azo dyes by sodium hypochlorite,” *Dye. Pigment.*, vol. 26, no. 1, pp. 33–50, 1994, doi: 10.1016/0143-7208(94)80028-6.

[118] K. Turhan, I. Durukan, S. A. Ozturkcan, and Z. Turgut, “Decolorization of textile basic dye in aqueous solution by ozone,” *Dye. Pigment.*, vol. 92, no. 3, pp. 897–901, 2012, doi: 10.1016/j.dyepig.2011.07.012.

[119] H. Liu, C. Wang, X. Li, X. Xuan, C. Jiang, and H. N. Cui, “A novel electro-Fenton process for water treatment: Reaction-controlled pH adjustment and performance assessment,” *Environ. Sci. Technol.*, vol. 41, no. 8, pp. 2937–2942, 2007, doi: 10.1021/es0622195.

[120] X. Q. Wang, C. P. Liu, Y. Yuan, and F. bai Li, “Arsenite oxidation and removal driven by a bio-electro-Fenton process under neutral pH conditions,” *J. Hazard. Mater.*, vol. 275, pp. 200–209, 2014, doi: 10.1016/j.jhazmat.2014.05.003.

[121] T. M. Zewail and N. S. Yousef, “Kinetic study of heavy metal ions removal by ion exchange in batch conical air spouted bed,” *Alexandria Eng. J.*, vol. 54, no. 1, pp. 83–90, 2015, doi: 10.1016/j.aej.2014.11.008.

[122] T. A. Kurniawan, G. Y. S. Chan, W. H. Lo, and S. Babel, “Physico-chemical treatment techniques for wastewater laden with heavy metals,” *Chem. Eng. J.*, vol. 118, no. 1–2, pp. 83–98, 2006, doi: 10.1016/j.cej.2006.01.015.

[123] F. Delval, G. Crini, J. Vebrel, M. Knorr, G. Sauvin, and E. Conte, “Starch-Modified Filters Used for the Removal of Dyes from Waste Water,” *Macromol. Symp.*, vol. 203, pp. 165–172, 2003, doi: 10.1002/masy.200351315.

[124] M. Sultana, M. H. Rownok, M. Sabrin, M. H. Rahaman, and S. M. N. Alam, “A review on experimental chemically modified activated carbon to enhance dye and heavy metals adsorption,” *Clean. Eng. Technol.*, vol. 6, no. 100382, 2022, doi: 10.1016/j.clet.2021.100382.

[125] J. PAN, R. LIU, and H. TANG, “Surface reaction of{\textless} i{\textgreater} {Bacillus} cereus{\textless}/i{\textgreater} biomass and its biosorption for lead and copper ions,” *J. Environ. Sci.*, vol. 19, no. 4, pp. 403–408, 2007.

[126] M. Tuzen, K. O. Saygi, C. Usta, and M. Soylak, “Pseudomonas aeruginosa immobilized multiwalled carbon nanotubes as biosorbent for heavy metal ions,” *Bioresour. Technol.*, vol. 99, no. 6, pp. 1563–1570, 2008, doi: 10.1016/j.biortech.2007.04.013.

[127] C. Quintelas, Z. Rocha, B. Silva, B. Fonseca, H. Figueiredo, and T. Tavares, “Biosorptive performance of an Escherichia coli biofilm supported on zeolite NaY for the removal of Cr(VI), Cd(II), Fe(III) and Ni(II),” *Chem. Eng. J.*, vol. 152, no. 1, pp. 110–115, 2009, doi: 10.1016/j.cej.2009.03.039.

[128] K. He, Y. Chen, Z. Tang, and Y. Hu, “Removal of heavy metal ions from aqueous solution by zeolite synthesized from fly ash,” *Environ. Sci. Pollut. Res.*, vol. 23, no. 3, pp. 2778–2788, 2016, doi: 10.1007/s11356-015-5422-6.

[129] V. Bobade and N. Eshtiagi, “Heavy Metals Removal from Wastewater by Adsorption Process : A Review,” *APCChE 2015 Congr. Inc. Chemeca 2015*, vol. 6, no. 6, pp. 312–317, 2015.

[130] R. Das, S. Das Tuhi, and S. M. J. Zaidi, “Adsorption, in Das R. (eds) Carbon Nanotubes for Clean Water.,” in *Carbon Nanostructures*, vol. Carbon Nan, 2018, pp. 85–106. doi: 10.1007/978-3-319-95603-9_4.

[131] S. Sircar, *Book reviews*, vol. Principles, no. 4. 1985.

[132] F. Ding and B. I. Yakobson, “Challenges in hydrogen adsorptions: From physisorption to chemisorption,” *Front. Phys.*, vol. 6, no. 2, pp. 142–150, 2011, doi: 10.1007/s11467-011-0171-6.

[133] F. Zhang, B. Wang, S. He, and R. Man, “Preparation of Graphene-Oxide/Polyamidoamine Dendrimers and Their Adsorption Properties toward Some Heavy Metal Ions,” *J. Chem. Eng. Data*, vol. 59, no. 5, pp. 1719–1726, 2014, doi: 10.1021/je500219e.

[134] R. L. White, C. M. White, H. Turgut, A. Massoud, and Z. R. Tian, “Comparative studies on copper adsorption by graphene oxide and functionalized graphene oxide nanoparticles,” *J. Taiwan Inst. Chem. Eng.*, vol. 85, pp. 18–28, 2018, doi: 10.1016/j.jtice.2018.01.036.

[135] L. P. Lingamdinne, J. R. Koduru, H. Roh, Y. L. Choi, Y. Y. Chang, and J. K. Yang, “Adsorption removal of Co(II) from waste-water using graphene oxide,” *Hydrometallurgy*, vol. 165, pp. 90–96, 2016, doi: 10.1016/j.hydromet.2015.10.021.

[136] L. Li, C. Luo, X. Li, H. Duan, and X. Wang, “Preparation of magnetic ionic liquid/chitosan/graphene oxide composite and application for water treatment,” *Int. J. Biol. Macromol.*, vol. 66, pp. 172–178, 2014, doi: 10.1016/j.ijbiomac.2014.02.031.

[137] J. Wang and B. Chen, “Adsorption and coadsorption of organic pollutants and a heavy metal by graphene oxide and reduced graphene materials,” *Chem. Eng. J.*, vol. 281, pp. 379–388, 2015, doi: 10.1016/j.cej.2015.06.102.

[138] P. Tan J. Sun, Y. Hu, Z. Fang, Q. Bi, Y. Chen, J. Cheng, “Adsorption of Cu2+, Cd2+ and Ni2+ from aqueous single metal solutions on graphene oxide membranes,” *J. Hazard. Mater.*, vol. 297, pp. 251–260, 2015, doi: 10.1016/j.jhazmat.2015.04.068.

[139] M. Khatamian, N. Khodakarampoor, and M. Saket-Oskoui, “Efficient removal of

arsenic using graphene-zeolite based composites," *J. Colloid Interface Sci.*, vol. 498, pp. 433–441, 2017, doi: 10.1016/j.jcis.2017.03.052.

[140] X. Yang, T. Zhou, B. Ren, A. Hursthouse, and Y. Zhang, "Removal of Mn (II) by Sodium Alginate/Graphene Oxide Composite Double-Network Hydrogel Beads from Aqueous Solutions," *Sci. Rep.*, vol. 8, no. 1, pp. 1–16, 2018, doi: 10.1038/s41598-018-29133-y.

[141] L. Chang Y. Pu, P. Jing, Y.Cui, G. Zhang, S. Xu, B.Cao, J. Guo, F.Chen, and C. Qiao, "Magnetic core-shell MnFe2O4@TiO2 nanoparticles decorated on reduced graphene oxide as a novel adsorbent for the removal of ciprofloxacin and Cu(II) from water," *Appl. Surf. Sci.*, vol. 541, no. September, p. 148400, 2021, doi: 10.1016/j.apsusc.2020.148400.

[142] X. Mi, G. Huang, W. Xie, W. Wang, Y. Liu, and J. Gao, "Preparation of graphene oxide aerogel and its adsorption for Cu 2+ ions," *Carbon N. Y.*, vol. 50, no. 13, pp. 4856–4864, 2012, doi: 10.1016/j.carbon.2012.06.013.

[143] K. R. Parmar, I. Patel, S. Basha, and Z. V. P. Murthy, "Synthesis of acetone reduced graphene oxide/Fe3O4 composite through simple and efficient chemical reduction of exfoliated graphene oxide for removal of dye from aqueous solution," *J. Mater. Sci.*, vol. 49, no. 19, pp. 6772–6783, 2014, doi: 10.1007/s10853-014-8378-x.

[144] F. Shoushtarian, M. R. A. Moghaddam, and E. Kowsari, "Efficient regeneration/reuse of graphene oxide as a nanoadsorbent for removing basic Red 46 from aqueous solutions," *J. Mol. Liq.*, vol. 312, p. 113386, 2020, doi: 10.1016/j.molliq.2020.113386.

[145] M. Z. Iqbal and A. A. Abdala, "Thermally reduced graphene: Synthesis, characterization and dye removal applications," *RSC Adv.*, vol. 3, no. 46, pp. 24455–24464, 2013, doi: 10.1039/c3ra43914c.

[146] R. Wijaya, G. Andersan, S. Permatasari Santoso, and W. Irawaty, "Green Reduction of Graphene Oxide using Kaffir Lime Peel Extract (Citrus hystrix) and Its Application as Adsorbent for Methylene Blue," *Sci. Rep.*, vol. 10, no. 1, pp. 1–9, 2020, doi: 10.1038/s41598-020-57433-9.

[147] J. H. Deng, X. R. Zhang, G. M. Zeng, J. L. Gong, Q. Y. Niu, and J. Liang, "Simultaneous removal of Cd(II) and ionic dyes from aqueous solution using magnetic graphene oxide nanocomposite as an adsorbent," *Chem. Eng. J.*, vol. 226, pp. 189–200, 2013, doi: 10.1016/j.cej.2013.04.045.

[148] K. D. Lokhande, D. A. Pethsangave, D. K. Kulal, and S. Some, "Remediation of Toxic Dye Pollutants by Using Graphene-Based Adsorbents," *ChemistrySelect*, vol. 5, no. 27, pp. 8062–8073, 2020, doi: 10.1002/slct.202002130.

[149] F. Mindivan, Ü. D. Gül, and M. Göktaş, "Application of graphene-based adsorbents in the treatment of dye-contaminated wastewater; kinetic and isotherm studies," *J. Vinyl Addit. Technol.*, vol. 27, no. 3, pp. 485–496, 2021, doi: 10.1002/vnl.21821.

[150] H. V. Tran, L. T. Hoang, and C. D. Huynh, "An investigation on kinetic and thermodynamic parameters of methylene blue adsorption onto graphene-based nanocomposite," *Chem. Phys.*, vol. 535, no. February, p. 110793, 2020, doi: 10.1016/j.chemphys.2020.110793.

[151] H. M. A. Hassan, M.R.El-Aassar, Mohammed A. El-Hashemy, Mohamed A.Betiha, Meshal Alzaid, Almah N.Alqhobisi, Linah A. Alzare, Ibrahim Hotan Alsohaimi Ph.D,

"Sulfanilic acid-functionalized magnetic GO as a robust adsorbent for the efficient adsorption of methylene blue from aqueous solution," *J. Mol. Liq.*, vol. Volume 361, 2022.

[152] Y. Satyawali and M. Balakrishnan, "Wastewater treatment in molasses-based alcohol distilleries for COD and color removal: A review," *J. Environ. Manage.*, vol. 86, no. 3, pp. 481–497, 2008, doi: 10.1016/j.jenvman.2006.12.024.

[153] M. Belhachemi and F. Addoun, "Adsorption of congo red onto activated carbons having different surface properties: Studies of kinetics and adsorption equilibrium," *Desalin. Water Treat.*, vol. 37, no. 1–3, pp. 122–129, 2012, doi: 10.1080/19443994.2012.661263.

[154] T. A. Kurniawan, G. Y. S. Chan, W. hung Lo, and S. Babel, "Comparisons of low-cost adsorbents for treating wastewaters laden with heavy metals," *Sci. Total Environ.*, vol. 366, no. 2–3, pp. 409–426, 2006, doi: 10.1016/j.scitotenv.2005.10.001.

[155] T. M. A. R. K. P. S. N. K. Jianying Shang and Rama Sinha., "Removal of hexavalent chromium via biochar-based adsorbents: State-of-the-art, challenges, and future perspectives," *J. Environ. Manage.*, vol. Volume 317, 2022, doi: https://doi.org/10.1016/j.jenvman.2022.115356.

[156] R. V. Hemavathy, P. S. Kumar, K. Kanmani, and N. Jahnavi, "Adsorptive separation of Cu(II) ions from aqueous medium using thermally/chemically treated Cassia fistula based biochar," *J. Clean. Prod.*, vol. 249, no. Ii, p. 119390, 2020, doi: 10.1016/j.jclepro.2019.119390.

[157] J. Pan, J. Jiang, and R. Xu, "Adsorption of Cr(III) from acidic solutions by crop straw derived biochars," *J. Environ. Sci. (China)*, vol. 25, no. 10, pp. 1957–1965, 2013, doi: 10.1016/S1001-0742(12)60305-2.

[158] D. Berihun, "Removal of Chromium from Industrial Wastewater by Adsorption Using Coffee Husk," *J. Mater. Sci. Eng.*, vol. 06, no. 02, pp. 6–11, 2017, doi: 10.4172/2169-0022.1000331.

[159] R. A. K. Rao, F. Rehman, and M. Kashifuddin, "Removal of Cr(VI) from electroplating wastewater using fruit peel of Leechi (Litchi chinensis)," *Desalin. Water Treat.*, vol. 49, no. 1–3, pp. 136–146, 2012, doi: 10.1080/19443994.2012.708211.

[160] G. Musumba, C. Nakiguli, C. Lubanga, P. Mukasa, and E. Ntambi, "Adsorption of Lead (II) and Copper (II) Ions from Mono Synthetic Aqueous Solutions Using Bio-Char from <i>Ficus natalensis</i> Fruits," *J. Encapsulation Adsorpt. Sci.*, vol. 10, no. 04, pp. 71–84, 2020, doi: 10.4236/jeas.2020.104004.

[161] F. Kebede, "Removal of Chromium and Azo Metal-Complex Dyes Using Activated Carbon synthesized from Tannery Wastes," *Open Access J. Sci. Technol.*, vol. 05, no. 02, pp. 1–30, 2017, doi: 10.11131/2017/101214.

[162] G. Z. Kyzas, E. A. Deliyanni, and K. A. Matis, "Activated carbons produced by pyrolysis of waste potato peels: Cobaltions removal by adsorption," *Colloids Surfaces A Physicochem. Eng. Asp.*, vol. 490, pp. 74–83, 2016, doi: 10.1016/j.colsurfa.2015.11.038.

[163] P. S. Katha, Z. Ahmed, R. Alam, B. Saha, A. Acharjee, and M. S. Rahman, "Efficiency analysis of eggshell and tea waste as Low cost adsorbents for Cr removal from wastewater sample," *South African J. Chem. Eng.*, vol. 37, no. June, pp. 186–195, 2021, doi: 10.1016/j.sajce.2021.06.001.

[164] D. Mohan, K. P. Singh, and V. K. Singh, "Trivalent chromium removal from wastewater using low cost activated carbon derived from agricultural waste material and activated carbon fabric cloth," *J. Hazard. Mater.*, vol. 135, no. 1–3, pp. 280–295, 2006, doi: 10.1016/j.jhazmat.2005.11.075.

[165] T. Bohli, A. Ouederni, N. Fiol, and I. Villaescusa, "Evaluation of an activated carbon from olive stones used as an adsorbent for heavy metal removal from aqueous phases," *Comptes Rendus Chim.*, vol. 18, no. 1, pp. 88–99, 2015, doi: 10.1016/j.crci.2014.05.009.

[166] H. Tounsadi, A. Khalidi, A. Machrouhi, M. Farnane, R. Elmoubarki, A. Elhalil, M. Sadiq, N. Barka, "Highly efficient activated carbon from Glebionis coronaria L. biomass: Optimization of preparation conditions and heavy metals removal using experimental design approach," *J. Environ. Chem. Eng.*, vol. 4, no. 4, pp. 4549–4564, 2016, doi: 10.1016/j.jece.2016.10.020.

[167] H. Tounsadi, A. Khalidi, M. Abdennouri, and N. Barka, "Activated carbon from Diplotaxis Harra biomass: Optimization of preparation conditions and heavy metal removal," *J. Taiwan Inst. Chem. Eng.*, vol. 59, pp. 348–358, 2016, doi: 10.1016/j.jtice.2015.08.014.

[168] T. Bohli and A. Ouederni, "Improvement of oxygen-containing functional groups on olive stones activated carbon by ozone and nitric acid for heavy metals removal from aqueous phase," *Environ. Sci. Pollut. Res.*, pp. 15852–15861, 2016, doi: 10.1007/s11356-015-4330-0.

[169] S. Abdulrazak, K. Hussaini, and H. M. Sani, "Evaluation of removal efficiency of heavy metals by low-cost activated carbon prepared from African palm fruit," *Appl. Water Sci.*, vol. 7, no. 6, pp. 3151–3155, 2017, doi: 10.1007/s13201-016-0460-x.

[170] R. Shahrokhi-Shahraki, C. Benally, M. G. El-Din, and J. Park, "High efficiency removal of heavy metals using tire-derived activated carbon vs commercial activated carbon: Insights into the adsorption mechanisms," *Chemosphere*, vol. 264, p. 128455, 2021, doi: 10.1016/j.chemosphere.2020.128455.

[171] K. Rambabu, F. Banat, G. S. Nirmala, S. Velu, P. Monash, and G. Arthanareeswaran, "Activated carbon from date seeds for chromium removal in aqueous solution," *Desalin. Water Treat.*, vol. 156, no. April 2018, pp. 267–277, 2019, doi: 10.5004/dwt.2018.23265.

[172] S. Mortazavian *et al.*, "Synthesis, characterization, and kinetic study of activated carbon modified by polysulfide rubber coating for aqueous hexavalent chromium removal," *J. Ind. Eng. Chem.*, vol. 69, pp. 196–210, 2019, doi: 10.1016/j.jiec.2018.09.028.

[173] N. Gupta, A. K. Kushwaha, and M. C. Chattopadhyaya, "Application of potato (Solanum tuberosum) plant wastes for the removal of methylene blue and malachite green dye from aqueous solution," *Arab. J. Chem.*, vol. 9, pp. S707–S716, 2016, doi: 10.1016/j.arabjc.2011.07.021.

[174] J. Georgin, G. L. Dotto, M. A. Mazutti, and E. L. Foletto, "Preparation of activated carbon from peanut shell by conventional pyrolysis and microwave irradiation-pyrolysis to remove organic dyes from aqueous solutions," *J. Environ. Chem. Eng.*, vol. 4, no. 1, pp. 266–275, 2016, doi: 10.1016/j.jece.2015.11.018.

[175] V. Gómez, M. S. Larrechi, and M. P. Callao, "Kinetic and adsorption study of acid dye removal using activated carbon," *Chemosphere*, vol. 69, no. 7, pp. 1151–1158, 2007,

doi: 10.1016/j.chemosphere.2007.03.076.

[176] M. Elkady, H. Shokry, and H. Hamad, "New activated carbon from mine coal for adsorption of dye in simulated water or multiple heavy metals in real wastewater," *Materials (Basel).*, vol. 13, no. 11, 2020, doi: 10.3390/ma13112498.

[177] W. Widiyastuti, M. Fahrudin Rois, N. M. I. P. Suari, and H. Setyawan, "Activated carbon nanofibers derived from coconut shell charcoal for dye removal application," *Adv. Powder Technol.*, vol. 31, no. 8, pp. 3267–3273, 2020, doi: 10.1016/j.apt.2020.06.012.

[178] S. Afshin, S. A. Mokhtari, M. Vosoughi, H. Sadeghi, and Y. Rashtbari, "Data of adsorption of Basic Blue 41 dye from aqueous solutions by activated carbon prepared from filamentous algae," *Data Br.*, vol. 21, pp. 1008–1013, 2018, doi: 10.1016/j.dib.2018.10.023.

[179] M. A. Ahmad, N. A. Ahmad Puad, and O. S. Bello, "Kinetic, equilibrium and thermodynamic studies of synthetic dye removal using pomegranate peel activated carbon prepared by microwave-induced KOH activation," *Water Resour. Ind.*, vol. 6, pp. 18–35, 2014, doi: 10.1016/j.wri.2014.06.002.

[180] M. A. Al-Ghouti and A. O. Sweleh, "Optimizing textile dye removal by activated carbon prepared from olive stones," *Environ. Technol. Innov.*, vol. 16, p. 100488, 2019, doi: 10.1016/j.eti.2019.100488.

[181] N. K. Amin, "Removal of direct blue-106 dye from aqueous solution using new activated carbons developed from pomegranate peel: Adsorption equilibrium and kinetics," *J. Hazard. Mater.*, vol. 165, no. 1–3, pp. 52–62, 2009, doi: 10.1016/j.jhazmat.2008.09.067.

[182] N. M. Mahmoodi, R. Salehi, and M. Arami, "Binary system dye removal from colored textile wastewater using activated carbon: Kinetic and isotherm studies," *Desalination*, vol. 272, no. 1–3, pp. 187–195, 2011, doi: 10.1016/j.desal.2011.01.023.

[183] P. K. Malik, "Dye removal from wastewater using activated carbon developed from sawdust: Adsorption equilibrium and kinetics," *J. Hazard. Mater.*, vol. 113, no. 1–3, pp. 81–88, 2004, doi: 10.1016/j.jhazmat.2004.05.022.

[184] M. Arulkumar, P. Sathishkumar, and T. Palvannan, "Optimization of Orange G dye adsorption by activated carbon of Thespesia populnea pods using response surface methodology," *J. Hazard. Mater.*, vol. 186, no. 1, pp. 827–834, 2011, doi: 10.1016/j.jhazmat.2010.11.067.

[185] S. Sarode, P. Upadhyay, M.A. Khosa, T. Mak, A. Shakir, S. Song, and A Ullah "Overview of wastewater treatment methods with special focus on biopolymer chitin-chitosan," *Int. J. Biol. Macromol.*, vol. 121, pp. 1086–1100, 2019, doi: 10.1016/j.ijbiomac.2018.10.089.

[186] C. P. J. Isaac and A. Sivakumar, "Removal of lead and cadmium ions from water using Annona squamosa shell: Kinetic and equilibrium studies," *Desalin. Water Treat.*, vol. 51, no. 40–42, pp. 7700–7709, 2013, doi: 10.1080/19443994.2013.778218.

[187] E. Abu-Danso, S. Peräniemi, T. Leiviskä, T. Y. Kim, K. M. Tripathi, and A. Bhatnagar, "Synthesis of clay-cellulose biocomposite for the removal of toxic metal ions from aqueous medium," *J. Hazard. Mater.*, vol. 381, no. June 2019, p. 120871, 2020, doi: 10.1016/j.jhazmat.2019.120871.

[188] X. Huang, H. Zhao, G. Zhang, J. Li, Y. Yang, and P. Ji, "Potential of removing Cd(II)

and Pb(II) from contaminated water using a newly modified fly ash," *Chemosphere*, vol. 242, p. 125148, 2020, doi: 10.1016/j.chemosphere.2019.125148.

[189] J. A. Sirviö and M. Visanko, "Lignin-rich sulfated wood nanofibers as high-performing adsorbents for the removal of lead and copper from water," *J. Hazard. Mater.*, vol. 383, no. May 2019, p. 121174, 2020, doi: 10.1016/j.jhazmat.2019.121174.

[190] I. Hegazy, M. E. A. Ali, E. H. Zaghlool, and R. Elsheikh, "Heavy metals adsorption from contaminated water using moringa seeds/ olive pomace byproducts," *Appl. Water Sci.*, vol. 11, no. 6, pp. 1–14, 2021, doi: 10.1007/s13201-021-01421-5.

[191] R. J. Nathan, C. E. Martin, D. Barr, and R. J. Rosengren, "Simultaneous removal of heavy metals from drinking water by banana, orange and potato peel beads: a study of biosorption kinetics," *Appl. Water Sci.*, vol. 11, no. 7, pp. 1–15, 2021, doi: 10.1007/s13201-021-01457-7.

[192] A. Stavrinou, C. A. Aggelopoulos, and C. D. Tsakiroglou, "Exploring the adsorption mechanisms of cationic and anionic dyes onto agricultural waste peels of banana, cucumber and potato: Adsorption kinetics and equilibrium isotherms as a tool," *J. Environ. Chem. Eng.*, vol. 6, no. 6, pp. 6958–6970, 2018, doi: 10.1016/j.jece.2018.10.063.

[193] M. Rafatullah, O. Sulaiman, R. Hashim, and A. Ahmad, "Adsorption of copper (II), chromium (III), nickel (II) and lead (II) ions from aqueous solutions by meranti sawdust," *J. Hazard. Mater.*, vol. 170, no. 2–3, pp. 969–977, 2009, doi: 10.1016/j.jhazmat.2009.05.066.

[194] G. F. Coelho *et al.*, "Removal of Cd(II), Pb(II) and Cr(III) from water using modified residues of Anacardium occidentale L.," *Appl. Water Sci.*, vol. 8, no. 3, pp. 1–21, 2018, doi: 10.1007/s13201-018-0724-8.

[195] K. Kaya, E. Pehlivan, C. Schmidt, and M. Bahadir, "Use of modified wheat bran for the removal of chromium(VI) from aqueous solutions," *Food Chem.*, vol. 158, no. September, pp. 112–117, 2014, doi: 10.1016/j.foodchem.2014.02.107.

[196] S. Bamukyaye and W. Wanasolo, "Performance of Egg-Shell and Fish-Scale as Adsorbent Materials for Chromium (VI) Removal from Effluents of Tannery Industries in Eastern Uganda," *OALib*, vol. 04, no. 08, pp. 1–12, 2017, doi: 10.4236/oalib.1103732.

[197] H. Rezaei, "Biosorption of chromium by using Spirulina sp.," *Arab. J. Chem.*, vol. 9, no. 6, pp. 846–853, 2016, doi: 10.1016/j.arabjc.2013.11.008.

[198] S. Gupta and B. V. Babu, "Removal of toxic metal Cr(VI) from aqueous solutions using sawdust as adsorbent: Equilibrium, kinetics and regeneration studies," *Chem. Eng. J.*, vol. 150, no. 2–3, pp. 352–365, 2009, doi: 10.1016/j.cej.2009.01.013.

[199] N. Itankar and Y. Patil, "Management of Hexavalent Chromium from Industrial Waste Using Low-cost Waste Biomass," *Procedia - Soc. Behav. Sci.*, vol. 133, pp. 219–224, 2014, doi: 10.1016/j.sbspro.2014.04.187.

[200] B. Nasernejad, T. E. Zadeh, B. B. Pour, M. E. Bygi, and A. Zamani, "Camparison for biosorption modeling of heavy metals (Cr (III), Cu (II), Zn (II)) adsorption from wastewater by carrot residues," *Process Biochem.*, vol. 40, no. 3–4, pp. 1319–1322, 2005, doi: 10.1016/j.procbio.2004.06.010.

[201] E. K. Guechi and O. Hamdaoui, "Evaluation of potato peel as a novel adsorbent for the removal of Cu(II) from aqueous solutions: equilibrium, kinetic, and thermodynamic

studies," *Desalin. Water Treat.*, vol. 57, no. 23, pp. 10677–10688, 2016, doi: 10.1080/19443994.2015.1038739.

[202] R. A. K. Rao and F. Rehman, "Adsorption studies on fruits of Gular (Ficus glomerata): Removal of Cr(VI) from synthetic wastewater," *J. Hazard. Mater.*, vol. 181, no. 1–3, pp. 405–412, 2010, doi: 10.1016/j.jhazmat.2010.05.025.

[203] A. K. Bhattacharya, T. K. Naiya, S. N. Mandal, and S. K. Das, "Adsorption, kinetics and equilibrium studies on removal of Cr(VI) from aqueous solutions using different low-cost adsorbents," *Chem. Eng. J.*, vol. 137, no. 3, pp. 529–541, 2008, doi: 10.1016/j.cej.2007.05.021.

[204] M. H. Dehghani, D. Sanaei, I. Ali, and A. Bhatnagar, "Removal of chromium(VI) from aqueous solution using treated waste newspaper as a low-cost adsorbent: Kinetic modeling and isotherm studies," *J. Mol. Liq.*, vol. 215, pp. 671–679, 2016, doi: 10.1016/j.molliq.2015.12.057.

[205] A. Ali, K. Saeed, and F. Mabood, "Removal of chromium (VI) from aqueous medium using chemically modified banana peels as efficient low-cost adsorbent," *Alexandria Eng. J.*, vol. 55, no. 3, pp. 2933–2942, 2016, doi: 10.1016/j.aej.2016.05.011.

[206] S. Kuppusamy, P. Thavamani, M. Megharaj, K. Venkateswarlu, Y. B. Lee, and R. Naidu, "Potential of Melaleuca diosmifolia leaf as a low-cost adsorbent for hexavalent chromium removal from contaminated water bodies," *Process Saf. Environ. Prot.*, vol. 100, pp. 173–182, 2016, doi: 10.1016/j.psep.2016.01.009.

[207] V. K. Gupta, A. Rastogi, and A. Nayak, "Adsorption studies on the removal of hexavalent chromium from aqueous solution using a low cost fertilizer industry waste material," *J. Colloid Interface Sci.*, vol. 342, no. 1, pp. 135–141, 2010, doi: 10.1016/j.jcis.2009.09.065.

[208] X. S. Wang, Y. P. Tang, and S. R. Tao, "Kinetics, equilibrium and thermodynamic study on removal of Cr (VI) from aqueous solutions using low-cost adsorbent Alligator weed," *Chem. Eng. J.*, vol. 148, no. 2–3, pp. 217–225, 2009, doi: 10.1016/j.cej.2008.08.020.

[209] Y. Wu *et al.*, "Functionalized agricultural biomass as a low-cost adsorbent: Utilization of rice straw incorporated with amine groups for the adsorption of Cr(VI) and Ni(II) from single and binary systems," *Biochem. Eng. J.*, vol. 105, pp. 27–35, 2016, doi: 10.1016/j.bej.2015.08.017.

[210] A. B. Albadarin, C. Mangwandi, A. H. Al-Muhtaseb, G. M. Walker, S. J. Allen, and M. N. M. Ahmad, "Kinetic and thermodynamics of chromium ions adsorption onto low-cost dolomite adsorbent," *Chem. Eng. J.*, vol. 179, pp. 193–202, 2012, doi: 10.1016/j.cej.2011.10.080.

[211] L. Chandana, K. Krushnamurty, D. Suryakala, and C. Subrahmanyam, "Low-cost adsorbent derived from the coconut shell for the removal of hexavalent chromium from aqueous medium," *Mater. Today Proc.*, vol. 26, no. xxxx, pp. 44–51, 2018, doi: 10.1016/j.matpr.2019.04.205.

[212] W. Cherdchoo, S. Nithettham, and J. Charoenpanich, "Removal of Cr(VI) from synthetic wastewater by adsorption onto coffee ground and mixed waste tea," *Chemosphere*, vol. 221, no. Vi, pp. 758–767, 2019, doi: 10.1016/j.chemosphere.2019.01.100.

[213] F. Sakr, A. Sennaoui, M. Dinne, S. Alahiane, I. Bakas, M. Belmoden, A. Assabbane,

"Application in chromium (VI) removal of natural and dried cactus," *Cienc. e Tecnol. dos Mater.*, vol. 29, no. 3, pp. 145–152, 2017, doi: 10.1016/j.ctmat.2018.01.001.

[214] N. Nordin, N. A. A. Asmadi, M. K. Manikam, A. A. Halim, M. M. Hanafiah, and S. N. Hurairah, "Removal of Hexavalent Chromium from Aqueous Solution by Adsorption on Palm Oil Fuel Ash (POFA)," *J. Geosci. Environ. Prot.*, vol. 08, no. 02, pp. 112–127, 2020, doi: 10.4236/gep.2020.82008.

[215] E. Malkoc, Y. Nuhoglu, and M. Dundar, "Adsorption of chromium(VI) on pomace-An olive oil industry waste: Batch and column studies," *J. Hazard. Mater.*, vol. 138, no. 1, pp. 142–151, 2006, doi: 10.1016/j.jhazmat.2006.05.051.

[216] T. S. Badessa, E. Wakuma, and A. M. Yimer, "Bio-sorption for effective removal of chromium(VI) from wastewater using Moringa stenopetala seed powder (MSSP) and banana peel powder (BPP)," *BMC Chem.*, vol. 14, no. 1, pp. 1–12, 2020, doi: 10.1186/s13065-020-00724-z.

[217] G. Moussavi and B. Barikbin, "Biosorption of chromium(VI) from industrial wastewater onto pistachio hull waste biomass," *Chem. Eng. J.*, vol. 162, no. 3, pp. 893–900, 2010, doi: 10.1016/j.cej.2010.06.032.

[218] M. Aschale, F. Tsegaye, and M. Amde, "Potato peels as promising low-cost adsorbent for the removal of lead, cadmium, chromium and copper from wastewater," *Desalin. Water Treat.*, vol. 222, pp. 405–415, 2021, doi: 10.5004/dwt.2021.27108.

[219] I. Ghorbel-Abid, K. Galai, and M. Trabelsi-Ayadi, "Retention of chromium (III) and cadmium (II) from aqueous solution by illitic clay as a low-cost adsorbent," *Desalination*, vol. 256, no. 1–3, pp. 190–195, 2010, doi: 10.1016/j.desal.2009.06.079.

[220] M. H. Karaoğlu, Ş. Zor, and M. Uğurlu, "Biosorption of Cr(III) from solutions using vineyard pruning waste," *Chem. Eng. J.*, vol. 159, no. 1–3, pp. 98–106, 2010, doi: 10.1016/j.cej.2010.02.047.

[221] L. Dai, Y. Li, R. Liu, C. Si, and Y. Ni, "Green mussel-inspired lignin magnetic nanoparticles with high adsorptive capacity and environmental friendliness for chromium(III) removal," *Int. J. Biol. Macromol.*, vol. 132, pp. 478–486, 2019, doi: 10.1016/j.ijbiomac.2019.03.222.

[222] A. Lodi, D. Soletto, C. Solisio, and A. Converti, "Chromium(III) removal by Spirulina platensis biomass," *Chem. Eng. J.*, vol. 136, no. 2–3, pp. 151–155, 2008, doi: 10.1016/j.cej.2007.03.032.

[223] S. Elabbas, L. Mandi, F. Berrekhis, M. N. Pons, J. P. Leclerc, and N. Ouazzani, "Removal of Cr(III) from chrome tanning wastewater by adsorption using two natural carbonaceous materials: Eggshell and powdered marble," *J. Environ. Manage.*, vol. 166, pp. 589–595, 2016, doi: 10.1016/j.jenvman.2015.11.012.

[224] L. Pietrelli, I. Francolini, A. Piozzi, M. Sighicelli, I. Silvestro, and M. Vocciante, "Chromium(III) removal fromwastewater by chitosan flakes," *Appl. Sci.*, vol. 10, no. 6, pp. 1–11, 2020, doi: 10.3390/app10061925.

[225] H. S. Mohamed, N. K. Soliman, D. A. Abdelrheem, A. A. Ramadan, A. H. Elghandour, and S. A. Ahmed, "Adsorption of Cd 2+ and Cr 3+ ions from aqueous solutions by using residue of Padina gymnospora waste as promising low-cost adsorbent," *Heliyon*, vol. 5, no. 3, p. e01287, 2019, doi: 10.1016/j.heliyon.2019.e01287.

[226] G. Campos-Flores, J. Gurreonero-Fernández, and R. Vejarano, "Passion-fruit shell

biomass as adsorbent material to remove chromium III from contaminated aqueous mediums," *IOP Conf. Ser. Mater. Sci. Eng.*, vol. 620, no. 1, pp. 0–7, 2019, doi: 10.1088/1757-899X/620/1/012110.

[227] A. H. Sulaymon, A. A. Mohammed, and T. J. Al-Musawi, "Comparative study of removal of cadmium (II) and chromium (III) ions from aqueous solution using low-cost biosorbent," *Int. J. Chem. React. Eng.*, vol. 12, no. 1, pp. 1–10, 2014, doi: 10.1515/ijcre-2014-0024.

[228] S. Tangjuank, N. Insuk, V. Udeye, and J. Tontrakoon, "Chromium (III) sorption from aqueous solutions using activated carbon prepared from cashew nut shells," *Int. J. Phys. Sci.*, vol. 4, no. 8, pp. 412–417, 2009.

[229] N. S. Barot and H. K. Bagla, "Desalination and Water Treatment Eco-friendly waste water treatment by cow dung powder (Adsorption studies of Cr (III), Cr (VI) and Cd (II) using tracer technique) Eco-friendly waste water treatment by cow dung powder (Adsorption studies of Cr (," *Tatlor Fr. Gr.*, no. May 2013, pp. 37–41, 2012.

[230] Z. H. Yang, S. Xiong, B. Wang, Q. Li, and W. C. Yang, "Cr(III) adsorption by sugarcane pulp residue and biochar," *J. Cent. South Univ.*, vol. 20, no. 5, pp. 1319–1325, 2013, doi: 10.1007/s11771-013-1618-4.

[231] M. Abbas, R. Nadeem, M. N. Zafar, and M. Arshad, "Biosorption of chromium (III) and chromium (VI) by untreated and pretreated Cassia fistula biomass from aqueous solutions," *Water. Air. Soil Pollut.*, vol. 191, no. 1–4, pp. 139–148, 2008, doi: 10.1007/s11270-007-9613-8.

[232] T. Guimarães, L. D. Paquini, B. R. Lyrio Ferraz, L. P. Roberto Profeti, and D. Profeti, "Efficient removal of Cu(II) and Cr(III) contaminants from aqueous solutions using marble waste powder," *J. Environ. Chem. Eng.*, vol. 8, no. 4, p. 103972, 2020, doi: 10.1016/j.jece.2020.103972.

[233] N. F. Fahim, B. N. Barsoum, A. E. Eid, and M. S. Khalil, "Removal of chromium(III) from tannery wastewater using activated carbon from sugar industrial waste," *J. Hazard. Mater.*, vol. 136, no. 2, pp. 303–309, 2006, doi: 10.1016/j.jhazmat.2005.12.014.

[234] R. A. Jacques, E. C. Lima, S. L. P. Dias, A. C. Mazzocato, and F. A. Pavan, "Yellow passion-fruit shell as biosorbent to remove Cr(III) and Pb(II) from aqueous solution," *Sep. Purif. Technol.*, vol. 57, no. 1, pp. 193–198, 2007, doi: 10.1016/j.seppur.2007.01.018.

[235] S. H. Ranasinghe, A. N. Navaratne, and N. Priyantha, "Enhancement of adsorption characteristics of Cr(III) and Ni(II) by surface modification of jackfruit peel biosorbent," *J. Environ. Chem. Eng.*, vol. 6, no. 5, pp. 5670–5682, 2018, doi: 10.1016/j.jece.2018.08.058.

[236] J. Liu, Y. Chen, S. Jiang, J. Huang, Y. Lv, Y. Liu, and M. Liu, "Rapid removal of Cr(III) from high-salinity wastewater by cellulose-g-poly-(acrylamide-co-sulfonic acid) polymeric bio-adsorbent," *Carbohydr. Polym.*, vol. 270, no. 2, 2021, doi: 10.1016/j.carbpol.2021.118356.

[237] A. Witek-Krowiak and D. Harikishore Kumar Reddy, "Removal of microelemental Cr(III) and Cu(II) by using soybean meal waste - Unusual isotherms and insights of binding mechanism," *Bioresour. Technol.*, vol. 127, pp. 350–357, 2013, doi: 10.1016/j.biortech.2012.09.072.

[238] S. Martini, S. Afroze, and K. Ahmad Roni, “Modified eucalyptus bark as a sorbent for simultaneous removal of COD, oil, and Cr(III) from industrial wastewater,” *Alexandria Eng. J.*, vol. 59, no. 3, pp. 1637–1648, 2020, doi: 10.1016/j.aej.2020.04.010.

[239] J. Wang, D. Zhang, S. Liu, and C. Wang, “Enhanced removal of chromium(III) for aqueous solution by EDTA modified attapulgite: Adsorption performance and mechanism,” *Sci. Total Environ.*, vol. 720, p. 137391, 2020, doi: 10.1016/j.scitotenv.2020.137391.

[240] H. Chen, J. Dou, and H. Xu, “Removal of Cr(VI) ions by sewage sludge compost biomass from aqueous solutions: Reduction to Cr(III) and biosorption,” *Appl. Surf. Sci.*, vol. 425, pp. 728–735, 2017, doi: 10.1016/j.apsusc.2017.07.053.

[241] F. Teshale, R. Karthikeyan, and O. Sahu, “Synthesized bioadsorbent from fish scale for chromium (III) removal,” *Micron*, vol. 130, no. September 2019, p. 102817, 2020, doi: 10.1016/j.micron.2019.102817.

[242] E. Hoseinzadeh, M. R. Samarghandi, G. McKay, N. Rahimi, and J. Jafari, “Removal of acid dyes from aqueous solution using potato peel waste biomass: A kinetic and equilibrium study,” *Desalin. Water Treat.*, vol. 52, no. 25–27, pp. 4999–5006, 2014, doi: 10.1080/19443994.2013.810355.

[243] Y. A. Öktem, S. G. Pozan Soylu, and N. Aytan, “The adsorption of methylene blue from aqueous solution by using waste potato peels; equilibrium and kinetic studies,” *J. Sci. Ind. Res. (India).*, vol. 71, no. 12, pp. 817–821, 2012.

[244] J. S. Piccin, C. S. Gomes, B. Mella, and M. Gutterres, “Color removal from real leather dyeing effluent using tannery waste as an adsorbent,” *J. Environ. Chem. Eng.*, vol. 4, no. 1, pp. 1061–1067, 2016, doi: 10.1016/j.jece.2016.01.010.

[245] D. P. Tiwari, S. K. Singh, and N. Sharma, “Sorption of methylene blue on treated agricultural adsorbents: equilibrium and kinetic studies,” *Appl. Water Sci.*, vol. 5, no. 1, pp. 81–88, 2015, doi: 10.1007/s13201-014-0171-0.

[246] M. Malakootian and M. R. Heidari, “Reactive orange 16 dye adsorption from aqueous solutions by psyllium seed powder as a low-cost biosorbent: kinetic and equilibrium studies,” *Appl. Water Sci.*, vol. 8, no. 7, pp. 1–9, 2018, doi: 10.1007/s13201-018-0851-2.

[247] M. K. Uddin and A. Nasar, “Walnut shell powder as a low-cost adsorbent for methylene blue dye: isotherm, kinetics, thermodynamic, desorption and response surface methodology examinations,” *Sci. Rep.*, vol. 10, no. 1, pp. 1–13, 2020, doi: 10.1038/s41598-020-64745-3.

[248] M. T. Islam, C. Chambers, and M. Toufiq Reza, “Effects of process liquid recirculation on material properties of hydrochar and corresponding adsorption of cationic dye,” *J. Anal. Appl. Pyrolysis*, vol. 161, no. October 2021, p. 105418, 2022, doi: 10.1016/j.jaap.2021.105418.

[249] N. S. Ali, N. M. Jabbar, S. M. Alardhi, H. Sh, and T. M. Albayati, “Heliyon Adsorption of methyl violet dye onto a prepared bio-adsorbent from date seeds : isotherm , kinetics , and thermodynamic studies,” *Heliyon*, vol. 8, no. March, p. e10276, 2022, doi: 10.1016/j.heliyon.2022.e10276.

[250] U. J. Etim, S. A. Umoren, and U. M. Eduok, “Coconut coir dust as a low cost adsorbent for the removal of cationic dye from aqueous solution,” *J. Saudi Chem. Soc.*,

vol. 20, pp. S67–S76, 2016, doi: 10.1016/j.jscs.2012.09.014.

[251] M. A. Al-Ajji and M. A. Al-Ghouti, "Novel insights into the nanoadsorption mechanisms of crystal violet using nano-hazelnut shell from aqueous solution," *J. Water Process Eng.*, vol. 44, no. October, p. 102354, 2021, doi: 10.1016/j.jwpe.2021.102354.

[252] E. H. Ezechi, S. R. B. M. Kutty, A. Malakahmad, and M. H. Isa, "Characterization and optimization of effluent dye removal using a new low cost adsorbent: Equilibrium, kinetics and thermodynamic study," *Process Saf. Environ. Prot.*, vol. 98, pp. 16–32, 2015, doi: 10.1016/j.psep.2015.06.006.

[253] G. B. Hong and Y. K. Wang, "Synthesis of low-cost adsorbent from rice bran for the removal of reactive dye based on the response surface methodology," *Appl. Surf. Sci.*, vol. 423, pp. 800–809, 2017, doi: 10.1016/j.apsusc.2017.06.264.

[254] M. K. Dahri, M. R. R. Kooh, and L. B. L. Lim, "Water remediation using low cost adsorbent walnut shell for removal of malachite green: Equilibrium, kinetics, thermodynamic and regeneration studies," *J. Environ. Chem. Eng.*, vol. 2, no. 3, pp. 1434–1444, 2014, doi: 10.1016/j.jece.2014.07.008.

[255] B. H. Hameed, "Removal of cationic dye from aqueous solution using jackfruit peel as non-conventional low-cost adsorbent," *J. Hazard. Mater.*, vol. 162, no. 1, pp. 344–350, 2009, doi: 10.1016/j.jhazmat.2008.05.045.

[256] N. Nasuha, B. H. Hameed, and A. T. M. Din, "Rejected tea as a potential low-cost adsorbent for the removal of methylene blue," *J. Hazard. Mater.*, vol. 175, no. 1–3, pp. 126–132, 2010, doi: 10.1016/j.jhazmat.2009.09.138.

[257] A. Asfaram, M. R. Fathi, S. Khodadoust, and M. Naraki, "Removal of Direct Red 12B by garlic peel as a cheap adsorbent: Kinetics, thermodynamic and equilibrium isotherms study of removal," *Spectrochim. Acta - Part A Mol. Biomol. Spectrosc.*, vol. 127, pp. 415–421, 2014, doi: 10.1016/j.saa.2014.02.092.

[258] M. R. Fathi, A. Asfaram, and A. Farhangi, "Removal of Direct Red 23 from aqueous solution using corn stalks: Isotherms, kinetics and thermodynamic studies," *Spectrochim. Acta - Part A Mol. Biomol. Spectrosc.*, vol. 135, pp. 364–372, 2015, doi: 10.1016/j.saa.2014.07.008.

[259] S. Jain and R. V. Jayaram, "Removal of basic dyes from aqueous solution by low-cost adsorbent: Wood apple shell (Feronia acidissima)," *Desalination*, vol. 250, no. 3, pp. 921–927, 2010, doi: 10.1016/j.desal.2009.04.005.

[260] S. Sarkar, N. Tiwari, A. Basu, M. Behera, B.Das, S. Chakrabortty, and S.K. Tripathy, "Sorptive removal of malachite green from aqueous solution by magnetite/coir pith supported sodium alginate beads: Kinetics, isotherms, thermodynamics and parametric optimization," *Environ. Technol. Innov.*, vol. 24, p. 101818, 2021, doi: 10.1016/j.eti.2021.101818.

[261] OriginLab, "Data analysis and graphing software," *OriginLab Corp., Northampton*. 2018.

[262] S. Wold, K. Esbensen, and P. Geladi, "Principal component analysis," *Chemom. Intell. Lab. Syst.*, vol. 2, no. 1, pp. 37–52, 1987, doi: https://doi.org/10.1016/0169-7439(87)80084-9.

[263] R. G. Brereton, *Chemometrics: data analysis for the laboratory and chemical plant*. John Wiley & Sons, 2003.

[264] B. E. L. Muñoz, R. R. Robles, J. L. I. García, and M. T. O. Gutiérrez, "Adsorption of basic chromium sulfate used in the tannery industries by calcined hydrotalcite," *J. Mex. Chem. Soc.*, vol. 55, no. 3, pp. 137–141, 2011.

[265] Z. Ahmad, A. Shamim, S. Mahmood, T. Mahmood, and F. U. Khan, "Biological Synthesis and Characterization of Chromium (iii) Oxide Nanoparticles," *Eng. Appl. Sci. Lett.*, vol. 1(2018), no. 2, pp. 23–29, 2018, doi: 10.30538/psrp-easl2018.0008.

[266] L. Li, Z. Wang, M. Y. Wang, and Y. Zhang, "Modulation of active Cr(III) complexes by bath preparation to adjust Cr(III) electrodeposition," *Int. J. Miner. Metall. Mater.*, vol. 20, no. 9, pp. 902–908, 2013, doi: 10.1007/s12613-013-0813-5.

[267] M. H. Armbruster and J. B. Austin, "The Adsorption of Gases on Plane Surfaces of Mica," *J. Am. Chem. Soc.*, vol. 60, no. 2, pp. 467–475, 1938, doi: 10.1021/ja01269a066.

[268] H. Freundlich, "Of the adsorption of gases. Section II. Kinetics and energetics of gas adsorption," *Trans. Faraday Soc.*, vol. 28, pp. 195–201, 1932.

[269] X. S. Wang, Y. P. Tang, and S. R. Tao, "Removal of Cr (VI) from aqueous solutions by the nonliving biomass of Alligator weed: Kinetics and equilibrium," *Adsorption*, vol. 14, no. 6, pp. 823–830, 2008, doi: 10.1007/s10450-008-9145-6.

[270] F. Teshale, R. Karthikeyan, and O. Sahu, "Synthesized bioadsorbent from fish scale for chromium (III) removal," *Micron*, vol. 130, no. Iii, p. 102817, 2020, doi: 10.1016/j.micron.2019.102817.

[271] M. A. Al-Ghouti, J. Li, Y. Salamh, N. Al-Laqtah, G. Walker, and M. N. M. Ahmad, "Adsorption mechanisms of removing heavy metals and dyes from aqueous solution using date pits solid adsorbent," *J. Hazard. Mater.*, vol. 176, no. 1–3, pp. 510–520, 2010, doi: 10.1016/j.jhazmat.2009.11.059.

[272] P. Miretzky and A. F. Cirelli, "Cr(VI) and Cr(III) removal from aqueous solution by raw and modified lignocellulosic materials: A review," *J. Hazard. Mater.*, vol. 180, no. 1–3, pp. 1–19, 2010, doi: 10.1016/j.jhazmat.2010.04.060.

[273] M. B. Aregu, S. L. Asfaw, and M. M. Khan, "Identification of two low-cost and locally available filter media (pumice and scoria) for removal of hazardous pollutants from tannery wastewater," *Environ. Syst. Res.*, vol. 7, no. 1, 2018, doi: 10.1186/s40068-018-0112-2.

[274] S. Nethaji, A. Sivasamy, and A. B. Mandal, "Adsorption isotherms, kinetics and mechanism for the adsorption of cationic and anionic dyes onto carbonaceous particles prepared from Juglans regia shell biomass," *Int. J. Environ. Sci. Technol.*, vol. 10, no. 2, pp. 231–242, 2013, doi: 10.1007/s13762-012-0112-0.

[275] G. Qiu, Q. Xie, H. Liu, T. Chen, J. Xie, and H. Li, "Removal of Cu(II) from aqueous solutions using dolomite-palygorskite clay: Performance and mechanisms," *Appl. Clay Sci.*, vol. 118, pp. 107–115, 2015, doi: 10.1016/j.clay.2015.09.008.

[276] N. Atar, A. Olgun, and S. Wang, "Adsorption of cadmium (II) and zinc (II) on boron enrichment process waste in aqueous solutions: Batch and fixed-bed system studies," *Chem. Eng. J.*, vol. 192, no. 3, pp. 1–7, 2012, doi: 10.1016/j.cej.2012.03.067.

[277] A. C. Kharake and V. S. Raut, "An assessment of water quality index of Godavari river water in Nashik city, Maharashtra," *Appl. Water Sci.*, vol. 11, no. 6, pp. 1–11, 2021, doi: 10.1007/s13201-021-01432-2.

[278] M. S. Islam, R. Afroz, and M. B. Mia, "Investigation of surface water quality of the

Buriganga river in Bangladesh: Laboratory and spatial analysis approaches," *Dhaka Univ. J. Biol. Sci.*, vol. 28, no. 2, pp. 147–158, 2019, doi: 10.3329/dujbs.v28i2.46501.

[279] F. J. Millero, R. Feistel, D. G. Wright, and T. J. McDougall, "The composition of Standard Seawater and the definition of the Reference-Composition Salinity Scale," *Deep. Res. Part I Oceanogr. Res. Pap.*, vol. 55, no. 1, pp. 50–72, 2008, doi: 10.1016/j.dsr.2007.10.001.

[280] E. V. Hatzikos, G. Tsoumakas, G. Tzanis, N. Bassiliades, and I. Vlahavas, "An empirical study on sea water quality prediction," *Knowledge-Based Syst.*, vol. 21, no. 6, pp. 471–478, 2008, doi: 10.1016/j.knosys.2008.03.005.

[281] J. R. Du, X. Zhang, X. Feng, Y. Wu, F. Cheng, and M. E. A. Ali, "Desalination of high salinity brackish water by an NF-RO hybrid system," *Desalination*, vol. 491, no. November 2019, p. 114445, 2020, doi: 10.1016/j.desal.2020.114445.

[282] P. G. Whitehead, G. Bussi, R. Peters, M.A. Hossain, L. Softley, S. Shawal, L. Jin, C.P.N. Rampley, P. Holdship, R. Hope, and G. Alabaster, "Modelling heavy metals in the Buriganga River System, Dhaka, Bangladesh: Impacts of tannery pollution control," *Sci. Total Environ.*, vol. 697, p. 134090, 2019, doi: 10.1016/j.scitotenv.2019.134090.

[283] P. G. Whitehead Z. Mimouni, D. Butterfield, G. Bussi, M. A. Hossain, R. Peters, S. Shawal, P. Holdship, C. P. N. Rampley, L. Jin, and D. Ager,, "A new multibranch model for metals in river systems: Impacts and control of tannery wastes in Bangladesh," *Sustain.*, vol. 13, no. 6, pp. 1–22, 2021, doi: 10.3390/su13063556.

[284] S. Bachrun, N. Ayurizka, S. Annisa, and H. Arif, "Preparation and characterization of activated carbon from sugarcane bagasse by physical activation with CO2 gas," *IOP Conf. Ser. Mater. Sci. Eng.*, vol. 105, no. 1, 2016, doi: 10.1088/1757-899X/105/1/012027.

[285] C. K. Singh, J. N. Sahu, K. K. Mahalik, C. R. Mohanty, B. R. Mohan, and B. C. Meikap, "Studies on the removal of Pb(II) from wastewater by activated carbon developed from Tamarind wood activated with sulphuric acid," *J. Hazard. Mater.*, vol. 153, no. 1–2, pp. 221–228, 2008, doi: 10.1016/j.jhazmat.2007.08.043.

[286] Z. Z. Chowdhury, S. M. Zain, R. A. Khan, and M. S. Islam, "Preparation and characterizations of activated carbon from kenaf fiber for equilibrium adsorption studies of copper from wastewater," *Korean J. Chem. Eng.*, vol. 29, no. 9, pp. 1187–1195, 2012, doi: 10.1007/s11814-011-0297-9.

[287] L. Zhang Y. Ren, Y. Xue, Z. Cui, Q. Wei, C. Han, and J. He, "Preparation of biochar by mango peel and its adsorption characteristics of Cd(ii) in solution," *RSC Adv.*, vol. 10, no. 59, pp. 35878–35888, 2020, doi: 10.1039/d0ra06586b.

[288] Z. Xiao, W. Chen, K. Liu, P. Cui, and D. Zhan, "Porous biomass carbon derived from peanut shells as electrode materials with enhanced electrochemical performance for supercapacitors," *Int. J. Electrochem. Sci.*, vol. 13, no. 6, pp. 5370–5381, 2018, doi: 10.20964/2018.06.54.

[289] A. Shariff, N. S. M. Aziz, and N. Abdullah, "Slow Pyrolysis of Oil Palm Empty Fruit Bunches for Biochar Production and Characterisation," *J. Phys. Sci.*, vol. 25, no. 2, pp. 97–112, 2014.

[290] M. Ajmal, A. Hussain Khan, S. Ahmad, and A. Ahmad, "Role of sawdust in the removal of copper(II) from industrial wastes," *Water Res.*, vol. 32, no. 10, pp. 3085–

3091, 1998, doi: 10.1016/S0043-1354(98)00067-0.

[291] Y. Wu, S. Zhang, X. Guo, and H. Huang, "Adsorption of chromium(III) on lignin," *Bioresour. Technol.*, vol. 99, no. 16, pp. 7709–7715, 2008, doi: 10.1016/j.biortech.2008.01.069.

[292] V. C. G. Dos Santos, A. D. P. A. Salvado, D. C. Dragunski, D. N. C. Peraro, C. R. T. Tarley, and J. Caetano, "Highly improved chromium (III) uptake capacity in modified sugarcane bagasse using different chemical treatments," *Quim. Nova*, vol. 35, no. 8, pp. 1606–1611, 2012, doi: 10.1590/s0100-40422012000800021.

[293] K. R. Hall, L. C. Eagleton, A. Acrivos, and T. Vermeulen, "Pore- and solid-diffusion kinetics in fixed-bed adsorption under constant-pattern conditions," *Ind. Eng. Chem. Fundam.*, vol. 5, no. 2, pp. 212–223, 1966, doi: 10.1021/i160018a011.

[294] M. Z. Iqbal, P. Pal, M. Shoaib, and A. A. Abdala, "Efficient removal of different basic dyes using graphene," *Desalin. Water Treat.*, vol. 68, no. May 2018, pp. 226–235, 2017, doi: 10.5004/dwt.2017.20213.

[295] Ş. Parlayici and E. Pehlivan, "Comparative study of Cr(VI) removal by bio-waste adsorbents: equilibrium, kinetics, and thermodynamic," *J. Anal. Sci. Technol.*, vol. 10, no. 1, 2019, doi: 10.1186/s40543-019-0175-3.

[296] Z. Droussi, V. D'orazio, M. R. Provenzano, M. Hafidi, and A. Ouatmane, "Study of the biodegradation and transformation of olive-mill residues during composting using FTIR spectroscopy and differential scanning calorimetry," *J. Hazard. Mater.*, vol. 164, no. 2–3, pp. 1281–1285, 2009, doi: 10.1016/j.jhazmat.2008.09.081.

[297] R. Shan, Y. Shi, J. Gu, Y. Wang, and H. Yuan, "Single and competitive adsorption affinity of heavy metals toward peanut shell-derived biochar and its mechanisms in aqueous systems," *Chinese J. Chem. Eng.*, vol. 28, no. 5, pp. 1375–1383, 2020, doi: 10.1016/j.cjche.2020.02.012.

[298] T. Adane and A. Dessie, "Adaptability of Teff husk activated carbon for removal of hexavalent chromium from tannery wastewater at optimized process condition," *Appl. Water Sci.*, vol. 10, no. 8, pp. 1–7, 2020, doi: 10.1007/s13201-020-01269-1.

[299] W. Yao W. Yao, S. Yu, J. Wang, Y. Zou, S. Lu, Y. Ai, N. S.Alharbi, A. Alsaedi, T. Hayat, and X. Wang, "Enhanced removal of methyl orange on calcined glycerol-modified nanocrystallined Mg/Al layered double hydroxides," *Chem. Eng. J.*, vol. 307, pp. 476–486, 2016, doi: 10.1016/j.cej.2016.08.117.

[300] Ş. Taşar, F. Kaya, and A. Özer, "Biosorption of lead(II) ions from aqueous solution by peanut shells: Equilibrium, thermodynamic and kinetic studies," *J. Environ. Chem. Eng.*, vol. 2, no. 2, pp. 1018–1026, 2014, doi: 10.1016/j.jece.2014.03.015.

[301] A. Maleki, H. Daraei, F. Khodaei, K. B. Aghdam, and E. Faez, "Direct blue 71 dye removal probing by potato peel-based sorbent: applications of artificial intelligent systems," *Desalin. Water Treat.*, vol. 57, no. 26, pp. 12281–12286, 2016, doi: 10.1080/19443994.2015.1048733.

[302] S. Lairini K. El Mahtal1, Y. Miyah, K. Tanji, S. Guissi, S. Boumchita, and F. Zerrouq, "The adsorption of Crystal violet from aqueous solution by using potato peels (Solanum tuberosum): Equilibrium and kinetic studies," *J. Mater. Environ. Sci.*, vol. 8, no. 9, pp. 3252–3261, 2017.

[303] Y. Chen, S. R. Zhai, N. Liu, Y. Song, Q. Da An, and X. W. Song, "Dye removal of activated carbons prepared from NaOH-pretreated rice husks by low-temperature

solution-processed carbonization and H3PO4 activation," *Bioresour. Technol.*, vol. 144, pp. 401–409, 2013, doi: 10.1016/j.biortech.2013.07.002.

[304] C. K. Enenebeaku, N. J. Okorocha, U. E. Enenebeaku, and I. C. Ukaga, "Adsorption and Equilibrium Studies on the Removal of Methyl Red from Aqueous Solution Using White Potato Peel Powder," *Int. Lett. Chem. Phys. Astron.*, vol. 72, no. May, pp. 52–64, 2017, doi: 10.18052/www.scipress.com/ilcpa.72.52.

[305] O. I. Maxwell, U. B. Chinwuba, and M. G. Onyebuchukwu, "Protein Enrichment of Potato Peels Using Saccharomyces cerevisiae via Solid-State Fermentation Process," *Adv. Chem. Eng. Sci.*, vol. 09, no. 01, pp. 99–108, 2019, doi: 10.4236/aces.2019.91008.

[306] N. A. El-Sersy, G. M. Abou-Elela, S. W. Hassan, and H. Abd-Elnaby, "Bioremediation of acid fast red dye by Streptomyces globosus under static and shake conditions," *African J. Biotechnol.*, vol. 10, no. 17, pp. 3467–3474, 2011, doi: 10.5897/ajb10.1989.

[307] M. A. Wahab, H. Boubakri, S. Jellali, and N. Jedidi, "Characterization of ammonium retention processes onto Cactus leaves fibers using FTIR, EDX and SEM analysis," *J. Hazard. Mater.*, vol. 241–242, pp. 101–109, 2012, doi: 10.1016/j.jhazmat.2012.09.018.

[308] A. I. Osman, J. Blewitt, J.K.A. Dahrieh, C. Farrell, A. H. Al-Muhtaseb, J Harrison, and D.W. .Rooney, "Production and characterisation of activated carbon and carbon nanotubes from potato peel waste and their application in heavy metal removal.," *Environ. Sci. Pollut. Res.*, vol. 26, no. 36, pp. 37228–37241, 2019, doi: 10.1007/s11356-019-06594-w.

[309] M. A. M. Salleh, D. K. Mahmoud, W. A. W. A. Karim, and A. Idris, "Cationic and anionic dye adsorption by agricultural solid wastes: A comprehensive review," *Desalination*, vol. 280, no. 1–3, pp. 1–13, 2011, doi: 10.1016/j.desal.2011.07.019.

[310] P. A. Ashis Kumar Samanta, "Application of natural dyes on textiles | Ashis Kumar Samanta | Request PDF", Accessed: Jul. 19, 2019. [Online]. Available: https://www.researchgate.net/publication/279573040_Application_of_natural_dyes_on_textiles

[311] C. Patawat, K. Silakate, S. Chuan-Udom, N. Supanchaiyamat, A. J. Hunt, and Y. Ngernyen, "Preparation of activated carbon fromDipterocarpus alatusfruit and its application for methylene blue adsorption," *RSC Adv.*, vol. 10, no. 36, pp. 21082–21091, 2020, doi: 10.1039/d0ra03427d.

Annex I- Publications

List of Publications

1. Fatema-Tuj-zohra, S. Ahmed, R. Sultana, M. Nurnabi, and M. Z. Alam, "Removal of Cr(III) from tanning effluent using adsorbent prepared from peanut shell," *Desalin. Water Treat.*, vol. 266, pp. 91–100, 2022, doi: 10.5004/dwt.2022.28621.

Desalination and Water Treatment
www.deswater.com

(2022) 1–10

doi: 10.5004/dwt.2022.28621

Removal of Cr(III) from tanning effluent using adsorbent prepared from peanut shell

Fatema-Tuj-Zohra[a,b], Sobur Ahmed[a,b], Razia Sultana[a], Md. Nurnabi[b,*], Md. Zahangir Alam[b,*]

[a]*Institute of Leather Engineering and Technology (ILET), University of Dhaka, Bangladesh, emails: fatema.ilet@du.ac.bd (Fatema-Tuj-Zohra), soburahmed@du.ac.bd (S. Ahmed), raziasultana.du53@gmail.com (R. Sultana)*
[b]*Department of Applied Chemistry and Chemical Engineering, University of Dhaka, Bangladesh, Tel. +8801711577225; Fax: +880-2-9667222; email: nabi@du.ac.bd (Md. Nurnabi), zahangir@du.ac.bd (Md. Z. Alam)*

Received 29 January 2022; Accepted 30 May 2022

ABSTRACT

This article describes the development of an adsorbent from peanut shell (PNS) for removing Cr(III) from tannery effluents. Adsorbent was prepared by pyrolysis of peanut shell followed by activation with NaOH and was characterized by different analytical methods. Adsorption capacity and removal rate of Cr(III) were determined. The adsorption capacity of activated PNS was investigated through batch experiments with the effect of pH, adsorbent doses, contact time, initial concentration, and temperature. Adsorption capacity and rate of removal of Cr(III) were 74.79 mg/g and 54.21%, respectively. The highest adsorption capacity (q_m) calculated from Langmuir isotherm was 104.82 mg/g. Adsorption isotherm of Cr(III) on PNS was studied by Langmuir and Freundlich models which revealed that Langmuir model fitted the best with a R^2 value of 0.999. The adsorption kinetics of Cr(III) on PNS followed pseudo-second-order reaction model with a R^2 value of 0.9879. The experimental data of Cr(III) adsorption were also fitted well with the pseudo-second-order kinetic model. Various physico-chemical parameters of chrome tanning effluent were also evaluated prior to and subsequent to adsorption.

Keywords: Activated carbon; Adsorption capacity; Adsorption isotherm; Peanut shell; Tannery effluent

1. Introduction

One of the most important environmental concerns of this century is the contamination of surface water with heavy metals. As we know, heavy metals cannot be degraded or destroyed; hence they are interminable in all parts of the environment [1,2]. Worldwide water sources are going under serious threat due to unplanned industrialization and urbanization. In the developing countries like Bangladesh, there is a tendency to set up industries beside the water bodies, and discharges untreated industrial waste to the surface water. Chromium compounds have gained extensive applications in leather tanning, textile dyeing, wood preservation, printing inks, paints and pigments, and metal plating [3]. Tannery effluents contain high chromium content and other organic and inorganic pollutants of a very heterogeneous group of elements in their properties and functions [4].

In leather tanning, 60%–70% of employed chromium is consumed by leather and the rest 30%–40% remains in the spent tan liquor [5]. It is reported that the waste and spent liquor from tanneries contain 10–50 and 2,900–4,500 mg/L of chromium, respectively [6]. The discharged unexploited

* Corresponding authors.